LCH Laboratoire de Constructions Hydrauliques
Laboratory of Hydraulic Constructions

ÉCOLE POLYTECHNIQUE
FÉDÉRALE DE LAUSANNE

Communication 39

An experimental study on main flow, secondary flow and turbulence in open-channel bends with emphasis on their interaction with the outer-bank geometry

Alexandre Duarte

Editeur : Prof. Dr A. Schleiss

Lausanne, 2009

Communications du Laboratoire de Constructions Hydrauliques ISSN 1661-1179
Ecole Polytechnique Fédérale de Lausanne
Editeur: Prof. Dr A. Schleiss

N° 14 2003 D. S. Hersberger
Wall roughness effects on flow and scouring in curved channels with gravel bed

N° 15 2003 Ch. Oehy
Effects of obstacles and jets on reservoir sedimentation due to turbidity currents

N° 16 2004 J.-L. Boillat, P. de Souza
Hydraulic System - Modélisation des systèmes hydrauliques à écoulements transitoires en charge

N° 17 2004 Cycle postgrade en aménagements hydrauliques
Collection des articles des travaux de diplôme postgrade

N° 18 2004 S. Emami
Erosion protection downstream of diversion tunnels using concrete prisms - Design criteria based on a systematic physical model study

N° 19 2004 Ph. Chèvre
Influence de la macro-rugosité d'un enrochement sur le charriage et l'érosion en courbe

N° 20 2004 S. André
High velocity aerated flows on stepped chutes with macro-roughness elements

N° 21 2005 Conférence sur la recherche appliquée en relation avec la troisième correction du Rhône - Nouveaux développements dans la gestion des crues

N° 22 2005 INTERREG IIIB - Projet ALPRESERV. Conférence sur la problématique de la sédimentation dans les réservoirs - Gestion durable des sédiments dans les réservoirs alpins

N° 23 2005 Master of Advanced Studies (MAS) in hydraulic schemes
Collection des articles des travaux de diplôme

N° 24 2006 S. Sayah
Efficiency of brushwood fences in shore protection against wind-wave induced erosion

N° 25 2006 P. Manso
The influence of pool geometry and induced flow patterns in rock scour by high-velocity plunging jets

N° 26 2006 M. Andaroodi
Standardization of civil engineering works of small high-head hydropower plants and development of an optimization tool

N° 27 2006 Symposium érosion et protection des rives lacustres
Bases de dimensionnement des mesures de protection des rives lacustres

PREFACE

Flow characteristics near river banks are still not fully understood, especially in river bends where the outer banks are most vulnerable to erosion. Dr. Alexandre Duarte investigated in his thesis the influence of the outer bank inclination and its roughness on the patterns of main flow, secondary flow, turbulence and boundary shear stress. Insight in these hydrodynamic parameters is relevant for river morphodynamics, water quality, river restoration, riparian ecology, bank protection, hazard mitigation, etc. Dr. Duarte has carried out 9 experiments in a laboratory flume with fixed horizontal sand bed under similar hydraulic conditions, thereby covering three different inclinations (30°, 45° and 90°) and three different roughness characteristics of the outer bank (hydraulically smooth, sand roughness identical to the bed and riprap-roughened). He focused on the influence of these parameters in straight and curved flows.

Bed and bank shear stresses in straight flows are commonly estimated by means of Chow's method (1959), which does not take into account the bank inclination and roughness. Based on a series of laboratory experiments, Knight (1994) has proposed empirical formulae for the bed and bank shear stresses that account for the bank inclination and roughness. Dr. Duarte has investigated the near-bank hydrodynamics and especially the intricate interaction between turbulence-induced cells of secondary flow and the main flow, which determines the distribution of the boundary shear stress. His analysis indicated that Chow's method overestimates/underestimates the bank/bed shear stress, validated Knight's formulae and extended them for configurations with roughened bank.

Curvature-induced secondary flow, also called helical flow, is a characteristic feature of flow in river bends. Beside the so-called center-region cell of secondary flow, a counter-rotating outer-bank cell has often been observed near the outer bank in laboratory flumes and natural rivers. In spite of its importance for the bank shear stress, little was known about the outer-bank cell's conditions of occurrence and dependence on the characteristics of the outer bank. Dr. Duarte's research has confirmed the protective effect of the outer-bank cell on the outer bank and the adjacent bed. Moreover, it has shown that roughness and steepness of the outer bank favour the outer-bank cell.

We would like to thank Prof. António Cardoso from Instituto Superior Técnico, Lisbon, Portugal, and Prof. Wim Uijttewaal from Delft University of Technology, The Netherlands, for their support and guidance and for their willingness to serve as jury members. Finally, we thank the Swiss National Science Foundation for financial support under grants 200020-103932 and 200020-119835/1.

Prof. Dr. Anton Schleiss Dr. Koen Blanckaert

Há duas coisas que a experiência deve ensinar: a primeira é que se torna indispensável corrigir muito; a segunda é que não se deve corrigir de mais

Delacroix

Dedico todo o meu esforço e ciência à mulher dos meus sonhos, Patrícia.

Acknowledgements

A three year Ph.D. project is a challenge. However, I've had a lot of support. My acknowledgements go to:

- Prof. Schleiss, for receiving me in his group, LCH, and providing the best conditions a Ph.D. student could possibly imagine. I am exceptionally grateful for the involvement of Dr. Koen Blanckaert in this project.

- The wonderful international team of LCH that without knowing, taught me more than they imagine.

- My friends in Lausanne: Bruno, Intan, Marcelo, Montse, Rafael, Juliano, Pedro, Janina, Luis, Paulo, Sabrina, Carlos, Luiz, Sameh, Ismael, Azin, Javier, Martin, Michael, Matteo, Fadi, Mario, Rui, Catia ...

- My parents, brother and sister, for all support and love.

- My beautiful wife, Patricia, for her unconditional support and love throughout these years. She kept her word and I did what I've promised to do.

ABSTRACT

This research focuses on the influence of bank inclination and roughness on near-bank flow patterns which is relevant for bank protection, bank erosion and design of stable river configuration. Foregoing studies have been carried out mostly in rectangular channels which are far from being representative of natural conditions.

In straight-channel flows large scale vortical structures, such as secondary currents or circulation cells of Prandtl's second kind, play a fundamental role. In curved flows mainly two circulation cells are generated, the center-region cell and the outer-bank cell. The outer-bank cell has a fundamental role in protecting the outer-bank by constraining the center-region cell and thereby decreasing the downstream velocity and turbulence. It is still not clear how the secondary circulation cells interact with varying channel shape and wetted perimeter roughness distribution in straight as in curved flows.

This work is a part of a joint research program. The project other three partners are: Delft University of Technology (TUD), WL | Delft Hydraulics (WL) and the Leibniz Institute of Freshwater Ecology and Inland Fisheries (IGB). The main goal is to improve the understanding of flow underlying mechanisms and to improve existing hydrodynamic and morphodynamic tools.

Despite the broader program where this research project is inserted, it is also self-contained. This research project is situated in the discipline of fluid dynamics applied to open-channel flows in the topic of dynamics of the mean-flow field and the turbulence in straight and curved channels. The two main goals are: i) To investigate, systematically in laboratory controlled conditions the influence of the outer-bank inclination and roughness on the patterns of main flow, secondary flow, turbulence and outer-bank shear stress in straight and curved flows; ii) To give insight in the flow mechanisms responsible for the observed patterns. The channel width of B = 1.3 m, water depth of H = 0.16 m and a bulk velocity of U = 0.43 m/s were kept constant. The bank inclination was varied between 90°, 45° and 30° whereas the bank roughness was varied between smooth PVC, sand (d = 0.002 m) and d = 0.03 m materials (simulating riprap). The measurements were performed using the Acoustic Doppler Velocimetry Profiler (ADVP). The ADVP is fundamental for the accomplishment of these goals due to its accuracy and profiler capabilities.

Straight channel results reveal that rectangular and trapezoidal channels have different flow patterns. The trapezoidal channels have less circulation cells than rectangular channels and a bed shear stress distribution with fewer oscillations. In trapezoidal channels the bed shear stress is higher than the cross-section averaged shear stress regardless the bank/bed roughness ratio. The bank shear stress value increases with outer-bank roughness. The experimental measurements were compared with methods for estimating mean and maximum bed and bank shear stresses, Chow (1959) and Knight et al. (1994). Chow (1959) wetted perimeter shear stress distribution is in agreement with trapezoidal channel experiments with homogeneous roughness distribution whereas for heterogeneous roughness distribution no agreement is verified. Knight (1994) estimations

are in good agreement with measurements suggesting its applicability as engineering expedite process.

In the curved flow experiments focus is given to the outer-bank roughness and inclination effect on the outer-bank flow region mainly on the outer-bank cell. Curved channel flow results reveal that the outer-bank roughness and inclination has a strong effect on the outer-bank cell, and as consequence, on the center-region cell and downstream velocity evolution along the bend. In all experiments the outer-bank cell constrains the outward limit of the center-region cell regardless its size or strength. In curved flows with rectangular channel, the outer-bank cell size increases with increasing outer-bank roughness and so further protect the bed close to the outer-bank. In curved flows with trapezoidal channel, the outer-bank cell is located over the outer-bank toe close to the free-surface even for low-bank inclination, however, the outer-bank basal zone is more exposed to higher shear stresses. In curved flows with trapezoidal channel, low outer-bank angle and varying bank roughness, the outer-bank cell does not increase with increasing outer-bank roughness.

The mechanisms underlying the outer-bank cell are disclosed by analyzing the downstream vorticity equation main terms. The centrifugal term and the cross-stream shear term favor the outer-bank cell rotation sense whereas cross-stream turbulent anisotropy term does not, for all experiments.

Keywords: open-channel flow, straight-channel flow, shear stress, curved flows, outer-bank cell, bank inclination, bank roughness, Acoustic Doppler Velocity Profiler (ADVP)

RÉSUMÉ

Cette recherche se concentre sur l'influence de l'inclination et de la rugosité de la berge sur l'écoulement proche de la rive. Les précédentes recherches sur le sujet ont principalement investigué les canaux de section rectangulaire, ce qui est loin d'être représentatif des conditions naturelles.

En écoulement droit, les structures de grande échelle comme les cellules de circulation ou les courants secondaires de Prandtl du deuxième ordre jouent un rôle fondamental dans l'écoulement. En écoulement courbe, deux cellules de circulation sont générées : la cellule-de-centre et la cellule-de-rive. La cellule-de-rive présente un rôle fondamental dans la protection de la rive extérieure de la cellule-de-centre en limitant la vitesse longitudinale et la turbulence. La compréhension de l'interaction des cellules de circulation avec la variation de géométrie du canal et avec la rugosité du périmètre mouillé n'est pas claire.

Ce travail de recherche fait partie d'une étude internationale. Les trois autres partenaires sont : Delft University of Technology (TUD), WL | Delft Hydraulics (WL) et le Leibniz Institute of Freshwater Ecology et Inland Fisheries (IGB). Les buts principaux sont d'améliorer la compréhension des mécanismes et des processus physiques existants et ainsi de développer les outils hydrodynamiques et morphodynamiques existants.

Malgré sa liaison avec d'autres projets ce travail est indépendant. Ce travail se situe dans la discipline de dynamique des fluides appliquée dans les écoulements à ciel ouvert, droit et en courbe, dans les domaines de champ moyen et turbulent. Les deux buts principaux sont : i) Investiguer expérimentalement en laboratoire d'une façon systématique l'influence de l'inclinaison de la rive et de la rugosité sur l'écoulement principal, l'écoulement secondaire, la turbulence, et le cisaillement à la rive extérieure pour des écoulements droits et courbes. ii) Comprendre les mécanismes et les processus physiques des phénomènes observés. La largeur du canal, $B = 1.3$ m, la hauteur d'eau, $H = 0.16$m et la vitesse longitudinale moyenne, $U = 0.43$ m/s, sont maintenus constantes. L'inclinaison de la rive extérieure varie entre 90°, 45° et 30° lorsque la rugosité de la rive oscille entre PVC lisse, sable (d = 0.002 m) et enrochement (d = 0.03 m). Les mesures sont faites en utilisant la technique Profiler Vélocimétrie Acoustique à effet Doppler (PVAD). Le PVDA est fondamental pour répondre aux objectifs, grâce à sa précision et sa capacité de Profileur.

Les résultats mesurés dans l'écoulement droit montrent que les géométries rectangulaires et trapézoïdales génèrent différents types d'écoulements. L'écoulement dans la section trapézoïdale génère moins de cellules de circulation et une distribution de cisaillement au fond moins oscillante. Pour la section trapézoïdale, le cisaillement au fond est plus grand que la valeur de référence malgré le ratio entre la rugosité de la rive et du lit. Le cisaillement sur rive augmente avec la rugosité de la rive. Les résultats expérimentaux ont été comparés avec les méthodes pour estimer le cisaillement moyen et maximal au fond et sur rive, Chow (1959) et Knight et al. (1994). L'estimation de Chow (1959) est en accord avec les mesures lorsque la rugosité du canal et homogène mais pas lorsque la

rugosité du canal est hétérogène. La méthode de Knight (1994) correspond aux mesures pour touts les cas étudiés et donc considéré valable.

Dans l'écoulement courbe, une attention particulière est donnée à l'influence de la rugosité et de l'inclinaison de la rive dans l'écoulement proche de la rive notamment dans la cellule-de-rive. Les résultats de l'écoulement courbe montrent que l'inclinaison et la rugosité de la rive ont un effet important dans la cellule-de-rive et par conséquent, dans la cellule-de-centre et l'écoulement principal. Dans toutes les expériences, la cellule-de-rive limite la cellule-de-centre indifférentement de sa taille. Dans l'écoulement courbe d'un canal rectangulaire, la taille de la cellule-de-rive augmente avec la rugosité de la rive. Par contre, la taille de la cellule-de-centre diminue avec la rugosité de la berge et donc augmente la protection de la rive. Dans l'écoulement courbe avec différentes géométries de canal (rectangulaire et trapézoïdal avec différents angles d'inclinaison de la rive), la cellule-de-rive se déplace vers l'intérieur du canal en fonction de la position de l'intersection de la rive avec le lit. Dans l'écoulement courbe en canal trapézoïdal, l'augmentation de la rugosité de la rive n'a presque aucun effet sur la taille de la cellule-de-rive et par conséquent, la cellule-de-centre n'est pas affectée non plus.

Les mécanismes responsables de la cellule-de-rive sont analysés avec l'étude des termes principaux de l'équation longitudinale de la vorticité. Les termes de la force centrifuge et de cisaillement de l'écoulement transversal favorisent la cellule de rive mais le terme de l'anisotropie ne favorise pas.

Mots clés : écoulement à ciel ouvert, écoulement droit, cisaillement, écoulement en courbe, cellule-de-rive, inclination de la rive, rugosité de la rive, Profiler Vélocimétrie Acoustique à effet Doppler (PVAD).

RESUMO

Esta investigação centra-se no escoamento de superfície livre perto da margem porque é relevante para o estudo de medidas de protecção contra a erosão e o desenho de configurações fluviais. A grande maioria das investigações precedentes foi feita em canais rectangulares que estão longe de representar condições naturais.

Num escoamento rectilíneo, existem estruturas de grande escala como as células de circulação ou correntes secundárias de Prandtl de segunda ordem que têm um papel relevante no escoamento principal. Num escoamento em curva, duas células de circulação são geradas: a célula helicoidal e a célula de margem exterior. A forma e intensidade e mesmo a existência das células são factos desconhecidas em geometrias (mais) naturais.

Como objectivo de avançar nos domínios experimental e numérico, diferentes grupos de investigação trabalham em conjunto. Este trabalho de investigação faz parte desse grupo. Os três outros participantes são: Delft University of Technology (TUD), WL | Delft Hydraulics (WL) e o Leibniz Institute of Freshwater Ecology e Inland Fisheries (IGB). Os objectivos principais são de aumentar o conhecimento existente neste tipo de escoamentos e assim ajudar a melhorar as ferramentas numéricas hidrodinâmicas e morfodinâmicas existentes.

Apesar da ligação estreita com os outros projectos, este trabalho continua a ser independente. Esta investigação situa-se na disciplina de mecânica de fluidos aplicada aos escoamentos de superfície livre rectilíneos e em curva nos campos médio e turbulento. Os dois objectivos principais são: i) Investigação em laboratório de uma forma sistemática a influência da inclinação da margem e da rugosidade no escoamento principal e secundário, turbulência, e tensões de corte ao longo do perímetro molhado em escoamentos rectilíneos e em curva; ii) Compreender os mecanismos e os processos físicos observados. A largura do canal, B = 1.3 m, a altura de água, H = 0.16 m, e a velocidade longitudinal média, U = 0.43 m/s foram mantidas constantes. A inclinação da margem foi variada entre 90°, 45° e 30° enquanto a rugosidade da margem foi variada entre PVC liso, areia (d = 0.002 m) e d = 0.03m (em simulação de enrocamento). As medições foram feitas com o instrumento *Acoustic Doppler Velocity Profiler* (ADVP). ADVP é fundamental para se atingir os objectivos deste trabalho, devido à sua precisão e capacidade de medir ao longo da coluna de água em diferentes pontos (*profiler*).

As medições mostram que os canais rectangulares e trapezoidais geram diferentes tipos de escoamento. O escoamento no canal trapezoidal gera menos células de circulação do que no canal rectangular e uma distribuição de tensão de corte ao longo do fundo menos oscilante. A tensão de corte no fundo é maior que o valor de referência independentemente do rácio entre as rugosidades da margem e do fundo para os canais trapezoidais. A tensão de corte na margem aumenta com a rugosidade. As medições experimentais são comparadas com métodos que estimam as tensões de corte média e máxima no fundo e na margem, Chow (1959) e Knight et al. (1994). A estimativa obtida com o método Chow (1959) está de acordo com as medições enquanto a rugosidade do canal é homogénea, mas quando a rugosidade do canal é heterogénea, as medições e as

estimativas deixam de estar em concordância. O método de Knight (1994) está em concordância com as medições para todos casos, e assim, é considerado como um método expedito passível de ser usado por engenheiros.

No escoamento em curva, atenção é dada à influência da rugosidade e da inclinação no escoamento próximo da margem, principalmente sobre a célula de margem. Os resultados obtidos no escoamento em curva mostram que a inclinação e a rugosidade da margem tem um efeito importante na célula de margem, que por sua vez, na célula helicoidal e finalmente no escoamento principal. Em todas as experiências a célula de margem limita a célula helicoidal, independentemente do seu tamanho. Num escoamento em curva, num canal rectangular, o tamanho da célula de margem aumenta com a rugosidade da margem. Num escoamento em curva com diferentes geometrias (rectangular e trapezoidal com duas diferentes inclinações da margem exterior) a célula de margem se move em direcção ao interior do canal em correlação com o ponto de intersecção da margem com o fundo, *bank toe*. Num escoamento em curva, num canal trapezoidal, o aumento da rugosidade da margem tem um efeito insignificante no tamanho da célula de margem e como consequência na célula helicoidal.

Os mecanismos responsáveis da célula de margem são analisados com o estudo dos termos principais na equação longitudinal da vorticidade. Os termos correspondentes à forca centrífuga e tensão de corte do escoamento secundário favorecem a célula da margem enquanto o termo anisotrópico não.

Palavras-chave: escoamento à superfície livre, escoamento rectilíneo, tensões de corte, escoamento em curva, célula de margem, inclinação da margem, rugosidade da margem, *Acoustic Doppler Velocity Profiler* (ADVP).

TABLE OF CONTENTS

INTRODUCTION 1
1 Background of research topic 2
2 Research groups 4
3 Objectives and work relevance 6
4 Structure of the report 7
5 State-of-the-art in experiments of curved flows with emphasis on near-bank flow patterns and circulation cells 8
6 Experimental set-up and instrumentation 11

INFLUENCE OF BANK INCLINATION AND ROUGHNESS ON HYDRODYNAMICS IN STRAIGHT OPEN-CHANNEL FLOW 17
ABSTRACT 18
1 Introduction 19
2 Experimental set-up and instrumentation 24
3 Theoretical background 26
4 Results 31
4.1 Rectangular channel experiments 31
4.2 Half-trapezoidal channel experiments 34
5 Discussion 40
6 Conclusions 42
REFERENCES 43

INFLUENCE OF OUTER-BANK ROUGHNESS ON HYDRODYNAMICS IN RECTANGULAR OPEN-CHANNEL BENDS....47
ABSTRACT....48
2 Experiments....51
3 Experimental results....53
3.1 Depth-averaged flow field....53
3.2 Patterns of cross-stream velocities in the cross-section at 90°....56
3.3 Patterns of downstream vorticity in the cross-section at 90°....58
3.4. Patterns of normalized downstream velocity, normalized boundary shear stress, normalized depth-averaged downstream velocity and Chezy factor in the cross-section at 90°....60
3.5 Patterns of normalized turbulent kinetic energy in the cross-section at 90°.64
3.6 Patterns of normalized normal stress difference in the cross-section at 90°.65
4 Mechanisms underlying circulation cells....67
4.1 Patterns of normalized centrifugal term in the cross-section at 90°....68
4.2 Patterns of normalized cross-stream anisotropy terms in the cross-section at 90°....69
4.3 Patterns of normalized cross-stream shear stress terms in the cross-section at 90°....70
4.4 Patterns of normalized cross-stream kinetic energy fluxes in the cross-section at 90°....71
4.5 Discussion....73
5 Conclusions....74
REFERENCES....75

INFLUENCE OF OUTER-BANK INCLINATION ON HYDRODYNAMICS IN OPEN-CHANNEL BENDS....77
ABSTRACT....78
2 Experiments....81
3 Experimental results....83
3.1 Depth-averaged flow field....83
3.2 Patterns of cross-stream velocities in the cross-section at 90°....86
3.3 Patterns of downstream vorticity in the cross-section at 90°....89
3.4. Patterns of normalized downstream velocity, boundary shear stress, normalized depth- averaged downstream velocity and Chezy factor in the cross-section at 90°....90
3.5 Patterns of turbulent kinetic energy in the cross-section at 90°....94
3.6 Patterns of normalized normal stress difference in the cross-section at 90°....95
4 Mechanisms underlying circulation cells....98
4.1 Patterns of normalized centrifugal term in the cross-section at 90°....99
4.2 Patterns of normalized cross-stream anisotropy terms in the cross-section at 90°....100
4.3 Patterns of normalized cross-stream shear stress terms in the cross-section at 90°....101
4.4 Patterns of normalized cross-stream kinetic energy fluxes in the cross-section at 90°....102
4.5 Explanation of underlying mechanisms....104
5 Conclusions....106
REFERENCES....108

INFLUENCE OF OUTER-BANK ROUGHNESS ON HYDRODYNAMICS IN TRAPEZOIDAL OPEN-CHANNEL BENDS WITH 30°-INCLINED OUTER-BANKS 111
ABSTRACT 112
1 Introduction 113
2 Experiments 115
3 Experimental results 117
3.1 Depth-averaged flow field 117
3.2 Patterns of cross-stream velocities in the cross-section at 90° 120
3.3 Patterns of downstream vorticity in the cross-section at 90° 123
3.4. Patterns of downstream velocity, boundary shear stress, normalized depth-averaged downstream velocity and Chezy factor in the cross-section at 90° ... 124
3.5 Patterns of normalized turbulent kinetic energy in the cross-section at 90° 128
3.6 Patterns of normalized normal stress difference in the cross-section at 90° 129
4 Mechanisms underlying circulation cells 132
4.1 Patterns of normalized centrifugal term in the cross-section at 90° 133
4.2 Patterns of normalized cross-stream anisotropy terms in the cross-section at 90° 134
4.3 Patterns of normalized cross-stream shear stress terms in the cross-section at 90° 136
4.4 Patterns of normalized cross-stream kinetic energy fluxes in the cross-section at 90° 137
5 Discussion 138
5.1 Explanation of underlying mechanisms 138
5.2 Comparison with Chapter III and Jin, Y-C et al (1990) 139
6 Conclusions 140
REFERENCES 141

CONCLUSIONS 145
1 Introduction and objectives 146
2 Conclusions 147
2.1 Straight-channel flow 147
2.2 Curved flow 148
3 Future work 150
3.1 CRC OBC separation locus 150
3.2 OBC strength 151

APPENDIX 153

LIST OF SYMBOLS

Alphabetic symbols

B	flume width
B/H	aspect ratio
$C = g^{1/2}(U/u_*)$	Chézy friction coefficient
$C2$	roughness parameter
d	roughness elements diameter
E_s	energy slope
f_n	normalized profile of v_n^*
$Fr = U/(gH)^{1/2}$	Froude number
$\left\langle \tilde{f}_n^{\,2} \right\rangle$	normalized strength of the cross-stream circulation
g	gravity acceleration
H	average flow depth
H/R	curvature ratio
k	turbulent kinetic energy
k_{sw}	roughness diameter of the bank material
k_{sb}	roughness diameter of the bed material
k_s	roughness diameter of the outer-bank material
n-axis	horizontal cross-stream direction of the flow
P	energy fluxes sum

P_b	bottom perimeter
P_w	wall or bank wetted perimeter
Q	flow discharge
R	bend radius
$Re = UH/\upsilon$	Reynolds number
R_h	hydraulics radius
s-axis	downstream direction of the flow
S_{circ}	sign of the cross-stream circulation cells used to label the rotation sense.
U	bulk velocity
U_s	downstream depth-averaged velocity
U_n	transverse depth-averaged velocity
$U^+ = v_s/u_*$	normalized downstream velocity
u_*	averaged shear velocity
u_*'	shear velocity value at z
v_s	downstream velocity
v_s'	fluctuating downstream velocity
v_n	transverse velocity
v_n'	fluctuating transverse velocity
v_n^*	circulation part of the transverse velocity
v_z	vertical velocity

$v_z^{'}$	fluctuating vertical velocity
z *–axis*	vertical cross-stream direction of the flow
z_0	the distance at which the log velocity profile indicates zero velocity
$Z^+ = z/k_s$	normalized vertical coordinate
$\%SF_w$	percentage of shear stress carried by the walls

Greek symbols

α	Knight's method parameter
α_s	transverse distribution of the downstream velocity
β	bend parameter
ε	turbulence dissipation ratio
Θ_{bank}	bank angle with horizontal bottom
κ	von Kármán's constant
$\overline{v_i v_j}$	Reynolds stresses
ρ	water density
$\overline{\tau_b}$	mean bottom shear stress
$\tau_{b\max}$	maximum bottom shear stress
$\overline{\tau_w}$	mean bank shear stress

$\tau_{w\max}$	maximum bank shear stress
τ_0	average shear stress
ν	kinematic viscosity
υ_t	kinematic eddy viscosity
ψ	streamfunction
ω	vorticity field (s,n,z)

LIST OF ACRONYMS

ADVP	Acoustic Doppler Velocity Profiler
CRC	centre region cell
CSS	cross-shear stress term (term of downstream vorticity equation)
CSTA	cross-shear anisotropy turbulence term (term of downstream vorticity equation)
CT	centrifugal term (term of downstream vorticity equation)
F16_90_00	experiment with 16 cm of water-depth, discharge of 90 l/s and outer-bank made of PVC
F16_90_02	experiment with 16 cm of water-depth, discharge of 90 l/s and outer-bank made of sand roughness of 2 mm
F16_90_30	experiment with 16 cm of water-depth, discharge of 90 l/s and outer-bank made of riprap roughness of 3 cm
F16_85_00	experiment with 16 cm of water-depth, discharge of 85 l/s and outer-bank made of PVC
F16_85_02	experiment with 16 cm of water-depth, discharge of 85 l/s and outer-bank made of sand roughness of 2 mm
F16_85_30	experiment with 16 cm of water-depth, discharge of 85 l/s and outer-bank made of riprap roughness of 3 cm
F16_80_00	experiment with 16 cm of water-depth, discharge of 80 l/s and outer-bank made of PVC
F16_80_02	experiment with 16 cm of water-depth, discharge of 80 l/s and outer-bank made of sand roughness of 2 mm
F16_80_30	experiment with 16 cm of water-depth, discharge of 80 l/s and outer-bank made of riprap roughness of 3 cm
$k-\varepsilon$	turbulence model
LOBC	lower outer-bank cell
OBC	outer-bank cell

tke	turbulence kinetic energy

CHAPTER I

INTRODUCTION

1 Background of research topic

In June 2008 the Mississippi river flooded once more vast areas. Unfortunately this is an example of periodic and worldwide occurrences. The lack of freedom in their alluvial plane is the main cause for these common and prejudicial occurrences. It is urgent to improve flood defense systems and to rehabilitate wherever possible the past works of rivers canalization. Figure 1 shows the magnitude of the problem that the hydraulic engineering community in this kind of disasters has to face. These images show the confluence of the Mississippi, Illinois, and Missouri Rivers just upstream of St. Louis. The left image shows the rivers in normal summer conditions (August 1991), while the right image shows the rivers at the end of the great floods of 1993 (August 1993). The consequences of worldwide flooding justify *per si* why every researcher in River Hydraulics has to be motivated, because, our work does make a difference at a regional scale.

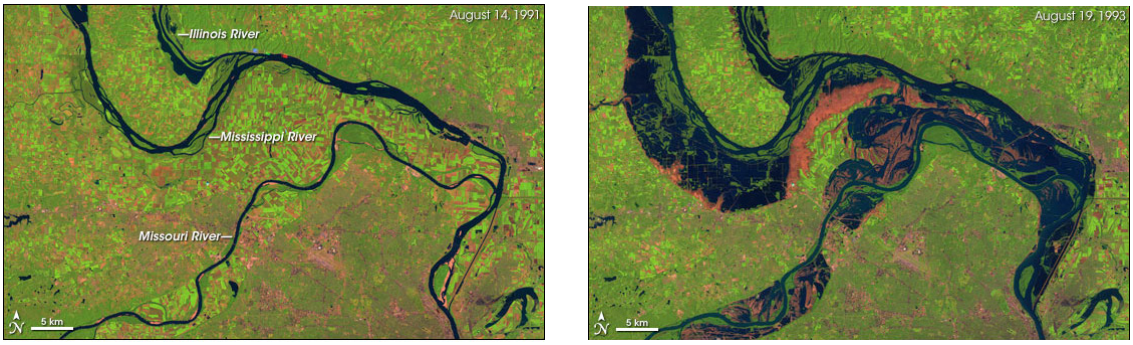

Figure 1
Confluence of the Mississippi, Illinois, and Missouri Rivers before (left) after (right) great floods of 1993 (Image by Jesse Allen, based on data provided by the Landsat Science Team)

Revitalization works are recently gaining importance. The so-called "3d correction of the Rhone river" is an example of an important river training and rehabilitation project in Switzerland: it is a 30-years project with an estimated cost of about 1 billion SF. So, security and revitalization are important trends in fluvial hydraulics in order to improve life standards and mainly to protect human life.

One of the important subjects within open-channel flows is the protection of banks against erosion. Bank failure may lead to correspondent inundations which unfortunately too often occur worldwide. So accurate and user friendly calculation processes are of paramount importance. Despite the progress hydraulic engineering are still far from being able to calculate and design safely any hydraulic structure in whatever situation. The computational fluid dynamics is the tool that will help substantially hydraulic engineering in the near-future but its development depends also on quality experimental data.

This research project is part of a research program built to tackle that need. A joint research program is carried out by École Polytechnique Fédérale de Lausanne (EPFL), Delft University of Technology (TUD), WL | Delft Hydraulics (WL) and the Leibniz Institute of Freshwater Ecology and Inland Fisheries (IGB) exploiting synergies between laboratory experiments at EPFL, field experiments at IGB and numerical research at Delft. Synergy between experimental and numerical activities is

fundamental and it is the backbone of this cluster program. Inserted in the cluster the main goals of this research project are to observe, to improve the understanding of the flow interaction with outer-bank characteristics and to provide data and guidelines to modelers. Moreover, the experimental data are already being used on validation of numerical codes for subsequent application in research and engineering.

2 Research groups

The joint research program is made up by four programs self-contained but complementary projects. The other three works are briefly present hereafter:

1) IGB Berlin: "An Environmental Fluid Dynamics Laboratory in the Field: studies and numerical modeling of hydro-, morpho-dynamics and invertebrates ecology in river meanders*"*. It focuses on measurements in natural river meanders. This project will be able to provide detailed field data on morphology, mean flow, secondary flow, turbulence, sediment transport, ecology etc... This data will enhance our insight into the relevant fluvial processes occurring in natural river meanders, including interactions between hydro-, morphodynamical and ecological processes. Comparison to idealized laboratory channels studies will allow evaluating the effect of scales related to flow shallowness and Reynolds number, and evaluating the relevance of results obtained under laboratory conditions. Acquired data will be used for model validation.

2) Delft University of Technology (TUD): "*LES-simulation of flow and turbulence in curved open-channel flows, with emphasis on transport and bank erosion processes*" It consists of the further development of an existing 3D LES code by accommodating it for irregular geometries and non-uniform flows, validating by means of the available experimental data and applying it to a broader parameter range. The main goal of this program is to study the near-bank shear stress distribution as function of near-bank patterns of circulation cells and turbulence. It will provide an improved parameterization of the bank shear stress and bank erosion processes for the development of quasi-3D morphodynamic code.

3) WL|Delft + TU Delft Hydraulics (WL): "*Development of a quasi-3D morphodynamic code and its application to meander dynamics at high curvature."* It consists of enhancing an existing *quasi*-3D morphodynamic code by implementing the non-linear closure submodel for circulation cells developed by Blanckaert & de Vriend (2003) and by using improved parameterization of the bank shear stress and bank erosion processes from the LES project. The main goal is to apply the model in meander dynamics at high curvature and river management.

Figure 2 schematizes the joint research program and its time table. Figure 2 also shows the main interactions between projects. Basically, 3D LES simulations use laboratory and field measurements for validation whereas quasi-3D morphodynamic simulations use LES information and field measurements for validation. Moreover the usefulness of the present research project data set is going to be evaluated by the to-be-obtained field measurements. It is going to be verified whether the scale effects, which laboratory imposes, is biasing the results.

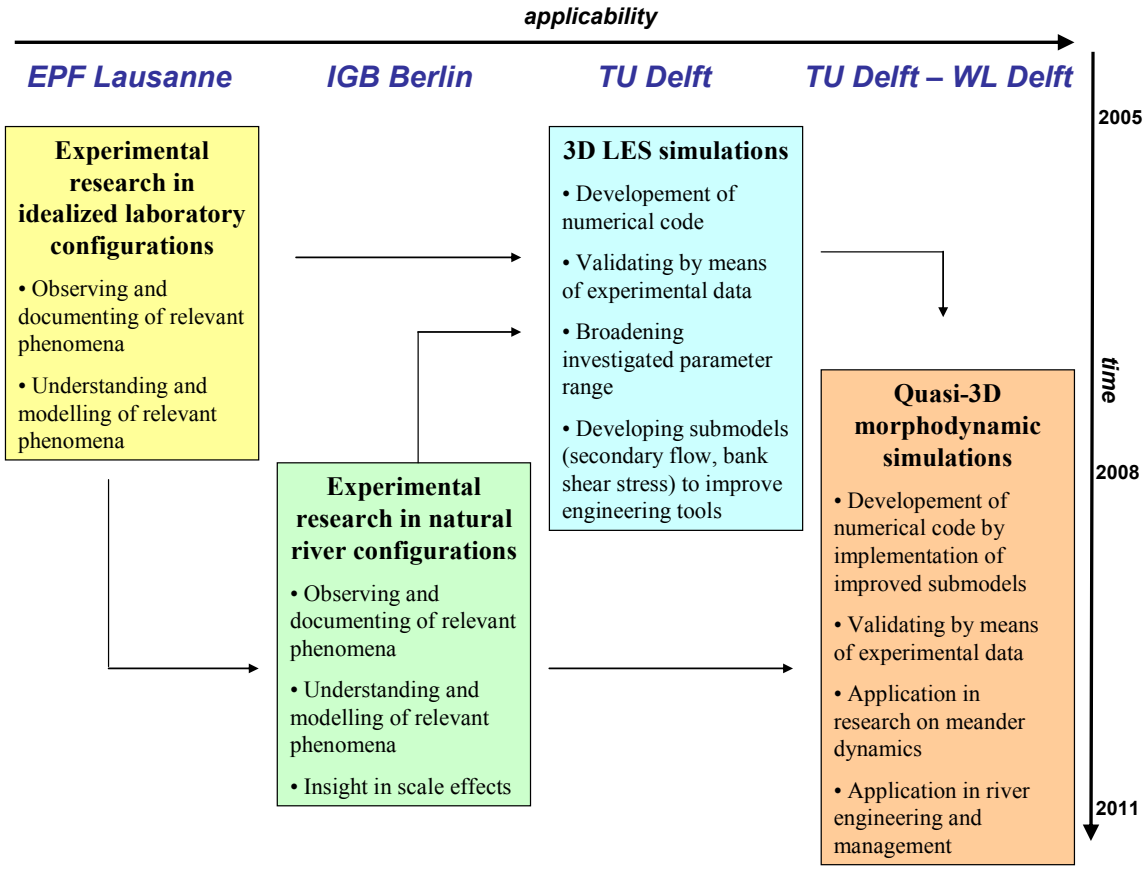

Figure 2
Joint-program applicability and time table

3 Objectives and work relevance

The present research project comes in the sequence of the study of Blanckaert (2002). He mainly found out that the outer-bank cell and reduced turbulence activity are fundamental processes in protecting the outer-bank against erosion. However, the foregoing research was limited to bend configurations with vertical and smooth outer-banks.

This research extends the available data set by investigating systematically the influence of the outer bank inclination and roughness on the patterns of main flow, secondary flow, turbulence and outer-bank shear stress in a straight and sharply curved open-channel laboratory bend. Nine experiments were carried out covering three different outer-bank inclinations and roughness values for straight and sharp curved flows.

The measurements were performed in a laboratory set-up designed not to be a prototype of any natural configuration but to enable the study of bank inclination and roughness on the fluid dynamics. So, some simplifications were made, such as: the bottom is horizontal, the inner bank is vertical, no sediment transport, a single bed, etc… in order to better isolate and thereby understand the bank inclination and roughness effect on the flow.

Hence, the main goals are:

1) To measure in a systematic way straight and curved open-channel flows with varying bank inclination and roughness, including all three mean velocity components and all six Reynolds stresses on a fine grid

2) To gain insight in the relevant physical mechanisms responsible for the patterns observed

3) To provide an extensive data set and guide lines for numerical modeling

4 Structure of the report

This report is divided into 6 Chapters. This Introduction will be followed by CHAPTER II "INFLUENCE OF BANK INCLINATION AND ROUGHNESS ON HYDRODYNAMICS IN STRAIGHT OPEN-CHANNEL FLOW" in which the influence of outer-bank roughness and inclination on straight channel flow patterns are investigated with special emphasis on the bank flow zone and on the bank shear stress. In Chapter II, the downstream velocity distribution, the wetted perimeter shear stress, the pattern of secondary circulation cells and the turbulent kinetic energy are shown.

CHAPTER II is followed by the core of this dissertation, CHAPTER III, CHAPTER IV and CHAPTER V, where the influence of bank inclination and roughness on curved flows patterns are investigated. In these Chapters the patterns of downstream and cross-stream flow velocities, the turbulent kinetic energy, the normal stresses anisotropy, the downstream vorticity are shown. Moreover the investigation of the circulation cells' underlying mechanisms by means of term-by-term analysis of the downstream vorticity equation and the kinetic energy transfer between mean flow and turbulence was performed.

CHAPTER III "INFLUENCE OF OUTER-BANK ROUGHNESS ON HYDRODYNAMICS IN RECTANGULAR OPEN-CHANNEL BENDS" presents experimental data and fundamental research of outer-bank roughness effect on flow patterns in rectangular open-channel bends with special focus in the near outer-bank zone.

CHAPTER IV "INFLUENCE OF OUTER-BANK INCLINATION ON HYDRODYNAMICS IN OPEN-CHANNEL BENDS" presents experimental data and fundamental research of outer-bank inclination effect on flow patterns in open-channel bends with special focus in the near outer-bank zone.

CHAPTER V "INFLUENCE OF OUTER-BANK ROUGHNESS ON HYDRODYNAMICS IN TRAPEZOIDAL OPEN-CHANNEL BENDS WITH 30°-INCLINED OUTER-BANK" presents experimental data and fundamental research of outer-bank roughness effect on flow patterns in trapezoidal open-channel bends with 30°-inclined outer-bank with special focus in the near outer-bank zone.

CHAPTER VI "CONCLUSIONS" presents the summary of the findings.

Note: This dissertation is a compilation of papers that are being prepared for submission. By making each one of them self-contained, repetition of some parts (such as the presentation of the experimental setup) was necessary.

5 State-of-the-art in experiments of curved flows with emphasis on near-bank flow patterns and circulation cells

Bankline stabilization is an important issue in river management. In order to control bankline geometries it is fundamental to understand bank erosion in open-channel flows. Thorne (1985) has recognized two dominant processes of bank erosion: basal erosion and geotechnical bank failure. Basal erosion steepens the bank and intermittently causes mass bank failure. It was noticed in Blanckaert & Graf (2001) that the outer-bank shear stress is smaller than the bottom shear stress in curved flows.

The current knowledge of curved open-channel flows is still incomplete, especially concerning near bank flow field and bank erosion as function of bank geometry. Blanckaert's PhD research at EPFL indicated two mechanisms that may protect outer banks from erosion: a cell of reverse secondary circulation adjacent to the outer bank, called outer-bank cell; a reduced turbulence activity near the outer bank.

Due to the importance of the cross-stream circulation cells and turbulence in such type of flow, a resume of its physical processes is presented hereafter based on detailed analysis of the cross-stream circulation cells and turbulence reported by Blanckaert & Graf (2001), Blanckaert (2002), Blanckaert & de Vriend (2003), Blanckaert & de Vriend (2004), and Blanckaert & de Vriend (2005).

The center-region cell redistributes the velocity and the boundary shear stress and shapes the bed topography. The center-region cell is formed by the imbalance of the vertical gradient of the centrifugal force, $\left(\frac{\partial}{\partial z}\right)\left(\frac{v_s^2}{R}\right)$ and the inward pressure gradient caused by the super-elevation of water against the outer-bank. An important feedback exists between the strength of the center-region cell and the vertical profile of v_s. The v_s-profile is flattened by the influence of the center-region cell. The resulting centrifugal force, v_s^2 / R, gets more uniform over the depth, which results in weaker center-region cell. Linear numerical models that do not account for the feedback mechanism over predict the strength of the center-region cell. Blanckaert de Vriend (2003) have proposed a model that accounts for this feedback

Outer-bank cells have since long been observed in laboratory flows (Mockmore 1943, Einstein & Harder 1954, Rozowski 1957, etc.) as well in natural flows (Bathurst et al. 1979, Dietrich & Smith 1983, de Vriend & Geldof 1983, etc.). Thorne and Hey (1979) and Thorne et al.(1985) have identified an outer-bank cell of secondary flow in some of their investigated bends, and pointed to its importance with respect to bank erosion. Thorne and Furbish (1995) have shown that the interaction between the outer bank roughness and the flow field is relevant with respect to the meander evolution.

In several experiments (Blanckaert, 2002) an outer-bank cell of secondary circulation close to the outer-bank was identified and measured besides the classical center-region cell. Both cells are important because of their effects on the flow. In the investigated configurations with vertical banks, the outer-bank cell reveals to have a protective effect on the outer-bank erosion, by keeping the high-velocity core away from the bank. The

outer-bank cell is often observed adjacent to the outer-bank and the free-surface in sharply curved turbulent open-channel flows with vertical outer bank. The outer-bank cell strengthens with bend curvature. Similar outer-bank cells are also present in curved laminar flows and in straight turbulent flows. In curved laminar flows the outer-bank cell formation is linked to the Dean number, defined as a combination of Reynolds number and curvature. In straight turbulent flows, the responsible mechanism of the outer-bank cell formation is the anisotropy of turbulence (Nezu and Nakagawa 1993) which is not possible to simulate with the standard $k-\varepsilon$ turbulence closure. In curved turbulent flows, both the centrifugal force and the cross-stream turbulent stresses contribute to the generation of the outer-bank cell.

Hersberger (2002) experimentally investigated the influence of macro-roughness elements on the outer bank on the bed topography and flow pattern and discovered that their application shifts away the core of downstream velocity from the outer-bank and hence reduces bend scour. He measured also an increase in size of the outer-bank cell with the application of macro-roughness on the outer-bank.

Figures 3 to 5 shows some essential results of above-mentioned works. Figure 3*a* shows the location of the maximum downstream velocity, which is clearly away from the water surface, whereas in straight turbulent flow it is close to the water surface. Figure 3*b* illustrates the above mentioned bi-cellular pattern of secondary circulation with the classical center-region cell and the outer-bank cell.

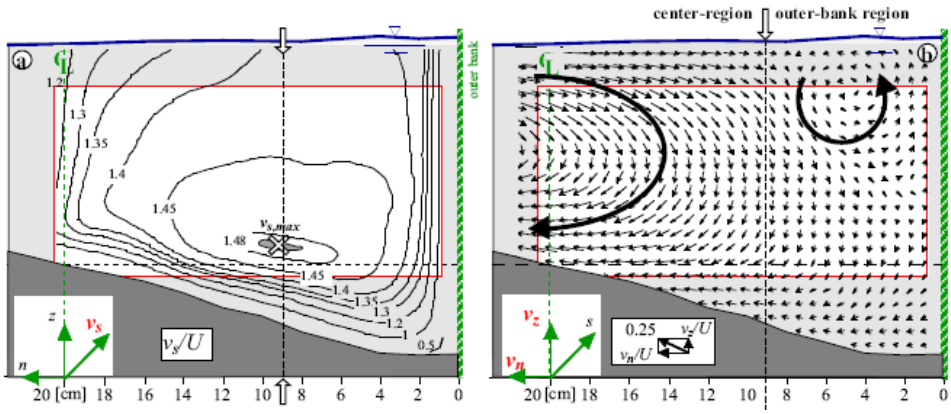

Figure 3

a) Isolines of normalized downstream velocity v_s/U, b) Vector representation of normalized cross-sectional motion $\sqrt{v_n^2+v_z^2}/U$, Blanckaert & Graf (2001)

Figure 4 shows the effect of macro-roughness elements applied at the outer-bend, wherein it is possible to see the increase in size and strength of the outer-bank cell (Hersberger, 2002).

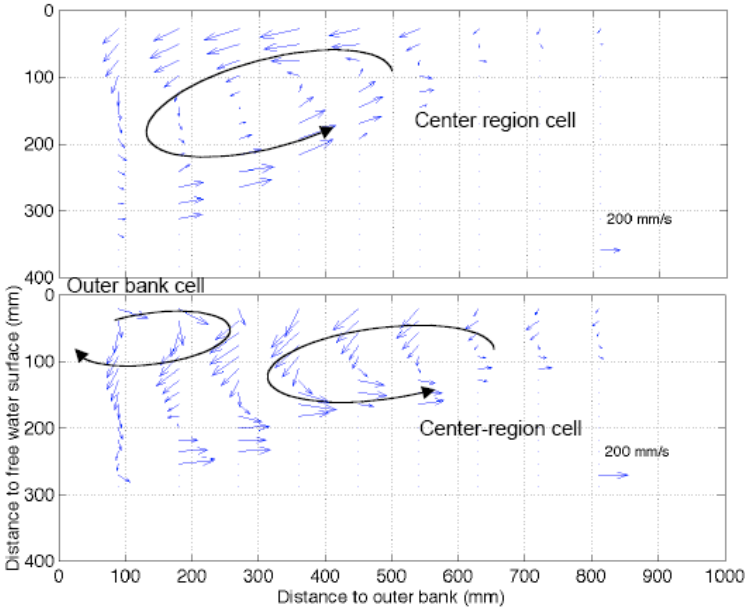

Figure 4
Measured pattern of secondary flow in an open channel bend under similar hydraulic conditions a) smooth outer-bank; b) macro-roughness elements applied the outer-bank
Hersberger (2002)

Figure 5 shows the reduced turbulent kinetic energy in the near-outer bank zone, including the core of lowest values, $k_{\min}$. This reduced turbulence activity reduces the flow's erosive capacity on the outer-bank, as observed in experiments by Blanckaert & Graf 2001 and analyzed and explained by Blanckaert & de Vriend (2005).

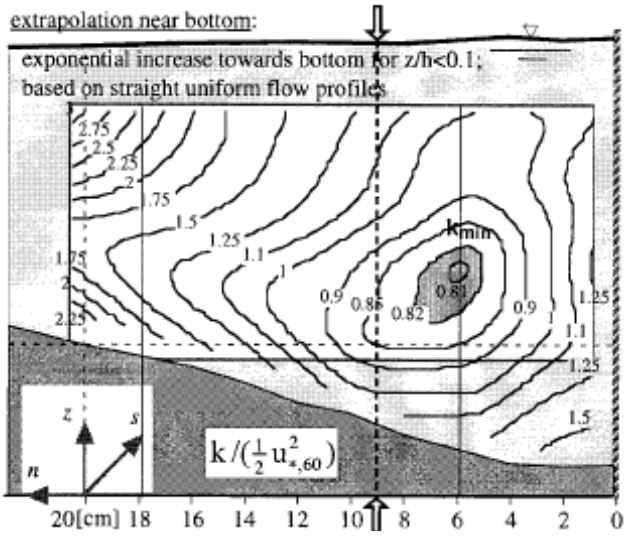

Figure 5
Turbulent kinetic energy, Blanckaert & Graf (2001)

6 Experimental set-up and instrumentation

Experiments were carried out in a laboratory open-channel. It consists of a 9 m long straight entry reach, followed by a 193° bend with constant centerline radius of curvature of R = 1.7 m and a 5 m long straight exit reach. The flume width is B = 1.3 m. The bed of the flume has glued quasi-uniform sediments of d = 0.002 m. The inner bank is made of smooth PVC. Table 1 presents the varying channel shapes and outer-bank roughness combinations used in the straight channel and bend channel flow measurements. Three rectangular and six half-trapezoidal cross-sections were measured covering three different outer-bank roughnesses and inclinations.

Table 1
Straight and curved channel experiments with varying outer-bank inclination and roughness
F16_90_00 stands for **flat** bottom with **16 cm** of water-depth, **90°** outer-bank angle with the bottom and **00** the outer-bank k_s equivalent roughness

Inclination of outer bank ⇒ / ***Roughness of outer bank*** ⇓	30°	45°	90°
Smooth PVC	F16_30_00	F16_45_00	F16_90_00
k_s = 0.002 m (sand)	F16_30_02	F16_45_02	F16_90_02
k_s = 0.03 m (riprap)	F16_30_30	F16_45_30	F16_90_30

Figure 6 shows the laboratory set-up.

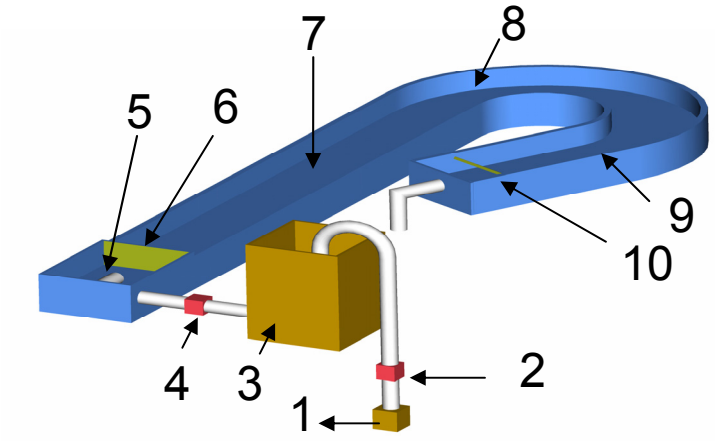

Figure 6 Laboratory Set-up
1 stands for the pump; **2** stands for valve #1; **3** stands for the intermediate tank; **4** stands for the valve #2; **5** stands for the inlet; **6** stands for the honeycomb and screens; **7** stands for the 9-m approach channel; **8** stands for the 193°-bend with a radius of 1.7 m; **9** stands for the exit channel and **10** stands for the weir.

Figure 7 shows the cross-section and the axis system. s-axis is in the downstream direction of the flow. z-axis zero is at the bed of the cross-section and increases towards

the free-surface. *n*-axis positive values are located in the outer part of the channel. In order to be uniform with foregoing and on-going projects the outer-bank is represented on the right of all Figures. All experiments have been investigated under similar hydraulic conditions with an overall mean velocity of $U \sim 0.43$ m/s and flow depth of $H \sim 0.16$ m.

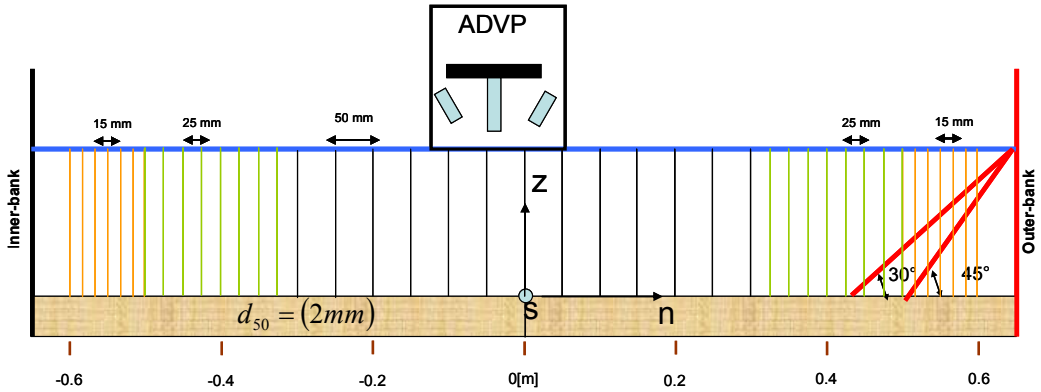

Figure 7
Cross-section measuring grids and shapes

Measurements were made on a refine grid throughout the flume in order to investigate the adaptation of flow to curvature changes. Moreover, measurements were made in straight upstream of the bend. Non-intrusive measurements were made with the Acoustic Doppler Velocity Profiler (ADVP) (Rolland 1994, Shen 1997, Hurther 2001, Blanckaert and Lemmin 2006). Figure 8 shows a schematic of the ADVP. The ADVP consists of a central emitter and four wide-angle receivers placed around the center placed in a water-filled housing that touches the water surface causing a minor flow perturbation. ADVP allows redundancy of the signal reducing the signal noise and the ability to check the velocity measurements quality. So, ADVP permits the measurement of quasi-instantaneous 3D velocity field over a column of water enabling the derivation of the mean velocity vector $\vec{v} = (v_s, v_n, v_z)$, fluctuating velocity vector, $\vec{v}' = (v_s', v_n', v_z')$ and all turbulent correlations $\overline{v_i'^a v_j'^b}$ (*i,j=s,n,z; a* and *b* are integers). The vertical profiles were divided into discrete cylindrical measuring volumes of size $(\pi \times 0.7^2 / 4) \times 0.3 = 0.12 cm^3$. The sampling frequency was 31.25 Hz and the acquisition time was 180 s. Details about the working principle of the ADVP, data treatment procedures and estimates of measuring uncertainty are summarized in Blanckaert (2009).

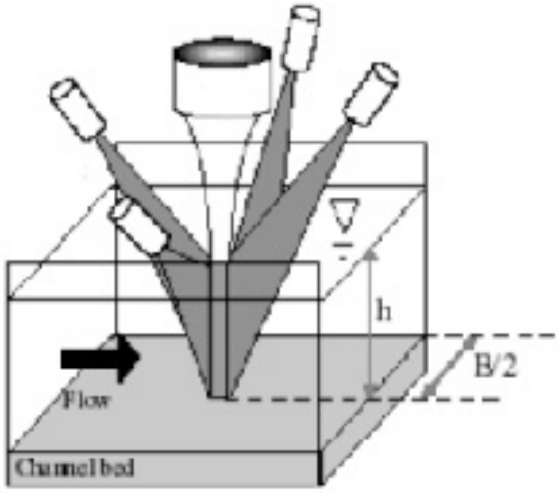

Figure 8
Multistatic configuration of the ADVP (Hurther, 2001)

Besides the ADVP, a complementary experimental technique is used to measure the cross section water depths at different angles throughout the bend. It consists of 8 acoustic limnimeters, mounted on a carriage that covers the width of the set-up, and so allowing the measurement of the water depth height differences from the inner bend to the outer bend.

Figures 9*a* shows the curved channel of the set-up. Figure 9*a* also shows the ADVP inside the box support by a movable carriage. The ADVP system (carriage, box and ADVP) is handled in a way that enables a slight contact with the water surface which is fundamental to measure the flow. Figure 9*b* shows the approach channel and the limnimeters mounted on a carriage. Figure 10 shows the inclined-outer-bank with k_s = 0.03 m elements simulating riprap protection.

a) b)

Figure 9
a) Bend b) Approach-channel

.

Figure 10
Inclined-outer-bank with k_s = 0.03 m elements simulating riprap protection

REFERENCES

Bathurst, J.C., Thorne, C.R. & Hey, R.D. (1979). "Secondary flow and shear stress at river bends." J. Hydr. Div. 105(10): 1277-1295.

Blanckaert, K., & Graf, W.H. (2001). "Mean flow and turbulence in open-channel bend." J. Hydr. Engng. 127(10):835-847.

Blanckaert, K., (2002). "Flow and turbulence in sharp open-channel bends." PhD dissertation N°. 2545, Swiss Federal Institute of Technology, Lausanne.

Blanckaert, K., & de Vriend, H.J. (2003). "Non-linear modeling of mean flow redistribution in curved open channels." Water Resources Research, AGU, 39 (12): 1375.

Blanckaert, K., & de Vriend, H.J. (2004). "Secondary flow in sharp open-channel bends." J. Fluid Mech., Cambridge Univ. Press, 498: 353-380.

Blanckaert, K. & de Vriend, H.J. (2005). "Turbulence characteristics in sharp open-channel bends." J. Fluid Mech., Cambridge Univ. Press.

Blanckaert, K. & Lemmin, U. (2006). "Means of noise reduction in acoustic turbulence measurements."J. Hydr. Research, IAHR, 44(1), 3-17.

Blanckaert, K. (2009). "Laboratory experiments on straight and sharply curved open-channel flows. Experimental techniques, data treatment and selected results." In preparation for submission.

Booij, R. (2003). "Measurements and large eddy simulation of flows in some curved flumes." J. Turbulence, 008.

de Vriend, H.J. & Geldof, H.J. (1983). "Main flow velocity in short and sharply curved river bends." Report No.83-6. Dep. Civil. Eng., Delft.

Dietrich, W.E. & Smith, J.D. (1983). "Influence of the point bar on flow through curved channels." Water Resourc. Res., 19(5):1173-1192.

Einstein, H.A. & Harder, J.A. (1954). "Velocity distributions and the distributions and the boundary layer at channel bends." Trans. AGU, 35(1): 114-120.

Hersberger, D. (2002). "Measurement of 3D flow field in a 90° bend with ultrasonic Doppler velocity." Proc.3th Int. Symp. ultrasonic Doppler Meth. for fluid Mech. and Fluid Eng., Lausanne, Switzerland, 59-66.

Hurther, D. (2001). "3-D Acoustic Doppler velocimetry and turbulence in open-channel flow." PhD dissertation N° 2395, Swiss Federal Institute of Technology, Lausanne.

Hurther, D. & Lemmin, U. (2001). “A correction method for turbulence measurements with 3-D acoustic Doppler profile measurements in open channel flow.” J. Atm. Oc. Techn., 18: 446-458.

Lemmin, U. & Rolland,T. (1997). “Acoustic velocity profiler for laboratory and field studies.” J.Hydr. Engng. 123(12):1089-1098.

Mockmore, C.A. (1943). “Flow around bends in stable channels.” Transactions ASCE 109: 593-628 (incl. discussions).

Nezu, I. & Nakagawa, H. (1993). “Turbulence in open-channel flows.” IAHR-monograph, Balkema.

Roland, T. (1994). “ Développment d’un instrumentation Doppler ultrason adaptée à l’étude hydraulique de la turbulence dans les canaux.” PhD dissertation N°.1281, Swiss Federal Institute of Technology, Lausanne.

Rozowski, I.L.(1957). “Flow of Water in Bends of Open Channels.” Ac. Sc. UKr.SSR, Isr. Progr. Sdc. Transl.

Shen, C. (1997). “An acoustic instantaneous flux profiler for turbulence flow.” PhD dissertation N°.1630, Swiss Federal Institute of Technology, Lausanne.

Thorne, C.R. & Hey, R.D. (1979). ”Direct measurements of secondary currents at a river inflexion point.” Nature, 280, 226-228.

Thorne, C.R., Zevenbergen, L. W., Pitlick, J. C., Rais, S., Bradely, J.B., & Julien, P.Y. (1985). “Direct measurement of secondary currents in a meandering sand-bed river.” Nature, 315(6022), 746-747.

Thorne, C.R., & Furbish, D.J. (1995). “Influences of coarse bank roughness on flow within a sharply curved river bend.” Geomorphology, vol.12, 241-257.

CHAPTER II

INFLUENCE OF BANK INCLINATION AND ROUGHNESS ON HYDRODYNAMICS IN STRAIGHT OPEN-CHANNEL FLOW

INFLUENCE OF BANK INCLINATION AND ROUGHNESS ON HYDRODYNAMICS IN STRAIGHT OPEN-CHANNEL FLOW

ABSTRACT

Even in straight channels bank protection is a crucial part of open-channel design. In order to protect banks against erosion several techniques, such as, riprap, covering banks with vegetation, lining etc... are used. The design of bank protection schemes requires knowledge on the bank shear stress and its dependence on bank inclination and roughness.

Hydraulic community widely uses the wetted perimeter shear stress distribution presented in Chow (1959) despite being based on channels with homogeneous wetted perimeter roughness distribution measurements. More recently the so-called *Knight's method* developed in a series of papers and summarized in Knight et al. (1994) are used to calculate mean and maximum shear stress values as function of the bed and bank wetted perimeter and roughness ratios. However, *Knight's method* for channels with non-homogeneous wetted perimeter roughness was made based on few experiments.

The cross-stream velocities are fundamental despite being only 2% of the bulk velocity. Their existence affects the downstream velocity, sediment transport and morphology. The influence of bank inclination and roughness on circulation cells and thereby on flow patterns and on the wetted perimeter shear stress distribution is not fully understood due to the complexity of the phenomena and the scarcity of experimental data. Hence, this paper investigates the influence of bank inclination (vertical, 45° and 30°) and bank roughness (smooth Plexiglas, sediments of $k_s \sim 2$ mm and $k_s \sim 30$ mm which models a bank protection by means of riprap) on straight open-channel flow. The flow experiments were performed in channels with an aspect ratio of $B/H = 8$ and bed roughness of $k_s \sim 2$ mm. The instrumentation Acoustic Doppler Velocity Profiler is used, which enables three-dimensional velocity measurements with high spatial and temporal resolution.

Chow (1959) is in agreement with the measurements for channels with homogeneous roughness distribution regardless the bank angle. However for channels with heterogeneous roughness the measurements diverge from Chow (1959) wetted perimeter shear stress distribution. *Knigth's method* is in general in agreement with the measurements which reinforces its validity range even for channels with heterogeneous wetted perimeter roughness distribution.

1 Introduction

The evaluation of shear stress distribution along the channel wetted perimeter is of paramount importance for channel design. Chow (1959) wetted perimeter shear stress distribution for smooth trapezoidal is widely used, see Figure 1. Knight's empirical formulas (Knight et al., 1994), also known as *Knight's method,* are also used to calculate mean and maximum shear stress in open-channels. However, these methods were developed with scarce data from channels with banks rougher than bed.

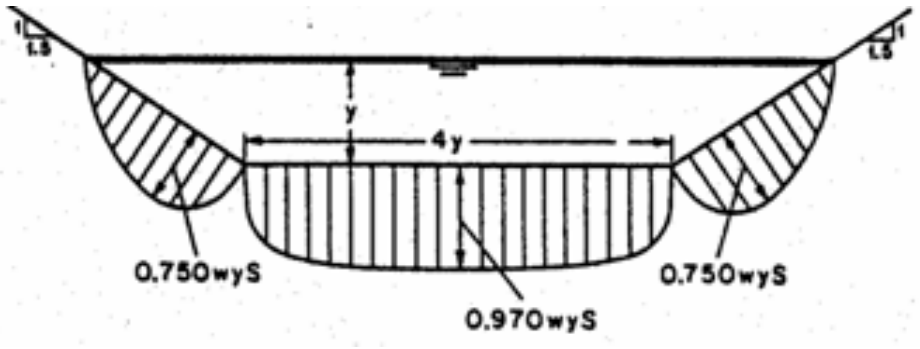

Figure 1
Chow (1959) wetted perimeter shear stress distribution

For engineering practice the downstream velocity patterns and the wetted perimeter stress distribution are very important information. However straight channel flow transverse and vertical velocities, the circulation cells, have a strong interplay with the downstream velocity patterns and the wetted perimeter stress distribution. Circulation cells are typically 2% of mean velocity and their energy being negligible (0.04% of the primary flow energy) however they are responsible for the redistribution of downstream velocity, boundary shear and sediment transport, Knight at al. (1984,1985) and Nezu et al.(1985). The straight channel circulation cells are turbulence driven, so they are also known as secondary current Prandtl's second kind (Prandtl, 1942). Figure 2 illustrates by means of measurements the interplay between downstream velocity patterns with the associated upflows downflows pairs or bulges and the circulation cells (Albayrak, 2007). The bulges are highlighted by arrows and the circulation cells are schematically shown in Figure 2. In regions where the arrows point up low velocities are lifted into the water column, whereas in regions where the arrows point down high velocities are advected towards the bed. This interplay is treated in this paper by means of experiments.

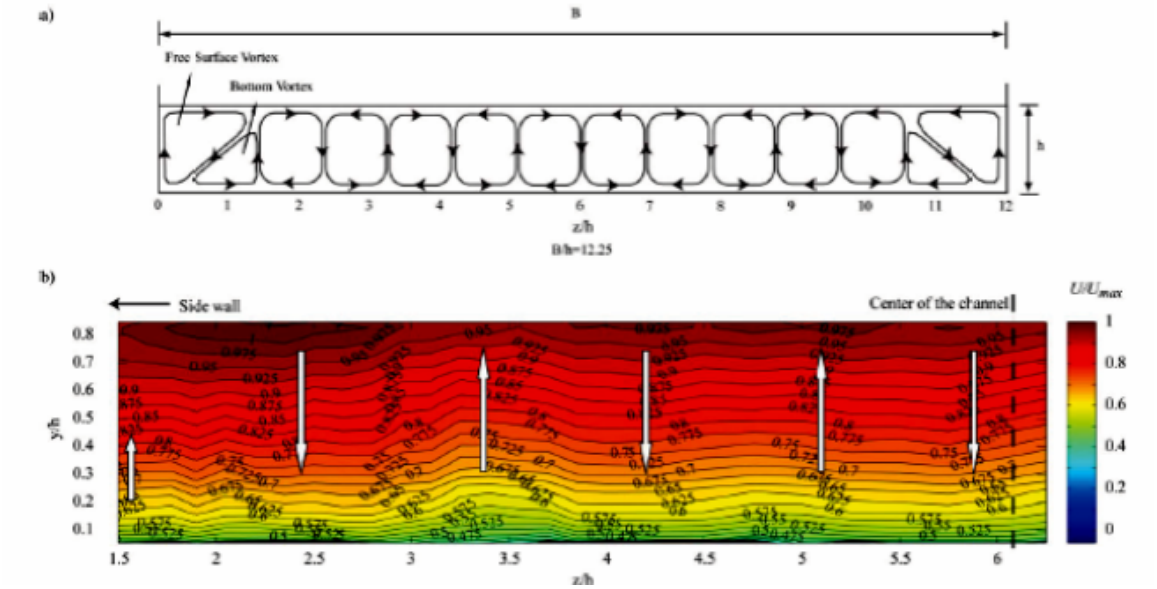

Figure 2
Contour lines of stream functions and upflows downflows pairs (up)
Contour lines of normalized downstream velocity, $v_s / U_{\max}$, upflows downflows pairs with arrows
Albayrak (2007)

Channel geometry and aspect ratio affect the wetted perimeter shear stress distribution. Wide and narrow open-channels generate different flow characteristics. Open-channel flow is considered as wide if its aspect ratio is higher than 5.5 or narrow if its aspect ratio is lower than 5.5. In narrow open-channels the maximum velocity core is located beneath the free-surface due to velocity dip contrasting with wide open-channels where no velocity dip is present and so the maximum velocity is located at free-surface. In wide open-channel the sidewall effect does not reach the central part of the channel and thereby 2D flow properties exist there (Nezu et al., 1993). Wetted perimeter roughness distribution also significantly affects the flow patterns. Bed roughness effect on flow patterns is different from the bank roughness effect. Studerus (1982) shows that shear stress over a rough bed strip is higher than over smooth zone in horizontal bed. In the case of vertical banks, increasing bank roughness pushes away high momentum flow from the vertical bank (Tominaga et al., 1989) reducing the bed shear stress in the vicinity of the bank toe which is important for scouring.

Table 1 shows a summary of foregoing experiments. Two main references listed in Table 1 were used in this paper. First, Tominaga et al. (1989) investigated the effects of the aspect ratio, the shape of the channel and wall roughness on circulation cells and shear stress. The results shown were explained through the longitudinal vorticity equation. They concluded: i) The 3D structure of the primary mean velocity; turbulences intensities and Reynolds stresses are affected by the circulation cells; ii) With different boundary roughness conditions the basic structure of the circulation cells are unchanged despite its different spanwise vortex scale; iii) The secondary flow structure in a trapezoidal open channel flow differs from rectangular channel, i.e. the velocity dip in a trapezoidal open channel does not appear; iv) as the angle of the bank wall is reduced from vertical to below 45° downstream velocity changes from rectangular characteristics into trapezoidal channel ones.

Table 1
Literature review of experimental research on straight open-channel flow

Literature	Type of Set-up Experimental technique	Cross-section	Flow regime	Size of measuring grid	Measured variables
Chow (1959)	**Laboratory measurements Membrane analogy technique Water flow**	**Trapezoidal channel 1<B/H <10**	-	-	-
Nezu et al. (1984)	**Laboratory LDA measurements Air flow**	**Rectangular channel with artificial longitudinal ridge attached on the walls B/H= 7.5**	**Re=1.3*10^4**	**280 and 340 measuring points**	$v_s\ v_n\ v_z$ $\overline{v_s'^2}\ \overline{v_n'^2}\ \overline{v_z'^2}$
Nezu et al. (1985)	**Laboratory measurements Air flow**	**Smooth Rectangular channel B/H= 10, 6, 4, 3 and 2**	**$3*10^4$<Re <$5*10^4$**	**300 measuring points in 20 cm**	$v_s\ v_n\ v_z$ $\overline{v_s'^2}\ \overline{v_n'^2}\ \overline{v_z'^2}$
Tominaga et al. (1989)	**Laboratory measurements X-type hot-film anemomneter Water flow**	**Rectangular channels with varying B/H and roughness distributions. Trapezoidal channels with fix roughness distribution but varying bank inclinations 2<B/H< 8**	**0.18<Fr<0.69 $3*10^4$<Re< $7.3*10^4$**	**100 points per half section**	$v_s\ v_n\ v_z$ $\overline{v_s'^2}\ \overline{v_n'^2}\ \overline{v_z'^2}$ **bed and bank shear stress**
Knight et al. (1992)	**Laboratory measurements. Preston tube measurements**	**Trapezoidal channels with varying bank roughness 0.85<B/H<10 Bank/Bed roughness ratio= 679 and 419**	**0.39<Fr<0.89 $3.4*10^4$<Re <$1.6*10^5$**	**5mm over the bed and 10 mm over the walls**	v_s **and bed and bank shear stresses values**
Nezu et al. (1993)	**Field measurements EM flow meters Water flow**	**B/H=8 and 2.5**	**Fr = 0.08 and 0.11 Re = $8*10^5$ and $6{,}1*10^5$**	**270 and 72 points**	$v_s\ v_n\ v_z$ $\overline{v_s'^2}\ \overline{v_n'^2}\ \overline{v_z'^2}$
Knight et al (1994)	**Laboratory measurements Preston tube measurements Water flow**	**Rectangular and trapezoidal cross-sections 0<B/H<20**	**0<Fr<3.2**	**No data given**	v_s **and bed and bank shear stresses values**

Table 1 (continuation)
Literature review of experimental research on straight open-channel flow

Literature	Type of Set-up Experimental technique	Cross-section	Flow regime	Size of measuring grid	Measured variables
Knight et al (2000)	**Laboratory measurements PrestonTube Water flow**	**244-mm internal diameter pipe. Surface flow with or without horizontal bed**	**0.38<Fr<1.9 $6.5*10^4$<Re<$3.4*10^5$**	**No data given**	v_s **and bed and bank shear stresses values**
Mohamadi et al (2004)	**Laboratory measurements Preston Tube Water flow**	**V-shaped channel 2<B/H< 8**	**Fr = 0.3 Re = $1.9*10^5$**	**15 mm of interval per profile**	v_s **and bed and bank shear stresses values**
Wang et al. (2006)	**Laboratory measurements LDA and UVP Water flow**	**7.75<B/H<8 Rectangular channel with longitudinal bedforms**	**0.55<Fr<0.62 $44*10^3$<Re<$46*10^5$**	**41 profiles with 7.5 mm space 5mm space on sidewalls UVP**	$v_s\ v_n\ v_z$ $\overline{v_s'^2}\ \overline{v_n'^2}\ \overline{v_z'^2}$ $\overline{v'_{sn}}$
Albayrak (2007)	**Laboratory measurements ADVP and PIV Water flow**	**Rectangular B/H=12.25**	**0.1<Fr<0.4 $2.9*10^4$<Re<$10*10^4$**	**One profile every 2.5 cm**	$v_s\ v_n\ v_z$ $\overline{v_s'^2}\ \overline{v_n'^2}\ \overline{v_z'^2}$ $\overline{v'_{sn}}\ \overline{v'_{sz}}\ \overline{v'_{nz}}$ **and bed shear stress**
Rodrigues et al. (2007)	**Laboratory measurements ADV Water flow**	**Rectangular B/H=8.5&6.3**	**0.42<Fr<0.59**	**One profile every 5 cm**	$v_s\ v_n\ v_z$ $\overline{v_s'^2}\ \overline{v_n'^2}\ \overline{v_z'^2}$ $\overline{v'_{sn}}\ \overline{v'_{sz}}$ **and bed shear stress**
Present Study	**Laboratory measurements ADVP Water flow**	**Rectangular and trapezoidal sections covering 3 different bank inclination and roughness B/H=8**	**Fr = 0.33 Re = $69*10^3$**	**Each profile every 15 mm near-wall, 25 mm and 50 mm at channel center**	$v_s\ v_n\ v_z$ $\overline{v_s'^2}\ \overline{v_n'^2}\ \overline{v_z'^2}$ $\overline{v'_{sn}}\ \overline{v'_{sz}}\ \overline{v'_{nz}}$ **bed and bank shear stresses**

Second, a group of articles summarized in Knigth et al. (1994) should be referred due to their aim to derive equations for mean and maximum shear stress on bed and banks. *Knight's method* calculates mean and maximum shear stress from bed and bank as function of perimeter and roughness ratios. These researches data set are available at www.flowdata.bham.ac.uk which is valuable for the development of theoretical and empirical models. However for the best of the author's knowledge few measurements were made on channels with non-homogeneous roughness distribution which may lead to erroneous estimations in such cases.

This paper investigates the interaction between boundary shear stresses, downstream velocity and circulation cells in straight open-channel flow as function of bank roughness and inclination by means of detailed laboratory measurements (Table 2). The data was obtained by a dense measurement grid with a state-of-the-art measuring technique, Acoustic Doppler Velocity Profile (ADVP).

Table 2
Straight channel experiments with varying outer-bank inclination and roughness
F16_90_00 stands for **flat** bottom with **16 cm** of water-depth, **90°** outer-bank angle with the bottom and **00** the outer-bank k_s equivalent roughness.

Inclination of outer bank ⇒ / ***Roughness of outer bank*** ⇓	90°	45°	30°
Smooth PVC	F16_90_00	F16_45_00	F16_30_00
k_s = 0.002 m (sand)	-	F16_45_02	F16_30_02
k_s = 0.03 m (riprap)	-	F16_45_30	F16_30_30

This paper addresses the following questions:

1) What are the effects of varying outer-bank inclination and roughness on the interaction between primary flow patterns, wetted perimeter shear stress distribution, circulation cells and turbulence?

2) Are the commonly used empirical methods (Chow, 1959 and Knight at al., 1994) able to calculate bed and bank mean and maximum shear stresses for trapezoidal cross-sections?

2 Experimental set-up and instrumentation

Table 3
Hydraulic and geometric conditions in the systematic series of experiments
Q is the flow discharge, H is the fume averaged water depth, U is the averaged velocity, R_h is the hydraulics radius, E_s is the energy slope, u_* is the averaged shear velocity, $u_* = \sqrt{gR_hE_s}$, $C = g^{1/2}(U/u_*)$ is the Chézy friction coefficient, $Re = UH/\upsilon$ is the Reynolds number, $Fr = U/(gH)^{1/2}$ is the Froude number, B is the flume width, k_s is the roughness diameter of the outer bank material, and Θ_{bank} is the inclination of the outer bank.

Label	Q [ls^{-1}]	H [m]	U [ms^{-1}]	R_h [m]	u_* ms^{-1}	C m$^{1/2}$s^{-1}	E_s [‰]	Re [10^3]	Fr [-]	R/H [-]	B/H [-]	Θ_{bank} [°]	k_s,bank [m]
F16_90_00	89	0.163	0.43	0.128	0.029	36	1.1	69	0.3	10.3	8.1	90	PVC
F16_45_00	83	0.162	0.43	0.125	0.028	39	0.9	69	0.3	10.7	7.7	45	PVC
F16_45_02	83	0.162	0.43	0.125	0.032	38	1.1	69	0.3	10.7	7.7	45	2
F16_45_30	83	0.162	0.44	0.125	0.034	36	1.2	69	0.3	10.8	7.7	45	30
F16_30_00	78	0.162	0.43	0.121	0.034	40	0.9	68	0.3	10.8	7.4	30	PVC
F16_30_02	78	0.162	0.43	0.121	0.037	40	0.9	68	0.3	10.8	7.4	30	2
F16_30_30	78	0.162	0.44	0.121	0.038	36	1.2	68	0.3	10.8	7.4	30	30

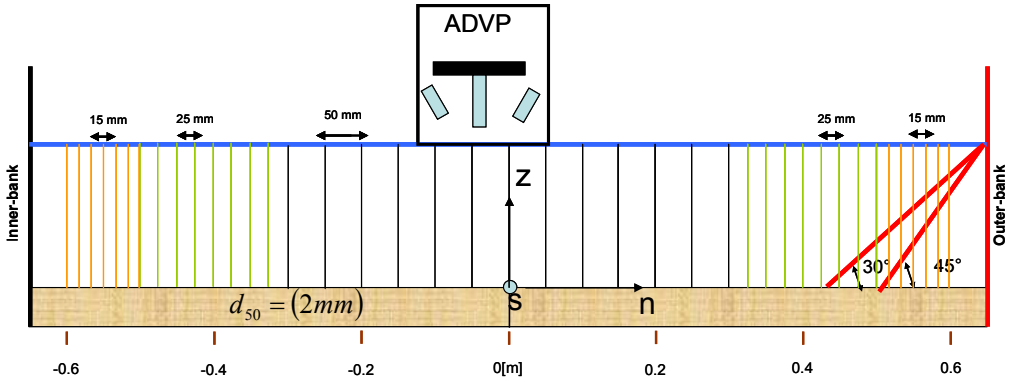

Figure 3
Cross-section schematic and measuring grid

Experiments were carried out in a long 9 m laboratory straight open-channel. Honeycomb and mesh screens were set-up at the flume entrance to provide uniform flow. Table 3 summarizes the hydraulic and geometric conditions. All Experiments have been carried out under similar hydraulic conditions with an overall mean velocity of $U \sim 0.43$ m/s and flow depth of H~0.16 m by means of discharge variation.

Figure 3 shows the cross-section and the axis system. s-axis is in the downstream direction of the flow, z-axis zero is at the bed of the cross-section and increases towards the free-surface, n-axis positive values are located in the outer-bank part of the channel.

Figure 3 illustrates the cross-section shapes located at 6.5 m from the flume's entrance. The inner bank was vertical in order to achieve a wider channel as possible. The bottom width is 1.14 m and 1.03 m for 45°-bank and 30°-bank inclinations, respectively.

Non-intrusive measurements were carried out with an Acoustic Doppler Velocity Profiler (ADVP), developed at EPFL (Rolland 1994, Shen 1997, Hurther 2001, Blanckaert & Lemmin, 2006). ADVP measures simultaneously and quasi-instantaneously profiles of the three velocity components from which the calculation of the mean velocity vector $\vec{v} = (v_s, v_n, v_z)$ and all turbulent correlations $\overline{v_i'^a v_j'^b}$ (*i,j=s,n,z*; *a* and *b* are integers) are possible. Contrary to most available commercial acoustic instruments, the ADVP measures entire flow profiles at one go, thereby allowing high spatial resolution measurements. The vertical profiles were divided into discrete cylindrical measuring volumes of size $(\pi \times 0.7^2/4) \times 0.3 = 0.12 cm^3$. The sampling frequency was 31.25 Hz and the acquisition time was 180 s which enables a record length of 600 times the estimated macro time scales of the flow, (Nezu and Nakagawa, 1993). Blanckaert (2009) reports more information on the ADVP and on the data treatment procedures, as well as on the estimation of the uncertainty of the experimental data. The estimated uncertainty is 4 % for downstream velocity, v_s, 10 % for cross-stream velocities, (v_n, v_z) ,and 10 % for turbulent kinetic energy, k.

The cross-section was measured on a grid that refines towards the banks (Figure 3) extending from n = - 0.6 m to n = 0.6 m for the trapezoidal configurations wherein the number of measuring points is about 1500.

3 Theoretical background

Several quantities used in this paper are described hereafter.

i) The circulation cells are parameterized by means of the streamfunction ψ, defined as (Batcheleor, 1967):

$$v_n = \frac{d\psi}{dz} \tag{1}$$

$$v_z = -\frac{d\psi}{dn} \tag{2}$$

$$\psi(n,z) = \int_{zb}^{z} v_n \, dz = \int_{-B/2}^{n} v_z \, dn = 0.5 * \left(\int_{zb}^{z} v_n \, dz + \int_{-B/2}^{n} v_z \, dn \right) \tag{3}$$

The uncertainty of the streamfunction, ψ, quantity is about 20% (Blanckaert & de Vriend, 2004).

ii) Turbulent kinetic energy is defined as:

$$k = \frac{1}{2}\left(\overline{v_s'^2} + \overline{v_n'^2} + \overline{v_z'^2}\right) \tag{4}$$

where $\overline{v_s'^2}$ is the turbulence intensity in downstream direction, $\overline{v_n'^2}$ is the turbulence intensity in transverse direction $\overline{v_z'^2}$ is the turbulence intensity in vertical direction.

Figure 4 compares measured $\overline{v_s'^2}$ $\overline{v_n'^2}$ $\overline{v_z'^2}$ profiles to the semi-theoretical profiles proposed by Nezu and Nakagawa (1993), Equations 5 to 7. It is concluded that $\overline{v_s'^2}$ and $\overline{v_n'^2}$ experimental values agree well with Equations 5 and 6 profiles but $\overline{v_z'^2}$ experimental values measured in this work are underestimated when comparing with those from Equation 7.

$$\overline{v_s'^2} \Big/ u_*^2 = 5.29 e^{(-2z/H)} \tag{5}$$

$$\overline{v_n'^2} \Big/ u_*^2 = 2.66 e^{(-2z/H)} \tag{6}$$

$$\overline{v_z'^2} \Big/ u_*^2 = 1.61 e^{(-2z/H)} \qquad (7)$$

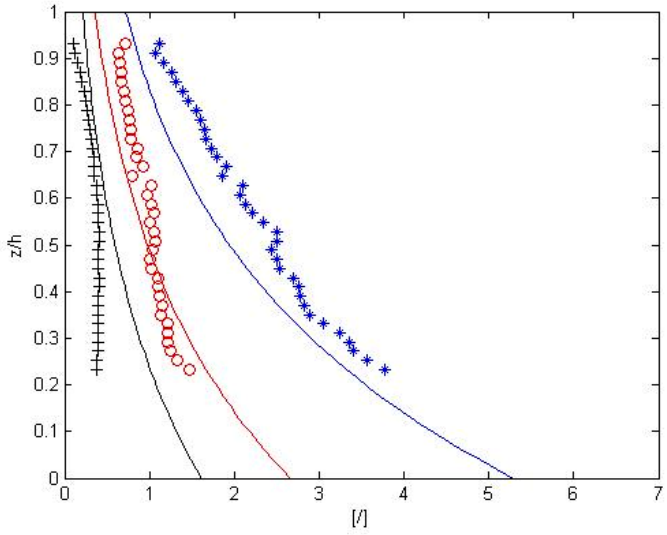

Figure 4

$\overline{v_s'^2}$ $\overline{v_n'^2}$ $\overline{v_z'^2}$ experimental (* o +) and Nezu's equation (-) profiles

iii) Shear stress estimation

In order to obtain the boundary shear stress distribution direct or indirect methods are normally used. The direct method consists of measuring directly the shear stress on the wall and so no assumption regarding the nature of the velocity distribution is necessary. The most know direct method is the hot-film anemometry widely used in hydraulics, mechanical engineering etc... The indirect method could estimate local shear stress through the measurement of velocity and pressure profiles normal to the wall. Several indirect methods exist in literature. In this work an indirect method is used which correlates the velocity and wall shear via the Karman-Prandtl logarithmic velocity distribution law. Ghosh & Roy (1970) and others compare several direct and indirect methods, including the one used in this work and conclude good accuracy of the indirect methods, although in general they overestimate the local shear stress value. The indirect methods have to be used with caution due to existing 3D flow characteristics. Straight channel flows also have 3D flow characteristics, e.g. see Figure 2, mainly in the outer region of a velocity profile. However in the lowest 20% of water depth the logarithmic velocity profile is possible to apply as the 3D effects are expected to be small.

The shear velocity along the bed was estimated via Equation 8 whereas the shear stress over the inclined bank was estimated using Equation 8 or Equation 9 as function of bank roughness.

$$\frac{v_s}{u_*} = \frac{1}{\kappa}\ln\left(\frac{z}{z_0}\right) \tag{8}$$

$$\frac{v_s}{u_*} = \frac{1}{\kappa}\ln\left(\frac{y \cdot u_*}{\upsilon}\right) + 5.3 \tag{9}$$

where v_s is the downstream velocity at a distance z from the boundary, κ is the von Kármán's constant and $z_0 = k_s/30$ is the distance at which the log velocity profile indicates zero velocity.

For each pair of water depth, z, and flow velocity, v_s, one shear velocity, u_*, is obtained calculated via Equations 8 or 9.That means, at each measuring point, within a velocity profile (comprising 51 points), a single $u_*^{'}$ value is obtained. The local shear velocity shown hereafter is an average of $u_*^{'}$ calculated within 10% to 20% of the water column where the loglaw is expected to be respected. So, the semilogarithmic plot between normalized downstream velocity, $U^+ = v_s/u_*$, and the normalized vertical coordinate, $Z^+ = z/k_s$ must be linear at least within the 10% to 20% range.

Figure 5 shows a linear relation between U^+ and Z^+ well beyond the range mentioned above in for profiles measured at different spanwise locations, as well as spanwise average of all measured profiles.

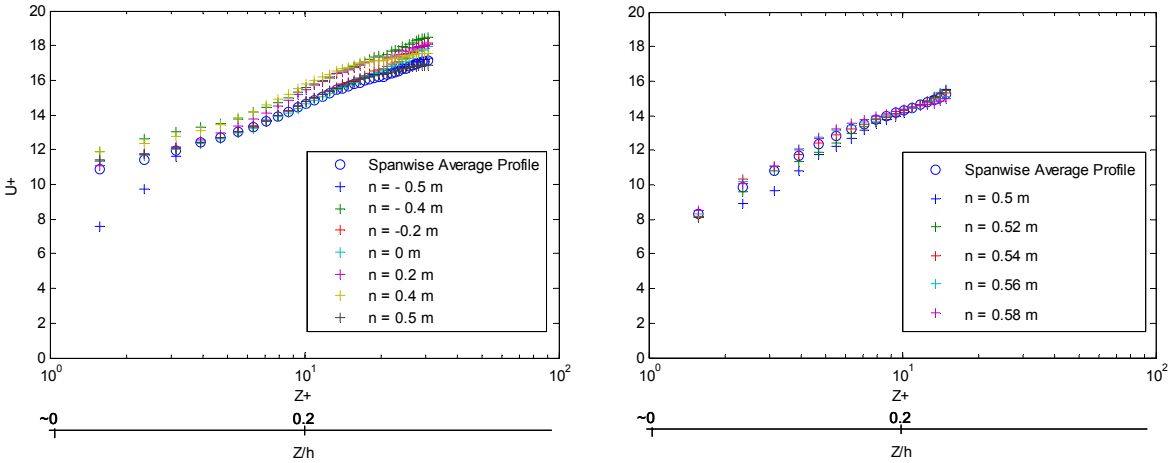

a) b)

Figure 5
Log-law plots of mean velocity in the spanwise direction in the channel ('+') and spanwise average ('0') a) bed b) inclined bank

Figure 6*ab* shows spanwise shear velocity evolution over the bed and inclined bank, respectively for F16_45_00. The local shear velocity is estimated three times from three different intervals 5-10%, 10-15% and 15-20% of *H,* respectively. Differences in these estimates suggest an uncertainty in the obtained boundary shear stress of almost 10% which is in agreement with Nezu & Nakagawa (1993).

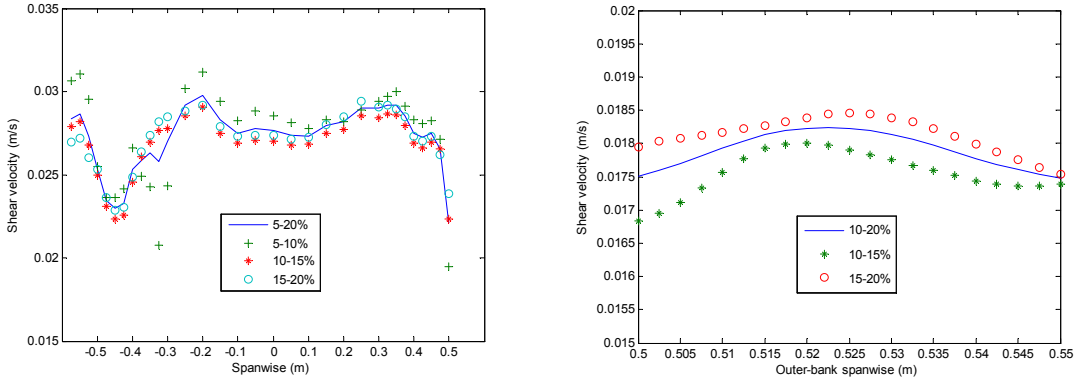

a) b)

Figure 6
Spanwise shear stress distribution as parameter of water depth intervals
(5-10% '+' ; 10-15% '0' ; 15-20% '*' ; 10-20% '-')
a) bed b) inclined-bank

iv) Knight (1994) equations

Knight et al. (1994) estimates the mean and maximum bed and wall shear stresses as:

$$\frac{\overline{\tau_w}}{\tau_0} = 0.01\%SF_w\left[1.0+\frac{P_b}{P_w}\right] \tag{10}$$

$$\frac{\overline{\tau_b}}{\tau_0} = \left(1-0.01\%SF_w\right)\left[1.0+\frac{1}{\left(P_b/P_w\right)}\right] \tag{11}$$

$$\frac{\tau_{w\max}}{\tau_0} = 0.01\%SF_w\left[2.37+\left(\frac{P_b}{P_w}\right)^{0.85}\right] \tag{12}$$

$$\frac{\tau_{b\max}}{\tau_0} = \left(1-0.01\%SF_w\right)\left[0.8+\left(\frac{P_b}{P_w}\right)^{-0.35}\right] \tag{13}$$

$$\%SF_w = e^{\alpha} \tag{14}$$

$$\alpha = -3.23\log_{10}\left(\frac{P_b}{P_w C2}+1\right)+4.6052 \quad (15)$$

$$C2 = 1.50\left(k_{sw}/k_{sb}\right)^{0.2115} \quad (16)$$

where k_{sw} and k_{sb} are the Nikuradse equivalent roughness height for wall and bed respectively, τ_0 is the cross-section average shear stress value. P_b is the bottom perimeter, P_w is the wall or bank wetted perimeter , $\tau_{w\max}$ is the maximum bank shear stress, $\tau_{b\max}$ is the maximum bottom shear stress, $\overline{\tau_w}$ is the mean bank shear stress, $\overline{\tau_b}$ is the mean bottom shear stress , $C2$ is the roughness parameter, α is *Knight's method* parameter, $\%SF_w$ is the percentage of shear stress carried by the walls.

The Knight's method could be explained by the following sequence: 1) from known P_b, P_w, α (Equation 15) and $C2$ (equation 16) Equation 14 calculates the $\%SF_w$. 2) Mean and maximum bed and bank normalized shear stresses can now be calculated via Equations 10 to 13.

4 Results

4.1 Rectangular channel experiments

Transverse and vertical velocity patterns prove the presence of circulation cells. In Figures 7*ab* normalized transverse and vertical velocities, $100*v_n/U$ and $100*v_z/U$ are shown. The consecutive positive and negative values in spanwise and vertical directions visible in $100*v_n/U$ and $100*v_z/U$ patterns correlate and suggest the presence of secondary circulation cells. The maximum $100*v_n/U$ and $100*v_z/U$ correspond close to 2 % of the mean velocity which is in agreement with Tominaga et al. (1989) and Melling & Whitelaw (1976). In all Figures hereafter non-color contour zones indicate extrapolations made in zones close to the free-surface or/and bottom. Blanckaert (2009) give more details about the extrapolations.

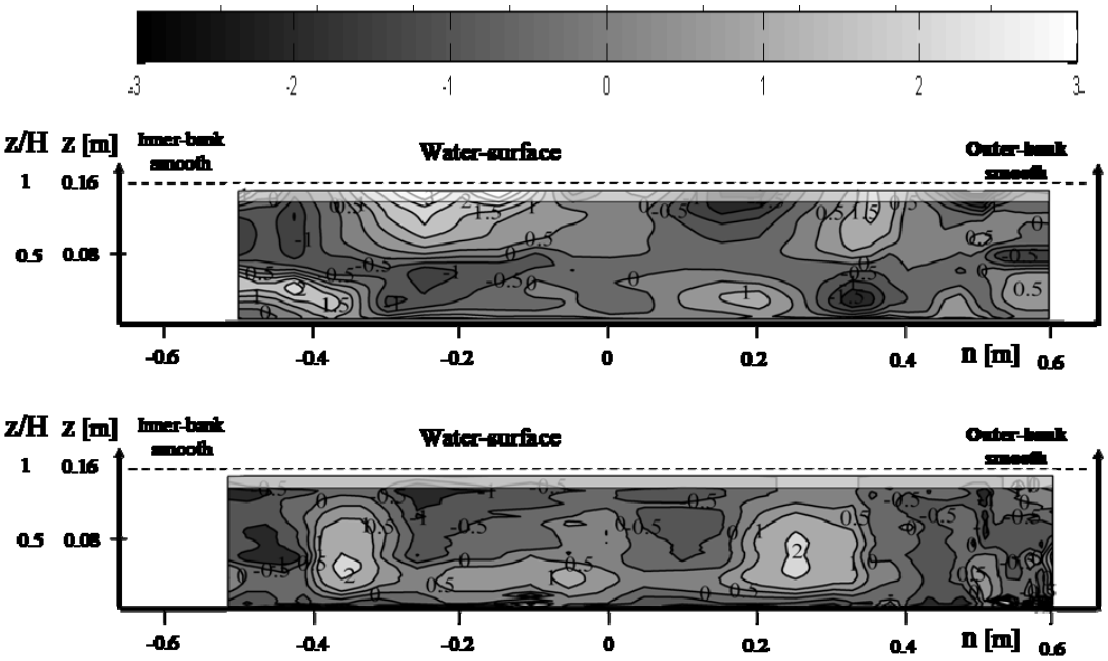

Figure 7
Contour lines of normalized transverse $(100*v_n/U)$ (up) and vertical $(100*v_z/U)$ (bottom) velocities for experiment F16_90_00

Figures 8 illustrates the patterns of secondary circulation cells by means of the $1000\psi/(UH)$. Figure 8 clearly shows 5 circulation cells between *n* = -0.5 and *n* = 0.6. In the outer-bank the bottom cell is hardly observed. In the inner outer-bank two more cells are expected. So in total 8 circulation cells exist. However in the channel center it is not clear if more circulation cells exist.

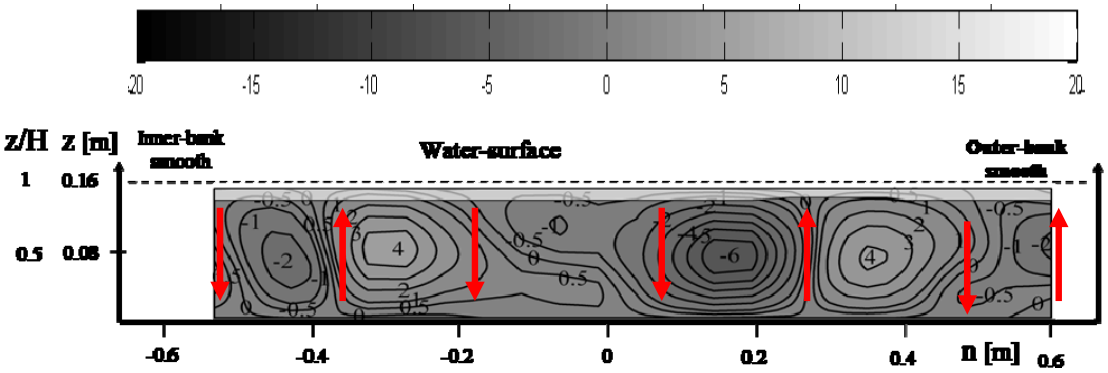

Figure 8
Contour lines of stream functions for experiment F16_90_00

Figure 9 shows the measured patterns of k/u_*^2 wherein bulges are observed. This result suggests that circulation cells influence turbulence field despite its lower energy. The upwelling/downwelling zones correspond to high/low *tke (turbulence kinetic energy)* zones. Hence higher downstream velocity (increased capacity of sediment transport) is located in reduced turbulent kinetic energy.

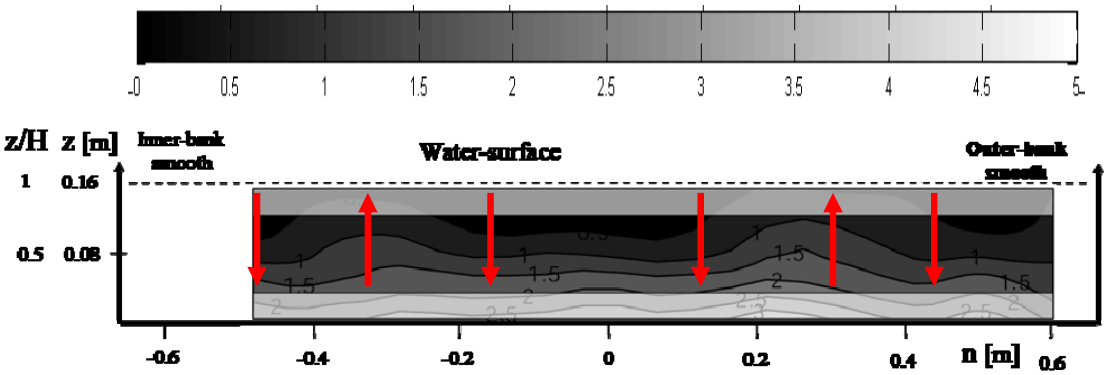

Figure 9
Contour lines of normalized turbulent kinetic energy for F16_90_00

Figure 10 shows the isolevels of normalized downstream velocity, v_s/U, and normalized shear stress, τ/τ_0. τ_0 is the mean of local shear stress values along the wetted perimeter, obtained via loglaw where velocity profiles were measured, and analytical computation where no measurements were made.

No velocity-dip phenomenon was observed being in agreement with literature as the aspect ratio B/H is greater than 5.5, its critical value. The maximum velocity, $v_{s\max}/U$, is equal to 1.2 being located at the free-surface. Lower downstream velocity zones from where the contour lines bulge towards the free-surface are located at n (m) = [-0.35 -0.1 0.25 0.55]. Higher downstream velocity zones from where the contour lines bulge towards the bed are located at n (m) = [-0.5 -0.2 0.1 0.4]. These "bulges"

correspond to upwelling and downwelling, zones of lower and higher velocities, respectively, corresponding to low and high bed shear stress. Bed shear stress amplitude undulation range is about 0.2 τ_0 which is in agreement with literature (e.g. Albayrak, 2007).

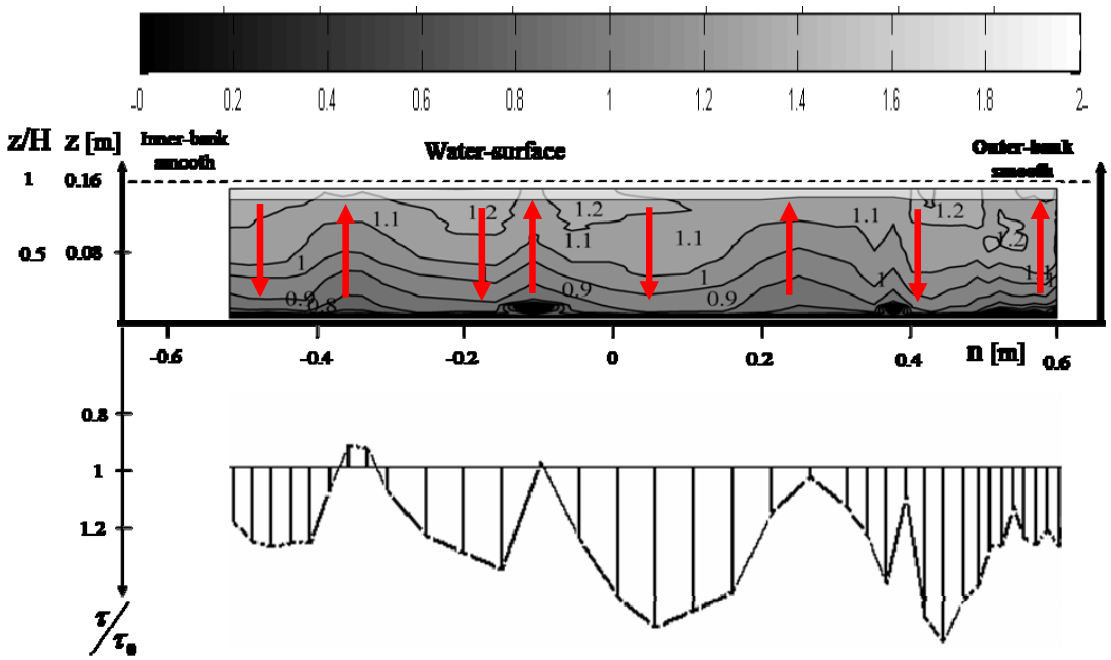

Figure 10

Contour lines of normalized downstream velocity, v_s / U, & bed and wall shear stress distribution τ / τ_0 for experiment F16_90_00

Figure 10 shows bulges at channel center suggesting the presence of two more circulation cells at about channel center, and so being in disagreement with Nezu (1985), who stated that no circulation cells are generated in the central part of smooth channel for aspect ratio $B/H > 4$ and with Tamburrino and Gulliver (1999) who makes the correspondence between B/H and the number of circulation cells for wide channels. However Albayrak (2007) measured 14 circulation cells in a rectangular channel with *B/H* = 12.25 (see Figure 2) and again measuring circulation cells at channel center.

4.2 Half-trapezoidal channel experiments

Figure 11 illustrates the measured patterns of the normalized streamfunctions $1000\psi/UH$, in all experiments with half-trapezoidal cross-section.

For 45°-bank trapezoidal, the number of circulation cells is reduced in comparison with the rectangular channel, F16_90_00. Experiments F16_45_00 and F16_45_02 show 3 and 4 circulation cells, respectively, which none is located at about channel center. Experiment F16_45_30 shows 6 circulation cell and possible 7 thorough the entire cross-section inclusively at channel center. In general, the cells' intensity increases with bank roughness, however, not uniformly along the channel, attributed to the measurement uncertainty.

For the 30°-bank inclination trapezoidal cases the number of circulation cells is 3, 4 and 4 for F16_30_00, F16_30_02 and F16_30_30, respectively. The cells reveal to be wider and their intensity increase with bank roughness. This is in agreement with Tominaga & Nezu (1993) who examined the effects of side-wall roughness and bed roughness on primary flows and secondary flows and discover that roughness leads to stronger circulation cells.

Figure 12 shows the patterns of normalized downstream velocity, v_s/U and normalized boundary shear stress, τ/τ_0 for 45°-bank and 30°-bank inclination cases.

For 45°-bank inclination cases the maximum normalized downstream velocity, $v_{s\max}/U$, is about 1.3. $v_{s\max}/U$ is concentrated at about n = -0.2 m and n= 0.2 m for F16_45_00 and F16_45_02. For F16_45_30, riprap elements on the outer-bank, the maximum normalized downstream velocity, $v_{s\max}/U$, is about 1.4 and it is concentrated at about n = -0.1 m.

The bed shear spanwise undulation is in agreement with the downstream velocity bulges. The maximum normalized bed shear stress tends to be at about n=-0.2 m and n = 0.2 m for F16_45_00 and F16_45_02 however for F16_45_30 the maximum is at about the channel center. The maximum and mean bank shear normalized stresses increase with outer-bank roughness. The amplitude of the bank shear stresses increase with bank roughness. The maximum shear stress location gets closer to the bank toe with increasing outer-bank roughness. It is also noticed that the adjacent bed zone to the outer-bank is protected with increasing outer-bank roughness due to the decrease of v_s.

For 30°-bank inclination cases the maximum normalized downstream velocity, $v_{s\max}/U$, is equal to 1.4 and it is located at about n = -0.1 m of the cross-section for all experiments. With increasing bank roughness the flow momentum near the channel center increases due to the velocity deficit over the outer-bank.

The undulation in bed shear is in agreement with the downstream velocity bulges. The maximum bed shear stress is located at about channel center for all Experiments. The maximum bank shear stress increases and gets closer to the bank toe with increasing outer-bank roughness. The bank shear stress undulation increases strongly with bank roughness, as for 45°-bank inclination experiments. As for the 45°-bank inclination cases, the adjacent bed zone to the outer-bank is protected with increasing outer-bank roughness due to the decrease of v_s .

Figure 13 illustrates the patterns of normalized turbulent kinetic energy. For the 45°-bank inclination trapezoidal experiments, fewer bulges are observed than in the rectangular experiment which is in agreement with the downstream velocity patterns. Experiment F16_45_00 shows high values at about channel center and low values close to the inclined bank whereas Experiment F16_45_30 shows that the maximum values are shifted outwards to about n = 0.15 m and the values over the bank are higher than Experiment F16_45_00 ones, which is logical due to the bank riprap effect on the flow.

For the 30°-bank inclination trapezoidal experiments fewer bulges are observed than in the 45°-bank inclination trapezoidal experiments. Experiment F16_30_00 shows high values at about channel center and low values close to the inclined bank as in 45°-bank inclination experiments. Experiment F16_30_30 also shows that the maximum values are shifted outwards and the values over the bank are higher than in Experiment F16_30_00 due to the bank riprap.

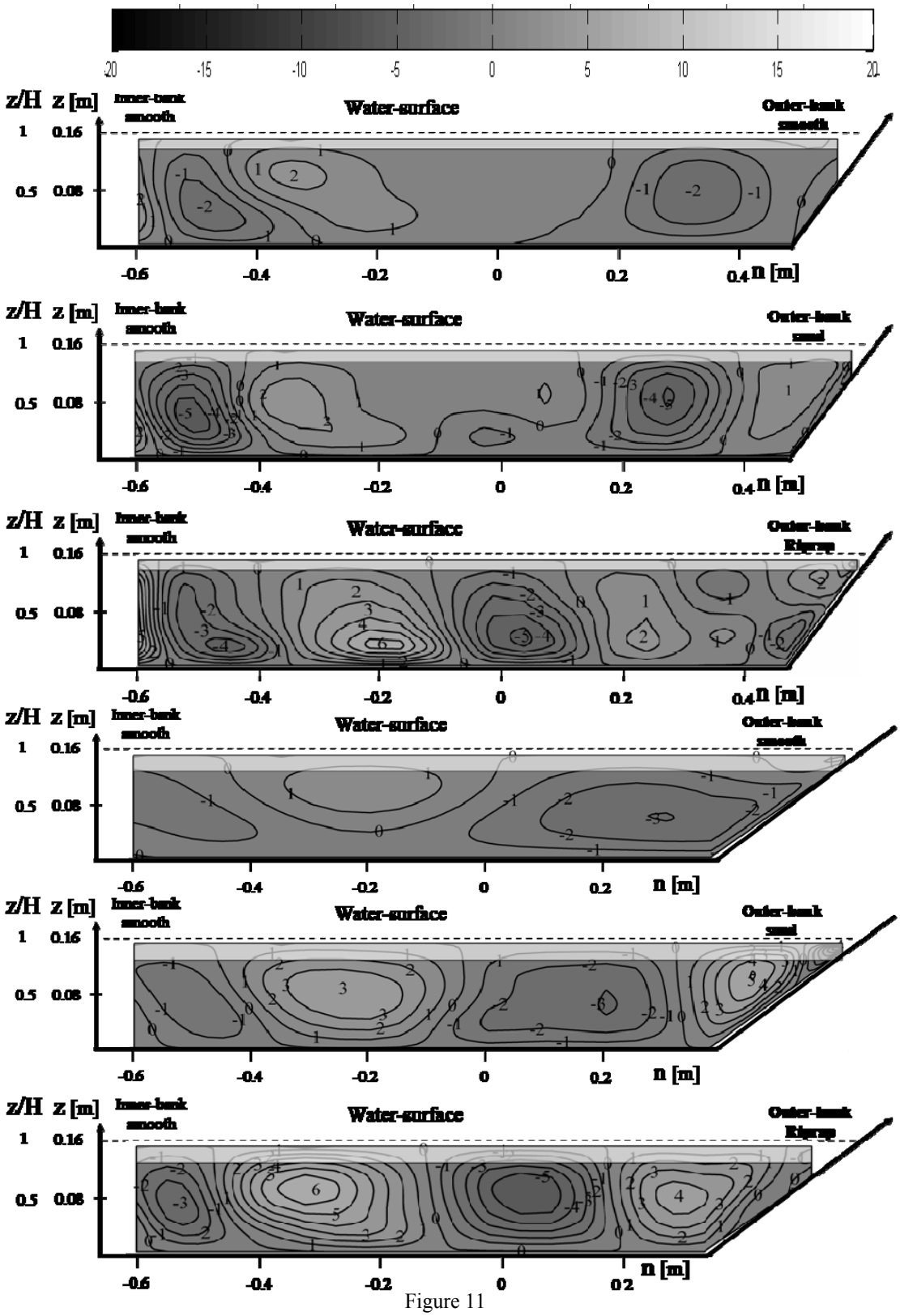

Figure 11
Contour lines of stream functions for trapezoidal experiments
From top to bottom: F16_45_00; F16_45_02;F16_45_30;F16_30_00;F16_30_02:F16_30_30

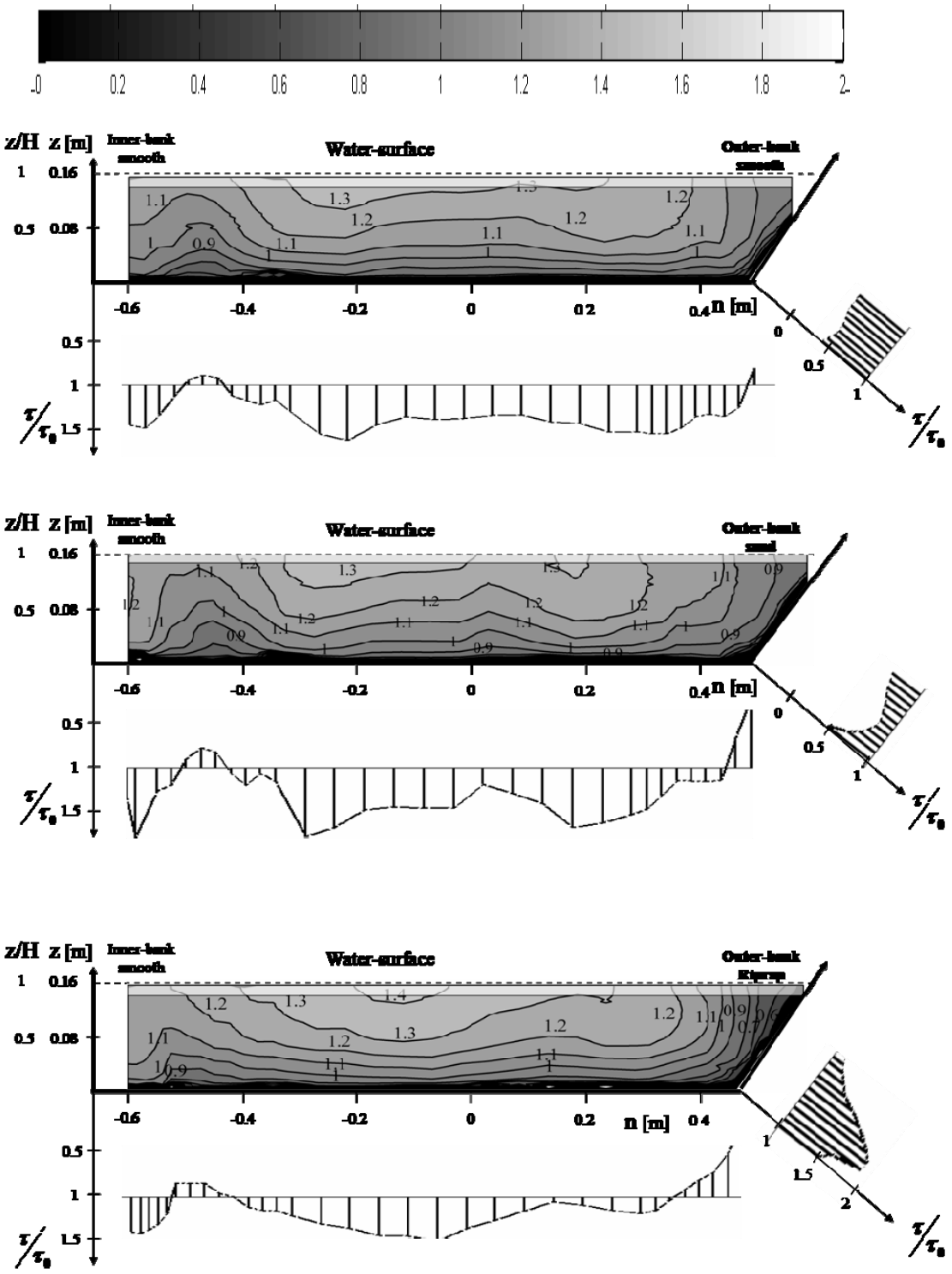

Figure 12

Contour lines of normalized downstream velocity, v_s / U, & bed and wall shear stress distribution τ / τ_0

From top to bottom: F16_45_00; F16_45_02; F16_45_30;

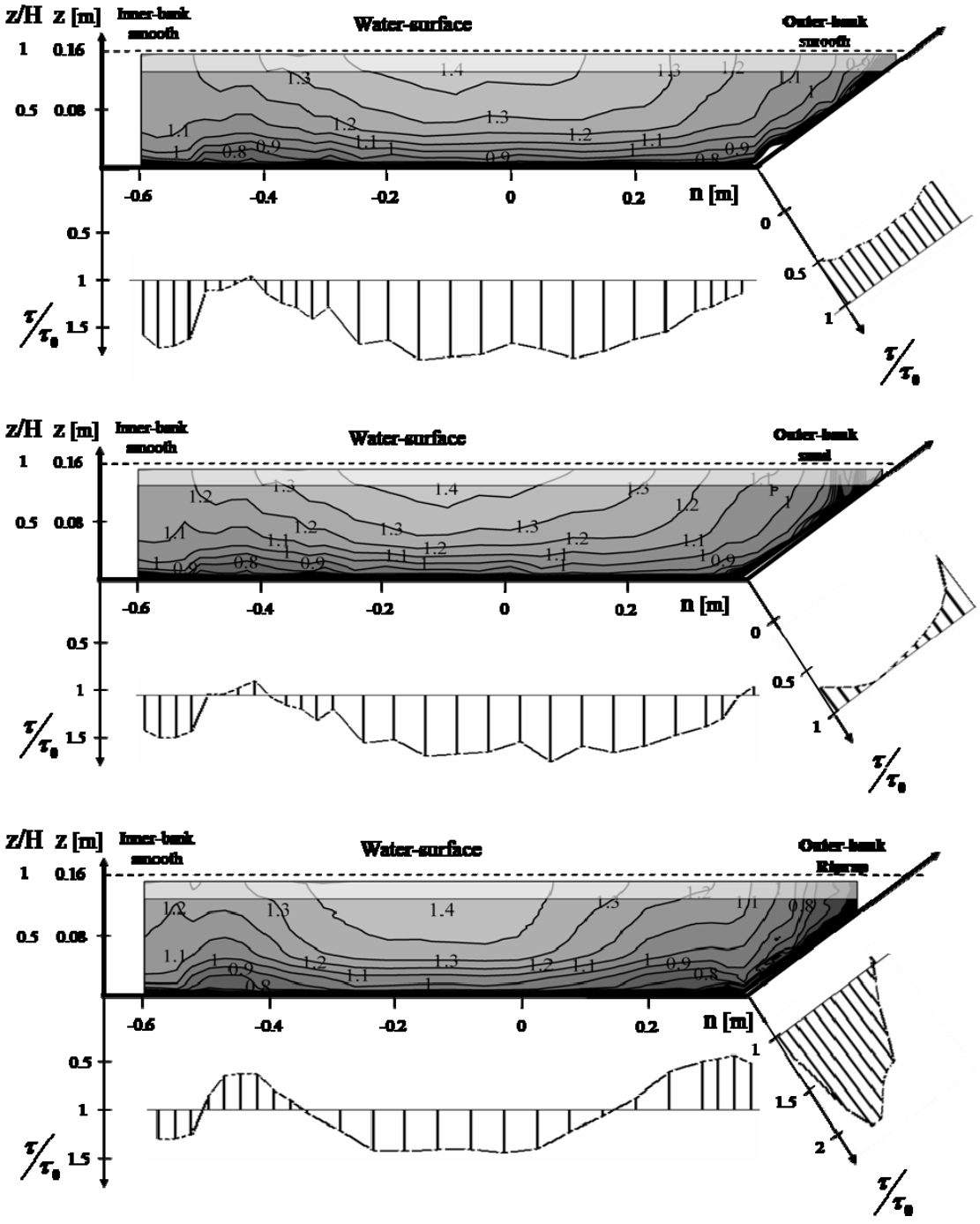

Figure 12 (continuation)
Contour lines of normalized downstream velocity, v_s / U, & bed and wall shear stress distribution τ / τ_0
From top to bottom: F16_30_00; F16_30_02:F16_30_30

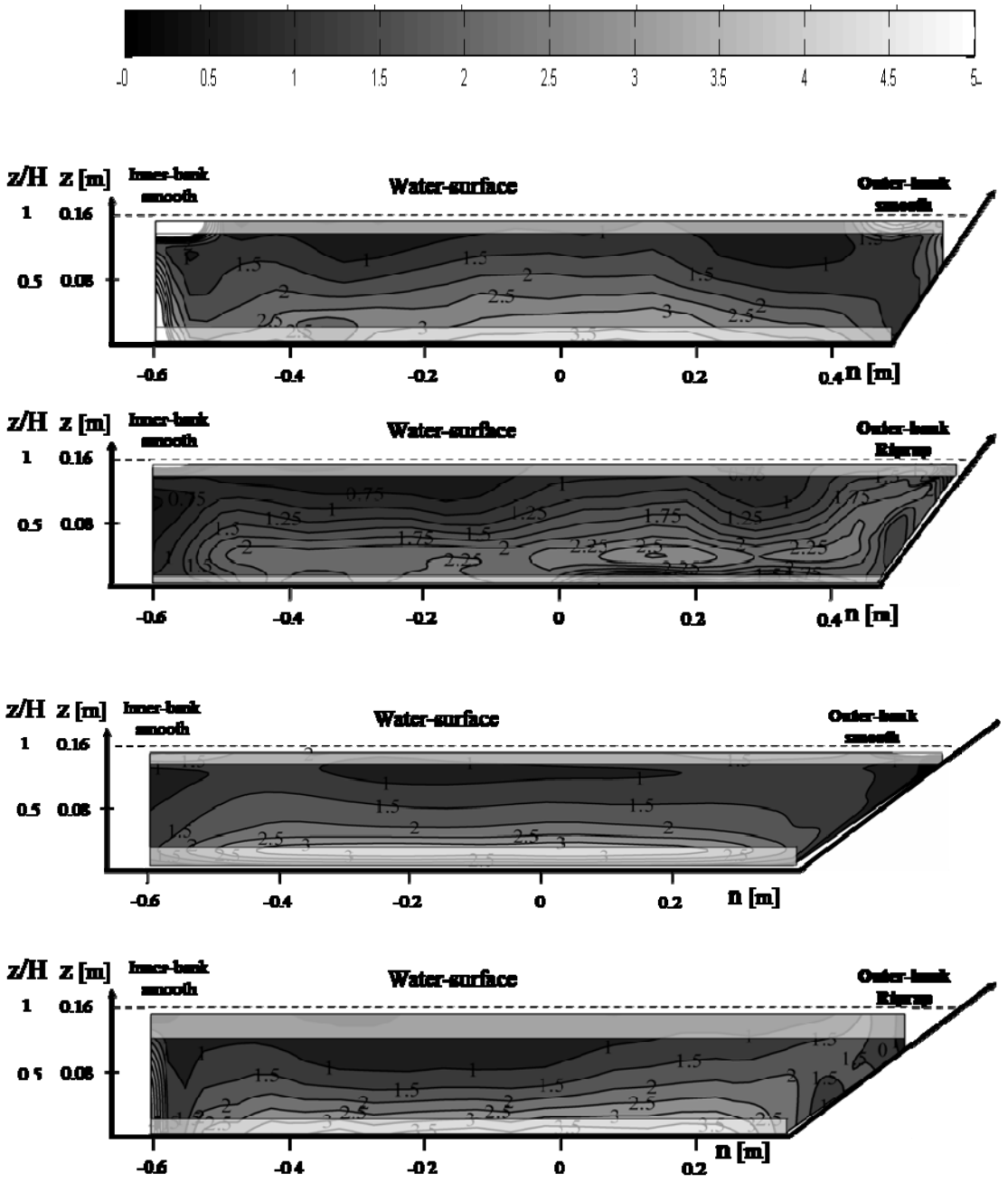

Figure 13
Contour lines of normalized turbulent kinetic energy
From top to bottom: F16_45_00; F16_45_30;F16_30_00; F16_30_30

5 Discussion

Table 4 Normalized mean and maximum bed and bank shear stresses

	$\overline{\tau}_b / \tau_0$	$\overline{\tau}_w / \tau_0$	$\tau_{b\max} / \tau_0$	$\tau_{w\max} / \tau_0$
F16_90_00	1.22	-	1.5	-
F16_45_00	1.26	0.54	1.52	0.57
F16_45_02	1.16	0.87	1.49	0.92
F16_45_30	1.07	1.54	1.33	2.05
F16_30_00	1.31	0.56	1.58	0.61
F16_30_02	1.22	0.83	1.5	1.03
F16_30_30	0.99	1.66	1.34	2.08

Table 4 resumes the normalized mean and maximum bed and bank shear stresses in order to quantify the effect of bank inclination and roughness on wetted perimeter shear stress, it shows: i) normalized bank shear stress increases with increasing bank roughness regardless the bank slope; ii) normalized bed shear stress decreases with increasing bank roughness regardless the bank slope; iii) the mean and maximum normalized bed shear stress values are equal or higher than τ_0 for all experiments.

In Tables 5, 6 and 7 the measurements are compared with Chow (1959) and Knight (1994). Tables 5, 6 compare the mean and maximum shear stresses whereas Table 7 compares $\%SF_w$. In Tables 5 and 6 the values obtained via measurements are different from Table 4 due to different normalization. In Tables 5 and 6 the values obtained via measurements are normalized by the average shear stress from the bed and inclined wall in order to be comparable with Knight (1994). It is assumed the cross-section as half-trapezoidal and so neglecting the inner vertical smooth wall effect on the flow. $\%SF_w$ parameter is compared in Table 7 in order to better evaluate the Knight (1994) method due to its central role.

Evaluation of Chow (1959) estimations

Chow (1959) maximum bed and bank shear stress is of $0.97\,\tau_0$ and $0.75\,\tau_0$ measured for homogeneous roughness channel considering $\tau_0 = \rho g H E_s$. Using instead $\tau_0 = \rho g R_h E_s$, the normalized maximum bed and bank shear stress are $1.3\,\tau_0$ and $1\,\tau_0$, respectively.

Hence, Chow (1959) estimations are in agreement with experiments for F16_45_02 and F16_30_02. However, as expected, with different outer-bank and bed roughness values the estimations diverge from the measurements as Chow (1959) distribution was obtained from channels with homogeneous roughness distribution.

Evaluation of Knight's equations

Knight (1994) method estimations are in fine agreement with the measurements as the magnitudes of the mean and maximum bed and bank shear stresses are similar to those from the measurements, moreover the results trend as function of outer-bank roughness and inclination are also in agreement. The only case of some divergence is the F16_45_02 test. Table 7 shows that $\%SF_w$ values from experiments are in agreement with Knight (1994) method regardless outer-bank inclination or outer-bank roughness which reinforces the validity of Knight (1994) method as a good expedite method for engineers.

Table 5
Maximum normalized bank shear stress values for trapezoidal channels obtained in this work, Chow (1959) [ ] and Knight's equations ( )

Inclination of outer bank ⇒ / ***Roughness of outer bank*** ⇓	30°	45°
Smooth PVC	0.52[1] (0.57)	0.5 [1] (0.49)
k_s = 0.002 m (sand)	0.9 [1] (1.28)	0.89 [1] (1.18)
k_s = 0.03 m (riprap)	1.8[1] (2.1)	1.8[1] (2)

Table 6
Maximum normalized bed shear stress values for trapezoidal channels obtained in this work, Chow (1959) [ ] and Knight's equations ()

Inclination of outer bank ⇒ / ***Roughness of outer bank*** ⇓	30°	45°
Smooth PVC	1.44 [1.3] (1.33)	1.33 [1.3] (1.29)
k_s = 0.002 m (sand)	1.3 [1.3] (1.17)	1.3 [1.3] (1.19)
k_s = 0.03 m (riprap)	1.16[1.3] (0.98)	1.15 [1.3] (1)

Table 7
$\%SF_w$ values for trapezoidal channels obtained in this work and by Knight's equations ()

Inclination of outer bank ⇒ / ***Roughness of outer bank*** ⇓	30°	45°
Smooth PVC	7 (9)	4(5)
k_s = 0.002 m (sand)	17 (20)	8 (12)
k_s = 0.03 m (riprap)	34 (33)	17(22)

6 Conclusions

Seven experiments covering different bank inclination and roughnesses were performed using ADVP measurements.

1) Outer-bank inclination –

The results show that the patterns of circulation cells, downstream velocity (v_s/U), bed and bank shear stress and turbulence depend on the cross-section shape. With decreasing outer-bank angle: i) the number of circulation cells decreases; ii) the maximum downstream velocity increase at about channel center; iii) the bed shear stress evolution presents less peaks although wider; iv) maximum bank shear stress gets closer from the bank toe; v) Turbulence is slightly affected by the cross-section shape as high and low k values are generated over the bed and bank, respectively.

2) Outer-bank roughness –

For trapezoidal cross-sections not only the cross-section shape is of paramount importance but also the roughness distribution on the wetted perimeter. With increasing outer-bank roughness: i) number of circulation cells increase; ii) circulation cells' intensity increase; iii) the maximum downstream velocity increase, at about channel center; iv) bed mean and maximum shear stresses decrease whereas bank mean and maximum shear stresses increase; v) maximum bank shear stress shifts closer to the bank toe; vi) k over the bank increases and shifts the k maximum value from the channel center outwards.

3) Combined cross-section trapezoidal shape and wetted perimeter roughness distribution effect –

Experiments F16_45_00 and F16_30_30 comparison illustrates well the effect of bank angle and roughness combination on flow patterns. F16_30_30 main differences with respect with F16_45_00 are: i) The circulation cells increase in number and in intensity; ii) The downstream velocity in the central part is narrowed in the spanwise sense and enlarged in vertical sense; iii) Maximum bank shear stress increases; iv) k over the bank increases and maximum k shifts from about the channel center outwards.

4) Chow (1959) and *Knight's equations*-

Chow (1959) is in agreement with the measurements for channel with homogeneous roughness distribution. However, for heterogeneous roughness distribution channels Chow (1959) is not suitable to be used. *Knigth's method* is in fine agreement with the measurements, being so, its validity reinforced. It is recommended to be used by engineers as an expedite process.

REFERENCES

Albayrak, I. (2007). "An experimental study of coherent structures, secondary currents and surface boils and their interrelation in open-channel flow." Ph.D thesis N°. 4112, Ecole Polytechnique Fédérale Lausanne, Switzerland.

Batcheleor, G.K. (1967). "An introduction to fluid dynamics" Cambridge Univ. press, Cambridge, U.K.

Blanckaert, K. (2002). "Flow and turbulence in sharp open-channel bends." Ph.D thesis N°. 2045, Ecole Polytechnique Fédérale Lausanne, Switzerland.

Blanckaert, K. & Lemmin, U. (2006). "Means of noise reduction in acoustic turbulence measurements." J. Hydr. Res., 44(1), 3-17.

Blanckaert, K. (2009). "Laboratory experiments on straight and sharply curved open-channel flows. Experimental techniques, data treatment and selected results." In preparation.

Chow, V.T. (1959). "Open-channel hydraulics" McGraw-Hill Book Co., New York, N.Y.

Gosh, S.N. & Roy, N. (1970). "Boundary shear stress distribution in open-channel flow." J. Hydr. Div., ASCE, 96(4), 967-994.

Gosh, S.N. (1972). "Boundary shear distribution in channels with varying wall roughness." Proc. of the Institute of Civil Engineers, Inst. of Civ. Engrs., 53(2), 471-430.

Hurther, D., & Lemmin, U. (2001). "A correction method for turbulence measurements with a 3-D acoustic Doppler velocity profiler." J. Atm. Oc. Techn, Vol.18, 446-458.

Knight, D.W., Demetriou, J.D., & Hamed, M.E. (1984). "Boundary shear in smooth rectangular channel." J. Hydr. Eng., ASCE, vol. 110, No4, April, pp 405-422.

Knight, D.W. & Patel, J. (1985). "Boundary shear in smooth rectangular ducts." J. Hydr. Div., ASCE, Vol.111, Proc. Paper 19408, pp.29-47.

Knight, D.W., Alhamid A.A.I & Yuen, K.W.H. (1992). "Boundary shear in differentially roughened trapezoidal channels." in Hydraulics and Environmental Modeling. Estuarine and River waters, Ch.1, (eds. R.A. Falconer, K. Shiono & R.G.S. Mathew), aSHGATE, pp. 3-14.

Knight, D.W., Alhamid A.A.I & Yuen, K.W.H. (1994). "Boundary shear stress distributins in open-channel flow." in Physical Mechanisms of mixing and transport in the environment, Ch.4, (ed. K. Beven, P. Chatwin & J. Millbank), J. Wiley, pp 51-87.

Knight, D.W. & Sterling, M. (2000). “Boundary shear in circular pipes running partially full.” J.Hydr. Engrg., Volume 126, issue 4, pp.263-275.

Melling, A. & Whitelaw, J.H. (1976). “Turbulent flow in a rectangular duct.” J. Fluid Mech. 78, pp 289-315.

Mohammadi, M. & Knight, D. W. (2004). “Boundary shear stress distribution in a V-shaped channel.” Hydraulics of dams and rivers structures, Taylor & Francis Group, London.

Nezu, I. & Nakagawa, H. (1984). “Cellular secondary currents in straight conduit” J. Hydr.Engr., ASCE, 110(2), 173-193.

Nezu, I., Nakagawa, H. & Tominaga, A. (1985). “Secondary currents in a straight channel flow and the relation to its aspect ratio” Turbulent shear flows 4, Springer-Verlag., 246-290.

Nezu, I. & Nakagawa, H. (1993). “Turbulence in open-channel flows.” Balkema, Rotterdam, The Netherlands.

Prandtl, L. (1942) “Füher durch die Strömungslehre”. Vieweg, Braunschweig.

Rodrigues, J. F. & Gárcia, M.H. (2008). “Laboratory measurements of 3-D flow patterns and turbulence in straight open channel with rough bed.” Journal of Hydraulic Research, Vol.46, N04, pp 454-465.

Rolland, T. (1994). “Dévelopment d’une instrumentation Doppler ultrasone adaptée à l’étude hydraulique de la turbulence dans les cannaux.” PhD dissertation N°. 1281, Swiss Federal Institute of Technology, Lausanne.

Shen, C. (1997). “An acoustic instantaneous particle flux profiler for turbulent flow.” PhD dissertation N°. 1630, Swiss Federal Institute of Technology, Lausanne.

Stearns, F.P. (1883). “A reason why the maximum velocity of water flowing in open channels is below the surface.” Trans.Am.Soc.Civ.Eng (7), pp.331-338.

Sterling, M. (1997). “The distribution of boundary shear stress in an open channel circular conduit running.” Part-full, Ph.D thesis, University of Birmingham, Birmingham, England.

Studerus, X. (1982). “Sekundarstromungen im offenen Gerinne uber rauhen Langsstreifen.” Ph.D thesis, RTH, Zurich, Switzerland.

Tominaga, A., Nezu, I., Ezaki, K. & Nakagawa, H. (1989). “Three-dimensional turbulent structure in straight open-channel flows.” J. Hydr. Res. 27,149-173.

Tamburrino, A., & Gulliver, J.S. (1999). “Large flow structures in a turbulent open-channel flow.” J. Hydr. Res., 37(3). 363-380.

Wang, Z.Q. & Cheng, N.S. (2006). “Time-mean structure of secondary flows in open channel with longitudinal bedforms.“ Advances in Water Resources, Volume 29, Issue 11, November 2006, Pages 1634-1649.

CHAPTER III

INFLUENCE OF OUTER-BANK ROUGHNESS ON HYDRODYNAMICS IN RECTANGULAR OPEN-CHANNEL BENDS

INFLUENCE OF OUTER-BANK ROUGHNESS ON HYDRODYNAMICS IN RECTANGULAR OPEN-CHANNEL BENDS

ABSTRACT

The influence of outer-bank roughness on hydrodynamics in open-channel bends is poorly known. The observation and understanding of underlying mechanisms are relevant for the design of bank protection schemes in river restoration projects.

In curved flows besides the classical helical motion, or center-region cell, an outer-bank cell is also observed. This outer-bank cell is counter-rotating, smaller and weaker than the center-region cell. Both cells are of fundamental importance for the outer bank erosion process therefore their understanding is a prerequisite for modeling the flow patterns in near-bank area. This paper investigates the influence of outer bank roughness on the flow pattern in a sharp laboratory open-channel bend with rectangular cross-section by means of high-resolution three-dimensional velocity measurements with an Acoustic Doppler Velocity Profiler.

In all measurements the pattern of cross-stream circulation is characterized by the existence of center-region cell and outer-bank cell. With increasing outer bank roughness, the outer bank cell amplifies and widens considerably constraining the center region cell, but does not significantly modify the evolution of its strength around the bend. It exerts a protective effect on the outer bank observed by the reduced turbulence and bed shear stress close to the outer-bank. The mechanism which underlines the widening of the outer-bank cell is observed via relevant downstream vorticity equation terms. The centrifugal force and the cross-stream turbulent stresses variation with outer-bank roughness favor the outer-bank cell widening.

1 Introduction

In order to better design river rehabilitation projects accurate and reliable engineering tools that account for complex features of three-dimensional flow patterns, such as circulation cells, are needed. Despite circulation cells being fundamental in three-dimensional open-channel flows little is known about their interaction with cross-sectional shape and cross-sectional roughness distribution.

To answer that need, series of experiment on flow in open-channel bends that systematically investigates the influence of isolated parameters, such as curvature ratio, bank topography and bank characteristics (Blanckaert 2009) have been performed. From that series 9 experiments have been carried out on the influence of roughness and inclination of the outer-bank, (Table 1). The present paper focus on the influence of the outer-bank roughness on flow patterns in rectangular cross-section (ellipse).

Table 1
EPFL bend channel measurements
F16_90_00 stands for **f**lat bottom with **16 cm** of water-depth, **90°** outer-bank angle with the bottom and **00** the outer-bank k_s equivalent roughness.

Inclination of outer bank ⇒ / ***Roughness of outer bank*** ⇓	30°	45°	90°
Smooth PVC	F16_30_00	F16_45_00	F16_90_00
k_s = 0.002 m (sand)	F16_30_02	F16_45_02	F16_90_02
k_s = 0.03 m (riprap)	F16_30_30	F16_45_30	F16_90_30

Globally, open-channel flows are driven by gravity and resisted by friction at flow boundaries. Figure 1 illustrates schematically the patterns of downstream (v_s) and cross-stream (v_n,v_z) velocities in an alluvial open-channel bend. Velocity and boundary shear stress are redistributed in the cross-section by the cross-stream velocities (Blanckaert and Graf 2004).

Figure 1 shows the cross-stream circulation cells, the center-region cell (CRC), also called spiral flow or secondary flow, and a counter-rotating cell, the outer-bank cell (OBC) in upper outer-bank part of the cross-section. The CRC is generated by the interplay between centrifugal force and pressure gradient induced by the superelevation of the water surface (Rozovskii 1957). The CRC advects momentum in outward/inward direction in the upper/lower part of the water column causing a gradually outward shift of the core of maximum downstream velocity. The OBC has been reported in the literature long ago (e.g. Mockmore 1943). Blanckaert & de Vriend (2004) found that turbulence is

an important mechanism in the OBC generation. OBC and near-bank hydrodynamics are relevant for bank protection, bank erosion and morphodynamics (Thorne, 1982, Blanckaert & Graf, 2004).

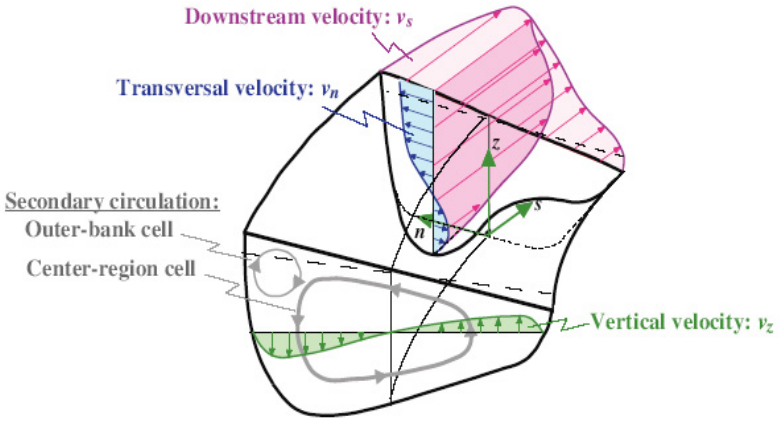

Figure 1
Definition sketch of curved open-channel flow, Blanckaert (2002)

This paper investigates experimentally curved open-channel flows with rectangular channel flow characteristics as function of varying outer-bank roughness. The outer-bank roughness varies between smooth PVC, sand and riprap. This work presents the patterns of downstream and cross-stream flow velocities, the turbulent kinetic energy, the normal stresses anisotropy, the downstream vorticity, and investigates the mechanisms underlying the CRC and OBC by means of term-by-term analysis of the downstream vorticity equation relevant terms and the kinetic energy transfer between mean flow and turbulence.

This paper addresses the following questions:

- What is the effect of increasing outer-bank roughness on downstream flow, cross-stream flow and turbulence in bends with rectangular cross-sections?

- How is the boundary shear stress distribution affected by varying outer-bank roughness in bends with rectangular cross-sections?

- Are the mechanisms underlying the OBC postulated by Blanckaert & de Vriend (2004) confirmed in bends with rectangular cross-section and varying outer-bank roughness?

2 Experiments

Figure 2 shows the laboratory open-channel bend used in this work. It consists of a 9 m long straight entry reach, followed by a 193° bend with constant centerline radius of curvature of R = 1.7 m and a 5 m long straight exit reach. The flume width is B = 1.3 m. The bed of the flume has glued quasi-uniform sediments of d =0.002 m. The inner bank is made of smooth PVC. The outer-bank roughness is varied between PVC, sand, d =0.002 m and d =0.03 m materials (simulating riprap). The approach channel has a downstream bed slope of 0.22%, whereas the bed in the bend and out-flow is horizontal. Figure 2 shows the physical model. Table 1 shows the hydraulic conditions.

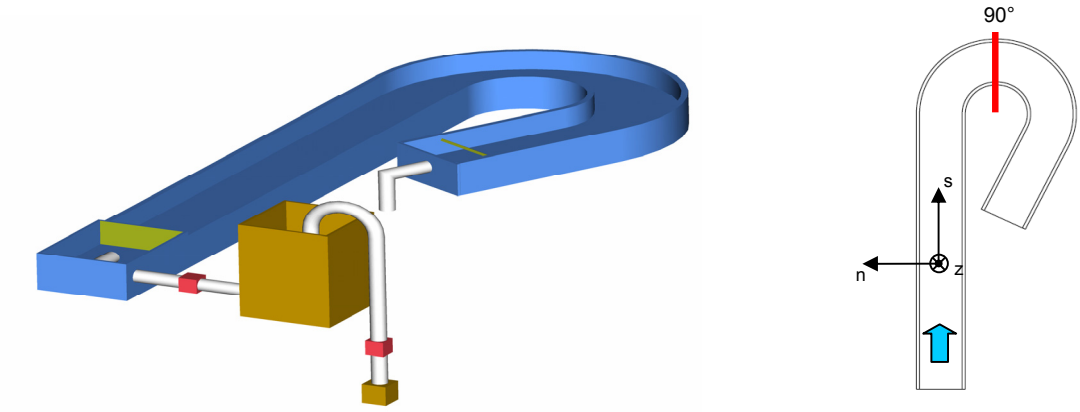

Figure 2
Experimental set-up

Table 2
Hydrodynamics conditions
Q is the flow discharge, H is the fume averaged water depth, U is the flume averaged velocity, u_* is the flume averaged shear velocity (based on hydraulic radius,R_h, and the average energy slope, E_s), $C = g^{1/2}(U/u_*)$ is the Chézy friction coefficient, $Re = UH/\nu$ is the Reynolds number, $Fr = U/(gH)^{1/2}$ is the Froude number, B is the flume width, k_s is the roughness diameter of the outer bank material

Label	Q [ls^{-1}]	H [m]	U [ms^{-1}]	R_h [m]	u_* [ms^{-1}]	C [m$^{1/2}$s^{-1}]	E_s [‰]	Re [10^3]	Fr [-]	R/H [-]	B/H [-]	K_{sb} [m]
F16_90_00	89	0.159	0.43	0.128	0.037	36	1.01	69	0.33	10.3	8.1	PVC
F16_90_02	89	0.159	0.43	0.128	0.037	36	1.13	69	0.33	10.3	8.1	2
F16_90_30	89	0.155	0.44	0.125	0.042	33	1.42	69	0.35	10.9	8.3	30

The water surface topography was measured by a set of 8 acoustic limnimeters that covers the channel width and was moved along the channel via a carriage.

Figure 3 shows the cross-section and the axis system. *s-axis* is in the downstream direction of the flow, *z*-axis zero is at the bed of the cross-section and increases towards the free-surface, *n*-axis positive values are located in the outer-bank part of the channel.

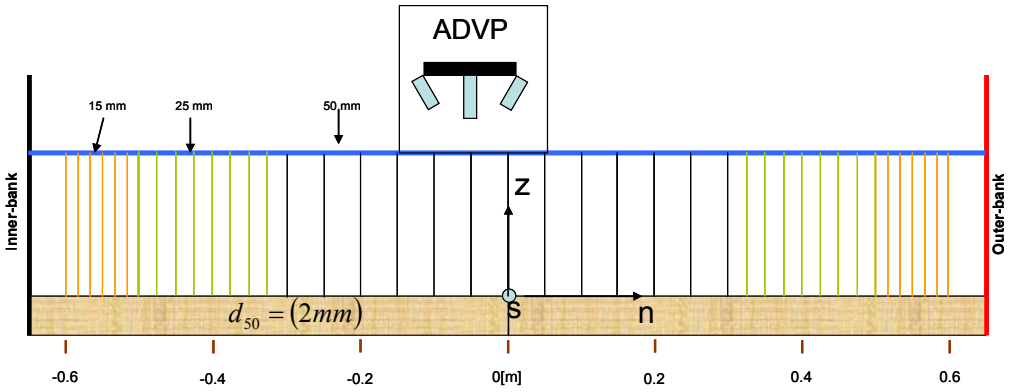

Figure 3
Cross-section measuring grids and shapes

Three dimensional velocity non-intrusive measurements were carried out with an Acoustic Doppler Velocity Profiler (ADVP) (Rolland 1994, Shen 1997, Hurther 2001, Blanckaert and Lemmin 2006). ADVP is placed in a water-filled housing that touches the water surface causing a minor flow perturbation. ADVP enables the derivation of the mean velocity vector $\vec{v} = (v_s, v_n, v_z)$, fluctuating velocity vector, $\vec{v}' = (v_s', v_n', v_z')$ and all turbulent correlations $\overline{v_i'^a v_j'^b}$ ($i,j=s,n,z$; a and b are integers). Cylindrical measuring volume of $(\pi \times 0.7^2 / 4) \times 0.3 = 0.12 cm^3$ is the spatial resolution of ADVP. The sampling frequency was 31.25 Hz and the acquisition time was 180 s which enables a record length of 600 times the estimated macro time scales of the flow, (Nezu and Nakagawa, 1993). In Blanckaert & de Vriend (2004) a resume of the uncertainty of ADVP measurements and derivate quantities is given. The uncertainty is 4 % for v_s, 10 % for (v_n, v_z), 10 % for turbulent kinetic energy, k, 20 % for downstream vorticity, ω_s, and 40% for the downstream vorticity equation terms.

Blanckaert (2009) reports more information on the ADVP, on the data treatment procedures and on the estimation of the uncertainty of the experimental data.

3 Experimental results

3.1 Depth-averaged flow field

A coarse measuring grid was used first along the bend at 15º, 30º, 60º, 90º, 120º, 150º and 180º. Vertical profiles were measured in the spanwise locations between n = -0.5 and n = 0.5 m with 0.1 m intervals. These measurements enabled the investigation of the flow parameters along the bend. However, flow in open-channel bends is highly non-uniform and spatially variable, which complicates comparison between different experiments. In our research we focus on comparison of the cross-section where maximum cross-stream circulation occurs (chapter 3.2).

Figures 4 and 5 show for the three experiments the evolution around the bend of the normalized depth-averaged downstream velocity, U_s/U and the normalized strength of the cross-stream circulation, $\left\langle \tilde{f}_n^{\,2} \right\rangle$, respectively. The latter is defined on the basis of the velocity decomposition

$$\left\langle \tilde{f}_n^{\,2} \right\rangle = \left\langle f_n^{\,2} \right\rangle * S_{circ} \tag{1}$$

Where

$$f_n = \frac{v_n - U_n}{U_s \dfrac{H}{R}} = \frac{v_n^*}{U_s \dfrac{H}{R}} \tag{2}$$

here $\langle\ \rangle$ indicates depth-averaged results; v_n is the transverse velocity components; U_n is v_n depth-averaged values; v_n^* is the transversal component of the cross-stream circulation; f_n is the normalized profiles of v_n^*; S_{circ} is the sign of the cross-stream circulation cells used to label the rotation sense. The curvature ratio H/R has been included in the normalization of v_n^* since the strength of the cross-stream circulation is expected to increase with H/R (van Bendgon 1947, Rozovskii 1957).

In all three experiments, the core of maximum depth-averaged downstream velocity (Figures 4 *abc*) crosses from the inner bank towards the outer bank along the bend. This redistribution of velocity is due to the advective momentum transport by the circulation cells (Blanckaert and Graf 2004).

Figure 5 shows circulation strength $\left\langle \tilde{f}_n^{\,2} \right\rangle$ along the bend. It grows from the bend entry to a value between 4 and 5 near the cross-section at 90° at the centerline for all experiments and then decreases quite sharply toward the bend exit, where its value is reduced to about 1. The maximum value, close to the cross-section at 90° varies only slightly with outer-bank roughness suggesting that the outer-bank roughness does not affect the CRC

strength. Hence, the cross-section at 90° is chosen for detailed measurements presented in chapters from 3.2 to 3.7 and 4.

"Rozovskii's model" predicts about $\left\langle \tilde{f}_n^{\,2} \right\rangle \approx$ 10 for F16_90_00 and F16_90_02 and $\left\langle \tilde{f}_n^{\,2} \right\rangle \approx$ 9 for F16_90_30. The "Rozovskii's model" adopts the straight-channel flow v_s profile and thus neglects the influence of curvature on the downstream velocity profile. It is well known that the curvature flattens the velocity profile, (de Vriend, 1981). To correct the linear model overestimation problem Blanckaert & de Vriend (2003) proposed a non-linear model that defined a corrector factor to be applied to the values of the linear model. This corrector factor depends on the "so-called" "bend parameter" β which regroups the Chezy friction factor *C*, *H/R* and the transverse distribution of the downstream velocity $\alpha_s = \frac{\partial v_s}{\partial n}\frac{R}{U_s}$ and is defined as Equation 3:

$$\beta = \left[\left(\sqrt{g} / C \right)^{-2.2} \left(H / R \right)^2 \left(\alpha_s + 1 \right) \right]^{0.25} \tag{3}$$

The "bend parameter" values, in cross-section at 90° obtained were about 0.92, 0.92 and 0.94, respectively, for F16_90_00, F16_90_02 and F16_90_30 corresponding to a correction factor of about 0.5 for all experiments (Figure 7 in Blanckaert de Vriend, (2003)) leading to a satisfactory agreement with the experimental results.

Figure 6 shows the evolution of the depth-averaged downstream velocity alongside the bend close to the outer-bank at *n* = 0.5 m $U_s(n = 0.5)$. In the beginning of the bend, between 15° and 30° cross-sections, $U_s(n = 0.5)$ slightly decreases for all experiments, mainly for F16_90_30. From cross-section at 30° the evolution of the depth-averaged downstream velocity increases onto the cross-section at 180° for all experiments. Between the three experiments differences are observed, as with increasing outer-bank roughness $U_s(n = 0.5)$ decreases, meaning so, that vertical outer-bank with riprap generates lower U_s in the vicinity of the outer-bank. Hence, it suggests that the outer-bank roughness protects the bottom close to the outer-bank from scouring.

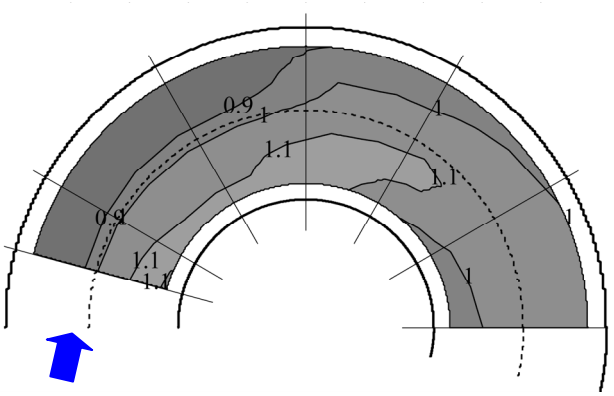

a) Outer-bank in PVC

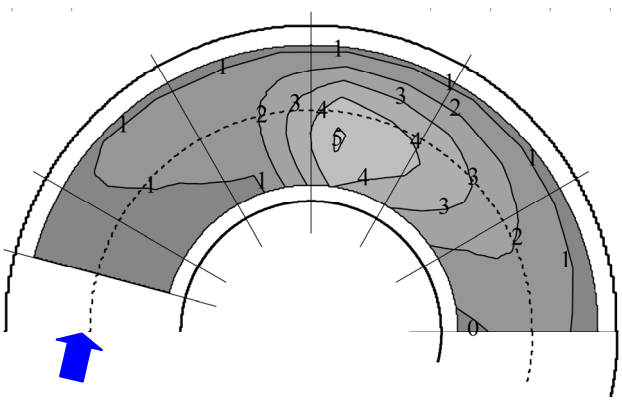

a) Outer-bank in PVC

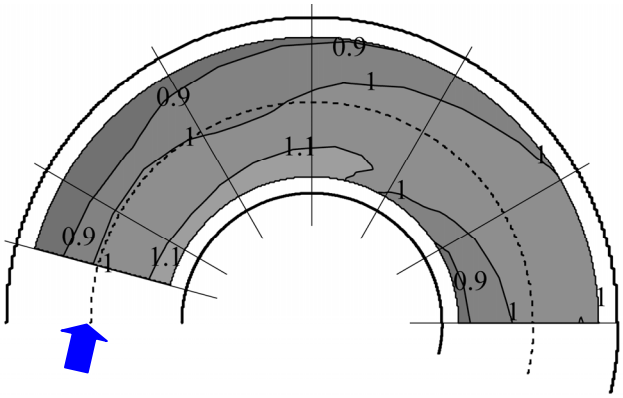

b) Outer-bank with sand (k_s = 2 mm)

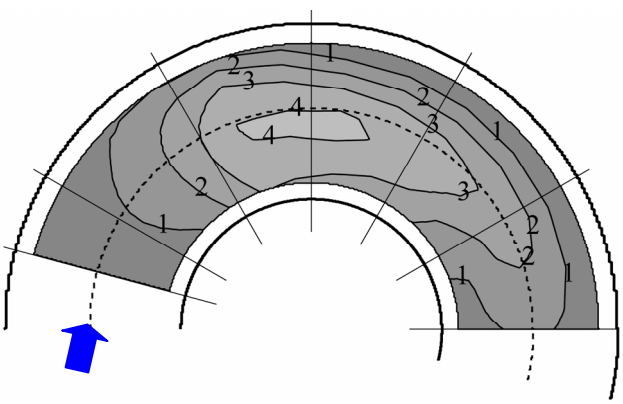

b) Outer-bank with sand (k_s = 2 mm)

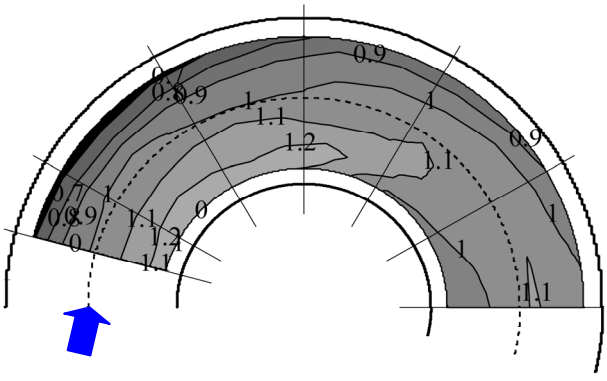

c) Outer-bank with Riprap (k_s = 30 mm)

Figure 4 a b c)
Pattern of normalized downstream depth-averaged velocity , U_s/U

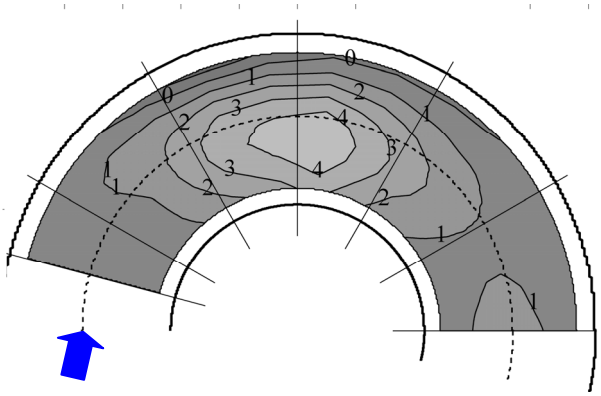

c) Outer-bank with Riprap (k_s = 30 mm)

Figure 5 a b c)
Pattern of normalized cross-stream circulation strength, $\langle \tilde{f}_n^{\,2} \rangle$

a) F16_90_00 (PVC); b) F16_90_02 (sand); c) F16_90_30 (riprap);

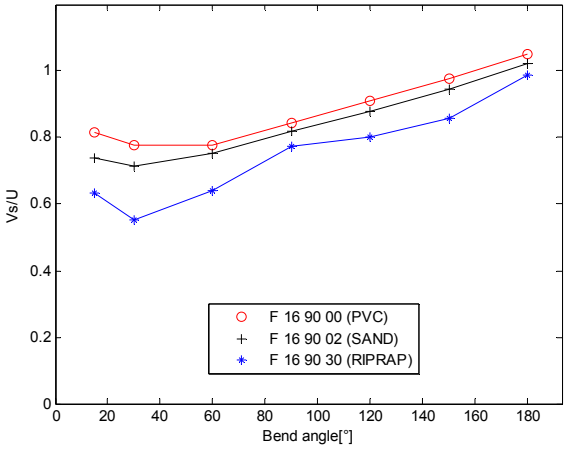

Figure 6
Depth-averaged downstream velocity evolution along the bend at spanwise n = 0.5 m
F16_90_00 (PVC) 'o'; F16_90_02 (SAND) '+' and F16_90_30 (RIPRAP) '*'

3.2 Patterns of cross-stream velocities in the cross-section at 90°

All Figures hereafter show measurement data and their derivatives from cross-section at 90°. A refined grid (Figure 3) that refines towards the banks was used. The average number of measurements points is about 1500. Close to the free-surface and in some cases also close to the bottom extrapolations towards the free-surface and bottom were made. In such cases non-color contour zones are shown. Blanckaert (2009) gives details about those extrapolations.

Figures 7 and 8 *abc* show the isolines of the normalized transverse velocity, v_n/U, and the isolines of the normalized vertical velocity, v_z/U, for the three experiments. In Figures 7 and 8 dashed lines were added to help visualize the circulation cells, their rotation sense and the separation location between them (CRC and OBC).

Figures 7 and 8 *abc* show the CRC at channel center with clockwise rotation sense covering the most part of the cross-section for all experiments. OBC is located in the upper outer zone with counter-clockwise rotation sense for all experiments. The separation between the CRC and the OBC is approximatively defined by the $v_n = 0$ contour line and $v_z < 0$ maximum values zone. Figures 7 and 8 *abc* also show a clockwise cell located beneath the OBC, hereafter referred as LOBC. LOBC is only clearly visible in F16_90_30 by the pair of $v_z > 0$ and $v_z < 0$ maximum values zones in the lower part of the outer-bank. The OBC and LOBC existence is in agreement with Bathurst et al. (1979) who mentioned the presence of a near outer-bank cells pair in rectangular bend flows. In the upper-inner part of the cross-section v_z/U negative values are attributed to flow separation.

Figures 7 and 8 *abc* shows that with increasing outer-bank roughness the OBC significantly widens in the spanwise direction. For F16_90_00 and F16_90_02 the width

of the OBC is about 0.2 and 0.23 m, respectively, from the outer-bank whereas for the F16_90_30 (riprap bank) experiment OBC width reaches about 0.35 m. OBC constrains the CRC outward limit, however the CRC inner limit is unchanged. Hence, CRC size decreases with OBC widening. LOBC also widens with increasing bank roughness. The widening of the OBC and LOBC with increasing outer-bank roughness may reduce the risk of erosion on the bank and adjacent bed. In Figures 7*ab* the outer-bank part is zoomed in order to help visualization.

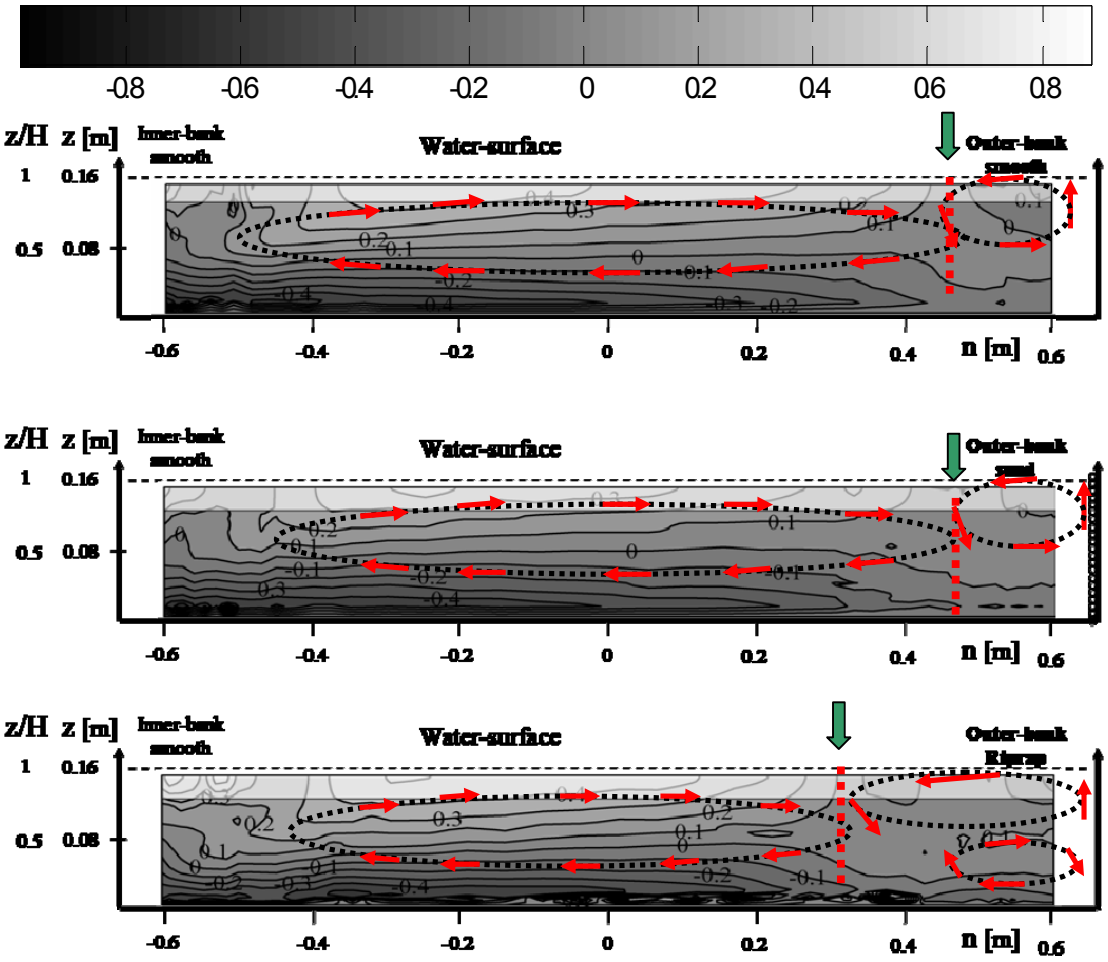

Figure 7.
Cross-section at 90°. Isolines of normalized transverse v_n/U.
F16_90_00 (Top); F16_90_02 (Middle) and F16_90_30 (Bottom).

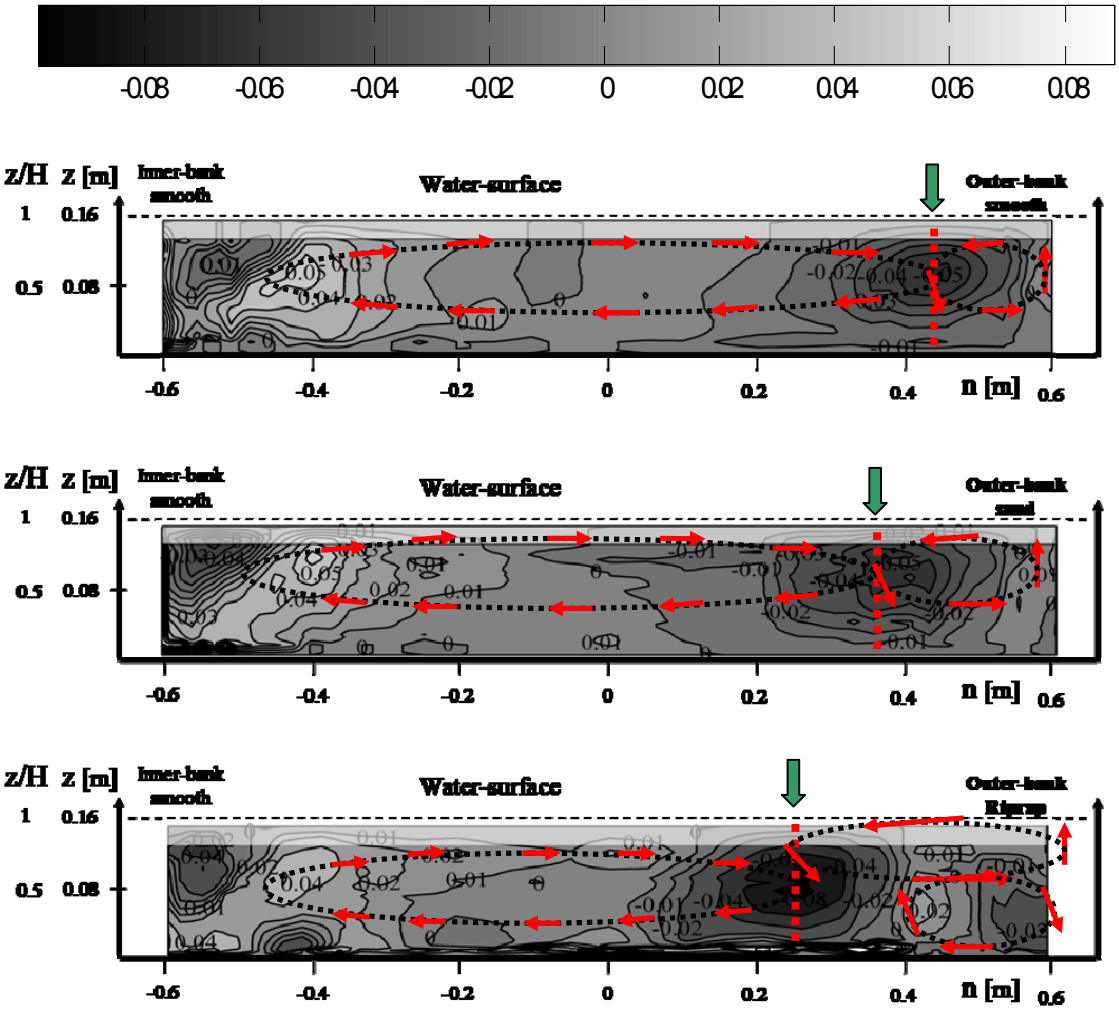

Figure 8.
Cross-section at 90°. Isolines of normalized vertical v_z/U.
F16_90_00 (Top); F16_90_02 (Middle) and F16_90_30 (Bottom).

3.3 Patterns of downstream vorticity in the cross-section at 90°

Cross-stream circulation cells are well visualized and quantified by the downstream vorticity, $\omega_s = \frac{\partial v_z}{\partial n} - \frac{\partial v_n}{\partial z}$. Moreover, the downstream vorticity equation terms allows analyzing the mechanisms underlying the circulation cells (see further in Chapter 4). CRC and OBC cells are well visible in Figure 9 by their negative and positive values, respectively. The maximum negative $\omega_s H/U$ values are located in the lower inward part for all experiments. CRC $\omega_s H/U$ negative values correspond to clock wise rotation sense whereas OBC $\omega_s H/U$ positive values correspond to counter-clock wise. CRC and OBC are separated by the $\omega_s H/U$ 0- isoline (marked by dashed line). LOBC is also visible by

$\omega_s H/U$ positive values mainly for F16_90_30 in the lower outer-bank part. In the upper inner part of the cross-section positive values are seen which are attributed to flow separation. With increasing outer-bank roughness the CRC decreases in size whereas OBC and LOBC increase. Regarding the maximum $\omega_s H/U$ values in the cells, the CRC strength is about constant (differences between the 3 experiments are within the 20% uncertainty by Blanckaert and de Vriend (2004)) whereas the OBC strengthens significantly from about 0.25 to 0.5 $\omega_s H/U$.

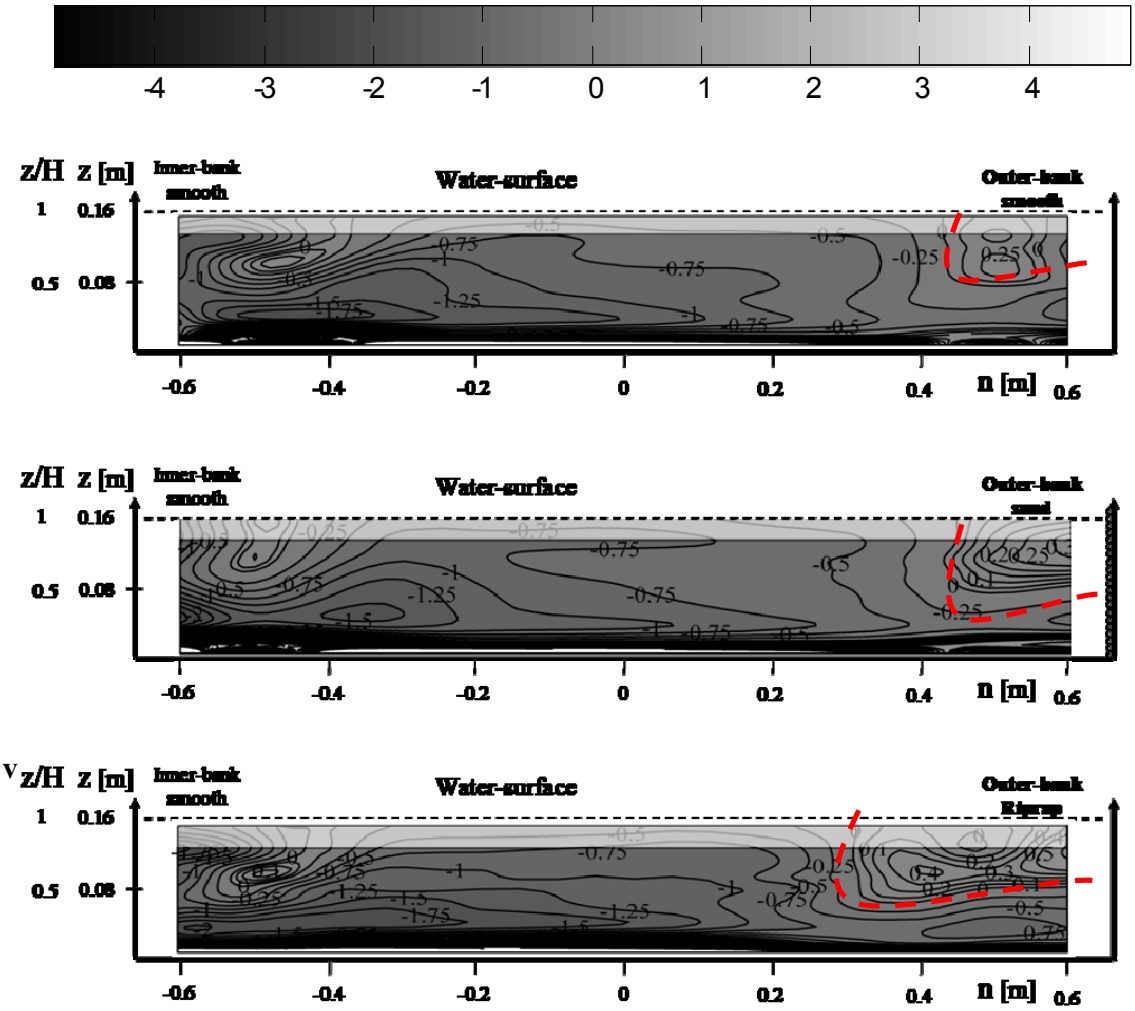

Figure 9

Cross-section at 90°. Isolines of normalized downstream vorticity $\omega_s H/U$

F16_90_00 (Top); F16_90_02 (Middle) and F16_90_30 (Bottom).

3.4. Patterns of normalized downstream velocity, normalized boundary shear stress, normalized depth-averaged downstream velocity and Chezy factor in the cross-section at 90°

Figure 10 shows the normalized downstream velocity, v_s/U, in the cross-section at 90° for the three experiments. Advective momentum transport by the cross-stream circulation cells strongly determines these patterns. Figure 10 shows that the core of maximum downstream velocity is still in the inner lower half of the cross-section and therefore hardly affected by the roughness of the outer bank. The effect of OBC (and LOBC) on v_s/U isolines is visible by the vertical isoline (red dashed line) which indicates the end of the CRC advection and thereby the separation between CRC and OBC. The OBC and LOBC are important also for the bank shear stress as they bring high momentum fluid towards the outer-bank at mid-depth. With increasing outer-bank roughness the vertical isolines shift inwards which is in agreement with the cross-stream velocities information.

Even though the boundary layer in curved flow is 3D, estimates of the boundary shear stress can be obtained by fitting a logarithmic law of the wall to the measured velocities. In the lowest 20% of water depth the logarithmic velocity profile is applied in this work to estimate the local shear stress along the bed (Equation 4). The procedure used is explained in Chapter 1 with more details.

$$\frac{v_s}{u_*} = \frac{1}{\kappa}\ln\left(\frac{z}{z_0}\right) \tag{4}$$

where v_s is the velocity at a distance z from the boundary, u_* is the shear velocity or shear stress, κ is von-Kármán constant and $z_0 = k_s/30$ is the distance at which the log velocity profile indicates zero velocity.

In Figure 11a the measured of primary velocity, $U^+ = v_s/u_*$, versus the vertical coordinate linear, $Z^+ = z/k_s$, shows a linear relation in the semilog plot for each spanwise location and also for their average within the water-depth range chosen to calculate the local shear velocity, 10-20%. Thus validating the water-depth range choice from where the shear velocity was derived.

Figure 11b shows spanwise shear stress evolution over the bed estimated from different water column intervals 10-15%, 15-20% and 10%-20% of H. Differences in these estimates suggest an uncertainty in the obtained boundary shear stress of almost 10% which is in agreement with Nezu & Nakagawa (1993).

Figure 10 also shows the normalized bed shear stress, $\tau/\tau_0 . \tau_0$ is the local shear stress values along the wetted perimeter, obtained via law of the wall method where velocity

profiles were measured, and analytical computation of τ/τ_0 where no measurements were made.

Figure 10 shows that τ/τ_0 maximum values are located at the inner bank as the maximum downstream velocity is still located in the inner part of the channel. The amplitude range slightly decreases with increasing bank roughness. It was noticed that the bed shear stress evolution crosses the τ_0 further away from the bank with increasing outer-bank roughness, suggesting that the adjacent part of the bed to the outer-bank is further protected. Insufficient accurate measurements close to the outer-bank did not allow estimating $\overline{\tau_w}$ via Equation 4. However, the maximum outer-bank shear stress is expected to be at about mid-depth wherein OBC and LOBC converge and where the maximum downstream velocity in that channel zone is located (Figure 10).

Figure 10 also shows U_s^2/U^2 and τ/τ_0 evolutions for all experiments where the divergence between them is noticed. This is not trivial as an important parameter to 2D depth-averaged numerical codes is the Chezy factor. Chezy factor is defined by Equation 5. In 2D simulations the Chezy factor is mostly considered as a constant factor. Figure 12 shows that the Chezy factor is not constant as decreases significantly outwards for all experiments. A dashed line is added to help the visualization. In the inner-part a strong oscillation is observed which is attributed to flow separation.

$$C = \sqrt{\rho g}\sqrt{\frac{U_s^2}{\tau}} \tag{5}$$

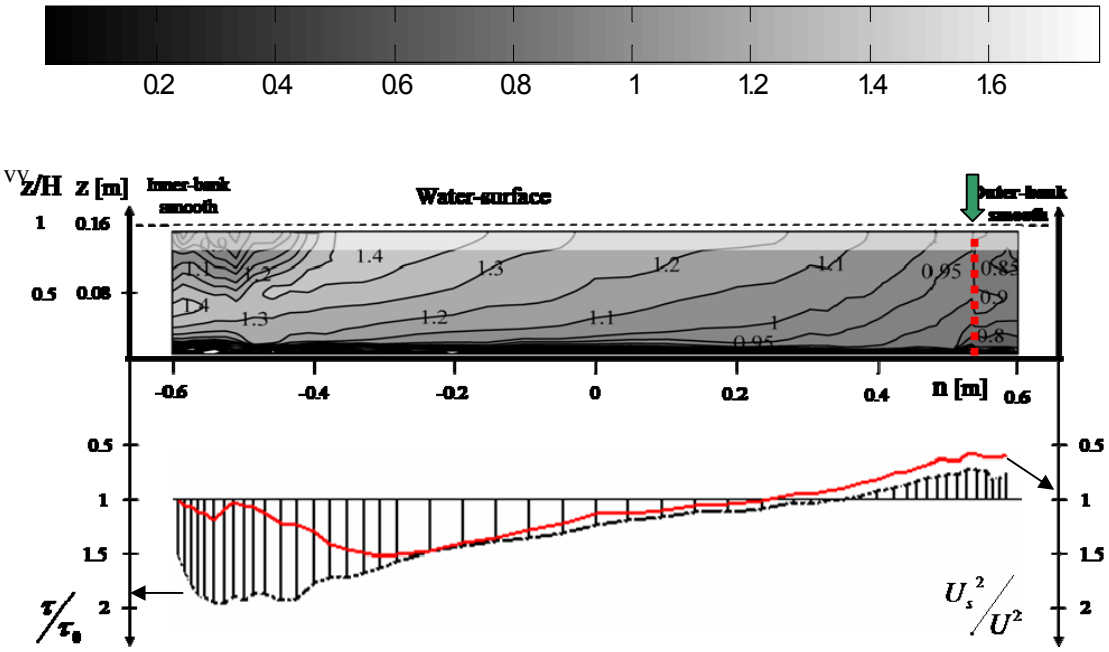

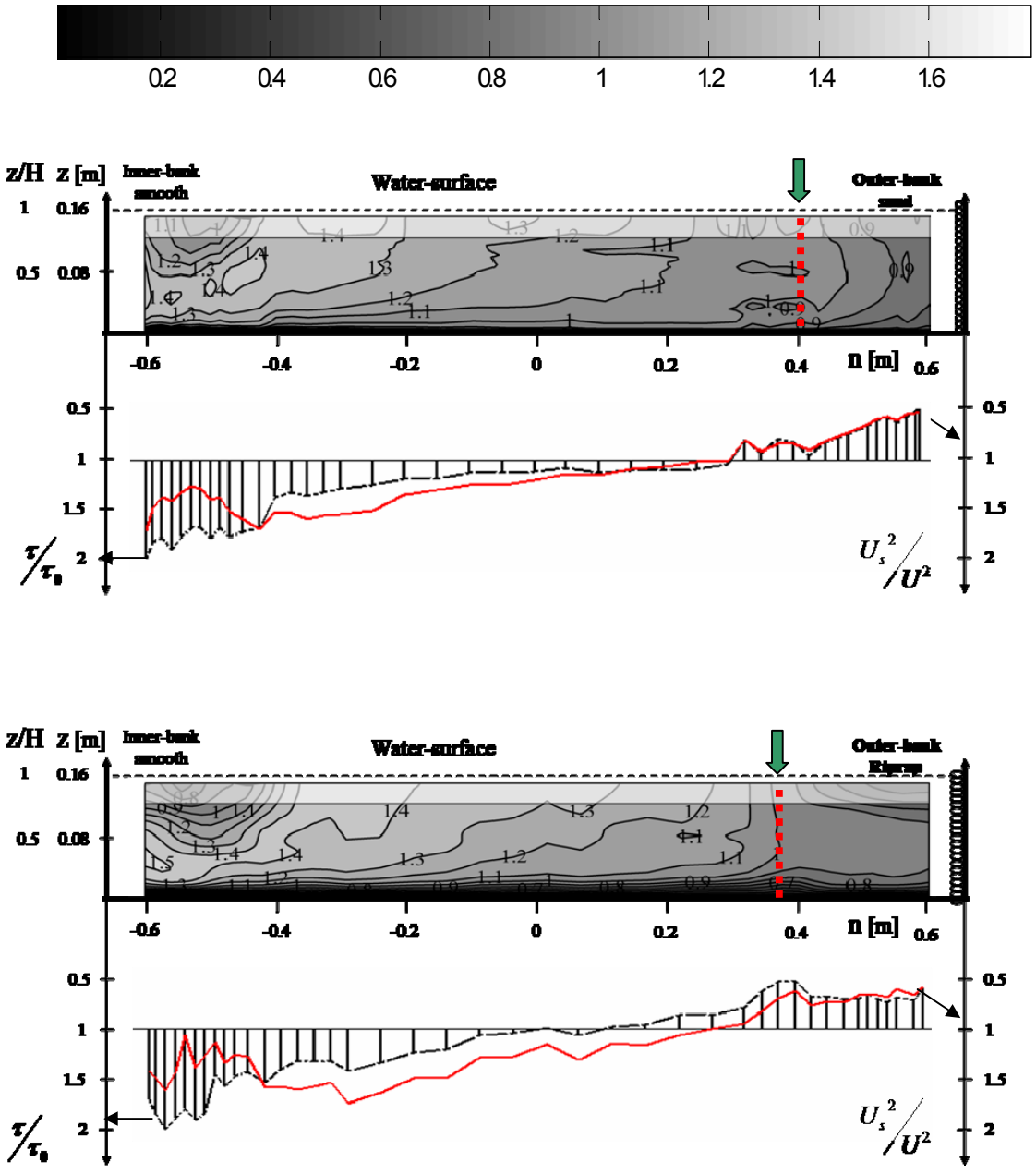

Figure 10
Cross-section at 90°. Isolines of normalized downstream velocity v_s/U, depth-averaged downstram velocity U_s^2/U^2 (red line) and boundary shear stress distribution τ/τ_o.
F16_90_00 (Top); F16_90_02 (Middle) and F16_90_30 (Bottom).

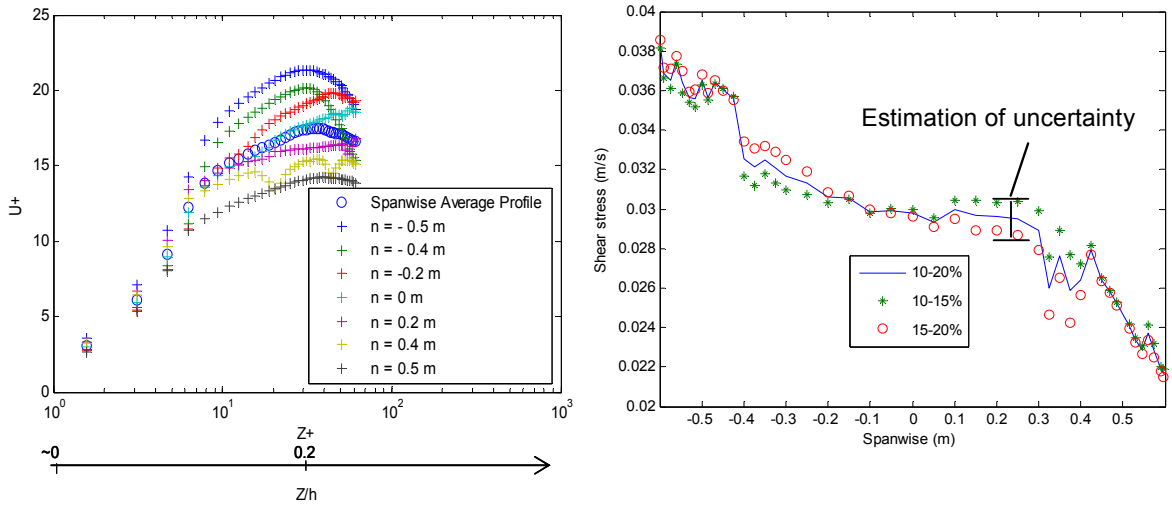

a) b)

Figure 11
a) Log-law plots of mean velocity in the spanwise direction over the width
b) Spanwise bed shear stress evolution obtained from loglaw as function of water-depth intervals

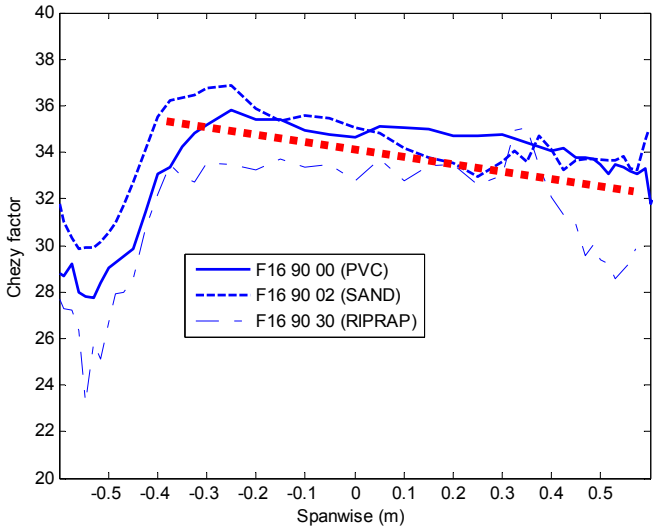

Figure 12
Chezy factor spanwise evolution
(- F16_90_00; * F16_90_02; F16_90_30)

3.5 Patterns of normalized turbulent kinetic energy in the cross-section at 90°

Figures 13 show the normalized turbulent kinetic energy, k/u_*^2, where $k = 0.5*\left(\overline{v_s'^2} + \overline{v_n'^2} + \overline{v_z'^2}\right)$. For all experiments a rather strongly reduced turbulence activity is seen near the outer bank over the OBC zone. The reduced activity is in agreement with Blanckaert & de Vriend (2004). The maximum k/u_*^2 values are located at CRC center and at separation of both cells (dashed line). The k/u_*^2 isolines are different from those measured in straight channel. In curved flow the k/u_*^2 values are higher and lower in the central and outer-bank zones, respectively, than in straight channel. So besides the lower downstream velocity in the vicinity of the outer-bank low turbulence values are also generated in the OBC zone. With increasing outer-bank roughness the maximum k/u_*^2 located close to the water-surface in the outer-bank zone shifts inwards as the separation of both cells locus (Figure 8).

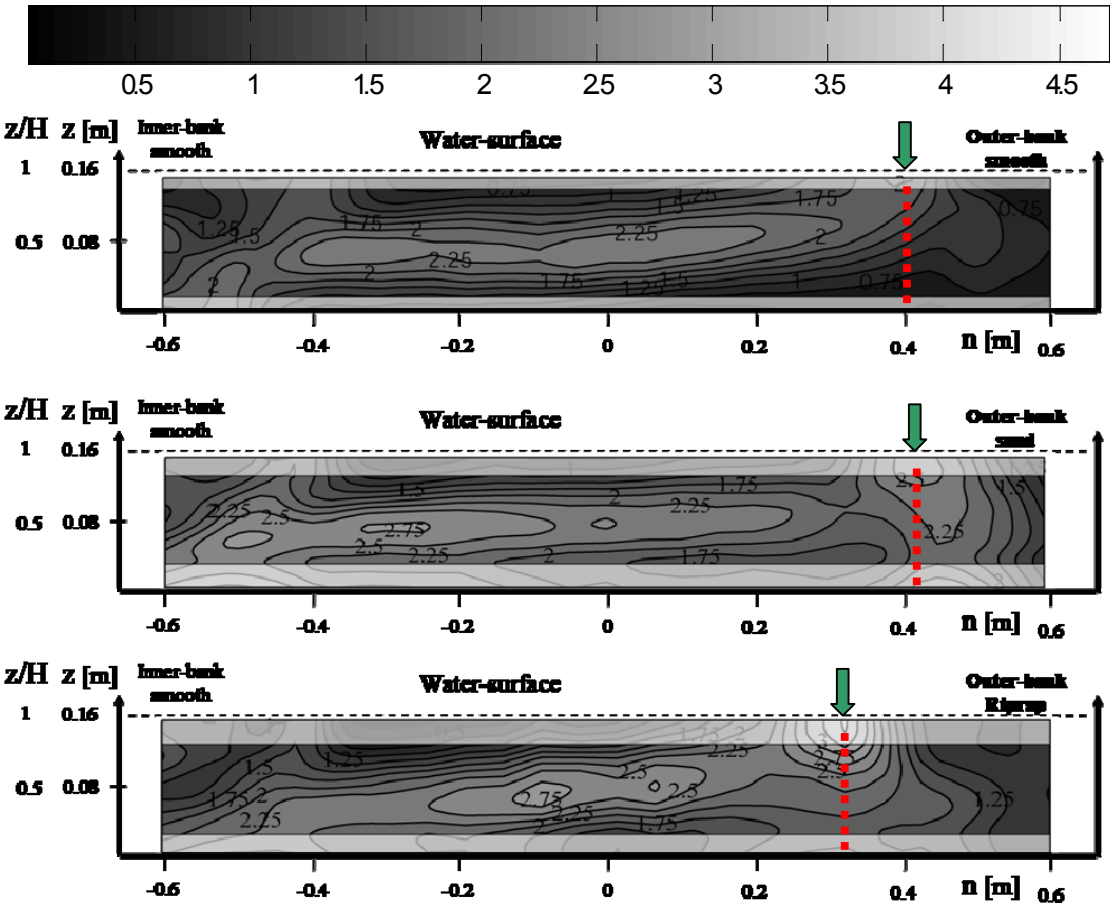

Figure 13

Cross-section at 90°. Isolines of normalized turbulent kinetic energy, k/u_*^2.
F16_90_00 (Top); F16_90_02 (Middle) and F16_90_30 (Bottom).

3.6 Patterns of normalized normal stress difference in the cross-section at 90°

Figure 14 shows the normalized normal stresses difference, $\left(\overline{v_n'^2} - \overline{v_z'^2}\right)/u_*^2$, which is known to be relevant with respect to the generation mechanisms of the OBC, Nezu and Nakagawa (1993). $\left(\overline{v_n'^2} - \overline{v_z'^2}\right)/u_*^2$ reflects the boundary conditions. In the regions close to the free-surface and bottom the vertical fluctuations are damped whereas close to the walls the transverse fluctuations are damped. Figure 14 shows that $\overline{v_n'^2}$ is always higher than $\overline{v_z'^2}$ even in the outer-wall zone, which is not in agreement with Tominaga et al. (1989). This fact is attributed to the $\overline{v_z'^2}$ underestimation by the measurements (Chapter II). The maximum values are at the same locations of k/u_*^2 maximums. The maximum value in the outer-bank zone varies with outer-bank roughness. It shifts inwards with increasing outer-bank roughness.

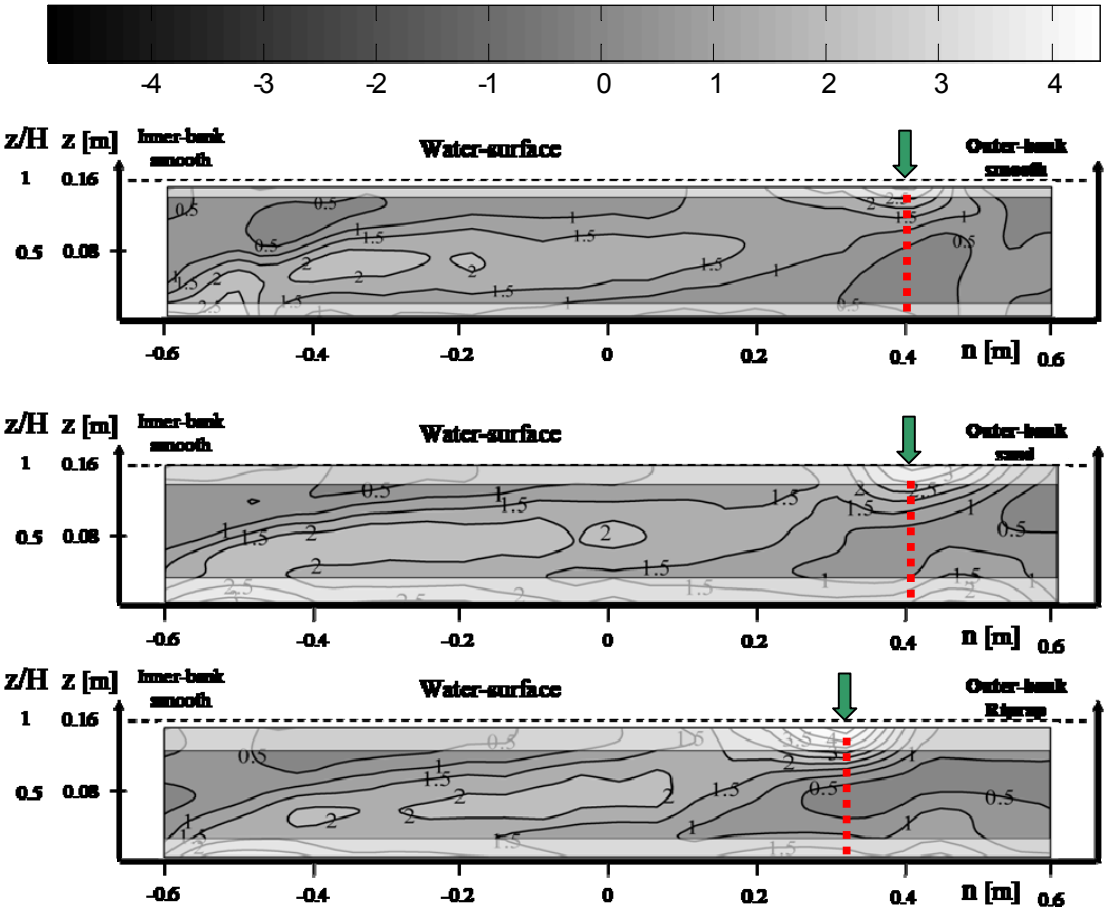

Figure 14
Cross-section at 90°. Isolines of normalized turbulent normal stress difference
F16_90_00 (Top); F16_90_02 (Middle) and F16_90_30 (Bottom).

3.7. Patterns of normalized cross-stream $\overline{v_n' v_z'}/u_*^2$ in the cross-section at 90°

Figures 15 shows high values of the normalized Reynolds shear stresses $\overline{v_n' v_z'}/u_*^2$ are located at the CRC center for all experiments. With increasing outer-bank roughness the center-region $\overline{v_n' v_z'}/u_*^2$ high values zone decrease in size. CRC values are constant regardless the outer-bank roughness. OBC values are not clear due to its small magnitude or scatter. $\overline{v_n' v_z'}/u_*^2$ quality measurement is important for the flow dynamics analysis hereafter.

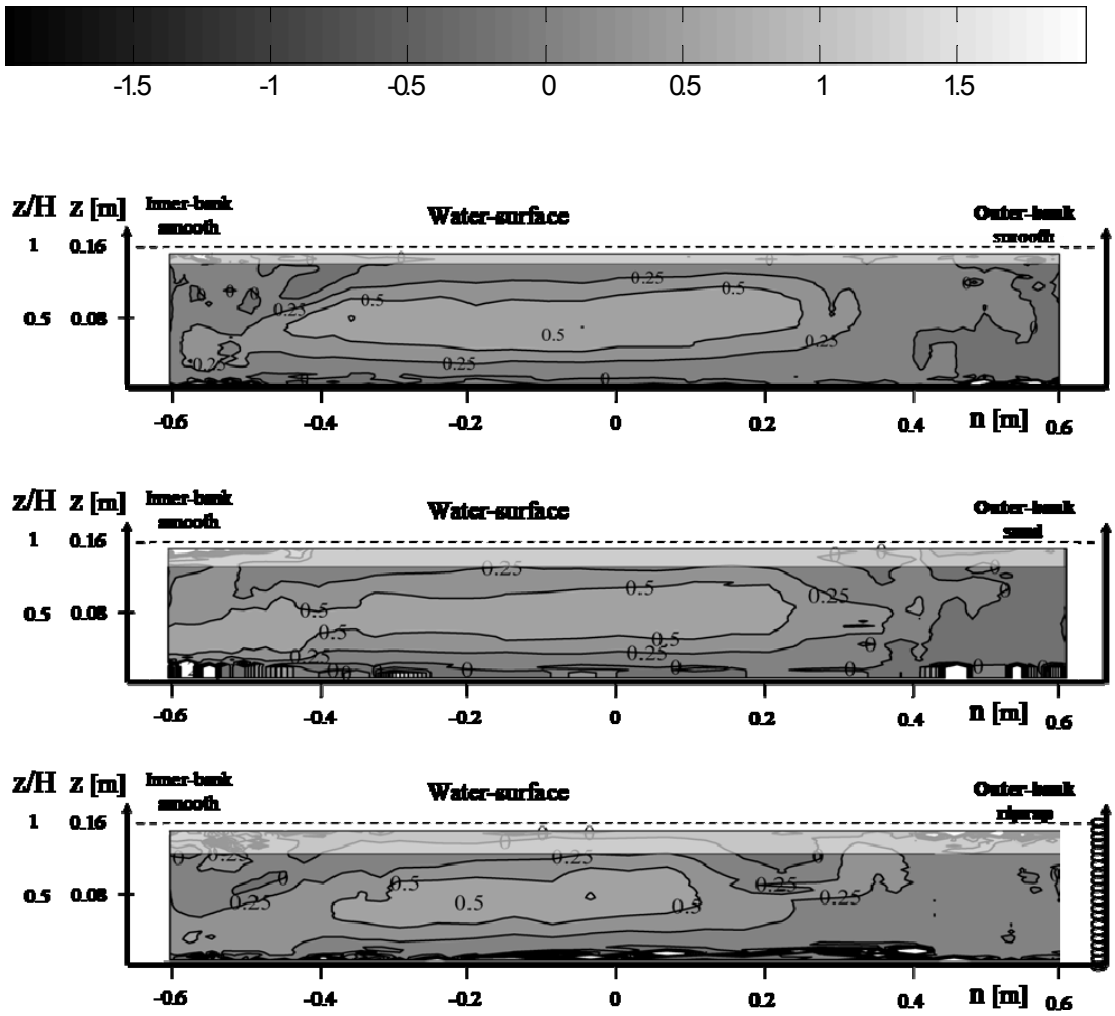

Figure 15

Cross-section at 90°. Isolines of turbulent shear stress $\overline{v_n' v_z'}/u_*^2$.

F16_90_00 (Top); F16_90_02 (Middle) and F16_90_30 (Bottom).

4 Mechanisms underlying circulation cells

In order to analyze the mechanisms underlying the cross-stream circulation cells the Blanckaert & de Vriend (2004) methodology is used, which consists of the analysis of the relevant terms of the downstream vorticity equation and the kinetic energy fluxes. The downstream vorticity equation, Equation (6), is obtained by cross-differentiation of the transverse and vertical momentum equations for incompressible flow (Schlichting & Gersten, 2000).

$$\frac{\partial \omega_s}{\partial t} = -\left(\frac{1}{1+n/R} v_s \frac{\partial \omega_s}{\partial s} + v_n \frac{\partial \omega_s}{\partial n} + v_z \frac{\partial \omega_s}{\partial z} \right)$$
$$+ \frac{1}{1+n/R} \omega_s \frac{\partial v_s}{\partial s} + \left[\omega_n \frac{\partial v_s}{\partial n} + \omega_z \frac{\partial v_s}{\partial z} + \frac{1}{1+n/R} \frac{v_n w_s}{R} - \frac{1}{1+n/R} \frac{v_s w_n}{R} \right] - \frac{1}{1+n/R} \frac{\partial}{\partial z} \left(\frac{\overline{v_s'^2}}{R} \right)$$
$$+ \frac{\partial^2}{\partial z \partial n} \left(\overline{v_n'^2} - \overline{v_z'^2} \right) + \frac{1}{1+n/R} \frac{1}{R} \left(\overline{\frac{\partial v_n'^2}{\partial z}} \right) + \left(\frac{1}{1+n/R} \frac{\partial^2}{\partial z^2} - \frac{\partial}{\partial n} \left(\frac{1}{1+n/R} \frac{\partial}{\partial n} \right) \right) \left((1+n/R) \overline{v_n' v_z'} \right)$$
$$+ \upsilon \left(\nabla^2 \omega_s + \frac{2}{(1+n/R)^2} \frac{1}{R} \frac{\partial \omega_n}{\partial s} - \frac{1}{(1+n/R)^2} \frac{1}{R^2} \omega_s \right) \qquad (6)$$

The dominant terms are indicated by rectangles. The terms from second line represent skewing induced vorticity redistribution by quasi-inviscid deflection of existing mean vorticity. Through several operations (e.g. Blanckaert & de Vriend, 2004) these terms are transformed into:

$$- \frac{1}{1+n/R} \frac{\partial}{\partial z} \left(\frac{v_s^2}{R} \right) + \frac{1}{1+n/R} \frac{v_n \omega_s}{R} + \left[\frac{1}{1+n/R} \frac{\partial v_n}{\partial s} \frac{\partial v_s}{\partial z} - \frac{\partial v_z}{\partial s} \frac{\partial}{\partial n} \left(\frac{1}{1+n/R} v_s \right) \right] \qquad (7)$$

Inside the rectangle the centrifugal force (CT) is indicated.

The third line represents the influence of cross-stream turbulent stress components on the vorticity field. The first term in the left is the cross-stream turbulent anisotropy term (CSTA) and the last term is the cross-stream shear term (CSS).

Blanckaert and de Vriend (2004) have postulated that the energy fluxes per unit mass between mean flow and turbulence play an important role with respect to the generation of the OBC. These fluxes take place through work done by the turbulent stresses as the

mean flow deforms. The sum of these energy fluxes is defined by (Batchelor 1970, p.600):

$$P = -\left[\left(\overline{v_s'^2} - \frac{2}{3}k\right)e_{ss} + \left(\overline{v_n'^2} - \frac{2}{3}k\right)e_{nn} + \left(\overline{v_z'^2} - \frac{2}{3}k\right)e_{zz} + 2\overline{v_s'v_n'}e_{sn} + 2\overline{v_s'v_z'}e_{sz} + 2\overline{v_n'v_z'}e_{nz}\right] \quad (8)$$

wherein e_{ij} (i,j = s,n,z) are the strain rates. P is mostly positive, the mean flow looses energy to turbulence.

The $2\overline{v_n'v_z'}e_{nz}$ term (within a rectangle) is shown hereafter as it is linked to the circulation cells.

4.1 Patterns of normalized centrifugal term in the cross-section at 90°

Figure 16 shows the patterns of the normalized centrifugal term, $CT/\left(U^2/H^2\right)$. The $CT/\left(U^2/H^2\right)$ is positive in the upper inner part of the channel due to the maximum downstream velocity mid-depth location in that flow zone, see Figure 10. The $CT/\left(U^2/H^2\right)$ is negative when integrated over the depth in the central part of the cross-section. The negative $CT/\left(U^2/H^2\right)$values are in compliance with the CRC rotation for all experiments (see the downstream vorticity patterns, Figure 9). In the upper outer part of the cross-section $CT/\left(U^2/H^2\right)$ values are positive as the maximum downstream velocity is at mid-depth. In the lower outer-part $CT/\left(U^2/H^2\right)$ values are negative in the LOBC zone. Hence $CT/\left(U^2/H^2\right)$ favors all cells.

$CT/\left(U^2/H^2\right)$ 0–contour isoline in the upper outer bank zone shifts inwards with increasing outer-bank roughness being in agreement with the shift inwards of all cells. In the channel center $CT/\left(U^2/H^2\right)$ values do not vary (differences within the experimental uncertainty) whereas in the OBC zone $CT/\left(U^2/H^2\right)$ values increase significantly as they are 0.2, 0.5 and 2 for F6_90_00, F16_90_02 and F16_90_30, respectively.

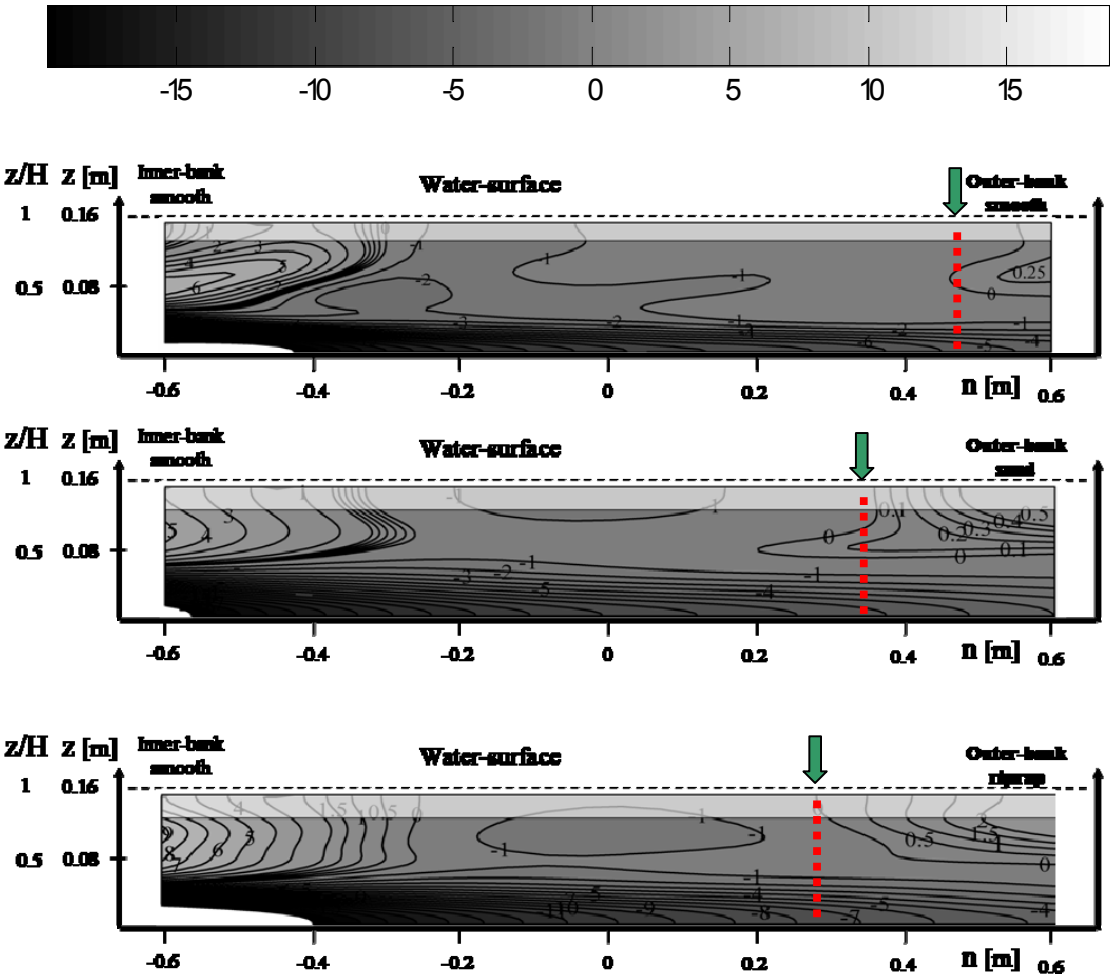

Figure 16

Cross-section at 90°. Isolines of normalized centrifugal term, $CT/\left(U^2/H^2\right)$

F16_90_00 (Top); F16_90_02 (Middle) and F16_90_30 (Bottom).

4.2 Patterns of normalized cross-stream anisotropy terms in the cross-section at 90°

Figure 17 shows normalized cross-stream turbulence anisotropy term $CSTA/\left(U^2/H^2\right)$. It is negative in the flow separation zone. It is slightly positive in the central part of the cross-section which does not favor the CRC. $CSTA/\left(U^2/H^2\right)$ presents a peak of positive values at the separation between the CRC and OBC. It is negative in the upper right part of the cross-section opposing the rotation sense of the OBC. $CSTA/\left(U^2/H^2\right)$ values are lower than $CT/\left(U^2/H^2\right)$ in the channel center although higher than $CT/\left(U^2/H^2\right)$ in the outer-bank.

With increasing outer-bank roughness the $CSTA/\left(U^2/H^2\right)$-0 isoline corresponding to the CRC and OBC separation moves inward (red dashed line). In the OBC zone $CSTA/\left(U^2/H^2\right)$ values do not increase with increasing outer-bank roughness. In the lower outer-bank zone positive $CSTA/\left(U^2/H^2\right)$ values zone widens with increasing outer-bank roughness.

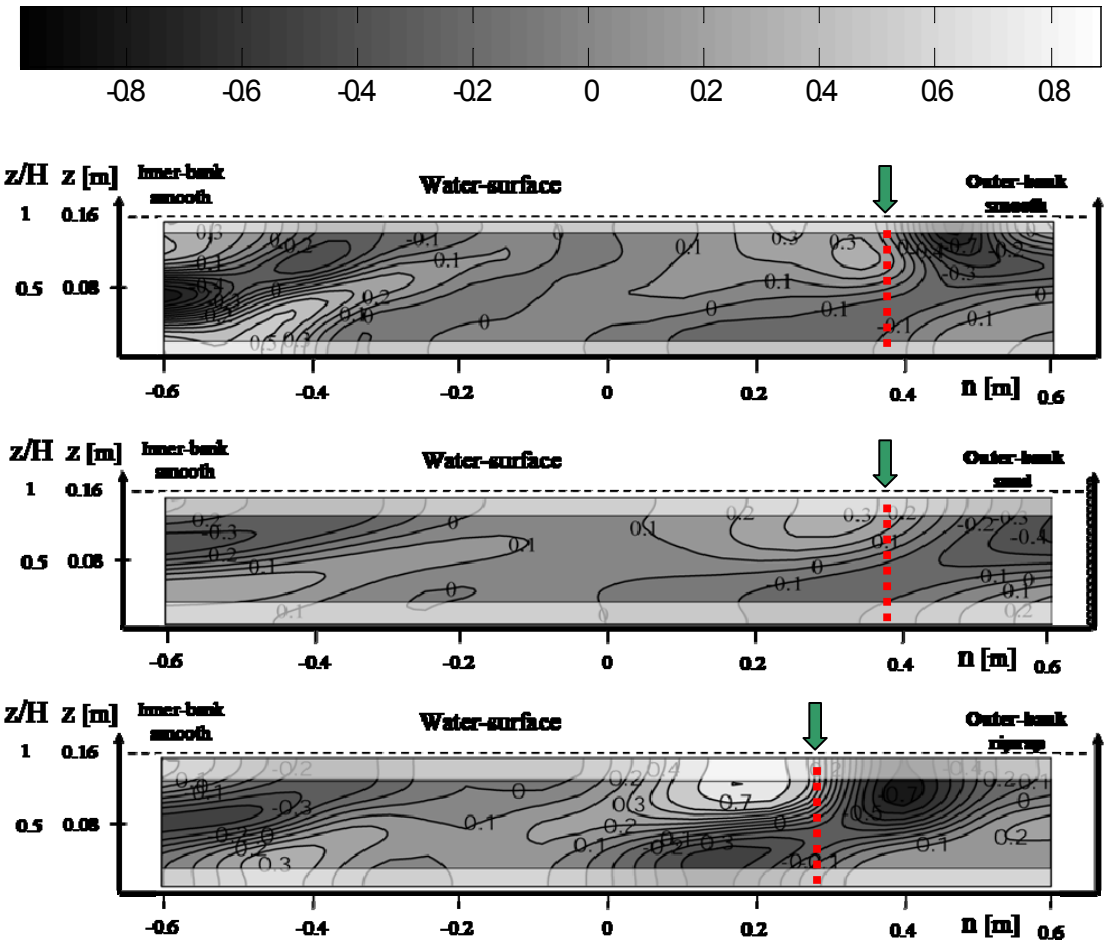

Figure 17

Cross-section at 90°. Isolines of normalized cross-stream turbulence anisotropy term $CSTA/\left(U^2/H^2\right)$ PVC F16_90_00 (Top); F16_90_02 (Middle) and F16_90_30 (Bottom).

4.3 Patterns of normalized cross-stream shear stress terms in the cross-section at 90°

Figure 18 shows patterns of normalized CSS by $\frac{U^2}{H^2}$. $CSS/\left(U^2/H^2\right)$ is opposed to the CRC and does not vary with outer-bank roughness within the uncertainty (Blanckaert & de Vriend 2004). The magnitude of this term is similar to $CT/\left(U^2/H^2\right)$ and so higher

than $CSTA/\left(U^2/H^2\right)$ in the channel center. $CSS/\left(U^2/H^2\right)$ is equal to $CT/\left(U^2/H^2\right)$ and $CSTA/\left(U^2/H^2\right)$ in the OBC zone. So, OBC is favored by $CSS/\left(U^2/H^2\right)$ in F16_90_00 and F16_90_02 experiments. However, in F16_90_30, $CSS/\left(U^2/H^2\right)$values are negative and so do not favor the OBC rotation sense.

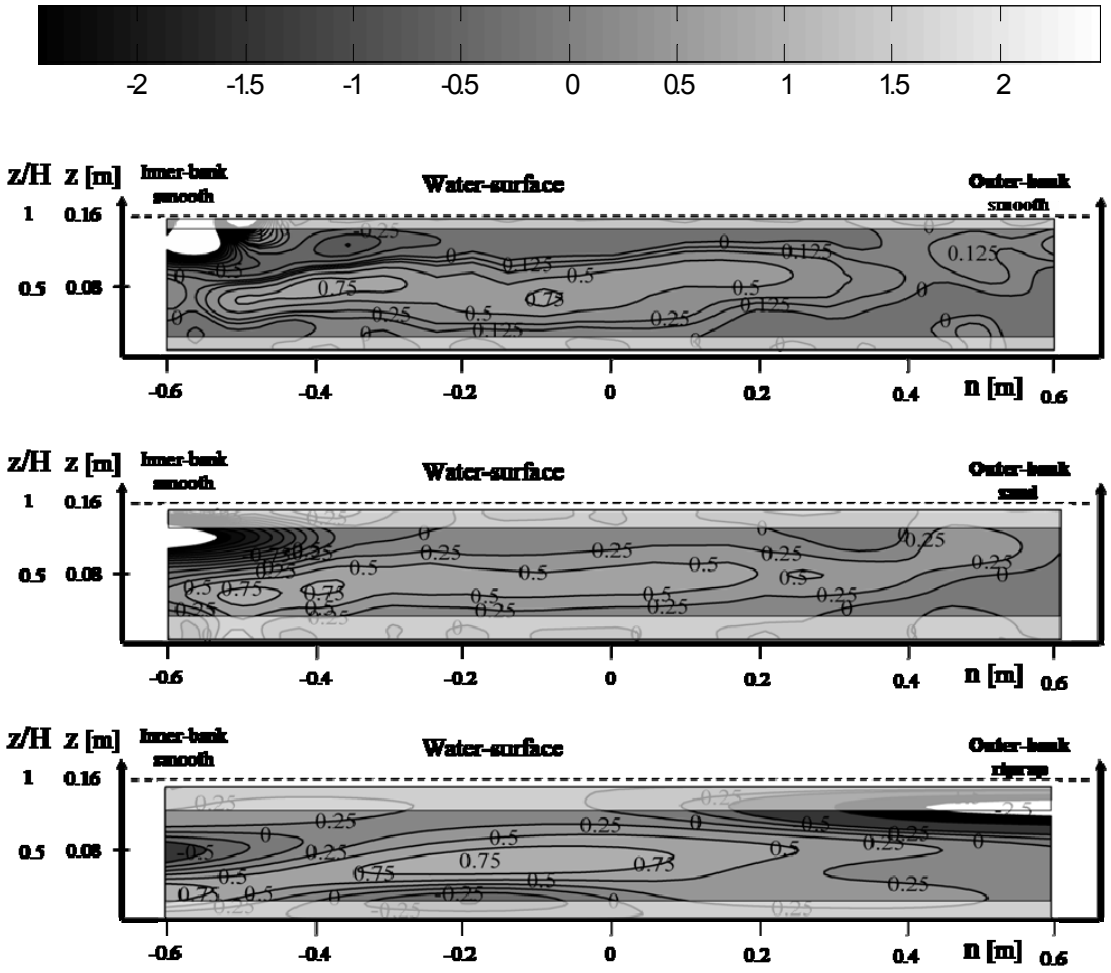

Figure 18

Cross-section at 90°. Isolines of normalized cross-stream turbulence shear stress term $CSS/\left(U^2/H^2\right)$ PVC F16_90_00 (Top); F16_90_02 (Middle) and F16_90_30 (Bottom).

4.4 Patterns of normalized cross-stream kinetic energy fluxes in the cross-section at 90°

Figure 19 shows normalized cross-stream kinetic energy fluxes via $\overline{v_n' v_z'}$ (cf. Equation 9) by $\left(u_*^3/H\right)$. High kinetic energy fluxes from mean flow to turbulence are observed in the CRC. In the OBC, kinetic energy fluxes are very small, which is in agreement with Blanckaert and de Virend (2004). Therefore, kinetic energy fluxes between turbulence

and mean flow in both senses exist in the outer-bank zone. A linear closure model with a scalar eddy viscosity is not able to reproduce the transfer in both senses, and so incapable of simulating correctly an OBC. However, a non-linear turbulence models, based on a non-linear relationship between the turbulent stresses and strain rates, are able to reproduce near-bank cells in turbulent straight flow and in curved flow (e.g., Speziale 1987, Jia et al. 2001).

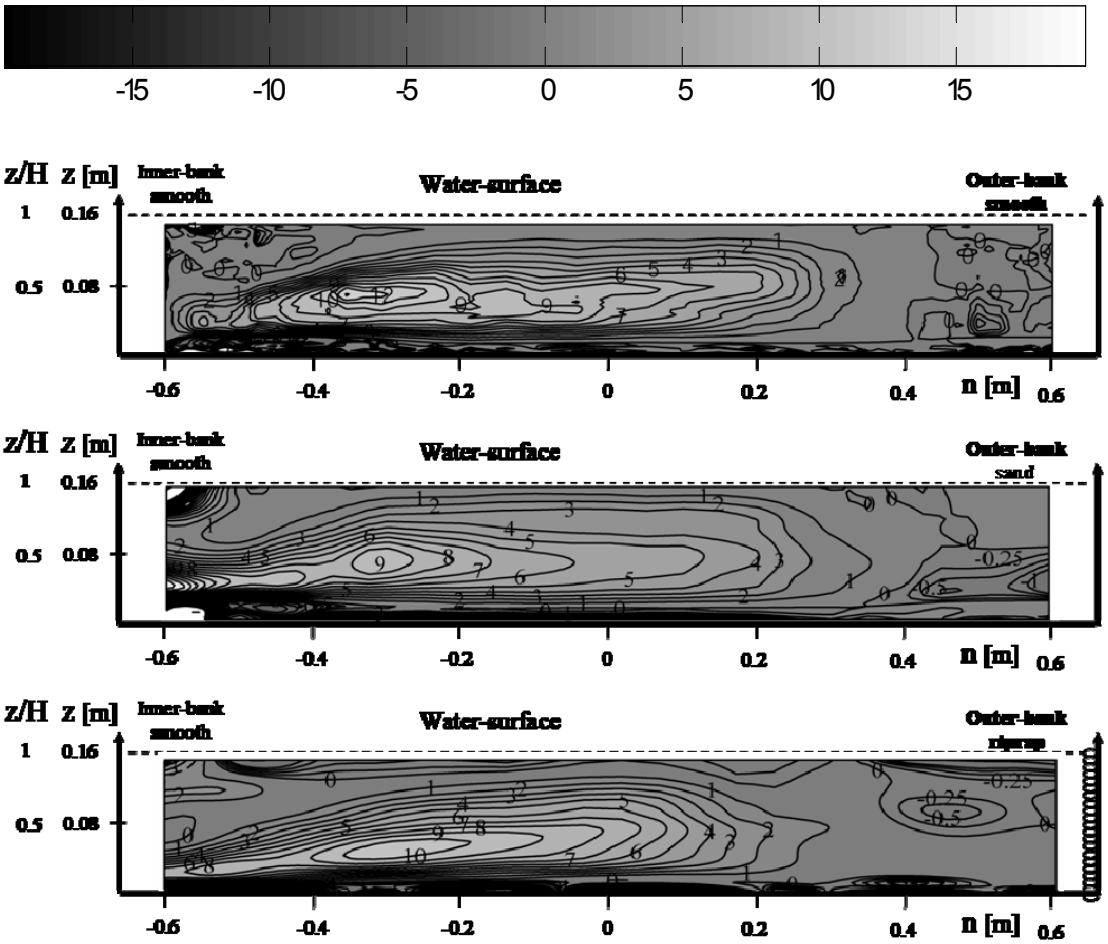

Figure 19

Cross-section at 90°. Isolines of normalized kinetic energy fluxes between mean flow and the turbulence via cross-stream turbulent stress, $\frac{2\overline{v_n' v_z'} e_{nz}}{\left(u_*^3 / H\right)}$

PVC F16_90_00 (Top); F16_90_02 (Middle) and F16_90_30 (Bottom).

4.5 Discussion

In order to understand the circulation cells patterns with varying outer-bank roughness the downstream vorticity equation and kinetic energy fluxes between mean flow and turbulence were analyzed as suggested by the Blanckaert & de Vriend (2004) methodology. Tables 3 and 4 summarize findings from Figures 9 and 16 to 19 of the relevant terms observed in the CRC and the OBC centers, respectively. The interpretation of these results takes into account the relatively high uncertainty in these terms due to the derivatives performed.

Table 3
Downstream vorticity equation relevant values and kinetic fluxes at CRC center

	$\omega_s H/U$ Figure 9	area/(BH)	$CT/\left(U^2/H^2\right)$ Figure 16	$CSTA/\left(U^2/H^2\right)$ Figure 17	$CSS/\left(U^2/H^2\right)$ Figure 18	$\frac{2\overline{v_n' v_z'} e_{nz}}{\left(u_*^3/H\right)}$ Figure 19
F16_90_00	**-0.75**	**0.46**	**-1**	**0.1**	**0.5**	**5**
F16_90_02	**-0.75**	**0.43**	**-1< CT <-0.5**	**0.1**	**0.5**	**5**
F16_90_30	**-0.75**	**0.34**	**-1**	**0.2**	**0.75**	**5**

Table 4
Downstream vorticity equation relevant values and kinetic fluxes at OBC center

	$\omega_s H/U$ Figure 9	area/(BH)	$CT/\left(U^2/H^2\right)$ Figure 16	$CSTA/\left(U^2/H^2\right)$ Figure 17	$CSS/\left(U^2/H^2\right)$ Figure 18	$\frac{2\overline{v_n' v_z'} e_{nz}}{\left(u_*^3/H\right)}$ Figure 19
F16_90_00	**0.25**	**0.06**	**0.25**	**-0.6**	**0.25**	**-0.1**
F16_90_02	**0.25**	**0.08**	**0.5**	**-0.6**	**0.25**	**<0**
F16_90_30	**0.5**	**0.14**	**2**	**-0.6**	**-2**	**-0.4**

Table 3 indicates that CRC is favored by CT (the same sign as ω_s) and opposed by CSS whereas CSTA is negligible. This is in agreement with simplified models for the CRC (e.g. van Bendegom, 1947, Rosovskii, 1957 or Blanckaert and de Vriend, 2004). The outer-bank roughness does not influence the mechanisms underlying the CRC. However the OBC widening due to outer-bank roughness variation narrows the CRC and so outer-bank roughness indirectly affects the CRC. Table 4 shows that the OBC strengthens and widens significantly with increasing outer-bank roughness. Table 4 also shows that OBC is favored by CT and opposed by CSTA for all experiments. CSS role is more complex as it favors OBC for F16_90_00 and F16_90_02 and not for F16_90_30. CSS negative values for F16_90_30 might be linked with high CT values in the OBC zone. Turbulent kinetic energy seems to also be restituted from turbulence (besides mean flow to turbulence sense) to mean flow via $v_n' v_z'$ which is in agreement with Blanckaert and de Vriend (2004) findings.

5 Conclusions

This paper analyzes the flow features occurring in a sharp open-channel bend of rectangular cross-section as function of outer-bank roughness.

The conclusions for the entire bend:

1) The maximum downstream velocity is advected by the center-region cell (CRC) from the inner bank at bed entrance towards the outer-bank at about bend exit regardless outer-bank roughness.

2) The depth-averaged downstream velocity at 15 cm from the bank toe along the bend varies as function of outer-bank roughness. With increasing outer-bank roughness the depth-averaged downstream velocity at 15 cm from the outer-bank decreases. This result suggests that scouring close to the wall could be reduced with increasing wall roughness.

The conclusions for the cross-section at 90°:

1) CRC and an outer-bank cell (OBC) with opposite rotation senses occur in all experiments. Moreover a lower outer-bank cell (LOBC) exists in the lower outer-bank zone with the CRC rotation sense.

2) With increasing outer bank roughness, the OBC widens and strengthens considerably. The OBC reveals its importance as downstream velocity and turbulence are reduced in the near-bank vicinity.

3) Chezy factor is not constant along the cross-section. It seems to decrease significantly in outwards direction for all experiments.

4) CRC is generated by centrifugal term (CT) and opposed by cross-stream shear term (CSS) and cross-stream turbulent anisotropy (CSTA). LOBC has the same underlying mechanisms. OBC is generated by CT and opposed by CSTA whereas CSS role is more complex as it could favor or not as function of outer-bank roughness.

5) Kinetic energy fluxes between mean flow and turbulence has a key role on the OBC generation in curved flows with rectangular channel. Positive and negative values are found in the OBC zone and so linear models are not able to simulate correctly the OBC and so confirming and extending Blanckaert & de Vriend (2004).

REFERENCES

Batcheleor, G.K. (1970). "An introduction to fluid dynamics." Cambridge Univ. press, Cambridge, U.K.

Bathurst, J.C., Throne, C.R. & Hey, R.D. (1979). "Secondary flow and shear stress at river bends." J. Hydr. Div., ASCE, 105 (10), 1277-1295.

Blanckaert, K., & Graf, W.H. (2001). "Mean flow and turbulence in open-channel bend." J. Hydr. Engng. 127(10):835-847.

Blanckaert, K. (2002). "Flow and turbulence in sharp open-channel bends." Ph.D dissertation No. 2545, Swiss Federal Institute of Technology, Lausanne.

Blanckaert, K., & de Vriend, H.J. (2003). "Non-linear modeling of mean flow redistribution in curved open channels." Water Resources Research, AGU, 39 (12):1375.

Blanckaert, K. & de Vriend, H.J. (2004). "Secondary flow in sharp open-channel bends." J. Fluid Mech., Cambridge Univ. Press, 498: 353-380.

Blanckaert, K. & Graf, W.H. (2004). "Momentum transport in sharp open-channel bends." J. Fluid Mech., Cambridge Univ. Press, Volume 130, Issue 3, pp. 186-198.

Blanckaert, K. & de Vriend, H.J. (2005). "Turbulence characteristics in sharp open-channel bends." J. Fluid Mech., Cambridge Univ. Press.

Blanckaert, K. & Lemmin, U. (2006). "Means of noise reduction in acoustic turbulence measurements." J.Hydr. Res., 44(1), 3-17.

Blanckaert, K. (2009). "Laboratory experiments on straight and sharply curved open-channel flows. Experimental techniques, data treatment and selected results." In preparation.

de Vriend, H.J. (1981) "Velocity redistribution in curved rectangle channels." J. Fluid Mech., Cambridge Univ. Press, Vol. 107(6), 429-439.

Einstein, H. A., & Li, H. (1958). "Secondary currents in straight channels." Trans. Am. Geophys. Union, 39 (6) , 1085-1088.

Gosh, S.N. & Roy, N. (1970). "Boundary shear stress distribution in open-channel flow." J. Hydr. Div., ASCE, 96(4), 967-994.

Hersberger, D. (2002). "Measurement of 3D flow field in a 90° bend with ultrasonic Doppler velocity." Proc.3th Int. Symp. ultrasonic Doppler Meth. for fluid Mech. and Fluid Eng., Lausanne, Switzerland, 59-66.

Hurther, D. & Lemmin, U. (2001). “A correction method for turbulence measurements with a 3-D acoustic Doppler velocity profiler.” J. Atm. Oc. Techn, Vol.18, 446-458.

Jia, Y., Blanckaert, K. & Wang, S.S. (2001). “Numerical simulation of secondary currents in curved channels.” Proc. 8th FMTM-congress, Tokyo.

Mockmore, C.A. (1943). “Flow around bends in stable channels.” Transactions, ASCE, Vol.109, 593-628.

Nezu, I., Nakagawa, H. & Tominaga, A. (1985). “Secondary currents in a straight channel flow and the relation to its aspect ratio.” Turbulent shear flows 4, Springer-Verlag., 246-290.

Nezu, I. & Nakagawa, H. (1993). “Turbulence in open-channel flows.” Balkema, Rotterdam, The Netherlands.

Perkins, H.J. (1970). “The formation of streamwise vorticity in turbulent flow.” J. Fluid Mech., 44(4), 721-740.

Prandtl, L. (1942) “Füher durch die Strömungslehre”. Vieweg, Braunschweig.

Rolland, T. (1994). “Dévelopment d’une instrumentation Doppler ultrasone adaptée à l’étude hydraulique de la turbulence dans les cannaux.” PhD dissertation N°. 1281, Swiss Federal Institute of Technology, Lausanne.

Rozowskii, I.L. (1957). “Flow of Water in Bends of Open-Channels.”Ac. Sc. Ukr. SSR, Isr. Progr. Sc.Transl., Jerusalem.

Shen, C. (1997). “An acoustic instantaneous particle flux profiler for turbulent flow.” PhD dissertation N°. 1630, Swiss Federal Institute of Technology, Lausanne.

Schlichting, H. & Gersten, K. (2000). “Boundary-Layer Theory.” 8th Edt, Springer, Berlin.

Speziale, C. G. (1987). “On nonlinear $k-l$ and $k-\varepsilon$ models of turbulence.” J. Fluid Mech.,178, 459-475.

Thorne, C. R. (1982). ‘‘Processes and mechanisms of river bank erosion.’’Gravel-bed rivers, R. D. Hey, J. C. Bathurst, et al., eds., Wiley, NewYork, 227–259.

Tominaga, A., Nezu, I., Ezaki, K. & Nakagawa, H. (1989). “Three-dimensional turbulent structure in straight open-channel flows.” J.Hydr. Res. 27,149-173.

van Bendegom, L. (1947). “Eenige beschouwingen over riviermorphologie en rivierverbetering.” De Ingenieur, 59(4), 1-11 (in Dutch).

CHAPTER IV

INFLUENCE OF OUTER-BANK INCLINATION ON HYDRODYNAMICS IN OPEN-CHANNEL BENDS

INFLUENCE OF OUTER-BANK INCLINATION ON FLOW PATTERNS IN OPEN-CHANNEL BENDS

ABSTRACT

In curved flows a center-region cell and a smaller and weaker counter-rotating cell in the upper outer-bank part are observed. For modeling the flow patterns in near-bank area both cells are of fundamental importance. Recently advances in the understanding of near-outer bank phenomena were obtained in rectangular channels, however, bank inclination variation effect on curved flows is still poorly known.

This paper investigates the influence of outer bank inclination on the flow pattern in a sharp laboratory open-channel bend. Three different cross-section geometries as function of varying outer-bank inclination (vertical, 45° and 30°) were investigated. Acoustic Doppler Velocity Profiler (ADVP) was used due to its three-dimensional velocity measurements with high-resolution capability.

In all measurements the pattern of cross-stream circulation is characterized by the existence of center-region cell and an outer bank cell. The results show that the outer-bank cell centre location is correlated with the outer-bank toe for most part of the bend. The outer-bank cell is analyzed via relevant downstream vorticity equation terms.

1 Introduction

Severe damages during floods are often caused by bank failure and lateral erosion. The most critical place for bank failure in a curved channel is the outer-bank due to the erosion process. Hence, it is fundamental to study curved flows with varying channel shapes to improve fluid mechanics knowledge and design practice.

Nine experiments covering three bank roughnesses and inclinations were made in order to systematically study the effect of outer-bank inclination and roughness on near outer-bank flow patterns (Table 1). The experiments cluster shown in Table 1 is part of a series of experiments on flow in open-channel bends that systematically investigate the influence of isolated parameters, such as curvature ratio, bank topography and bank characteristics (Blanckaert 2009) have been performed. Table 1 shows inside the ellipse the experiments presented in this paper. They enable the experimental investigation of curved open-channel flow characteristics as function of varying outer-bank inclination where the outer-bank was always made of smooth PVC.

Table 1
EPFL bend channel measurements
F16_45_00 stands for **f**lat bottom with **16 cm** of water-depth, **45°** outer-bank angle with the bottom and **00** the outer-bank k_{sw} equivalent roughness.

Inclination of outer bank ⇒ / ***Roughness of outer bank*** ⇓	30°	45°	90°
Smooth PVC	F16_30_00	F16_45_00	F16_90_00
k_s = 0.002 m (sand)	F16_30_02	F16_45_02	F16_90_02
k_s = 0.03 m (riprap)	F16_30_30	F16_45_30	F16_90_30

Curved flows major feature is the so-called center-region cell (CRC) generated by the interplay between centrifugal force and pressure gradient induced by the superelevation of the water surface (Rozovskii 1957). A second important cell is located in the upper outer-bank zone close to the water-surface known as outer-bank cell (OBC). OBC is generated by a different flow mechanism than the CRC. It is generated by the combination of turbulence driven and skewing induced mechanisms. The OBC has been investigated by several researchers (Bathurst et al. (1979), Thorne et al. (1985)) and more recently by Blanckaert and de Vriend (2004).

Blanckaert and de Vriend (2004) improved the knowledge on fluid dynamics in a curved flume as flow patterns, circulation cells and turbulence in a sharp bend were studied. Term-by-term evaluations of the relevant flow equation were made in order to understand the circulation cells, mainly the outer-bank cell mechanisms. They found out that OBC

protects the outer-bank by reducing downstream velocity and turbulence in near outer-bank area. They also found out that only turbulence models that simulate the energy transfer between mean flow and turbulence in both senses, i.e. anisotropic, are able to correctly simulate the OBC.

The circulation cells characteristics are fairly understood in a simple rectangular geometry. However, their response to varying channel shapes is still not clear. Some researches were made in this topic, such as, Ippen and Drinker (1962), and Yen (1965) Ghosh and Roy (1970), Naot (1983), Hicks et al. (1990) and Tominaga and Nagao (2002) where flow and shear stress in trapezoidal channels were investigated.

Two studies with similar goals to this paper are hereafter described. Tominaga and Nagao (2002) investigated the effects of cross-section shapes, trapezoidal and compound channels, on the circulation cells. The trapezoidal channels aspect ratio and the ratio of the curvature with the width were $B/H = 6$ and $R/B = 3$, respectively. They found that the OBC generated in narrow trapezoidal channels are smaller and less intense than in rectangular curved channel. Hicks et al. (1990) measure the shear and velocity distributions near a sloped bank in a 270° open channel bend in order to analyze the effect of sloped bank and the variation of the bank slope angle. They found an outward shift of the downstream velocity and shear stress on the sloped bank along the bend. From their measurements the bank toe reveals to be quite important on the cross-section flow patterns however the cross-stream cells were not measured.

This paper presents an investigation on curved open-channel flow characteristics as function of outer-bank inclination. The outer-bank inclination was varied between 90° (vertical), 45° (1:1) and 30° (1:2). The patterns of downstream and cross-stream flow velocities, the turbulent kinetic energy, the normal stresses anisotropy, the downstream vorticity, the downstream vorticity equation relevant terms and the kinetic energy transfer between mean flow and turbulence are presented and discussed.

Hence, the purpose of the experimental study was to provide data for a comprehensive analysis that allow answering the following questions:

- In a curved open-channel flow, how does the cross-section shape affect the downstream velocity along the bend?

- In a curved open-channel flow, how does the cross-section shape affect the circulation cells?

- In a curved open-channel flow, how does the cross-section shape affect the wetted perimeter shear stress distribution?

- What are the underlying mechanisms of the existing circulation cells?

2 Experiments

Experiments were carried out in a laboratory open-channel bend. It consists of a 9 m long straight entry reach, followed by a 193° bend with constant centerline radius of curvature of R=1.7 m and a 5 m long straight exit reach. The bend was originally rectangular in shape, 1.3 m wide, used in Experiment 1, the two others experiments were assembled by adding side slope of 30° and 45° inside the rectangular flume along the outside of the bank using flexible PVC. The inner bank was not slopped in order to achieve a wider channel as possible.

So the flume width at the bottom varied with outer-bank inclination 1.3 m, 1.14 m and 1.02 m, for 90°, 45° and 30° inclination of the outer-bank, respectively. The bed of the flume has glued quasi-uniform sediments of d = 0.002 m and the inner-bank and outer-bank were made of PVC for all experiments. The approach channel has a downstream bed slope of 0.22%, whereas the bed in the bend and out-flow is horizontal. Figure 1 shows the physical model.

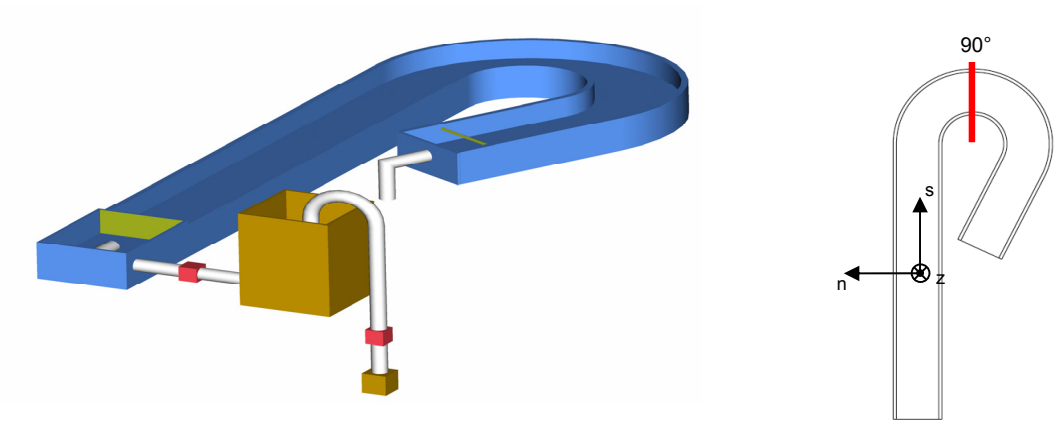

Figure 1 Experimental set-up

Table 2
Hydrodynamics conditions
Q is the flow discharge, H the flume-averaged flow depth, U is the flume averaged velocity, u_* is the flume averaged shear velocity (based on Hydraulic radius,R_h, and the average energy slope, E_s, $C = g^{1/2}(U/u_*)$ is the Chézy friction coefficient, $Re = UH/\nu$ is the Reynolds number, $Fr = U/(gH)^{1/2}$ the is Froude number, B is the flume width and Θ_{bank} the inclination of the outer bank.

Label	Q [ls^{-1}]	H [m]	U [ms^{-1}]	R_h [m]	u_* [ms^{-1}]	C [m$^{1/2}$s^{-1}]	E_s [‰]	Re [10^3]	Fr [-]	R/H [-]	B/H [-]	Θ_{bank} [°]
F16_90_00	89	0.159	0.43	0.128	0.037	36	1.1	69	0.33	10.3	8.1	90
F16_45_00	83	0.159	0.43	0.217	0.035	39	0.97	69	0.35	10.7	7.7	45
F16_30_00	78	0.157	0.43	0.121	0.035	40	0.93	68	0.35	10.8	7.4	30

Figure 2 shows the cross-section and the axis system wherein s-axis is in the downstream direction of the flow. z-axis zero is at the bed of the cross-section and increases towards

the free-surface. *n*-axis positive values are located in the outer-bank part of the channel. All three experiments have been investigated under similar hydraulic conditions with an overall mean velocity of $U \sim 0.43$ m/s and flow depth of $H \sim 0.16$ m.

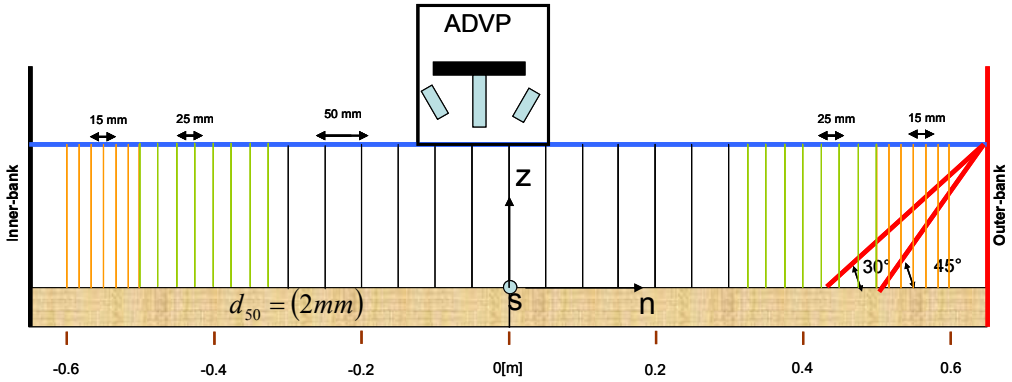

Figure 2 Cross-section measuring grids and shapes

Acoustic Doppler Velocity Profiler (ADVP), developed at EPFL (Rolland 1994, Shen 1997, Hurther 2001) enables three dimensional velocity non-intrusive measurements. ADVP permits the derivation of the mean velocity vector $\vec{v} = (v_s, v_n, v_z)$, fluctuating velocity vector, $\vec{v}' = (v_s', v_n', v_z')$ and all turbulent correlations $\overline{v_i'^a v_j'^b}$ (i,j=s,n,z; a and b are integers). The ADVP consists of four wide-angle receivers placed surrounding the central emitter. The emitter and receivers are placed in a water-filled housing that slightly touches the water surface hence the measurements are non-intrusive. The vertical profiles were divided into discrete cylindrical measuring volumes of size $(\pi \times 0.7^2/4) \times 0.3 = 0.12 cm^3$. The sampling frequency was 31.25 Hz and the acquisition time was 180 s. This enables a record length of 600 times the estimated macro time scales of the flow, (Nezu and Nakagawa, 1993). The measuring uncertainty for downstream velocity, v_s, and for cross-stream velocities, (v_n, v_z), is 4 % and 10 %, respectively, whereas 10 % for turbulent kinetic energy, k, 20 % for downstream vorticity and 40% for the downstream vorticity equation terms (Blanckaert & de Vriend, 2004). Details regarding the precision and accuracy of measurements made with ADVP and extrapolations and smooth procedures that enable the calculation of relevant downstream vorticity equation terms (some with double derivatives) are given in Blanckaert (2009).

3 Experimental results

3.1 Depth-averaged flow field

A coarse measuring grid was used along the bend. Vertical profiles were measured in the spanwise locations from n = -0.5 m to n = 0.5 m with 100 mm of interval. Flow in open-channel bends is highly non-uniform and spatially variable. To compare the experiments the cross-section with maximum cross-stream circulation for each experiment was chosen.

The normalized depth-averaged downstream velocity, U_s/U and the normalized strength of the cross-stream circulation, $\left\langle \tilde{f}_n^{\,2} \right\rangle$, respectively, for the three experiments are shown in Figures 3 and 4. $\left\langle \tilde{f}_n^{\,2} \right\rangle$ is defined based on the velocity decomposition

$$\left\langle \tilde{f}_n^{\,2} \right\rangle = \left\langle f_n^{\,2} \right\rangle * S_{circ} \tag{1}$$

where

$$f_n = \frac{v_n - U_n}{U_s \dfrac{H}{R}} = \frac{v_n^*}{U_s \dfrac{H}{R}} \tag{2}$$

here $\langle\ \rangle$ indicates depth-averaged results; v_n is the transverse velocity component; U_n its depth-averaged value; v_n^* is the transverse component of the cross-stream circulation; f_n is the normalized profiles of v_n^* respectively; S_{circ} is the sign of the cross-stream circulation strength used to label the rotation sense. The curvature ratio H/R has been included in the normalization of v_n^* since the strength of the cross-stream circulation is expected to increase with H/R (Rozovskii 1957).

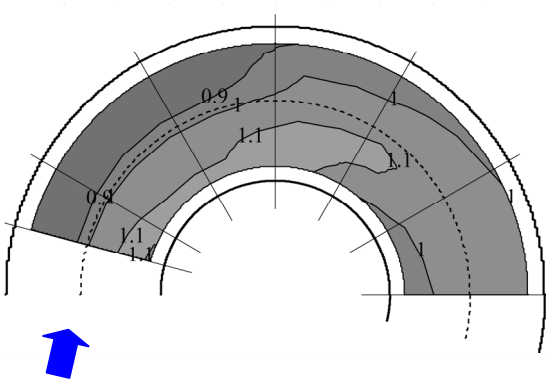

a) Outer-bank (vertical)

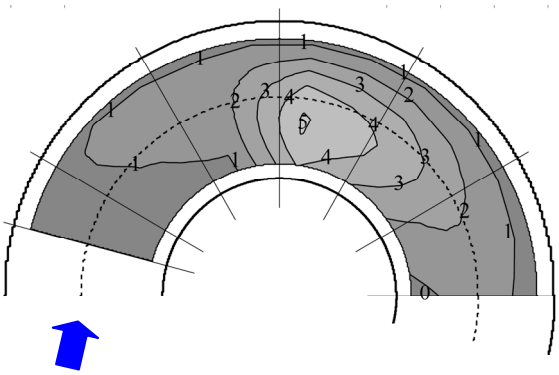

a) Outer-bank (vertical)

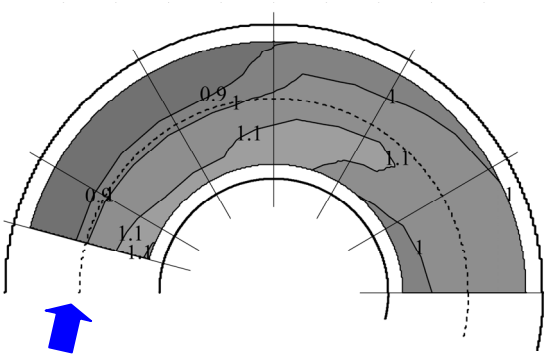

b) Outer-bank (1:1)

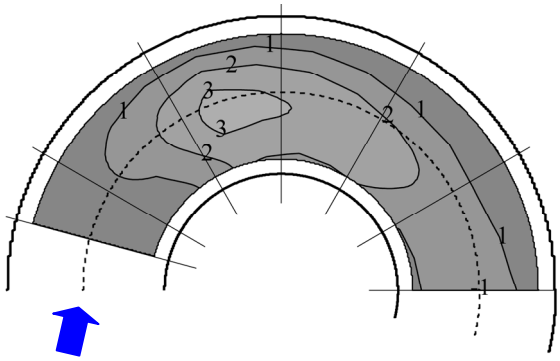

b) Outer-bank (1:1)

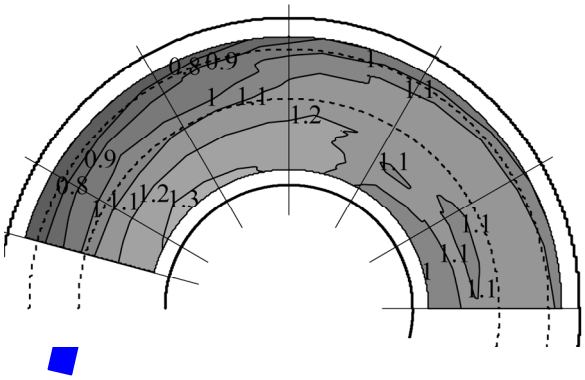

c) Outer-bank (1:2)

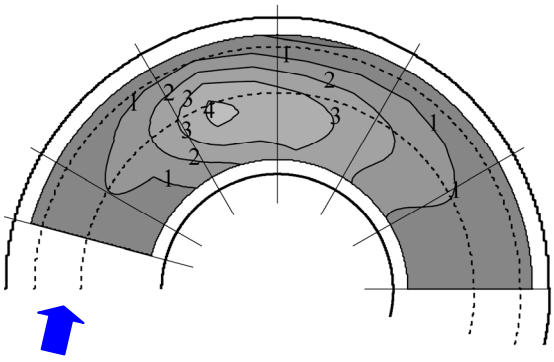

c) Outer-bank (1:2)

Figure 3 a b c)
Pattern of normalized downstream depth-averaged velocity , U_s/U

Figure 4 a b c)
Pattern of normalized cross-stream circulation strength, $\langle \tilde{f}_n^{\,2} \rangle$

a) F16_90_00 (vertical); b) F16_45_00 (1:1); c) F16_30_00 (1:2);

Figures 3 *abc* show the depth-averaged downstream velocity evolution along the bend wherein the core of maximum depth-averaged downstream velocity evolves from the inner bank at the bend entry, to the outer bank part at channel exit driven by the effects of circulation cells (Blanckaert and Graf 2004). Figure 4 *abc* show the strength of the CRC along the bend. For all experiments the maximum is located in cross-section at about 90° with $\left\langle \tilde{f}_n^{\,2} \right\rangle$ about 4, 4 and 3 at channel center for F16_90_00, F16_45_00 and F16_30_00, respectively. This is in contradiction with the "Rozovskii's model" which predicts about $\left\langle \tilde{f}_n^{\,2} \right\rangle \approx 10$ for all experiments. "Rozovskii's model" value is high as the computation of CRC strength is made adopting the straight-channel flow v_s profile and so neglecting the curvature flattening effect on the velocity profile (de Vriend, 1981).

To correct the linear model overestimation problem a non-linear model was developed, (Blanckaert & Graf, 2004).

$$\beta = \left[\left(\sqrt{g} / C \right)^{-2.2} \left(H / R \right)^2 \left(\alpha_s + 1 \right) \right]^{0.25} \qquad (3)$$

where C is the Chezy coefficient, H/R is the curvature ratio and $\alpha_s = \frac{\partial v_s}{\partial n} \frac{R}{U_s}$ is the transverse distribution of the downstream velocity.

Equation 3 values are about 1 for all experiments. The corresponding correction factor is about 0.5 which is obtained in Figure 7 in Blanckaert de Vriend, (2003). Multiplying the Rozovskii's model prediction and the correction factor a value close to the experimental measurement is obtained. So the non-linear model performs well even for sharp bends with quasi-homogeneous trapezoidal channels and outer-bank inclination of 30° and 45°, as well for sharp bends with rectangular channel.

The evolution of the outer-bank downstream depth-averaged velocities alongside the bend at n= 0.6 m, n= 0.5 m and n = 0.375 m for experiments F16_90_00, F16_45_00 and F16_30_00, respectively, is shown in Figure 5. For the half-trapezoidal experiments, F16_45_00 and F16_30_00, the depth-averaged velocity profiles compared are over the bank toe. F16_90_00 evolution is useful to compare the effect of bank inclination and so it is should be interpreted as reference.

Between cross-sections at 15° and 30° the depth-averaged downstream velocity is stable but from cross-section at 30° on it increases linearly onto cross-section at 180° for all experiments. Hence, the downstream velocity evolution over the bank toe is in agreement with Hicks et al. (1990). The location of the bank toe is important for trapezoidal channels (F16_30_00 and F16_45_00) because, regardless their bank slope angles, the depth-averaged downstream velocity values over the bank toe are similar. However, the downstream velocity close the bank toe is higher for the trapezoidal experiments than for rectangular channel. This observation is in agreement with Thorne (1995) where the vulnerability of bank basal zones in trapezoidal channels is referred.

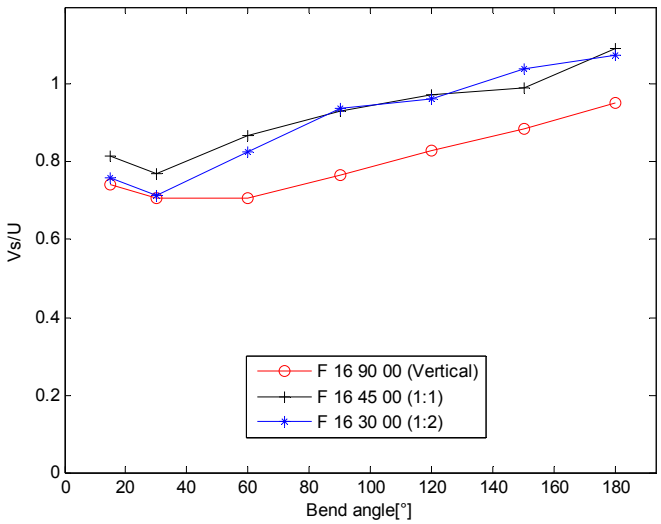

Figure 5
Depth-average downstream velocity evolution along the bend
Vertical bank 'o'; (1:1) bank '+' and (1:2) bank'*'

3.2 Patterns of cross-stream velocities in the cross-section at 90°

For each representative cross-section a refined grid of measurements was used. The vertical profiles are distributed with varying spanwise intervals, see Figure 2. In the central part of the channel, profiles are separated by 50 mm whereas in near-bank zones profiles were measured every 15 mm. In between the channel center and the near-bank zones 25 mm was taken, see Figure 2.

Figures 6 and 7*abc* show the isolines of the normalized transverse, v_n/U and vertical velocity v_z/U in the cross-section at 90° for the three experiments. Close to the free-surface and in some cases also close to the bottom extrapolations towards the free-surface or bottom were made, in such cases non-color contour zones are shown. Blanckaert (2009) gives details about those extrapolations.

The CRC is visible by the limits imposed by the maximum $v_z > 0$ and $v_z < 0$ in inner and outer-bank zones, respectively, and by the positive and negative v_n/U values in upper and lower water-depth channel center, respectively. The clockwise rotation cense of CRC is also observed by the v_n and v_z values. In the upper outer-bank part, the v_n/U sign is opposed to the upper channel central part and $v_z < 0$ $v_z > 0$ pair in the outer-bank suggest the presence of a counter-clockwise rotation cell, OBC, for all experiments (even for trapezoidal channels). Figures 6a and 7*a* also suggest the presence of a cell beneath the OBC in agreement with the findings of Bathurst et al. (1979) for bends with rectangular channels. The separation between the CRC and the OBC is approximatively defined by the core of maximum downward velocities, $v_z < 0$. In Figures 6 and 7 dashed lines were added to help visualize the separation between the circulation cells, and also their rotation sense. Figures 6*abc* and 7*abc* reveal that, with decreasing outer-bank slope, the CRC width diminishes whereas OBC shifts inwards maintaining constant size. The OBC center

is located over the bank toe for the half-trapezoidal experiments. Thus, the OBC is observed for all experiments which disagrees with Tominaga and Nagao (2002) work, where the OBC was only measured for curved flows with outer-bank slope higher than 45°.

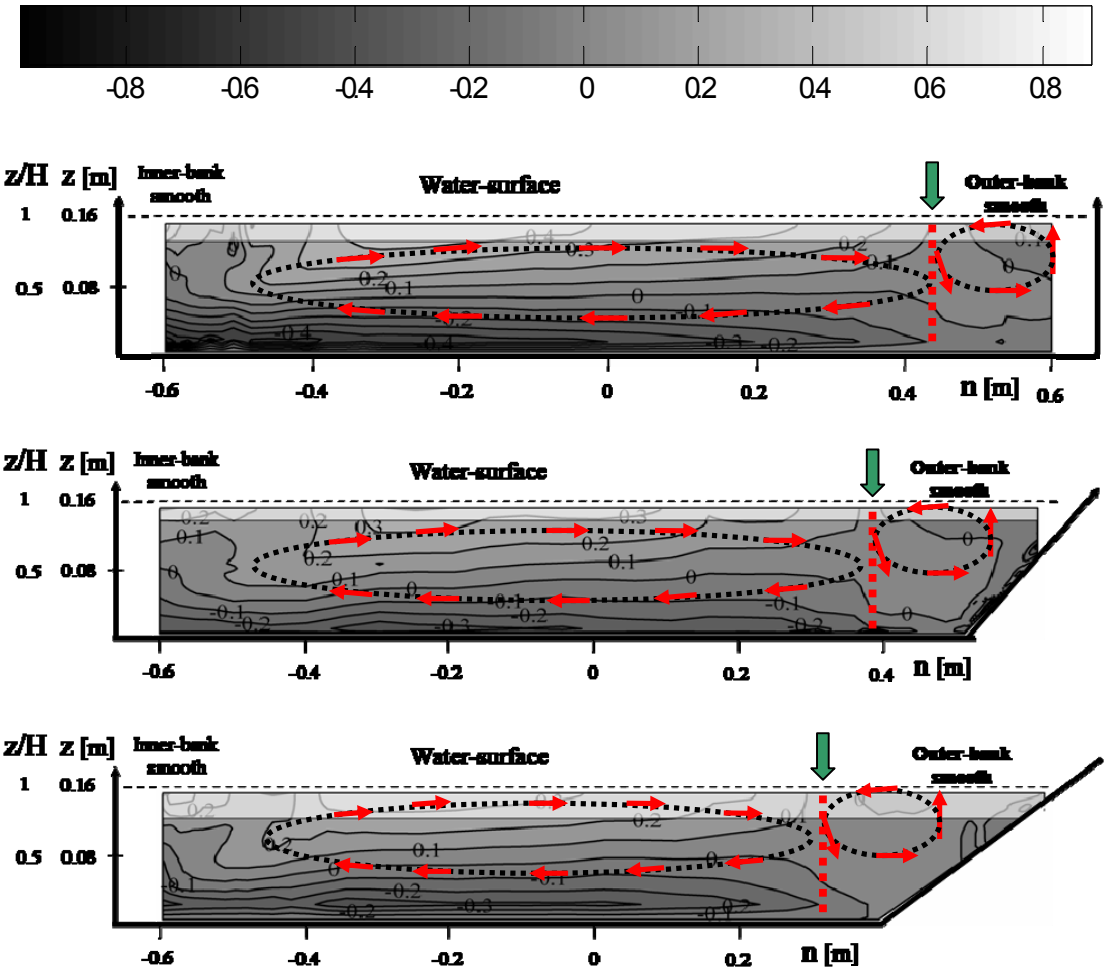

Figure 6.
Cross-section at 90°. Isolines of normalized transversal v_n/U.
F16_90_00 (Top); F16_45_00 (Middle) and F16_30_00 (Bottom).

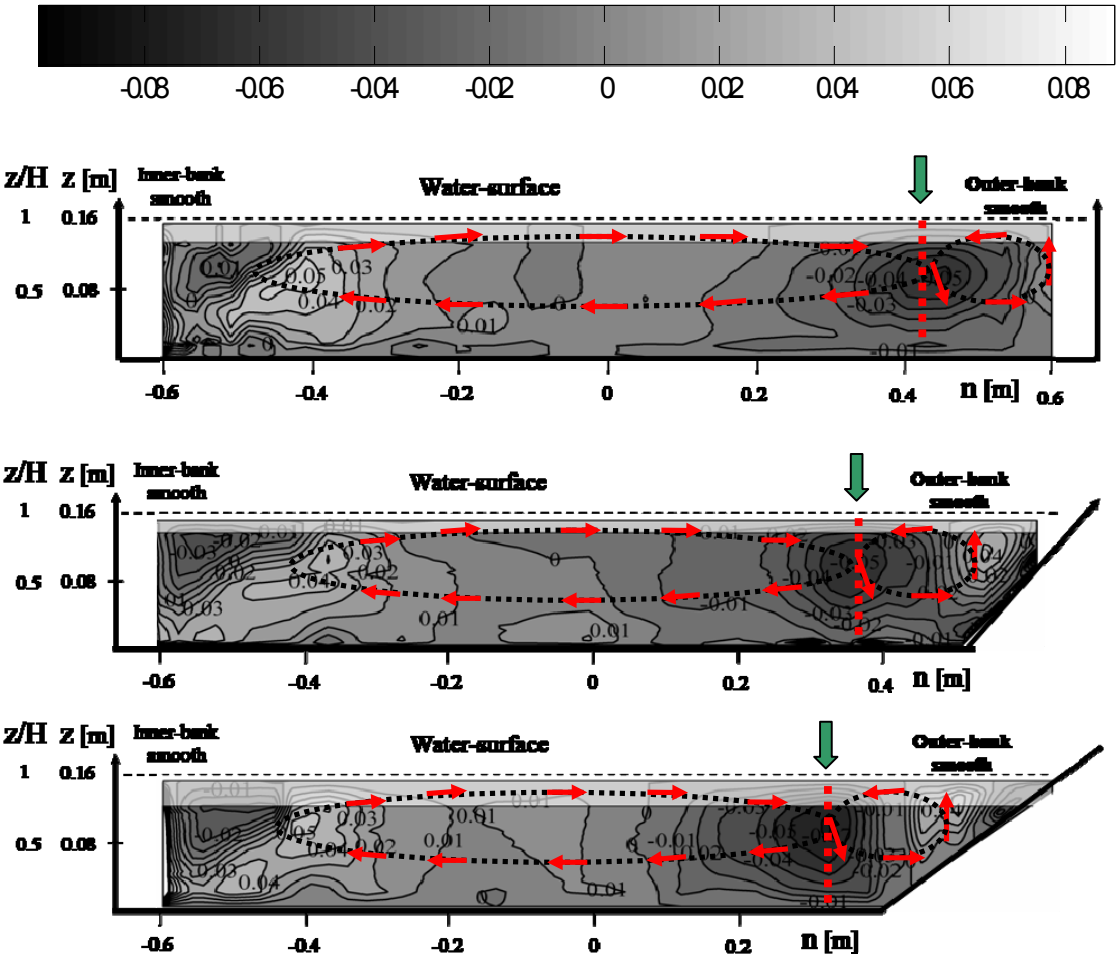

Figure 7.
Cross-section at 90°. Isolines of normalized vertical v_z/U.
F16_90_00 (Top); F16_45_00 (Middle) and F16_30_00 (Bottom).

3.3 Patterns of downstream vorticity in the cross-section at 90°

Figure 8 shows the normalized downstream vorticity, $\omega_s H/U$, where the CRC and the OBC are observed by the negative and positive values in the central and upper outer-bank zones. The maximum negative $\omega_s H/U$ values are located in the lower inward part. The negative $\omega_s H/U$ values spread over the cross-section except for the upper outward part. CRC and OBC are separated by the ω_s = 0-countour. OBC contour is well defined for all experiments.

With decreasing bank slope, the CRC size decreases although its magnitude is unaffected (except for F16_45_00 as the patterns were smoothened due to scatter). OBC moves inwards although with constant size. The OBC magnitude slightly decreases with decreasing bank slope which is in agreement with Tominaga and Nagao (2002). The OBC halts the CRC from reaching the outer-bank regardless its strength. Hence the CRC outward limit depends on the location of the OBC and not on its strength.

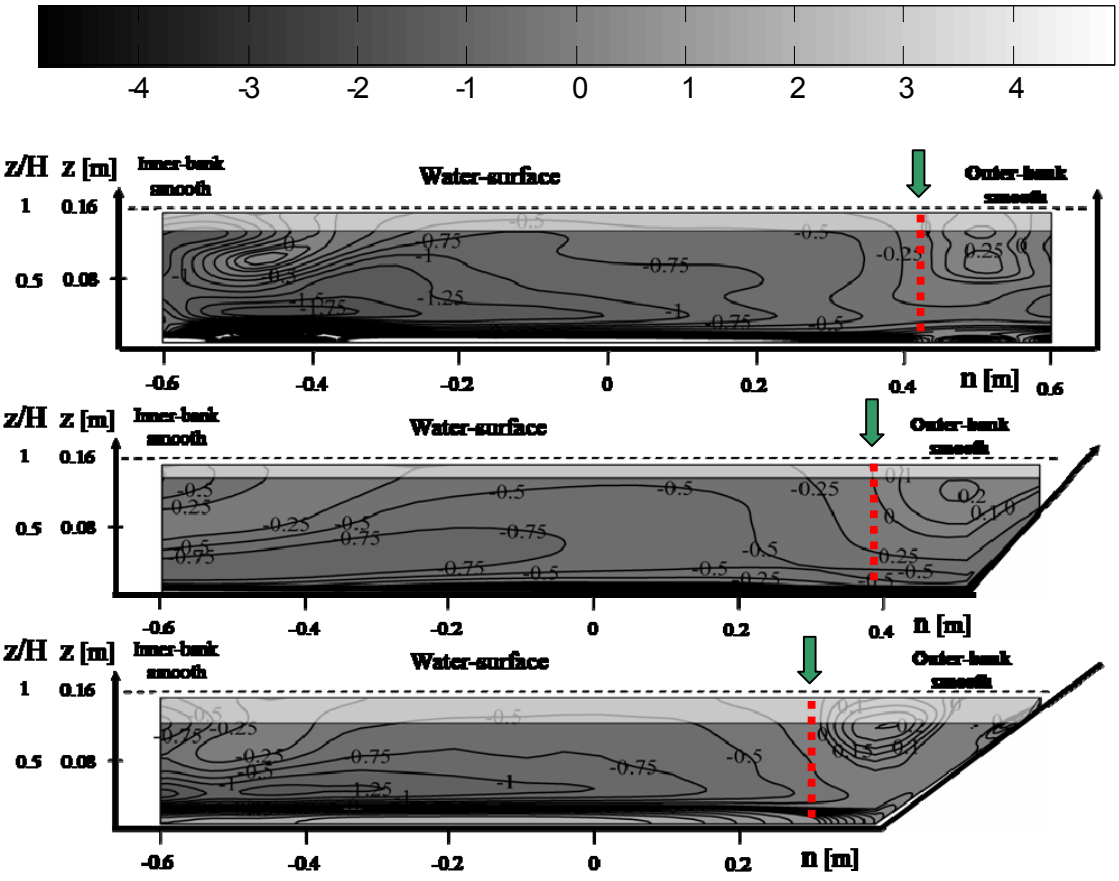

Figure 8

Cross-section at 90°. Isolines of normalized downstream vorticity $\omega_s H/U$.
F16_90_00 (Top); F16_45_00 (Middle) and F16_30_00 (Bottom).

3.4. Patterns of normalized downstream velocity, boundary shear stress, normalized depth- averaged downstream velocity and Chezy factor in the cross-section at 90°

The normalized downstream velocity, v_s/U, in the cross-section at 90° for the three experiments is shown in Figure 9. The maximum downstream velocity is still located in the lower inner bank therefore hardly affected by the slope of the outer-bank. The isolines reveal the presence of circulation cells. In the channel center the isolines are inclined outwards and so the CRC advects momentum in outward/inward direction in the upper/lower part of the water column. Vertical isolines near the water surface pinpoint the separation between CRC and OBC and the end of the CRC advection effect. With decreasing outer-bank slope the vertical isolines, which mark the separation between CRC and OBC, move inward following the bank toe.

The wetted perimeter shear stress distribution is also shown in Figure 9. It is estimated by fitting a logarithmic law of the wall (Equation 4) to the measured velocities. Figure 9 shows that cross-section shape does not influence the bed shear stress undulation range as the amplitude range is about $0.5\,\tau_0$ for all experiments. The normalized maximum outer-bank shear stress is located in different zones. For F16_90_00 the maximum shear-stress outer-bank value is located at mid-depth (where the downstream velocity is higher) whereas for F16_45_00 and F16_30_00 it is located close to the bank toe at about z/h = 0.2.

The logarithmic law of the wall method was used. Ghosh and Roy (1970) concluded that shear stresses distributions calculated from velocity profiles agreed well with those obtained from direct measurements and Nezu and Nakagawa (1993) states that shear stresses distributions calculated from velocity profiles are valid.

Equations 4 and 5 are used in the lowest 20% of the water-column due to the strong 3D flow present in a curved flow. The procedure used is explained in more detail in Chapter 1.

$$\frac{v_s}{u_*} = \frac{1}{\kappa}\ln\left(\frac{z}{z_0}\right) \tag{4}$$

$$\frac{v_s}{u_*} = \frac{1}{\kappa}\ln\left(\frac{y \cdot u_*}{\upsilon}\right) + 5.3 \tag{5}$$

where v_s is the velocity at a distance z from the boundary, u_* is the shear velocity or shear stress, κ is von-Kármán constant and $z_0 = {}^{k_s}\!/_{30}$ is the distance at which the log velocity profile indicates zero velocity.

Figure 10*ab* shows a linear relation in the semilogarithmic plot alongside spanwise direction and its average between normalized downstream velocity, $U^+ = v_s / u_*$, and the normalized vertical coordinate, $Z^+ = z/k_s$ over the bed and outer-bank. Hence, the applicability of this method in the lowest 20% of the water column is confirmed.

Figure 11*ab* shows spanwise shear stress evolution over the bed and inclined bank, respectively. The local shear stress is estimated three times from three different intervals 5-10%, 10-15% and 15-20% of *H,* respectively. Differences in these estimates suggest an uncertainty in the obtained boundary shear stress of about 15% which is in agreement with Nezu & Nakagawa (1993).

An important parameter to 2D depth-averaged numerical codes is the Chezy factor, Chezy factor is defined by Equation 6.

$$C = \sqrt{\rho g}\sqrt{\frac{U_s^2}{\tau_0}} \qquad (6)$$

The Chezy factor is mostly consider as constant factor in 2D simulations. Figure 12 shows that the Chezy factor is not constant over the bed for F16_90_00 and F16_45_00 whereas for F16_30_00 is constant over the central and outer parts of the bed. It seems that with decreasing bed slope the Chezy factor tends to a constant value over the bed (except in the inner bank zone for all experiments due to flow separation).

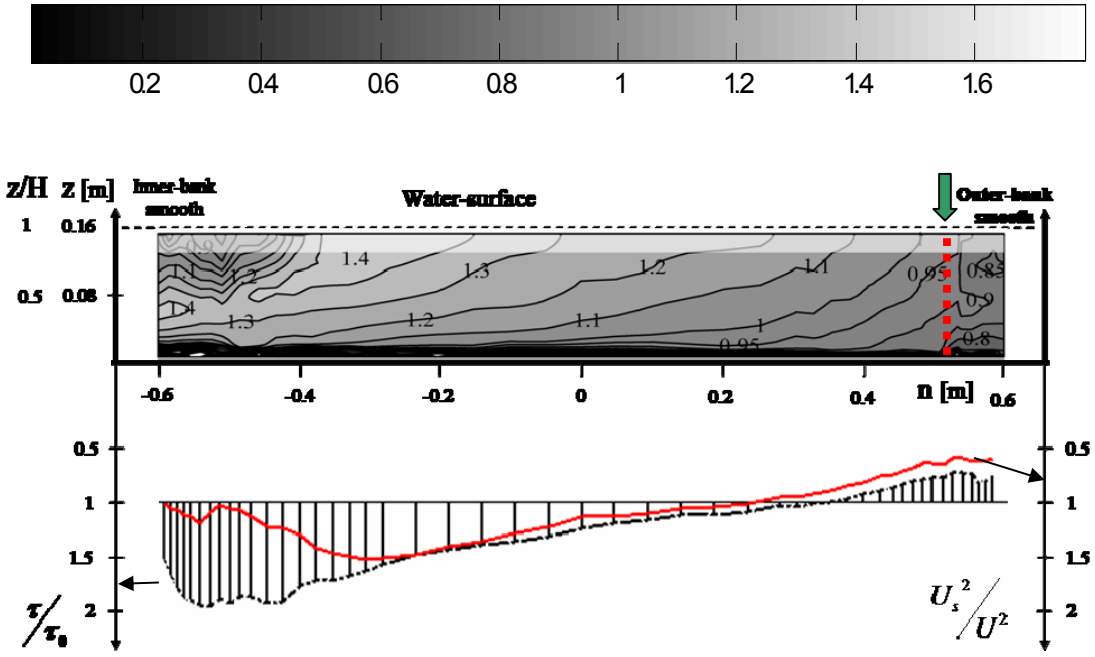

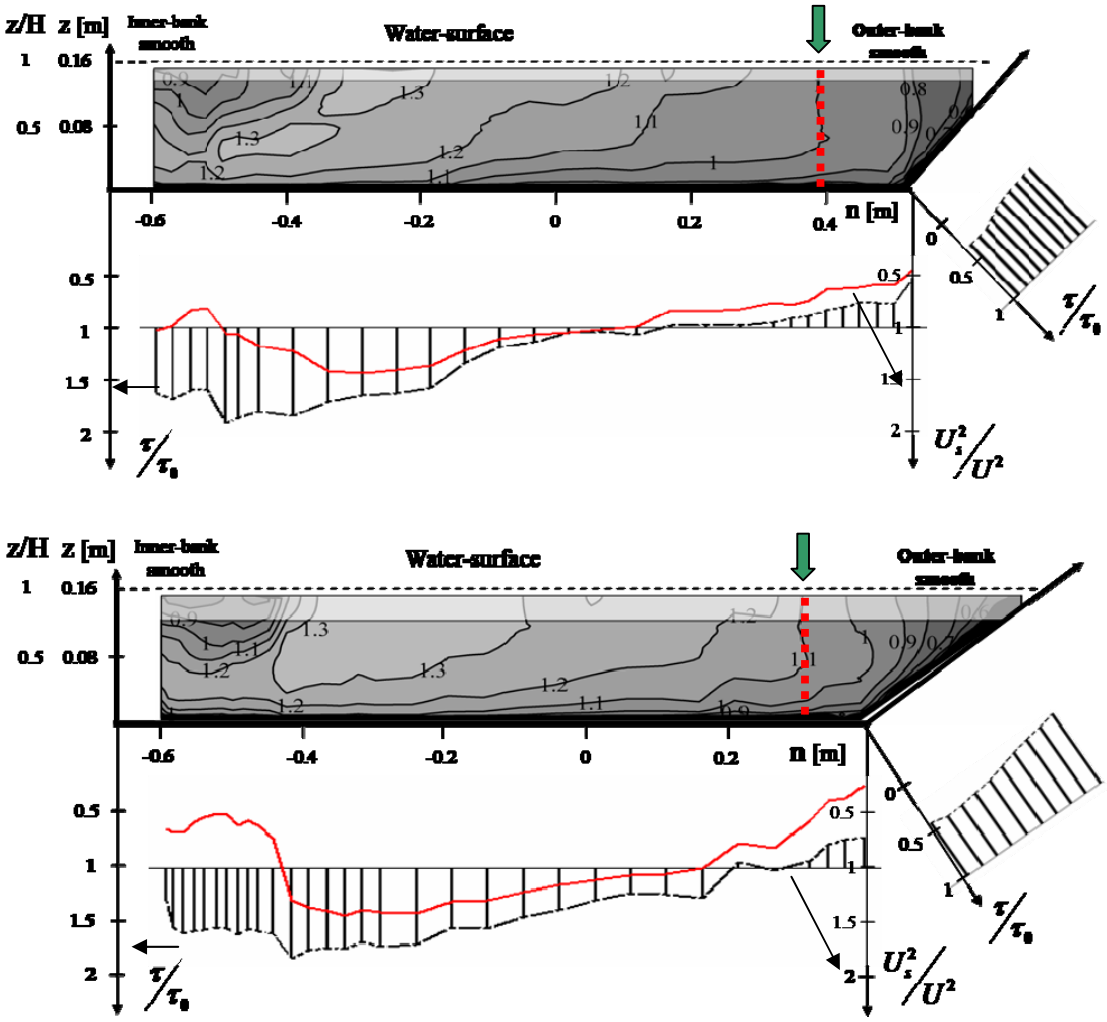

Figure 9
Cross-section at 90°. Isolines of normalized downstream velocity v_s/U , depth-averaged downstram velocity U_s^2/U^2 (red line) and boundary shear stress distribution τ/τ_o .
F16_90_00 (Top); F16_45_00 (Middle) and F16_30_00 (Bottom).

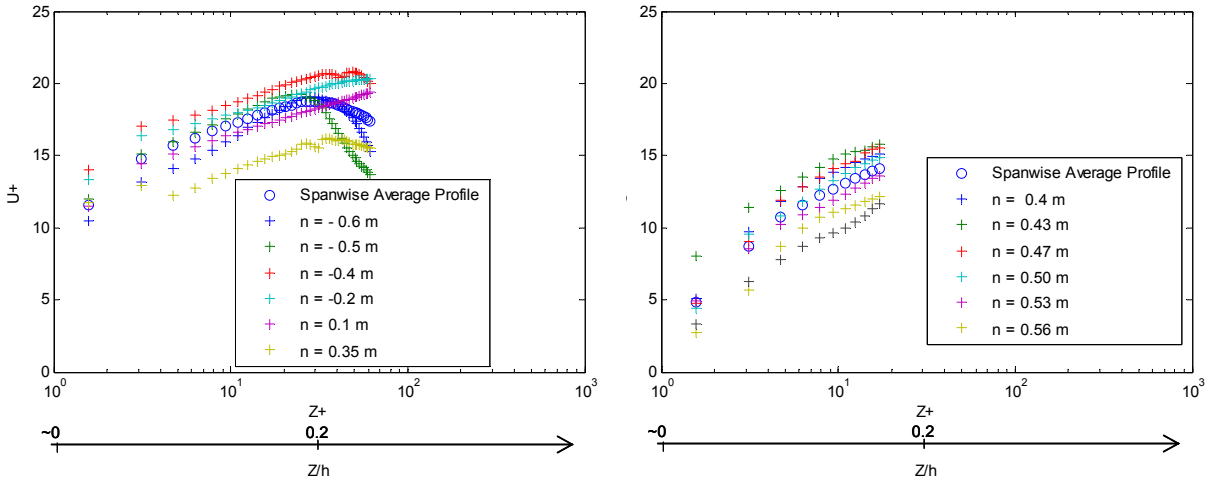

Figure 10
a) Log-law plots of mean velocity over the bottom
b) Log-law plots of mean velocity over the outer-ban

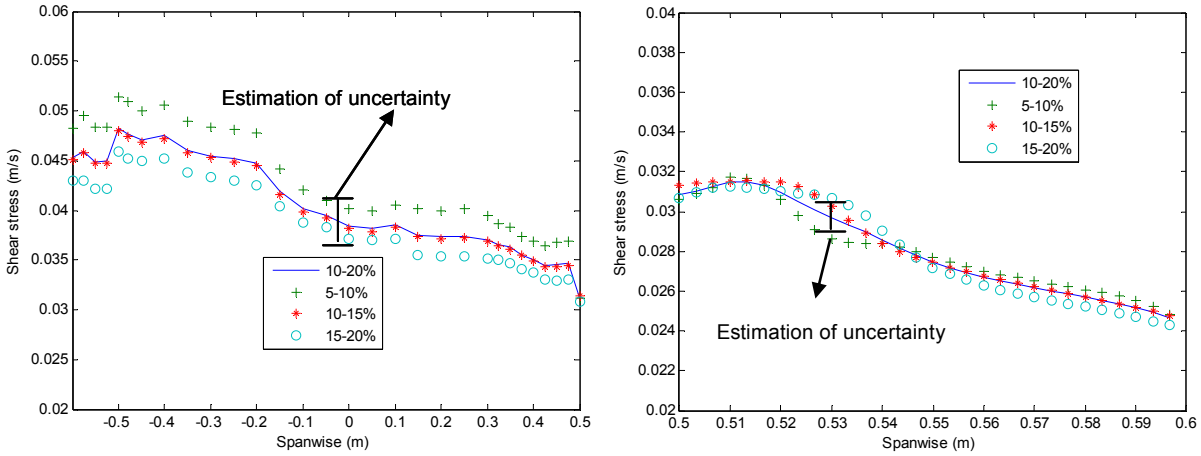

Figure 11
a) Spanwise bed shear stress evolution obtained from loglaw as functions of water-depth intervals
b) Spanwise outer-bank shear stress evolution obtained from loglaw as functions of water-depth intervals

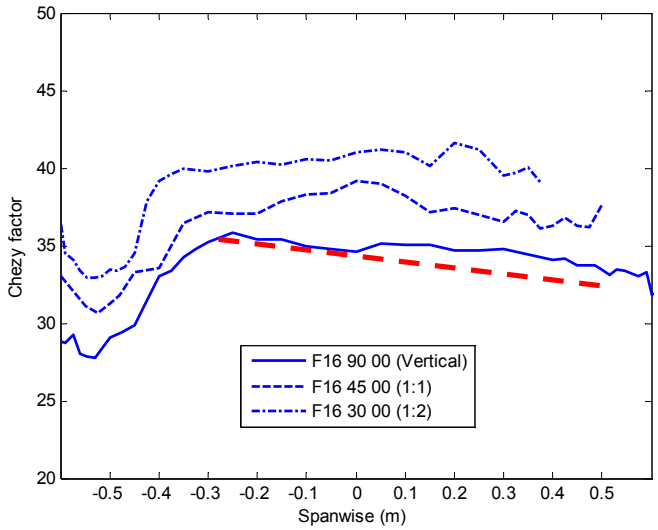

Figure 12
Chezy factor spanwise evolution
(- F16_90_00; * F16_45_00; F16_30_00)

3.5 Patterns of turbulent kinetic energy in the cross-section at 90°

The normalized turbulent kinetic energy, k/u_*^2 where, $k = 0.5*\left(\overline{v_s'^2} + \overline{v_n'^2} + \overline{v_z'^2}\right)$, is shown in Figures 13 for the three experiments. The maximum values are located at the channel center and in the upper outer-bank zone close to free-surface. The low turbulence values in the outer bank are in agreement with Blanckaert & de Vriend (2004).

With decreasing bank slope the, k/u_*^2 patterns are unchanged in the channel center, however, the maximum k/u_*^2 located in the outer-bank shifts inwards. Despite that, in the basal zone of the outer-bank, k/u_*^2 values increase with decreasing outer-bank slope. So, the high v_s/U and k/u_*^2 close to the outer-bank suggest more vulnerability to erosion especially for low bank angles channels.

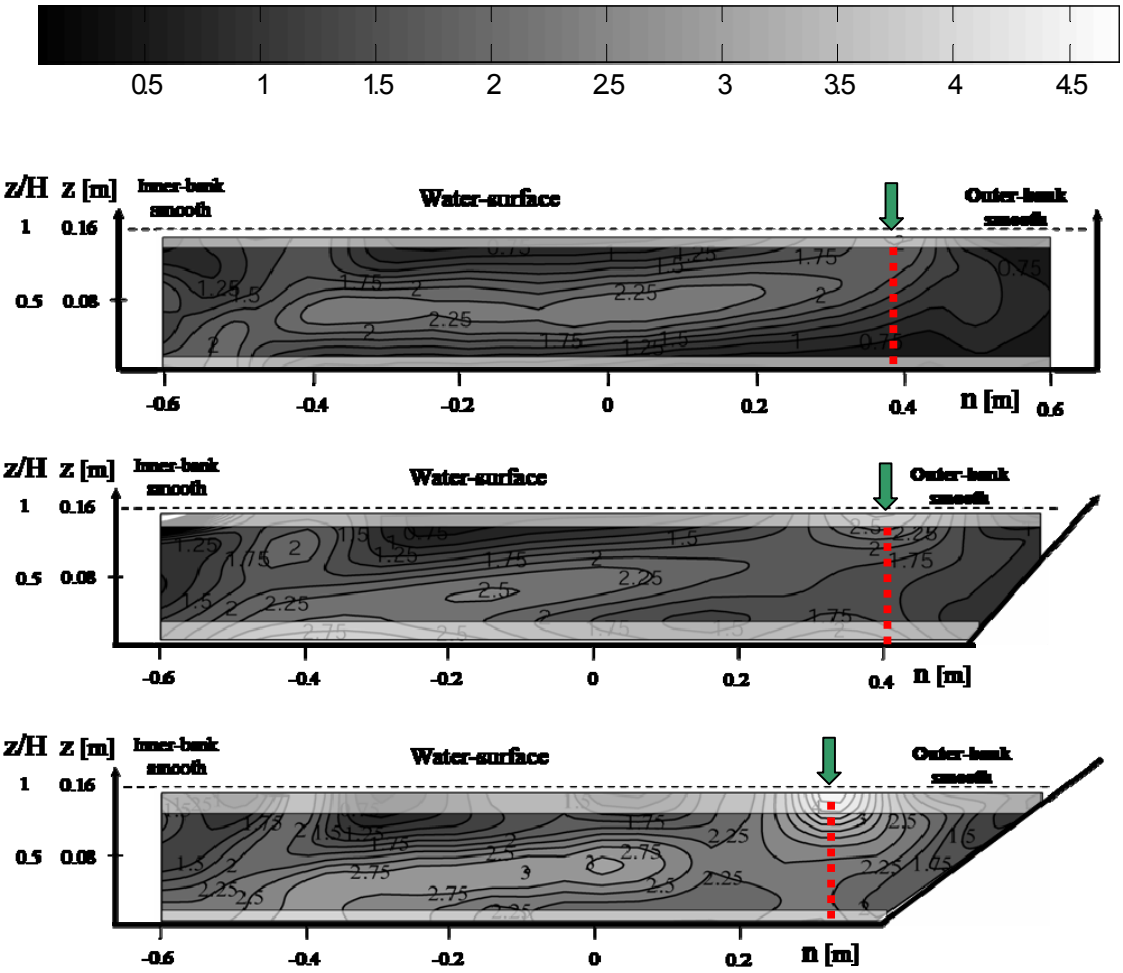

Figure 13

Cross-section at 90°. Isolines of normalized turbulent kinetic energy, k/u_*^2
F16_90_00 (Top); F16_45_00 (Middle) and F16_30_00 (Bottom).

3.6 Patterns of normalized normal stress difference in the cross-section at 90°

The normalized normal stresses difference, $\left(\overline{v_n'^2}-\overline{v_z'^2}\right)/u_*^2$, is shown in Figure 14. The maximum values are located at channel center and at free-surface in the outer part of the cross-section. There is a correlation between the location of the k/u_*^2 maximum values and $\left(\overline{v_n'^2}-\overline{v_z'^2}\right)/u_*^2$. With decreasing bank slope the maximum located at the free-surface shifts inwards (see dashed line). $\left(\overline{v_n'^2}-\overline{v_z'^2}\right)/u_*^2$ reflects the different boundary conditions. In the regions close to the free-surface and bottom, the vertical fluctuations are damped whereas close to the walls the transverse fluctuations are damped. Figure 14 shows that

$\overline{v_n'^2}$ is always higher than $\overline{v_z'^2}$ even in the outer-wall zone, which is not in agreement with Tominaga et al. (1989). $\left(\overline{v_n'^2} - \overline{v_z'^2}\right)/u_*^2$ measurement is essential for the downstream vorticity equation relevant terms analysis.

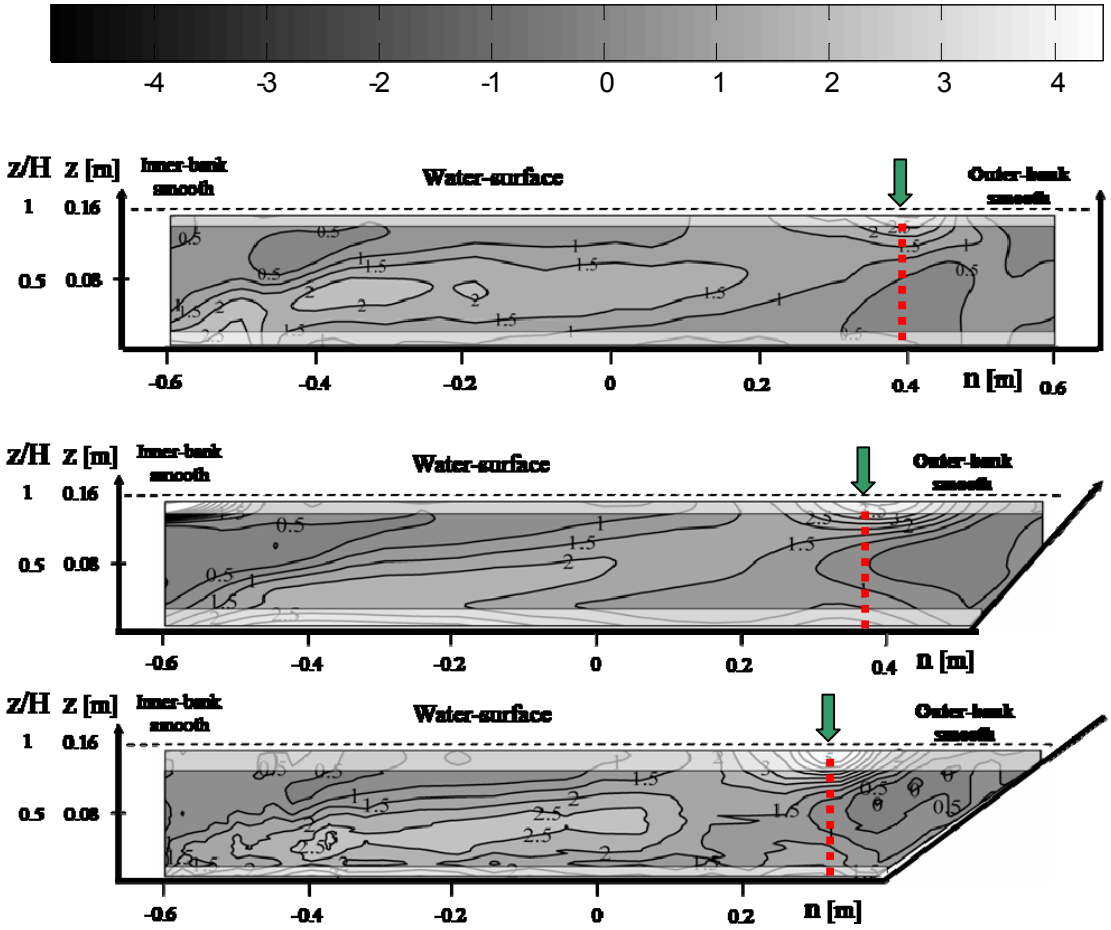

Figure 14
Cross-section at 90°. Isolines of normalized turbulent normal stress difference F16_90_00 (Top); F16_45_00 (Middle) and F16_30_00 (Bottom).

3.7. Patterns of cross-stream $\overline{v_n' v_z'}/u_*^2$ in the cross-section at 90°

Normalized cross-sectional turbulent shear stresses correlate well with CRC and OBC as two peaks of $\overline{v_n' v_z'}/u_*^2$ are observed in the CRC and OBC zones for F16_45_00 and F16_30_00. For F16_90_00 $\overline{v_n' v_z'}/u_*^2$ in the upper outward channel zone is not visible probably due to scatter.

With decreasing outer-bank slope the high $\overline{v_n' v_z'}/u_*^2$ values in the outer-bank shift inwards in agreement with the OBC shift. Decreasing bank slope angles generates higher negative

values in the bank toe zone. $\overline{v_n' v_z'} / u_*^2$ accurate measurements are also important for the downstream vorticity equation relevant terms analysis which is shown hereafter.

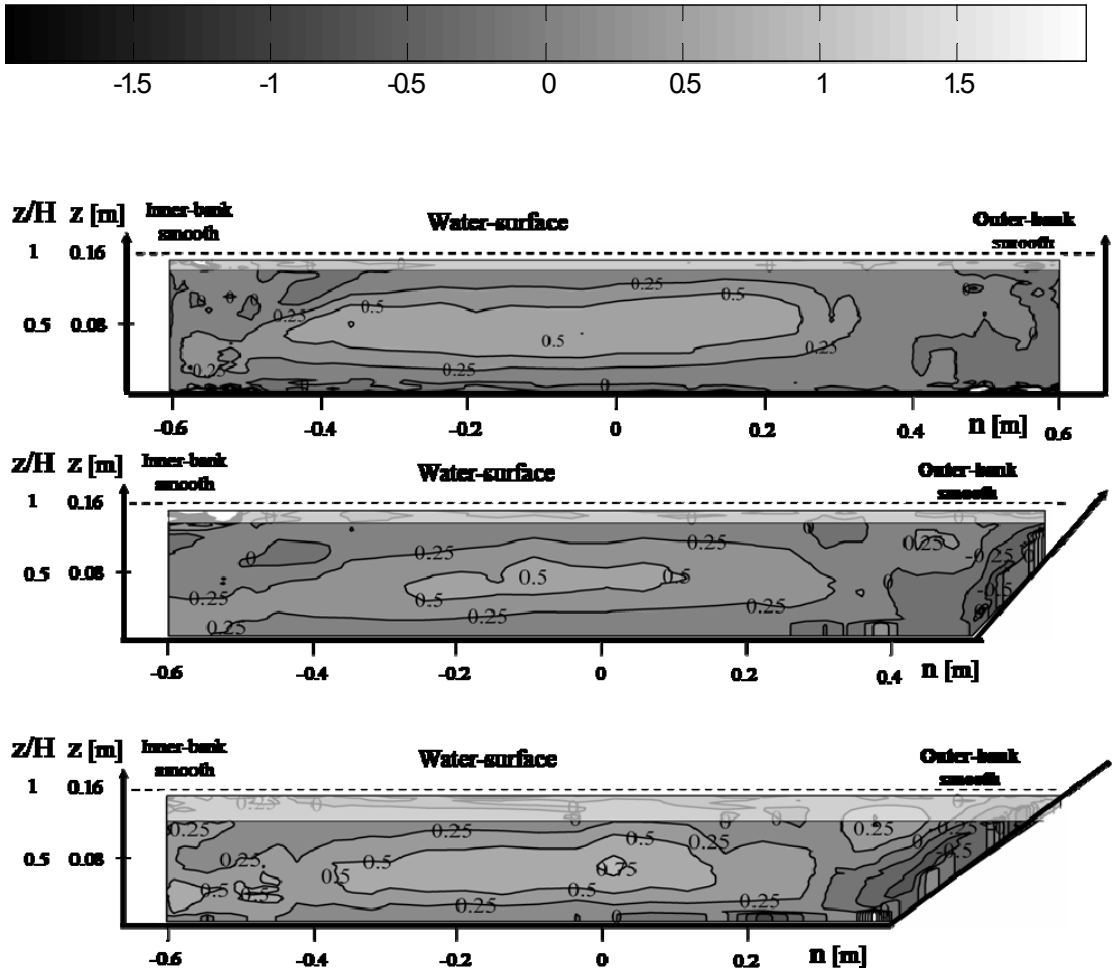

Figure 15

Cross-section at 90°. Isolines of turbulent shear stress $\overline{v_n' v_z'} / u_*^2$
F16_90_00 (Top); F16_45_00 (Middle) and F16_30_00 (Bottom).

4 Mechanisms underlying circulation cells

Relevant terms of the downstream vorticity equation and the kinetic energy fluxes analyses, Blanckaert & de Vriend (2004) methodology, are used to study the underlying mechanisms of the circulation cells. The downstream vorticity equation, Equation (7), is obtained by cross-differentiation of the transverse and vertical momentum equations for incompressible flow (Schlichting & Gersten, 2000).

$$\frac{\partial \omega_s}{\partial t} = -\left(\frac{1}{1+n/R} v_s \frac{\partial \omega_s}{\partial s} + v_n \frac{\partial \omega_s}{\partial n} + v_z \frac{\partial \omega_s}{\partial z} \right)$$
$$+ \frac{1}{1+n/R} \omega_s \frac{\partial v_s}{\partial s} + \left[\omega_n \frac{\partial v_s}{\partial n} + \omega_z \frac{\partial v_s}{\partial z} + \frac{1}{1+n/R} \frac{v_n w_s}{R} - \frac{1}{1+n/R} \frac{v_s w_n}{R} \right] - \frac{1}{1+n/R} \frac{\partial}{\partial z} \left(\frac{\overline{v_s'^2}}{R} \right)$$
$$+ \frac{\partial^2}{\partial z \partial n} \left(\overline{v_n'^2} - \overline{v_z'^2} \right) + \frac{1}{1+n/R} \frac{1}{R} \left(\overline{\frac{\partial v_n'^2}{\partial z}} \right) + \left(\frac{1}{1+n/R} \frac{\partial^2}{\partial z^2} - \frac{\partial}{\partial n} \left(\frac{1}{1+n/R} \frac{\partial}{\partial n} \right) \right) \left((1+n/R) \overline{v_n' v_z'} \right)$$
$$+ \upsilon \left(\nabla^2 \omega_s + \frac{2}{(1+n/R)^2} \frac{1}{R} \frac{\partial \omega_n}{\partial s} - \frac{1}{(1+n/R)^2} \frac{1}{R^2} \omega_s \right) \qquad (7)$$

The relevant terms for the application of the Blanckaert & de Vriend (2004) methodology are marked by rectangles. The terms from second line are transformed into (e.g. Blanckaert & de Vriend, 2004):

$$- \frac{1}{1+n/R} \frac{\partial}{\partial z} \left(\frac{v_s^2}{R} \right) + \frac{1}{1+n/R} \frac{v_n \omega_s}{R} + \left[\frac{1}{1+n/R} \frac{\partial v_n}{\partial s} \frac{\partial v_s}{\partial z} - \frac{\partial v_z}{\partial s} \frac{\partial}{\partial n} \left(\frac{1}{1+n/R} v_s \right) \right] \qquad (8)$$

Equation 8 represents skewing induced vorticity redistribution by quasi-inviscid deflection of existing mean vorticity. Inside the red rectangle the term associated with the centrifugal force (CT) is shown. Apparently, skewing-induced vorticity mainly results from CT.

In the third line the influence of cross-stream turbulent stress components on the vorticity field is represented. The first term corresponds to the cross-stream turbulent anisotropy term (CSTA) whereas the last term corresponds to the cross-stream shear term (CSS).

Equation 9 indicates that the energy fluxes per unit mass take place through work done by the turbulent stresses as the mean flow deforms. The sum of these energy fluxes is

mostly positive, i.e., from mean flow to turbulence. It is called the production or generation of turbulent kinetic energy.

$$P = -\left[\left(\overline{v_s'^2} - \frac{2}{3}k\right)e_{ss} + \left(\overline{v_n'^2} - \frac{2}{3}k\right)e_{nn} + \left(\overline{v_z'^2} - \frac{2}{3}k\right)e_{zz} + 2\overline{v_s'v_n'}e_{sn} + 2\overline{v_s'v_z'}e_{sz} + 2\overline{v_n'v_z'}e_{nz}\right] \quad (9)$$

wherein e_{ij} (i,j = s,n,z) are the strain rates (Batchelor 1970, p.600).

Equation 9 $2\overline{v_n'v_z'}e_{nz}$ term analysis the energy flux between mean flow and turbulence in the cells zones.

4.1 Patterns of normalized centrifugal term in the cross-section at 90°

Normalized CT by $\frac{U^2}{H^2}$ is shown in Figure 16. $CT/\left(U^2/H^2\right)$ is positive in the upper inner part of the channel which is attributed to flow separation. $CT/\left(U^2/H^2\right)$ values are in compliance with the CRC sense and extension for all experiments (CRC $\omega_s H/U$ values are negatives). In the upper outer part of the cross-section the values are positive in agreement with OBC $\omega_s H/U$ values. With decreasing outer-bank slope, the $CT/\left(U^2/H^2\right)$ contours corresponding to OBC shift inwards. OBC $CT/\left(U^2/H^2\right)$ values are not constant with decreasing outer-bank slope as they pass from 0.25 to 0.1. This result suggests that OBC shifts inwards and looses strength with decreasing bank slope.

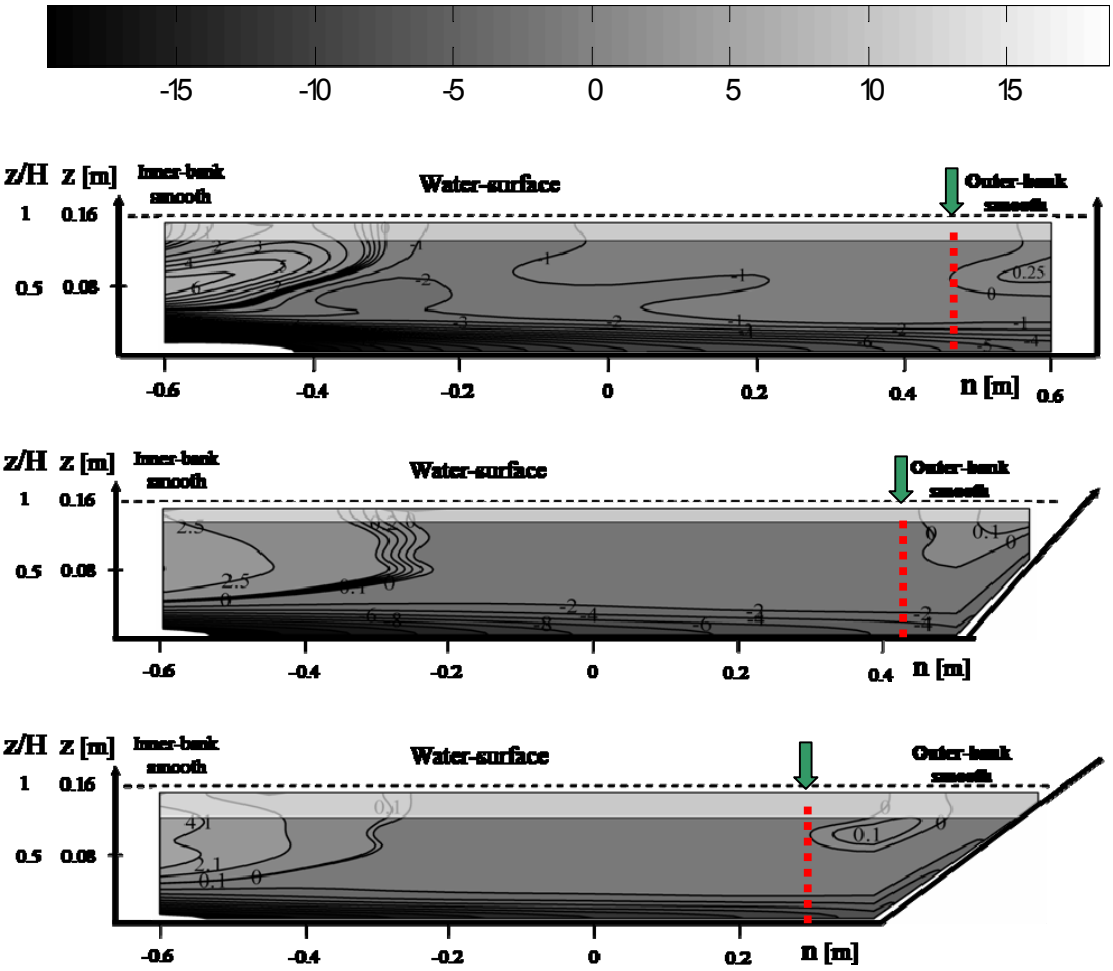

Figure 16

Cross-section at 90°. Isolines of vorticity equation centrifugal term $CT/\left(U^2/H^2\right)$
F16_90_00 (Top); F16_45_00 (Middle) and F16_30_00 (Bottom).

4.2 Patterns of normalized cross-stream anisotropy terms in the cross-section at 90°

Normalized $CSTA$ by $\frac{U^2}{H^2}$ is shown in Figure 17. $CSTA/\left(U^2/H^2\right)$ is negative in the upper inner part of the cross-section. $CSTA/\left(U^2/H^2\right)$ is slightly positive in the central part of the cross-section not favoring the CRC rotation sense. The maximum positive values of $CSTA/\left(U^2/H^2\right)$ are located near the free-surface at about the same location of CRC and OBC separation (dashed line). Over the OBC location $CSTA/\left(U^2/H^2\right)$ is negative. The negative sign of $CSTA/\left(U^2/H^2\right)$ does not favor the OBC counter-clockwise rotation sense. With decreasing bank slope, $CSTA/\left(U^2/H^2\right)$ shifts inwards being in agreement with OBC shift. However $CSTA/\left(U^2/H^2\right)$-0 isoline shift (dashed

line) is smaller than $CT/\left(U^2/H^2\right)$-0 isoline shift which could be explained by the increase of uncertainty due to the double derivatives performed.

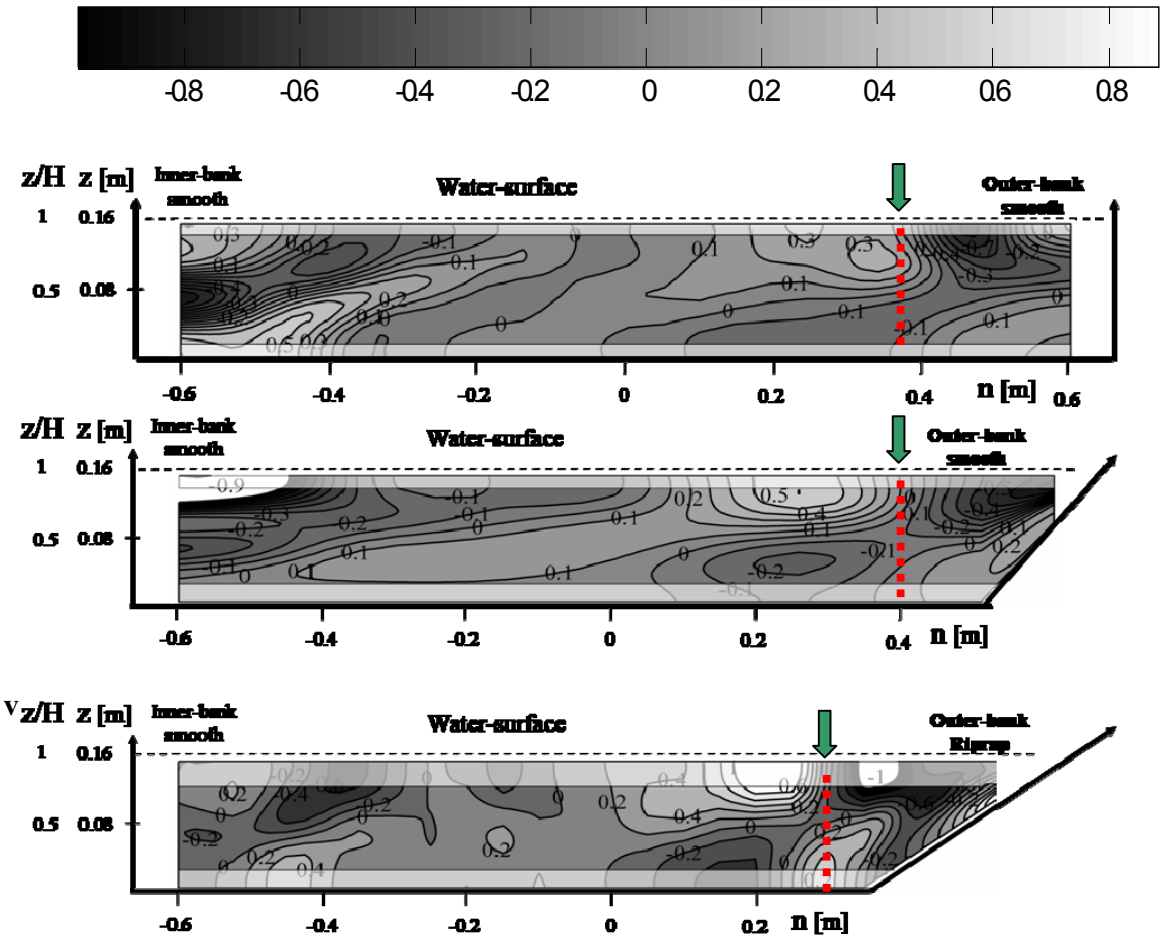

Figure 17

Cross-section at 90°. Isolines of normalized cross-stream turbulence anisotropy term $CSTA/\left(U^2/H^2\right)$ PVC F16_90_00 (Top); F16_90_02 (Middle) and F16_90_30 (Bottom).

4.3 Patterns of normalized cross-stream shear stress terms in the cross-section at 90°

Isolines of CSS normalized by $\frac{U^2}{H^2}$ are shown in Figure 18. $CSS/\left(U^2/H^2\right)$ maximum values are at channel center. The CRC rotation sense is not favored by $CSS/\left(U^2/H^2\right)$. In the near outer-bank zone the positive values seem to be located over the OBC zone indicating that $CSS/\left(U^2/H^2\right)$ term favors the OBC for all experiments. Beneath OBC zone negative values exist for all experiments. With decreasing bank slope $CSS/\left(U^2/H^2\right)$ values and patterns are unchanged.

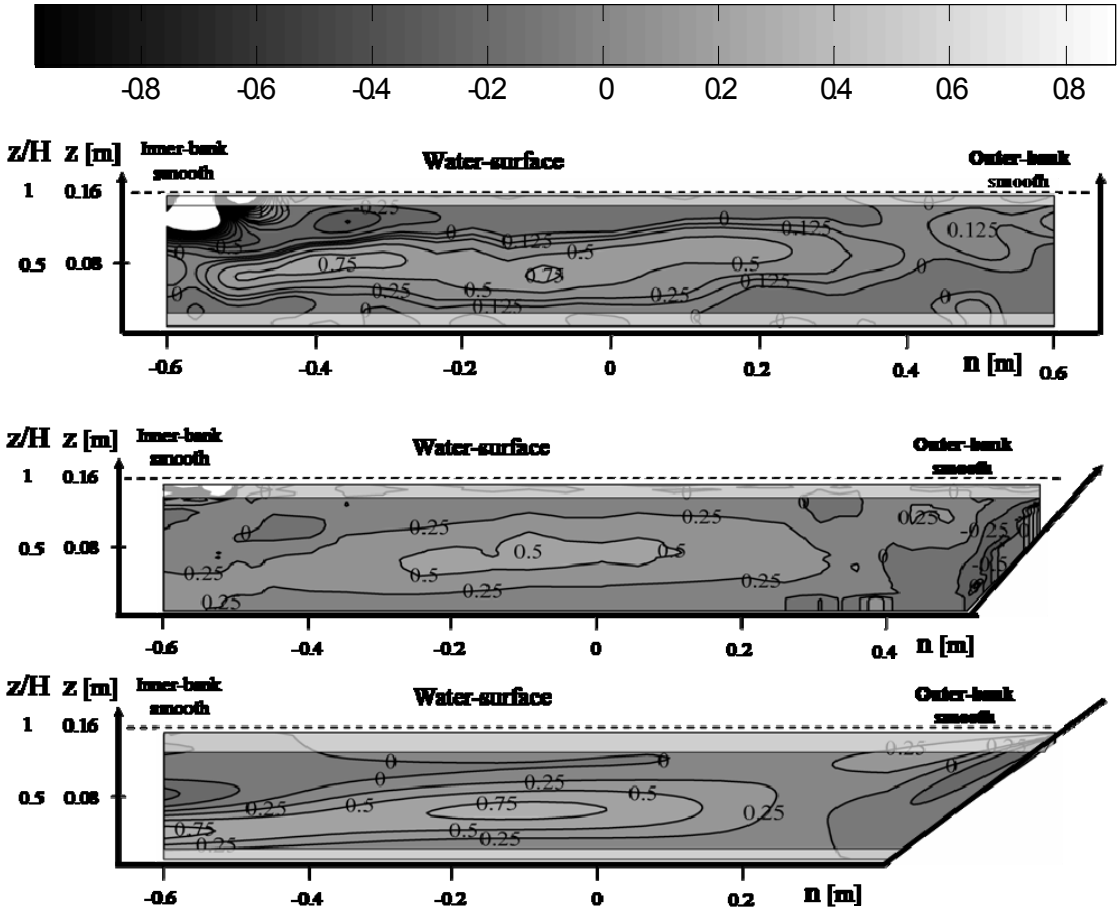

Figure 18

Cross-section at 90°. Isolines of normalized cross-stream turbulence shear stress term $CSS/\left(U^2/H^2\right)$ PVC F16_90_00 (Top); F16_90_02 (Middle) and F16_90_30 (Bottom).

4.4 Patterns of normalized cross-stream kinetic energy fluxes in the cross-section at 90°

Normalized cross-stream kinetic energy fluxes via $\overline{v_n' v_z'}$ (cf. Equation 9) by $\left(u_*^3/H\right)$ is shown in Figure 19. In the CRC center high positive values are observed corresponding to kinetic energy fluxes from mean flow to turbulence. In the outer-bank negative and positive values are noticed suggesting that energy fluxes are in both senses between turbulence and mean flow.

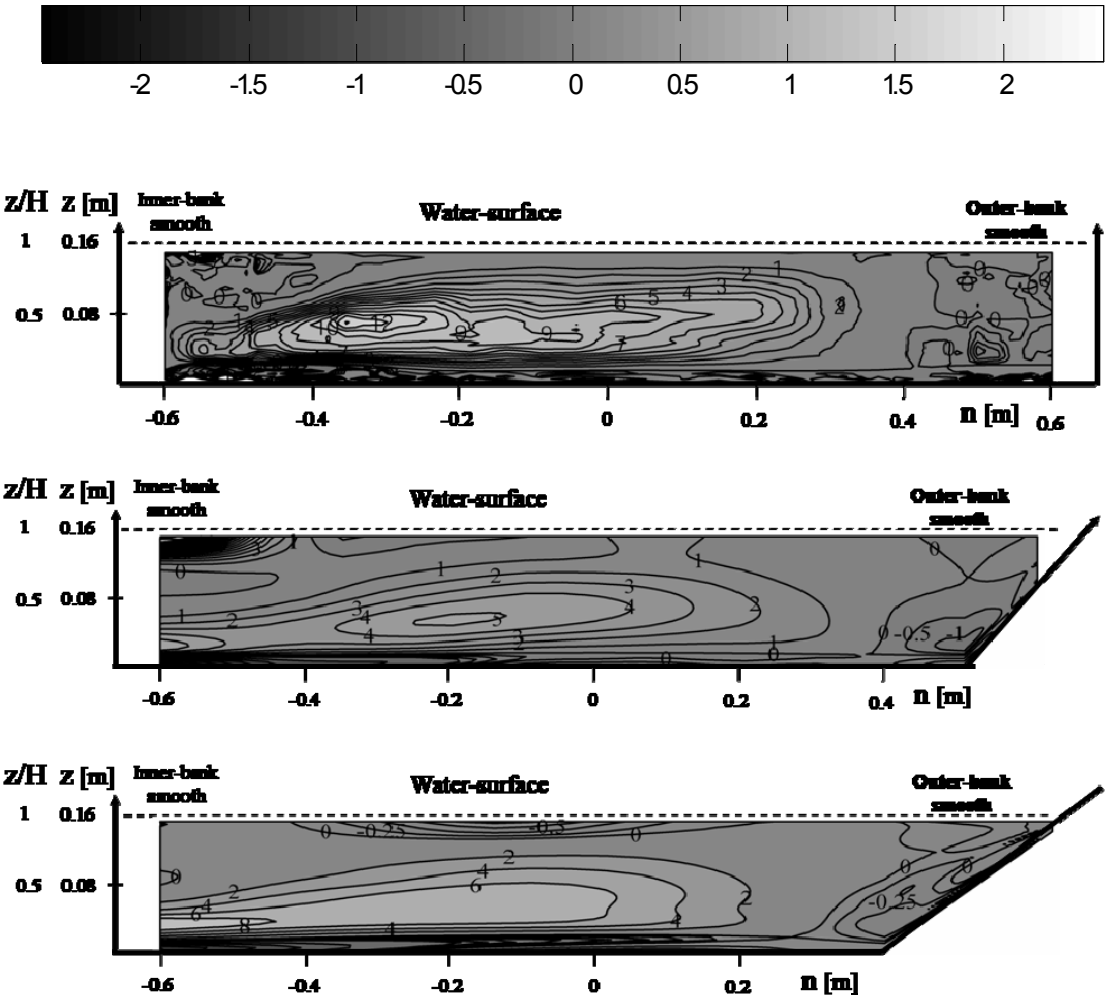

Figure 19

Cross-section at 90°. Isolines of the normalized kinetic energy fluxes between mean flow and the turbulence via cross-stream turbulent stress, $\frac{2\overline{v_n' v_z'} e_{nz}}{\left(u_*^3 / H\right)}$.

F16_90_00 (Top); F16_45_00 (Middle) and F16_30_00 (Bottom).

4.5 Explanation of underlying mechanisms

In order to understand the circulation cells patterns as function of channel geometry Blanckaert & de Vriend (2004) methodology is used. In the methodology used the downstream vorticity equation relevant terms and the kinetic energy fluxes via $\overline{v_n' v_z'}$ are analyzed. Tables 3 and 4 show $CT/\left(U^2/H^2\right)$, $CSTA/\left(U^2/H^2\right)$, area/(BH), $CSS/\left(U^2/H^2\right)$ and $\frac{2\overline{v_n' v_z'} e_{nz}}{\left(u_*^3/H\right)}$ values from the CRC and OBC centers. Tables 3 and 4 evaluations are only qualitatively due to the errors associated with derivatives and double derivatives of small quantities.

Table 3
CRC average downstream vorticity equation relevant values and kinetic fluxes

	$\omega_s H/U$ Figure 8	area/(BH)	$CT/\left(U^2/H^2\right)$ Figure 16	$CSTA/\left(U^2/H^2\right)$ Figure 17	$CSS/\left(U^2/H^2\right)$ Figure 18	$\frac{2\overline{v_n' v_z'} e_{nz}}{\left(u_*^3/H\right)}$ Figure 19
F16_90_00	**-0.75**	**0.46**	**-1**	**0.1**	**0.5**	**6**
F16_45_00	**-0.75**	**0.46**	**-1**	**0.1**	**0.5**	**6**
F16_30_00	**-0.75**	**0.4**	**-1**	**0.1**	**0.75**	**8**

Table 4
OBC average downstream vorticity equation relevant values and kinetic fluxes

	$\omega_s H/U$ Figure 8	area/(BH)	$CT/\left(U^2/H^2\right)$ Figure 16	$CSTA/\left(U^2/H^2\right)$ Figure 17	$CSS/\left(U^2/H^2\right)$ Figure 18	$\frac{2\overline{v_n' v_z'} e_{nz}}{\left(u_*^3/H\right)}$ Figure 19
F16_90_00	**0.25**	**0.07**	**0.25**	**-0.6**	**0.25**	**-0.1**
F16_45_00	**0.2**	**0.07**	**0.1**	**-0.6**	**0.25**	**<0**
F16_30_30	**0.2**	**0.07**	**0.1**	**-0.7**	**0.25**	**<0**

Table 3 shows that the centrifugal term $CT/\left(U^2/H^2\right)$ favors the CRC whereas the cross-stream turbulent shear stress terms (*CSS* and *CSTA*) do not. $CT/\left(U^2/H^2\right)$ is the leading term followed by $CSS/\left(U^2/H^2\right)$ whereas $CSTA/\left(U^2/H^2\right)$ values are negligible. $\frac{2\overline{v_n' v_z'} e_{nz}}{\left(u_*^3/H\right)}$ positive values indicate a flux of energy from the mean flow to turbulence.

With decreasing bank slope, $\omega_s H/U$ values are unchanged. In general, the downstream vorticity equation relevant terms at about CRC center are constant which is in agreement with CRC constant strength with decreasing bank slope.

Table 4 shows that $CSTA/\left(U^2/H^2\right)$ is the highest term at about OBC center, although CT and $CSS/\left(U^2/H^2\right)$ values have the same order of magnitude. These values suggest that OBC in trapezoidal channels have the characteristics of 1st and 2nd kind of Prandlt's secondary currents. $CSS/\left(U^2/H^2\right)$and $CT/\left(U^2/H^2\right)$ values are positive and so favoring the OBC rotation sense whereas $CSTA/\left(U^2/H^2\right)$ does not. $\frac{2\overline{v_n' v_z'} e_{nz}}{\left(u_*^3/H\right)}$ negative values indicate an existing flux of energy from turbulence to mean flow in the OBC zone. With decreasing outer-bank inclination the $\omega_s H/U_{\max}$ values slightly decrease which is in agreement with CT decrease.

5 Conclusions

This paper analyzed the flow features occurring in a sharp open-channel bend as function of outer-bank inclination.

The conclusions for the entire bend:

1) The maximum downstream velocity is advected by the center-region cell (CRC) from the inner bank at bed entrance towards the outer-bank at about bend exit.

2) The depth-averaged downstream velocity over the bank toe along the bend is similar for experiments with different outer-bank inclination angles.

The conclusions for the cross-section at 90°:

1) Besides CRC a second circulation cell is present between the outer-bank and the free-surface with an opposite rotation sense. It is known from literature as outer-bank cell (OBC). It is found that occurs for all channel shapes (rectangular and trapezoidal).

2) With decreasing outer bank slope, the OBC shifts inward with constant size. The OBC is over the bank toe for trapezoidal channels regardless the bank angle. Hence, CRC diminishes with decreasing bank slope as it is pushed inwards by the OBC.

3) Turbulence is reduced towards the outer-bank regardless the channel shape. Despite that, turbulence close to the outer-bank toe is affected by the channel shape as it increases with decreasing bank slope.

4) The outer-bank shear stress magnitude is higher for trapezoidal channels than for rectangular channels. The maximum bank shear stress location is at mid-depth and close to the outer-bank for rectangular and trapezoidal channels, respectively.

5) Despite being considered constant in 2D-depth averaged simulations measured Chezy factor is not constant over the bed, however, with decreasing bank angle tends to be at channel center.

6) CRC is generated by centrifugal term (CT) and opposed by cross-stream shear terms (CSS) and cross-stream turbulent anisotropy (CSTA) regardless the cross-section shape.

7) OBC is generated by CT and CSS and opposed by CSTA regardless the cross-section shape.

8) Kinetic energy fluxes between mean flow and turbulence has a key role on the OBC generation in curved flows. Positive and negative values are found in the OBC zone and so non-linear models are needed to simulate correctly the OBC.

REFERENCES

Batcheleor, G.K. (1970). "An introduction to fluid dynamics." Cambridge Univ. press, Cambridge, U.K.

Bathurst, J.C., Throne, C.R. & Hey, R.D. (1979). "Secondary flow and shear stress at river bends." J. Hydr. Div., ASCE, 105 (10), 1277-1295.

Blanckaert, K. (2002). "Flow and turbulence in sharp open-channel bends." Ph.D dissertation N°. 2545, Swiss Federal Institute of Technology, Lausanne.

Blanckaert, K., & de Vriend, H.J. (2003). "Non-linear modeling of mean flow redistribution in curved open channels." Water Resources Research, AGU, 39 (12):1375.

Blanckaert, K. & de Vriend, H.J. (2004). "Turbulence characteristics in sharp open-channel bends." J. Fluid Mech., Cambridge Univ. Press.

Blanckaert, K. & de Vriend, H.J. (2005). "Secondary flow in sharp open-channel Bends." J. Fluid Mech., Cambridge Univ. Press, 498: 353-380.

Blanckaert, K. & Lemmin, U. (2006). "Means of noise reduction in acoustic turbulence measurements." J.Hydr. Res., 44(1), 3-17.

Blanckaert, K. (2009). "Laboratory experiments on straight and sharply curved open-channel flows. Experimental techniques, data treatment and selected results." In preparation.

Booij, R. (2003). "Measurements and large eddy simulations of the flows in some curved flows." J. Turbulence 4 1-17.

de Vriend, H.J. (1981). "Velocity redistribution in curved rectangle channels." J. Fluid Mech., Cambridge Univ. Press, Vol. 107(6), 429-439.

Gosh, S.N. & Roy, N. (1970). "Boundary shear stress distribution in open-channel flow." J. Hydr. Div., ASCE, 96(4), 967-994.

Hersberger, D. (2002). "Measurement of 3D flow field in a 90° bend with ultrasonic Doppler velocity." Proc.3th Int. Symp. ultrasonic Doppler Meth. for fluid Mech. and Fluid Eng., Lausanne, Switzerland, 59-66.

Hurther, D. & Lemmin, U. (2001). "A correction method for turbulence measurements with a 3-D acoustic Doppler velocity profiler." J. Atm. Oc. Techn, Vol.18, 446-458.

Hicks, F.E., Jin, Y.C. & Steffler, P.M., (1990). "Flow near sloped bank in curved channel." J. Hydr. Eng., ASCE, 116(1).

Ippen, A.T. & Drinker, P.A. (1962). "Boundary shear stress in curved trapezoidal channels." J.Hydr. Div., ASCE, 88(5), 143-179.

Jin,Y.C., Peter, Steffler, M. & Hicks, F.E. (1990). "Roughness effects on flow and shear stress near outside bank of curved channel." J.Hydr. Div., ASCE, 88(5), 143-179.

Mockmore, C.A. (1943). "Flow around bends in stable channels." Transactions, ASCE, Vol.109, 593-628.

Naot, D. (1983). "Response of channel flow to roughness heterogeneity." J. Hydr. Eng., ASCE, 110(11), 1568-1587.

Nezu, I., Nakagawa, H. & Tominaga, A. (1985). "Secondary currents in a straight channel flow and the relation to its aspect ratio." Turbulent shear flows 4, Springer-Verlag.,246-290.

Nezu, I. & Nakagawa, H. (1993). "Turbulence in open-channel flows." Balkema, Rotterdam, The Netherlands.

Perkins, H.J. (1970). "The formation of streamwise vorticity in turbulent flow." J. Fluid Mech., 44(4), 721-740.

Prandtl, L. (1942) "Füher durch die Strömungslehre." Vieweg, Braunschweig.

Rolland, T. (1994). "Dévelopment d'une instrumentation Doppler ultrasone adaptée à l'étude hydraulique de la turbulence dans les cannaux". Ph.D Thesis N°. 1281, EPFL, Lausanne Switzerland.

Rozowskii, I.L. (1957). "Flow of Water in Bends of Open-Channels." Ac. Sc. Ukr.SSR, Isr. Progr. Sc.Transl., Jerusalem.

Shen, C. (1997). "An acoustic instantaneous particle flux profiler for turbulent flow." Ph.D thesis No.1630, Swiss Federal Institute of Technology, Lausanne, (1997).

Schlichting, H. & Gersten, K. (2000). "Boundary-Layer Theory", 8th edt, Springer, Berlin.

Thorne, C. R. (1982). ''Processes and mechanisms of river bank erosion.'' Gravel-bed rivers, R. D. Hey, J. C. Bathurst, et al., eds., Wiley, NewYork, 227–259.

Thorne, C.R., & Furbish, D.J. (1995). "Influences of coarse bank roughness on flow within a sharply curved river bend." Geomorphology, vol.12, 241-257.

Tominaga, A., Nezu, I., Ezaki, K. &Nakagawa, H. (1989). "Three-dimensional turbulent structure in straight open-channel flows." J.Hydr. Res. 27,149-173.

Tominaga, A. & Nagao, M. (2002). "Secondary flow structures in bends of narrow open channels with various cross-sections." Proc. Of 4th Intenational conference on hydroscience and Engineering, in CD-ROM.

van Bendegom, L. (1947). "Eenige beschouwingen over riviermorphologie en rivierverbetering." De Ingenieur, 59(4), 1-11 (in Dutch).

Yen, B.C. (1965) "Characteristics of subcritical flow in a meandering channel." Inst. for Hydr. Res., Univ. of Iowa, Iowa City, Iowa.

CHAPTER V

INFLUENCE OF OUTER-BANK ROUGHNESS ON HYDRODYNAMICS IN TRAPEZOIDAL OPEN-CHANNEL BENDS WITH 30°-INCLINED OUTER-BANKS

INFLUENCE OF OUTER-BANK ROUGHNESS ON HYDRODYNAMICS IN TRAPEZOIDAL OPEN CHANNEL BENDS WITH 30°-INCLINED OUTER-BANKS

ABSTRACT

The influence of outer-bank roughness on hydrodynamics in open-channel bends with trapezoidal channels is poorly known. The underlying mechanisms observation and understanding are relevant for the efficient use of riprap protection design.

In curved open-channel flows the center-region cell and the outer-bank cell are usually observed in channel center and in the upper outer-bank region, respectively. This outer-bank cell is counter-rotating, smaller and weaker than the center-region cell, despite its fundamental role. However little is known about the effect of outer-bank roughness on the circulation cells in sharp bends with trapezoidal channel.

This paper investigates experimentally the influence of outer-bank roughness on the flow pattern in a sharp laboratory open-channel bend with a 30°-inclined outer-bank by means of high-resolution three-dimensional velocity measurements obtained with an Acoustic Doppler Velocity Profiler.

The results reveal a pattern of cross-stream circulation consisting of a center-region cell and a counter rotating outer-bank cell. The circulation cells sizes and locations do not vary with outer bank roughness. This contrasts with previous results obtained in rectangular curved flow, where flow patterns were significantly influenced by outer bank roughness. The mechanism which underlines the outer-bank cell is observed via relevant downstream vorticity equation terms. The centrifugal force and the cross-stream turbulent stresses slight variation with outer-bank roughness are in compliance with the circulation cells patterns.

1 Introduction

Bank erosion on the outer-bank of a bend is a critical problem. In order to improve the insight on bank protection design more detailed information on the complex flow field in the vicinity of the outer-bank is needed. The effect of bank roughness and inclination on circulation cells and thereby on downstream velocity and shear stress distribution is badly known.

Series of experiments in open-channel bends that systematically investigates the influence of isolated parameters, such as curvature ratio, bank topography and bank characteristics (Blanckaert 2009) have been performed. From that series, 9 experiments have been carried out on the influence of roughness and inclination of the outer-bank, Table 1. The present paper focus on the influence of the outer-bank roughness on curved flow patterns in trapezoidal cross-sections with 30° bank inclination.

Table 1
EPFL bend channel measurements
F16_30_00 stands for **flat** bottom with **16 cm** of water-depth, **30°** outer-bank angle with the bottom and **00** the outer-bank k_s equivalent roughness

Inclination of outer bank ⇒ / ***Roughness of outer bank*** ⇓	30°	45°	90°
Smooth PVC	F16_30_00	F16_45_00	F16_90_00
k_s = 0.002 m (sand)	F16_30_02	F16_45_02	F16_90_02
k_s = 0.03 m (riprap)	F16_30_30	F16_45_30	F16_90_30

In bend flows, velocity and boundary shear stress are redistributed in the cross-section by the circulation cells (Blanckaert and Graf, 2004). Bend flows major feature is the so-called center-region cell (CRC). When flow is in a bend, an imbalance of the centrifugal force generates an outward motion near the free-surface and an inward near the bed, at the same time, a lateral slope of surface is induced in order to create the equilibrium between the lateral pressure force, centrifugal force, and the shear generated along the bed. A second important cell is located in the upper outer-bank zone close to the water-surface, known as outer-bank cell (OBC). It is generated by the combination of turbulence driven mechanism with skewing induced mechanism (de Vriend, 1981).

Blanckaert and de Vriend (2004) advanced further on the bend flow fluid mechanics knowledge as flow patterns, circulation cells and turbulence with vertical walls in a sharp bend were studied. Term-by-term evaluations of the relevant flow equation were made in order to understand the cross-stream cells mainly the outer-bank cell mechanisms. Their

main findings were: i) OBC protects the outer-bank by reducing downstream velocity and turbulence in near-bank area; ii) turbulence models that simulate the energy transfer between mean flow and turbulence in both senses, i.e. anisotropic, are able to simulate the OBC. However their findings were made in single rectangular cross-section and it is not known if they are valid for different channel geometries.

Research on the variation of the cross-section shape and wetted perimeter roughness distribution effect on bend flow patterns is scarce. Ippen and Drinker (1962), and Yen (1965) measured flow and shear stress in trapezoidal channels. The transverse variation of the shear stress along the sloped bank has been investigated by Ghosh and Roy (1970), Naot (1983) and others. Tominaga and Nagao (2002) found that the OBC generated in narrow trapezoidal channels are smaller and less intense than in rectangular bend channel.

A special reference is done to Jin Y-C et al. (1990) paper on the effect of outer-bank roughness on half-trapezoidal bend flows. Three test conditions covering varying outer-bank roughness (smooth, k_s = 0.56 mm, k_s = 9 mm) were measured. The general characteristics of the study are: R/B = 3.79; B/H =16 and bank slope angle of 20°. They found that with increasing bank roughness the downstream velocity and bank shear stress decreases and increases, respectively, over the bank. They justify the bank shear stress increase with increasing bank roughness and the circulation cells patterns. However, they did not measure the circulation cells.

This paper investigates experimentally curved open-channel with trapezoidal channel flow characteristics as function of varying outer-bank roughness. The outer-bank roughness varies between smooth PVC, sand and riprap. This work presents the patterns of downstream and cross-stream flow velocities, the turbulent kinetic energy, the normal stresses anisotropy, the downstream vorticity, the downstream vorticity equation relevant terms and the kinetic energy transfer between mean flow and turbulence.

The outer-bank roughness effect on trapezoidal bend channels flow patterns is not fully understood. Hence, this paper objective is to answer the following questions:

- What is the effect of increasing outer-bank roughness on downstream flow, cross-stream flow and turbulence in bends with trapezoidal cross-sections?

- How is the boundary shear stress distribution affected by varying outer-bank roughness in bends with trapezoidal cross-sections?

- What are the underlying mechanisms of the existing circulation cells?

2 Experiments

Laboratory open-channel bend is seen in Figure 1. It consists of a 9 m long straight entry reach, followed by a 193° bend with constant centerline radius of curvature of R=1.7 m and a 5 m long straight exit reach. The set-up is half-trapezoidal in shape with outer-bank inclination of 30° to horizontal plane hence with 1.3 m top width and 1.02 bottom width. The bed of the flume has glued quasi-uniform sediments of d = 0.002 m and the inner bank is made of PVC. The outer-bank roughness is varied between three values: PVC, d = 0.002 m and d = 0.03 m (simulating riprap elements). The approach channel has a downstream bed slope of 0.22%, whereas the bed in the bend and out-flow is horizontal. Figure 2 shows the physical model.

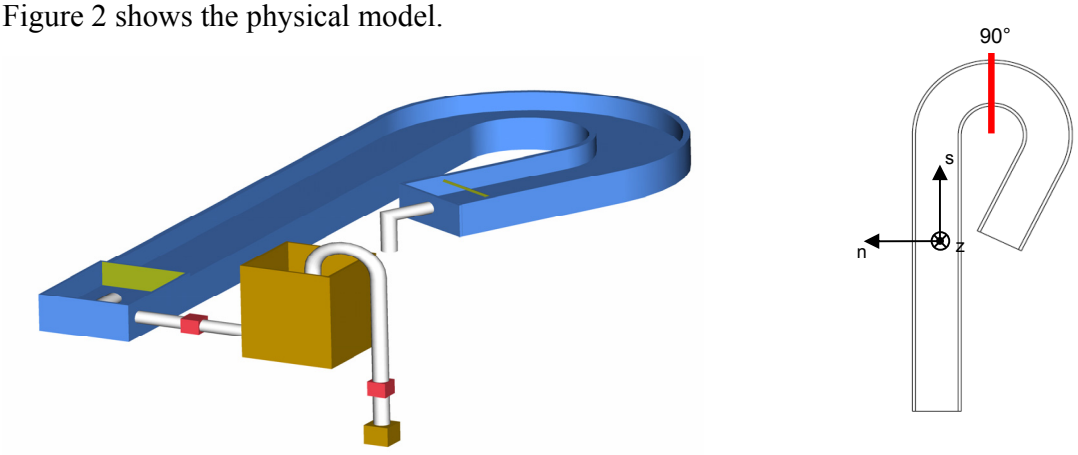

Figure 1 Experimental set-up

Table 2 Hydrodynamics conditions
Q is the flow discharge, H is the fume averaged water depth, U is the flume averaged velocity, u_* is the flume averaged shear velocity (based on hydraulic radius,R_h, and the average energy slope, E_s), $C = g^{1/2}(U/u_*)$ is the Chézy friction coefficient, $Re = UH/\nu$ is the Reynolds number, $Fr = U/(gH)^{1/2}$ is the Froude number, B is the flume width, k_s is the roughness diameter of the outer bank material

Label	Q [ls^{-1}]	H [m]	U [ms^{-1}]	R_h [m]	u_* [ms^{-1}]	C [m$^{1/2}$s^{-1}]	E_s [‰]	Re [10^3]	Fr [-]	R/H [-]	B/H [-]	k_s,bank [m]
F16_30_00	78	0.157	0.43	0.121	0.035	40	0.93	68	0.35	10.8	7.4	PVC
F16_30_02	78	0.157	0.43	0.121	0.035	40	0.92	68	0.35	10.8	7.4	2
F16_30_30	78	0.156	0.44	0.121	0.038	36	1.21	68	0.35	10.8	7.4	30

The water surface topography along the set-up was measured by a set of 8 acoustic limnimeters. The set covers the channel width and was moved along the channel via a carriage enabling longitudinal and transversal topographic data of the free-surface.

Figure 2 shows the cross-section and the axis system. s-axis is in the downstream direction of the flow. z-axis zero is at the bed of the cross-section and increases towards the free-surface. n-axis positive values are located in the outer-bank part of the channel.

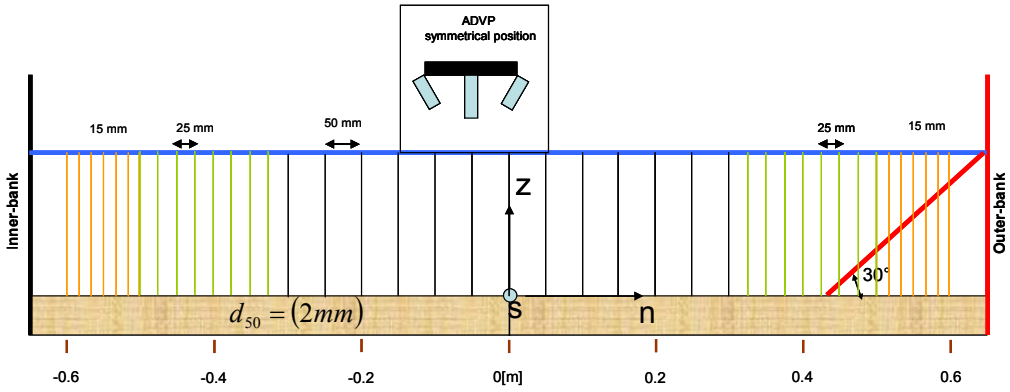

Figure2
Cross-section measuring grids and shapes

Three dimensional velocity non-intrusive measurements were carried out with an Acoustic Doppler Velocity Profiler (ADVP), developed at EPFL (Rolland 1994, Shen 1997, Hurther 2001). The ADVP is composed of a central emitter and four wide-angle receivers placed around the center. The ADVP is placed in a water-filled housing that touches the water surface causing a minor flow perturbation. Quasi-instantaneous 3D velocity field over a column of water enables the derivation of the mean velocity vector $\vec{v} = (v_s, v_n, v_z)$, fluctuating velocity vector, $\vec{v}' = (v_s', v_n', v_z')$ and all turbulent correlations $\overline{v_i'^a v_j'^b}$ ($i,j=s,n,z$; a and b are integers). The measuring spatial resolution is $(\pi \times 0.7^2 / 4) \times 0.3 = 0.12 cm^3$. The sampling frequency was 31.25 Hz and the acquisition time was 180 s. This enables a record length of 600 times the estimated macro time scales of the flow, (Nezu and Nakagawa, 1993). Details regarding the precision and accuracy of measurements made with ADVP are presented by Hurther and Lemmin (2001). Blanckaert (2009) reports more information on the ADVP, on the data treatment procedures and in the estimation of the uncertainty of the experimental data. The estimated uncertainty is 4 % for downstream velocity, v_s, 10 % for cross-stream velocities, (v_n, v_z), 10 % for turbulent kinetic energy, k, 20 % for downstream vorticity, ω_s, and 40% for the downstream vorticity equation terms.

3 Experimental results

3.1 Depth-averaged flow field

Flow in open-channel bends is highly non-uniform and spatially variable. To compare the experiments, the cross-section with maximum cross-stream circulation for each experiment was chosen. A coarse measuring grid composed of vertical profiles between *n* = -0.5 and n = 0.5 m with 0.1 m intervals was used along the bend at 15º, 30º, 60º, 90º, 120º, 150º and 180º. The measurements along the bend enable the computation of the normalized depth-averaged downstream velocity, U_s/U and the normalized strength of the cross-stream circulation, $\left\langle \tilde{f}_n^{\,2} \right\rangle$, respectively. $\left\langle \tilde{f}_n^{\,2} \right\rangle$ is defined as:

$$\left\langle \tilde{f}_n^{\,2} \right\rangle = \left\langle f_n^{\,2} \right\rangle * S_{circ} \tag{1}$$

where

$$f_n = \frac{v_n - U_n}{U_s \dfrac{H}{R}} = \frac{v_n^*}{U_s \dfrac{H}{R}} \tag{2}$$

$\langle\ \rangle$ indicates depth-averaged results; v_n is the transverse velocity component; U_n is the depth-averaged of v_n; v_n^* is the transverse component of the circulation cells; f_n is the normalized profiles of v_n^*; S_{circ} is the sign of the cross-stream circulation strength used to label the rotation sense. The curvature ratio H/R has been included in the normalization of v_n^* since the strength of the cross-stream circulation is expected to increase with H/R (Rozovskii 1957).

In all three experiments, the core of maximum depth-averaged downstream velocity (Figure 3 *abc*) is found near the inner bank at the bend entry, then gradually passing to the outer bank part of the channel towards over the bank toe along the bend. This redistribution of velocity around the bend is due to the advective momentum transport by the center-region cell (Blanckaert and Graf 2004).

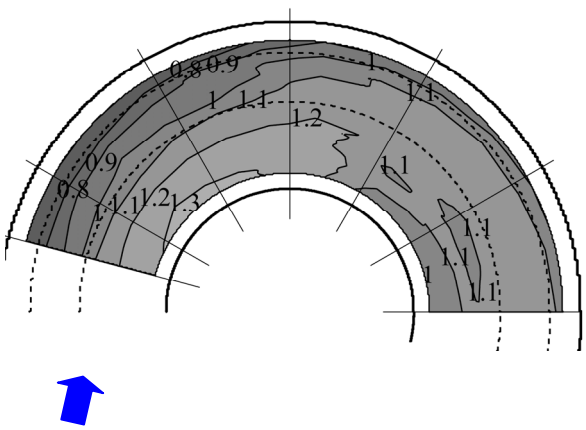

a) Outer-bank in PVC

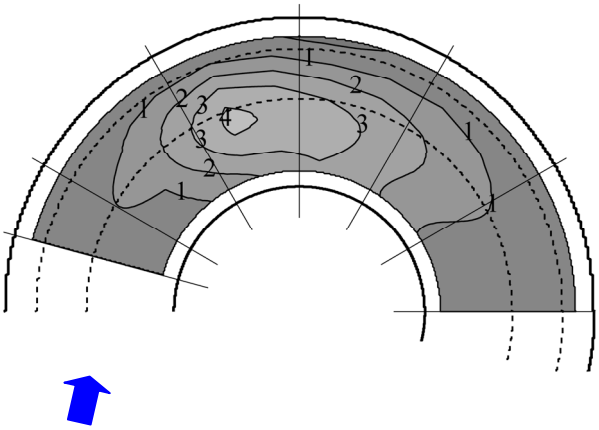

a) Outer-bank in PVC

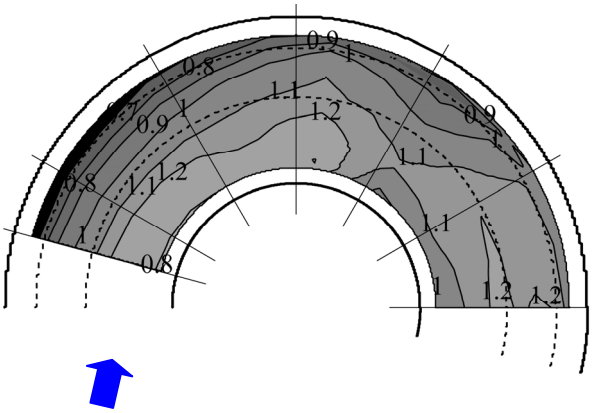

b) Outer-bank with sand (k_s = 2 mm)

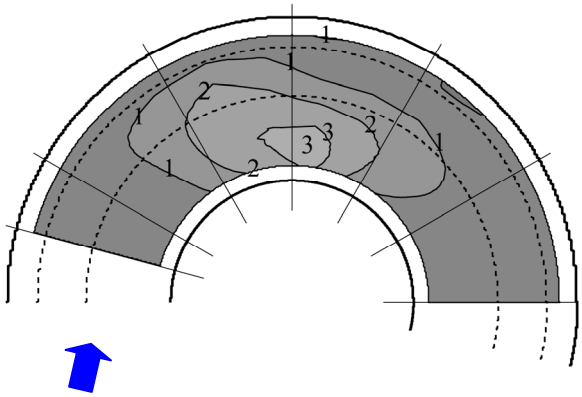

b) Outer-bank with sand (k_s=2 mm)

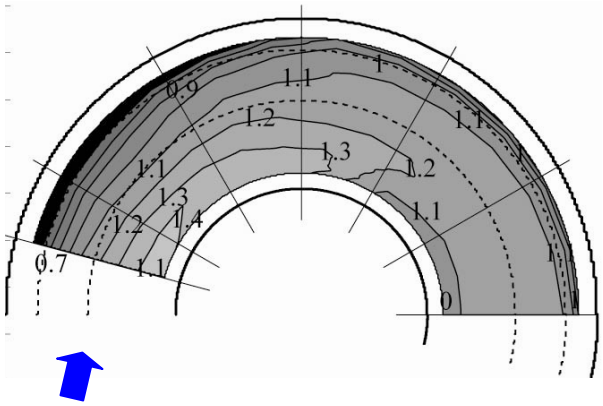

c) Outer-bank with riprap (k_s = 30 mm)

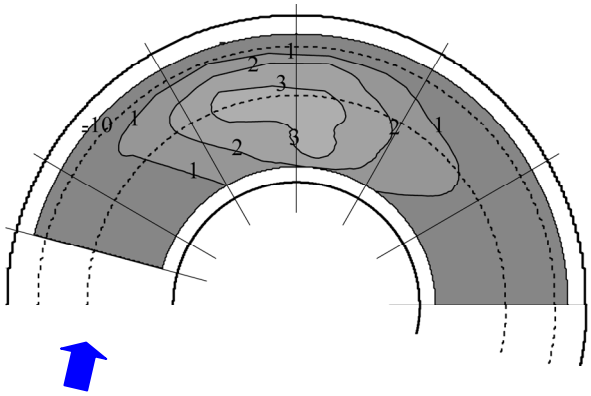

c) Outer-bank with riprap (k_s = 30 mm)

Figure 3 a b c)
Pattern of normalized downstream depth-averaged velocity , U_s/U

Figure 4 a b c)
Pattern of normalized cross-stream circulation strength, $\langle \tilde{f}_n^{\,2} \rangle$

a) F16_30_00 (PVC); b) F16_30_02 (sand); c) F16_30_30 (riprap)

Figure 4 shows circulation strength $\langle \tilde{f}_n^{\,2} \rangle$ along the bend. It grows from the bend entry to a value about 3, 4 and 4 at centerline for F16_30_00, F16_30_02 and F16_30_30, respectively, near the cross-section at 90° and then decreases quite sharply toward the bend exit, where its value is reduced to less than half of the maximum value. The maximum value, close to the cross-section at 90° varies slightly with outer-bank roughness suggesting that the outer-bank roughness in trapezoidal channels does not affect the center-region cell strength. Hence, cross-section at 90° is chosen to be measured by a refine grid for all experiments. The results are presented from chapters 3.2 to 3.7.

"Rozovskii's model" predicts $\langle \tilde{f}_n^{\,2} \rangle \approx 10$ as circulation strength maximum. The influence of curvature on the downstream velocity profile by adopting the straight-channel flow v_s profile is the reason why Rozovskii's model" overestimates the value, de Vriend (1981). To correct the linear model overestimation problem, a non-linear model was developed in Blanckaert & de Vriend (2004). The non-linear model uses, besides the Chezy coefficient, the curvature ratio, *H/R,* and the transverse distribution of the downstream velocity, parameterized by means of $\alpha_s = \frac{\partial v_s}{\partial n}\frac{R}{U_s}$. Briefly, the non-linear model correlates the "bend parameter", see Equation 3, with a correction factor to be applied to the values of the linear model. More details are given in Blanckaert & de Vriend (2004).

$$\beta = \left[\left(\sqrt{g} / C \right)^{-2.2} \left(H / R \right)^2 \left(\alpha_s + 1 \right) \right]^{0.25} \tag{3}$$

The "bend parameter" values, in cross-section at 90° obtained were about 1, respectively, for F16_30_00, F16_30_02 and F16_30_30 corresponding to a correction factor of about 0.5 for all experiments (Figure 7 in Blanckaert de Vriend, (2004)). So, this proves that the non-linear model works well even for trapezoidal sharp bends with varying outer-bank roughness.

Figure 5 shows the evolution of the outer-bank downstream depth average velocity, $U_s(n = 0.375)$, alongside the bend over the bank toe at spanwise *n*=0.375 m for all experiments. $U_s(n = 0.375)$ is stable mainly between cross-sections at 15° and 30° for all experiments whereas $U_s(n = 0.375)$ values increase for all experiments between 60° and 180°. The effect of outer-bank roughness is small on $U_s(n = 0.375)$ until cross-section at 150° whereas form 150° on divergence between the experiments is noticed, $U_s(n = 0.375)$ for F16_30_30 is lower than for F16_30_00 and F16_30_02.

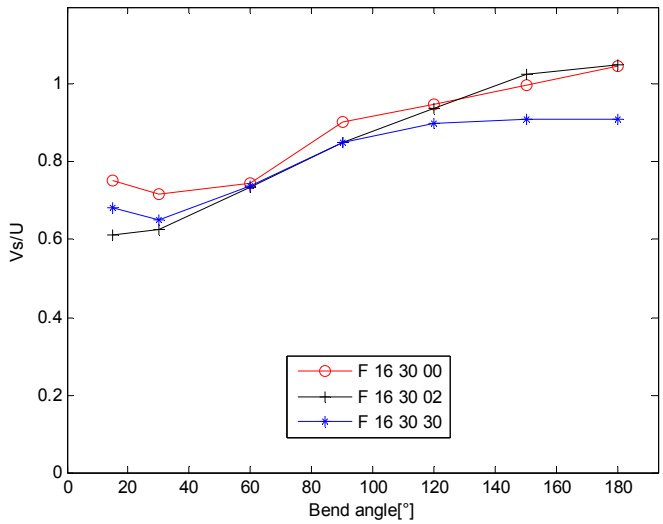

Figure 5
Depth-average downstream velocity evolution along the bend
F16_30_00 (PVC) 'o'; F16_30_02 (SAND) '+' and F16_30_30 (RIPRAP) '*'

3.2 Patterns of cross-stream velocities in the cross-section at 90°

The isolines of the normalized transverse, v_n/U and the isolines of the normalized vertical velocity v_z/U in the cross-section at 90° where the cross-stream circulation is maximal are shown in Figures 6 and 7*abc*. This cross-section has been measured on a refined grid (Figure 2). In Figures 6 and 7, dashed lines were added to help visualize the circulation cells locations, rotation sense and the location of CRC OBC separation. Close to the free-surface and in some cases also close to the bottom, extrapolations towards the free-surface or bottom were made, in such cases non-color contour zones are shown. Blanckaert (2009) gives details about those extrapolations.

The v_n/U positive and negative values in upper and lower water depth channel, respectively, and $v_z > 0$ $v_z < 0$ maximum values at the inner and outer-bank part reveal the CRC size and rotation sense. The CRC outward limit is over the bank toe for all experiments. The maximum positive and negative v_n/U values are 0.4 and -0.3, respectively, at about n = -0.3 m for all experiments whereas the maximum positive and negative v_z/U values are about 0.05 and -0.06.

In the upper outer-bank part v_n/U sign seems to be negative only very close to the free-surface (the ADVP slight intrusive effect on the free-surface does not allow measuring accurately the v_n negative values in upper outer-bank). The (negative) maximum vertical velocity, $v_z < 0$, is close to the bank toe whereas $v_z > 0$ maximum is over the outer-bank. So, the patterns of v_n/U and v_z/U reveal the presence of the OBC in trapezoidal bends with outer-bank angle of 30°.

Figures 6 and 7 *abc* show that with increasing outer bank roughness, the isolines do not vary significantly suggesting that the two circulation cells do not shift or widen with outer-bank roughness. This fact contrasts with the circulation cells widening with outer-bank roughness observed for curved flows with rectangular channel, Chapter III. The CRC and OBC separation line is close to the bank toe hence advecting high momentum flow towards the outer part of the bed which may endanger the bank stability.

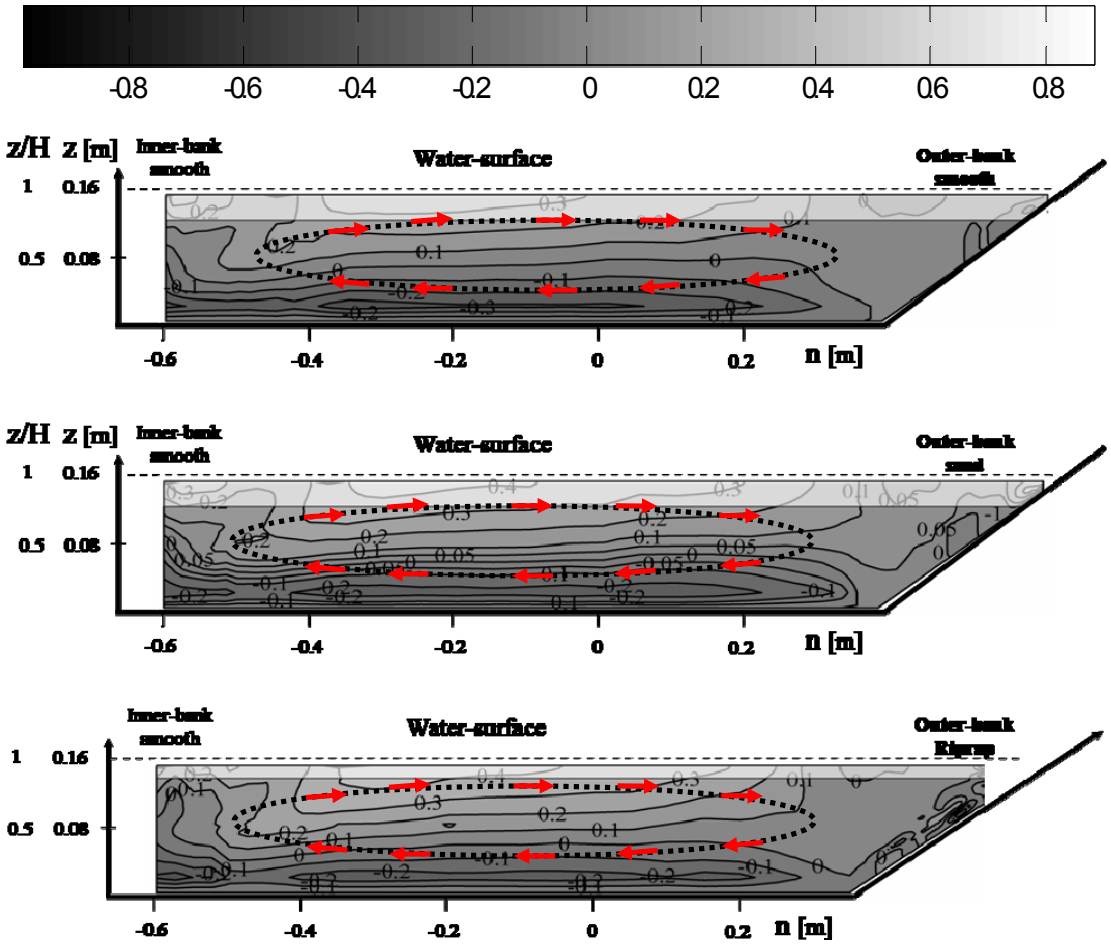

Figure 6.
Cross-section at 90°. Isolines of normalized vertical v_n/U.
F16_30_00 (Top); F16_30_02 (Middle) and F16_30_30 (Bottom).

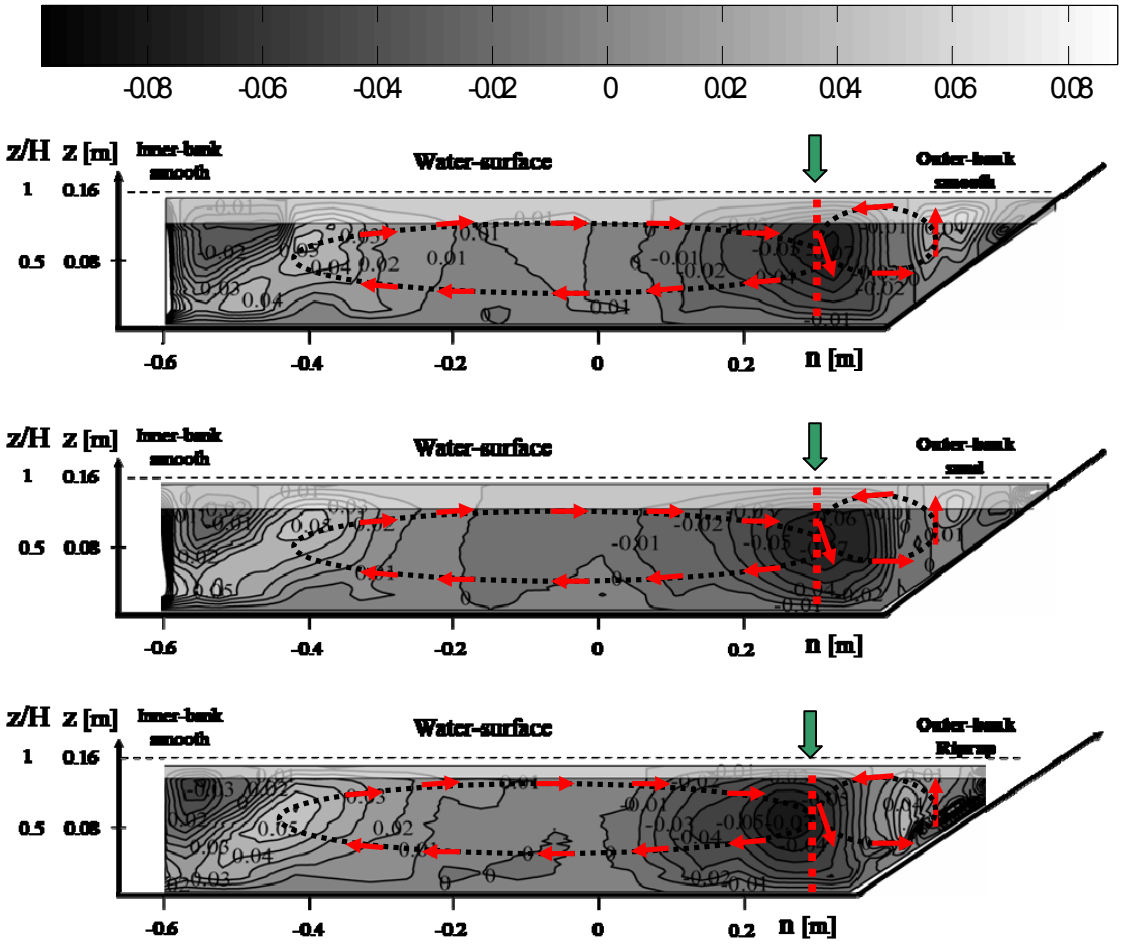

Figure 7.
Cross-section at 90°. Isolines of normalized vertical v_z/U.
F16_30_00 (Top); F16_30_02 (Middle) and F16_30_30 (Bottom).

3.3 Patterns of downstream vorticity in the cross-section at 90°

The downstream vorticity, $\omega_s = \frac{\partial v_z}{\partial n} - \frac{\partial v_n}{\partial z}$, clearly shows CRC and OBC cells at the center and outer-bank upper zone by their negative and positive values respectively. The maximum negative $\omega_s H/U$ values are located in the lower inward part. The negative values spread over the cross-section except between the inclined outer-bank and the free surface. CRC and OBC are separated by the ω_s = 0-countour. The increase of the outer-bank roughness does not affect the CRC. OBC strength, size and location are also unchanged for all experiments. This contrasts with Chapter III where the OBC strength, size and location change with increasing vertical bank roughness.

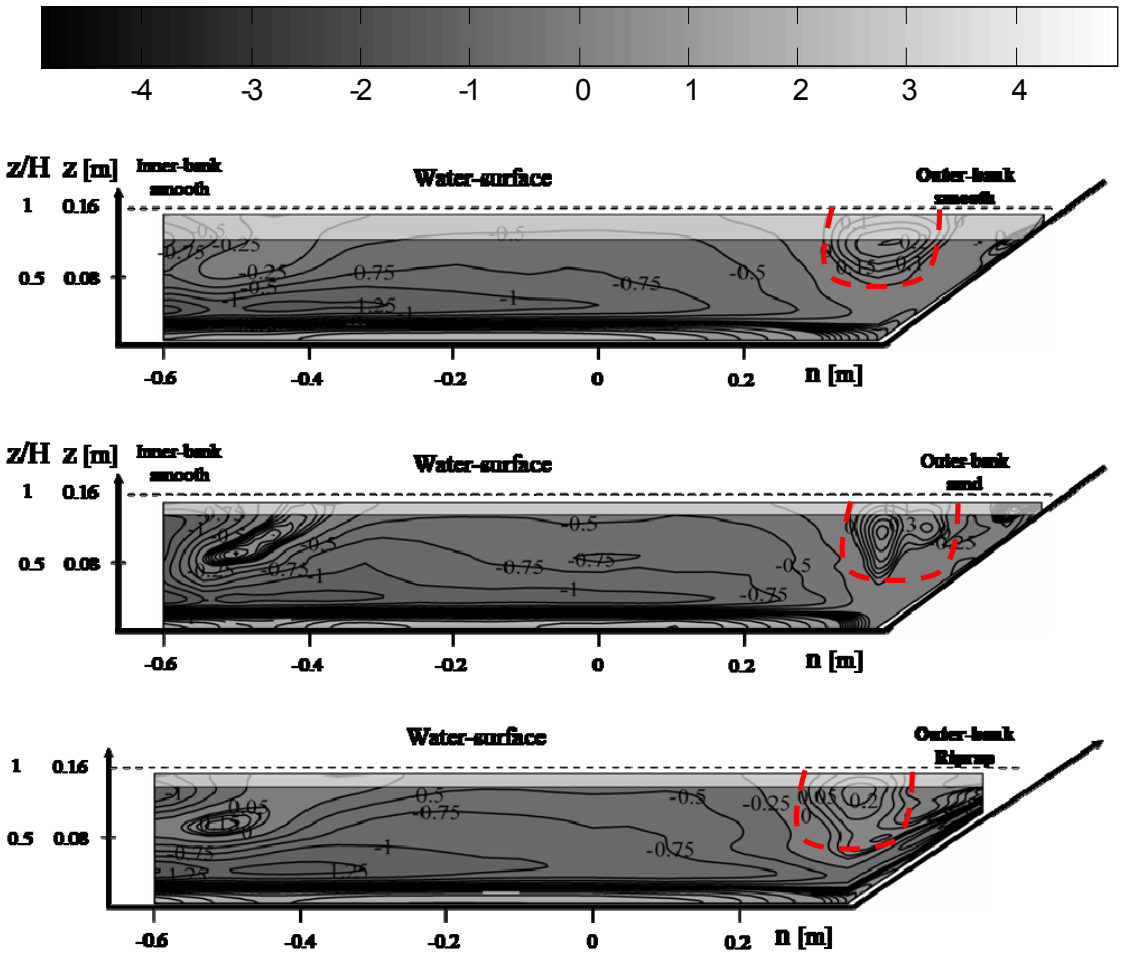

Figure 8

Cross-section at 90°. Isolines of normalized downstream vorticity $\omega_s H/U$.

F16_30_00 (Top); F16_30_02 (Middle) and F16_30_30 (Bottom)

3.4. Patterns of downstream velocity, boundary shear stress, normalized depth-averaged downstream velocity and Chezy factor in the cross-section at 90°

The normalized downstream velocity, v_s/U, in the cross-section at 90° for the three experiments is shown in Figure 9. The maximum downstream velocity location in the lower inner bank is due to the CRC advection, potential vortex effect at bend entry and flow separation. The advection due to CRC is also responsible for the gradually outward shift of the core of maximum downstream velocity along the bend. In the central part of the cross-section the isolines are inclined (up and to the right) suggesting the CRC sense. Over the bank toe that inclination disappears suggesting the halt of the CRC due to the OBC presence.

With increasing outer-bank roughness, the core of maximum downstream velocity is unaffected. The isolines suggesting the presence of OBC zone are slightly shift inward which is in agreement with the slight shift already detected by the cross-stream velocities patterns.

The wetted perimeter shear stress distribution (Figure 9) is estimated by fitting a logarithmic law of the wall (Equations 4 and 5) to the measured velocities even with the strong 3D flow present in a curved flow. Equation 4 represents the velocity profile in the lowest 20% of water depth. Ghosh and Roy (1970) and others concluded that shear stresses distributions calculated from velocity profiles agreed well with those obtained from direct measurements. Still the applicability of the procedure used (which is explained in Chapter 1 in more detail) is verified hereafter.

$$\frac{v_s}{u_*} = \frac{1}{\kappa}\ln\left(\frac{z}{z_0}\right) \tag{4}$$

$$\frac{v_s}{u_*} = \frac{1}{\kappa}\ln\left(\frac{y \cdot u_*}{\upsilon}\right) + 5.3 \tag{5}$$

where v_s is the downstream velocity at a distance z from the boundary, u_* is the shear velocity or shear stress, κ is von-Kármán constant and and $z_0 = {k_s}/{30}$ is the distance at which the log velocity profile indicates zero velocity.

Figure 10a shows a linear relation between normalized measured of primary velocity, the normalized velocity $U^+ = \frac{V_s}{u_*}$, and the normalized vertical coordinate, $Z^+ = \frac{z}{k_s}$ over the bed. Figure 10b also shows a linear relation in the semilogarithmic plot alongside the bank.

Figures 11*ab* shows the spanwise bed and bank shear stress values calculated from different water-depth intervals revealing the same trend despite the intervals taken. The shear stress uncertainty is between 10% and 15% for bed and outer-bank respectively.

Figure 9 shows that amplitude of normalized bed shear stress reduces with outer-bank roughness due to the increase of τ_0. The outer-bank maximum shear stresses are located close to the bank toe for all experiments. The normalized outer-bank maximum and mean shear stresses increase strongly with outer-bank roughness, as its amplitude distribution along the bank. The bed shear stress in the vicinity of the bank toe does not change with outer-bank roughness suggesting that the protection of the adjacent bottom is not extended with outer-bank roughness increase in cross-section at 90°.

An important parameter to 2D depth-averaged numerical codes is the Chezy factor, Chezy factor is defined by Equation 6.

$$C = \sqrt{\rho g}\sqrt{\frac{U_s^2}{\tau_0}} \tag{6}$$

The Chezy factor is mostly considered as a constant factor for 2D simulations. Figure 12 shows that the Chezy factor is constant over the central part of the bed regardless outer-bank roughness. However, in the inner part of the channel flow a big oscillation of the Chezy factor due to flow separation is noticed. Figure 9 shows similar spanwise evolutions of $\frac{\tau}{\tau_0}$ and U_s^2/U confirming the Chezy factor spanwise evolution.

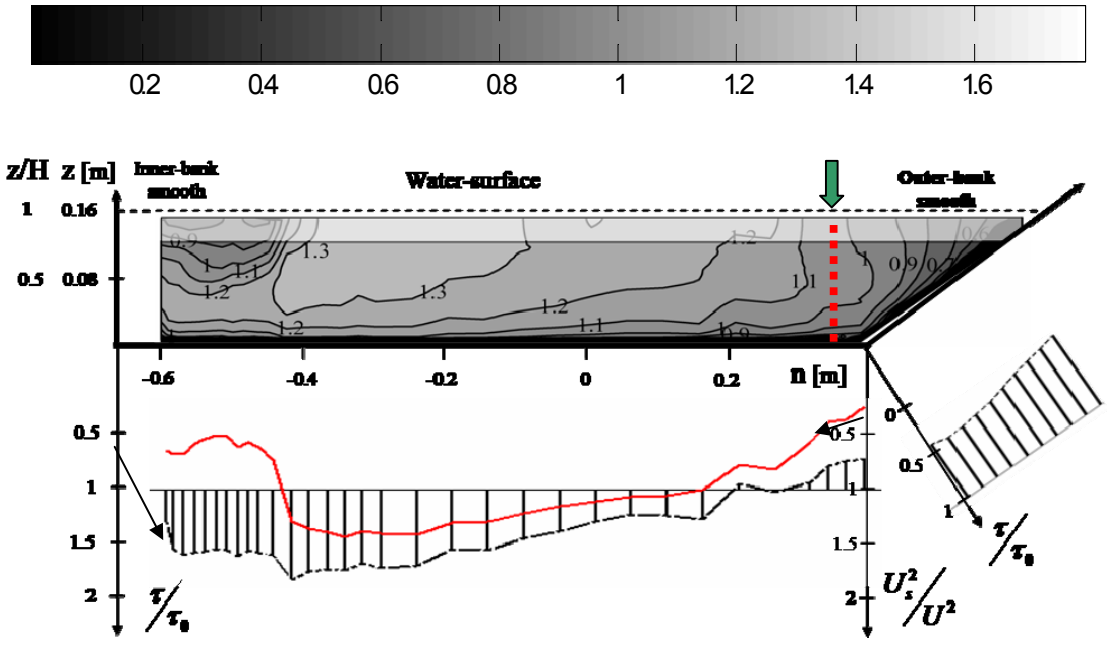

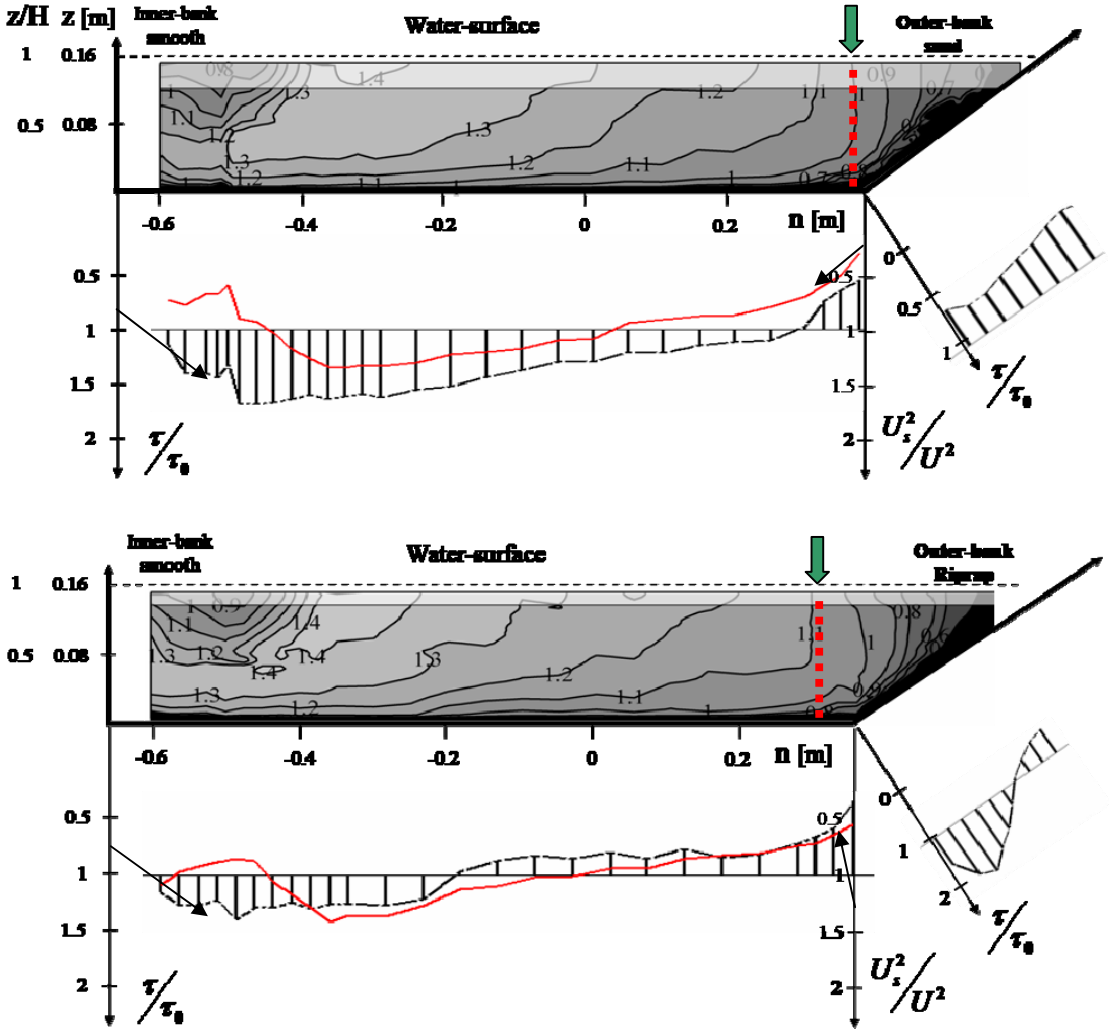

Figure 9

Cross-section at 90°. Isolines of normalized downstream velocity v_s/U , depth-averaged downstram velocity U_s^2/U^2 (red line) and boundary shear stress distribution.

F16_30_00 (Top); F16_30_02 (Middle) and F16_30_30 (Bottom).

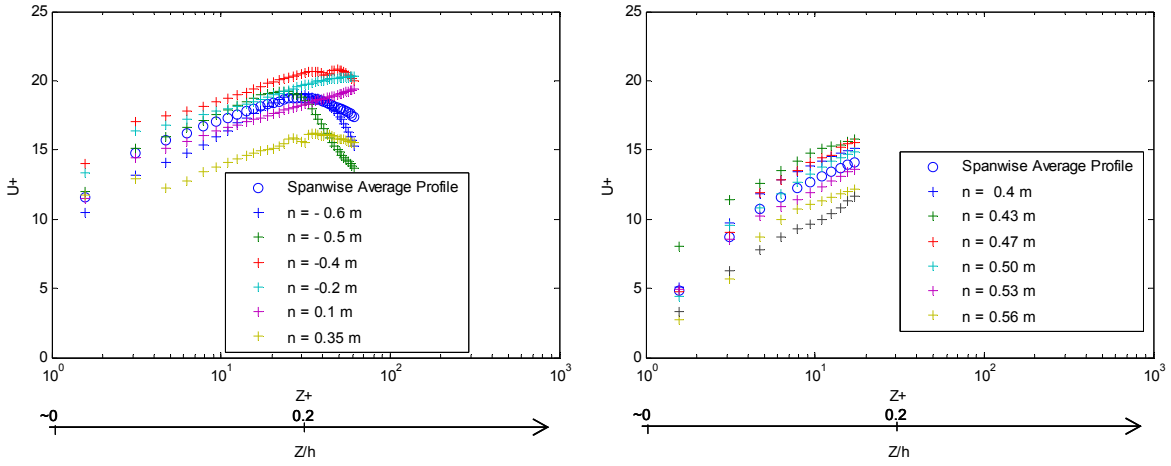

a) b)

Figure 10
a) Log-law plots of mean velocity over the bottom
b) Log-law plots of mean velocity over the outer-bank

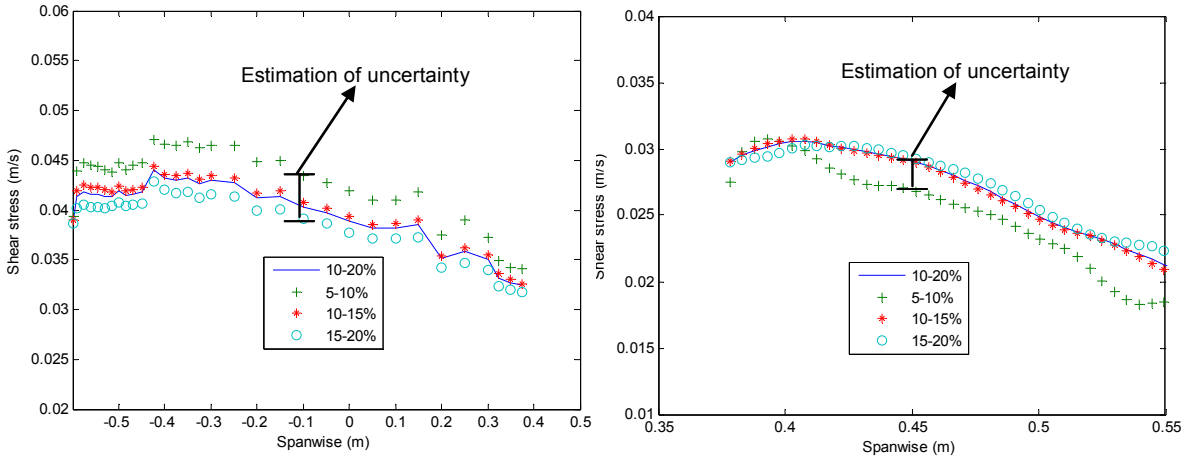

a) b)

Figure 11
a) Spanwise bed shear stress evolution obtained from loglaw as functions of water-depth intervals
b) Spanwise outer-bank shear stress evolution obtained from loglaw as functions of water-depth intervals

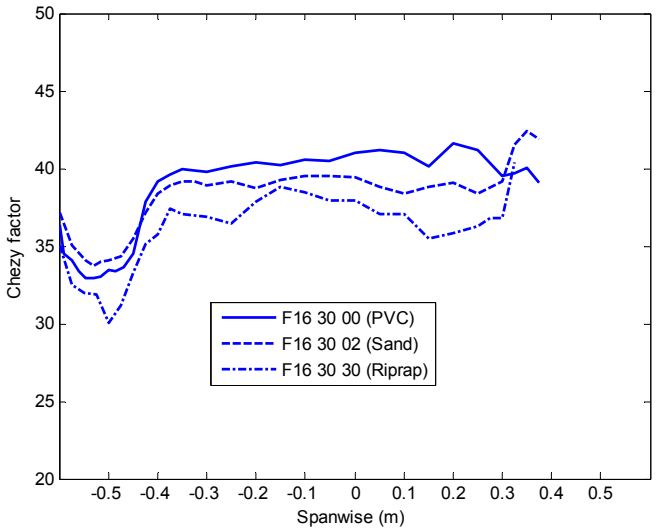

Figure 12
Chezy factor spanwise evolution
(- F16_30_00 (PVC); * F16_30_02 (SAND); F16_30_30 (RIPRAP))

3.5 Patterns of normalized turbulent kinetic energy in the cross-section at 90°

The normalized turbulent kinetic energy, $k = 0.5 * \left(\overline{v_s'^2} + \overline{v_n'^2} + \overline{v_z'^2} \right)$ is shown in Figures 13. The maximum k/u_*^2 locations are at channel center and over bank toe at free-surface (dashed line). In the outer-bank zone k/u_*^2 low values are noticed even for the riprap outer-bank experiment. The OBC flow zone is characterized by low k/u_*^2 which is in agreement with Blanckaert & de Vriend (2004) and Chapters III, IV. With increasing outer-bank roughness, the k/u_*^2 isolines are not changed whereas the k/u_*^2 magnitudes vary slightly which is attributed to the normalization values used.

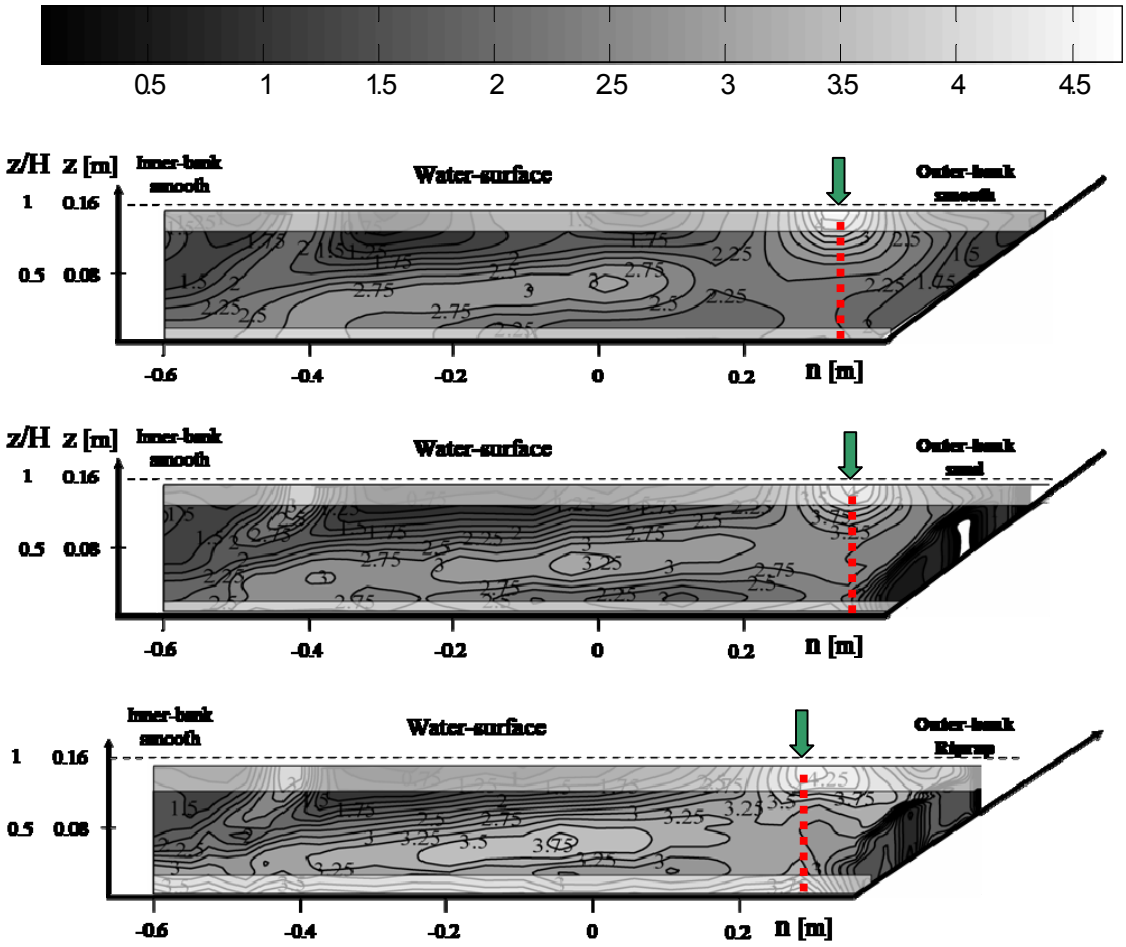

Figure 13

Cross-section at 90°. Isolines of normalized turbulent kinetic energy, k/u_*^2
F16_30_00 (Top); F16_30_02 (Middle) and F16_30_30 (Bottom).

3.6 Patterns of normalized normal stress difference in the cross-section at 90°

Figures 14 show the normalized normal stresses difference, $\left(\overline{v_n'^2}-\overline{v_z'^2}\right)/u_*^2$. Near the flow boundaries, the velocity fluctuations are hindered by geometrical constrains. Near the bottom and near the water surface $v_n'^2 > v_z'^2$ is obtained which is in agreement with (Tominaga et al., 1989). Near the inclined bank it is supposed to be $v_n'^2 < v_z'^2$ (Tominaga et al., 1989) which is not verified. It is attributed to v_z' underestimation (Chapter II). Even so a low values zone close to the outer-bank is visible. With increasing outer-bank roughness, the trapezoidal bend $\left(\overline{v_n'^2}-\overline{v_z'^2}\right)/u_*^2$ patterns are unchanged which is not the case for rectangular curved flows with varying outer-bank roughness experiments, (Chapter III). $\left(\overline{v_n'^2}-\overline{v_z'^2}\right)/u_*^2$ is part of the generation mechanism of circulation cells, to be discussed after, and so its accurate measurement is of paramount importance.

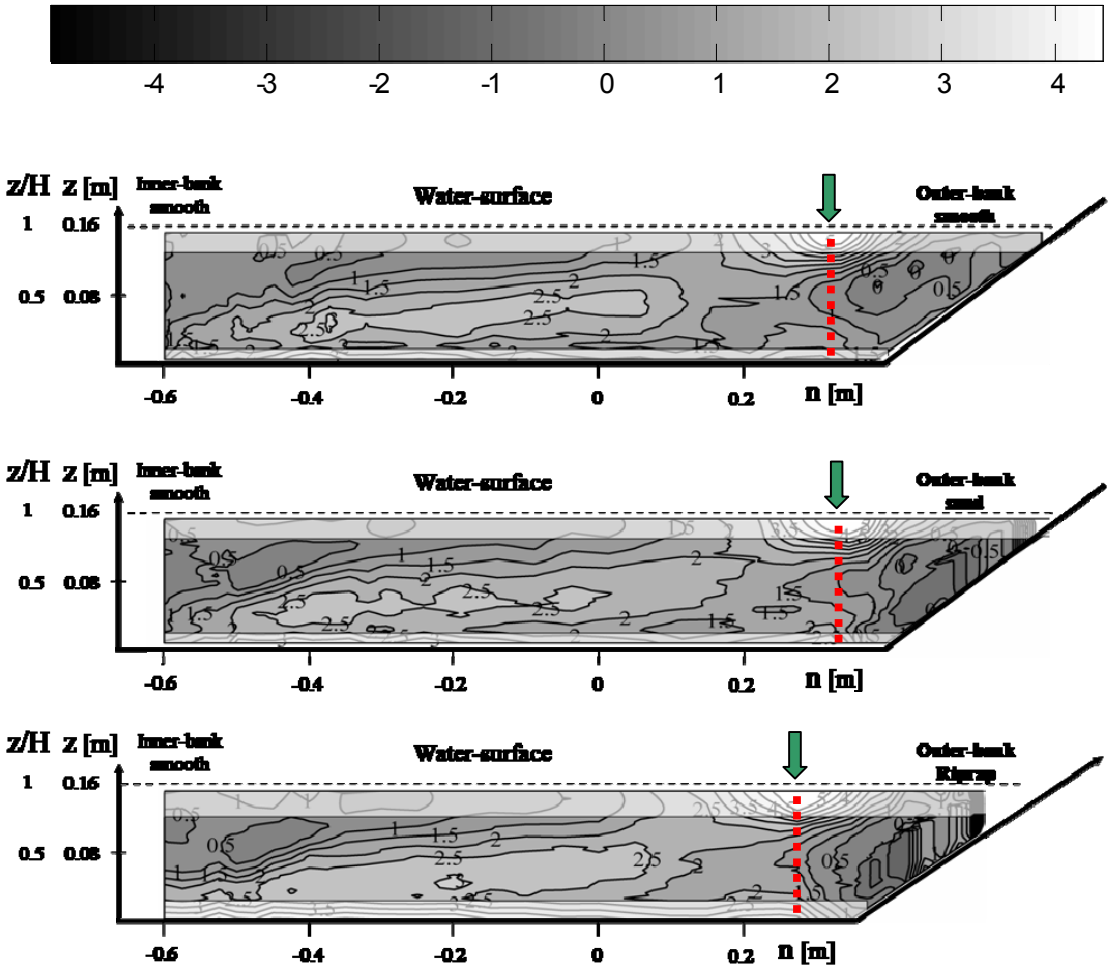

Figure 14
Cross-section at 90°. Isolines of normalized turbulent normal stress difference
F16_30_00 (Top); F16_30_02 (Middle) and F16_30_30 (Bottom).

3.7. Patterns of normalized cross-stream $\overline{v_n' v_z'}/u_*^2$ in the cross-section at 90°

Normalized cross-sectional turbulent shear stresses, $\overline{v_n' v_z'}/u_*^2$, are shown in Figure 15. Figure 15 shows two peaks of $\overline{v_n' v_z'}/u_*^2$ in the center and in the upper outer part. These peaks correlate well with the CRC and OBC cells. Negative values $\overline{v_n' v_z'}/u_*^2$ are seen over the bank toe. With increasing outer-bank roughness the high values peaks do not shift significantly. $\overline{v_n' v_z'}/u_*^2$ accurate measurement is also important for the flow dynamics analysis as downstream vorticity equation relevant terms depend on $\overline{v_n' v_z'}/u_*^2$.

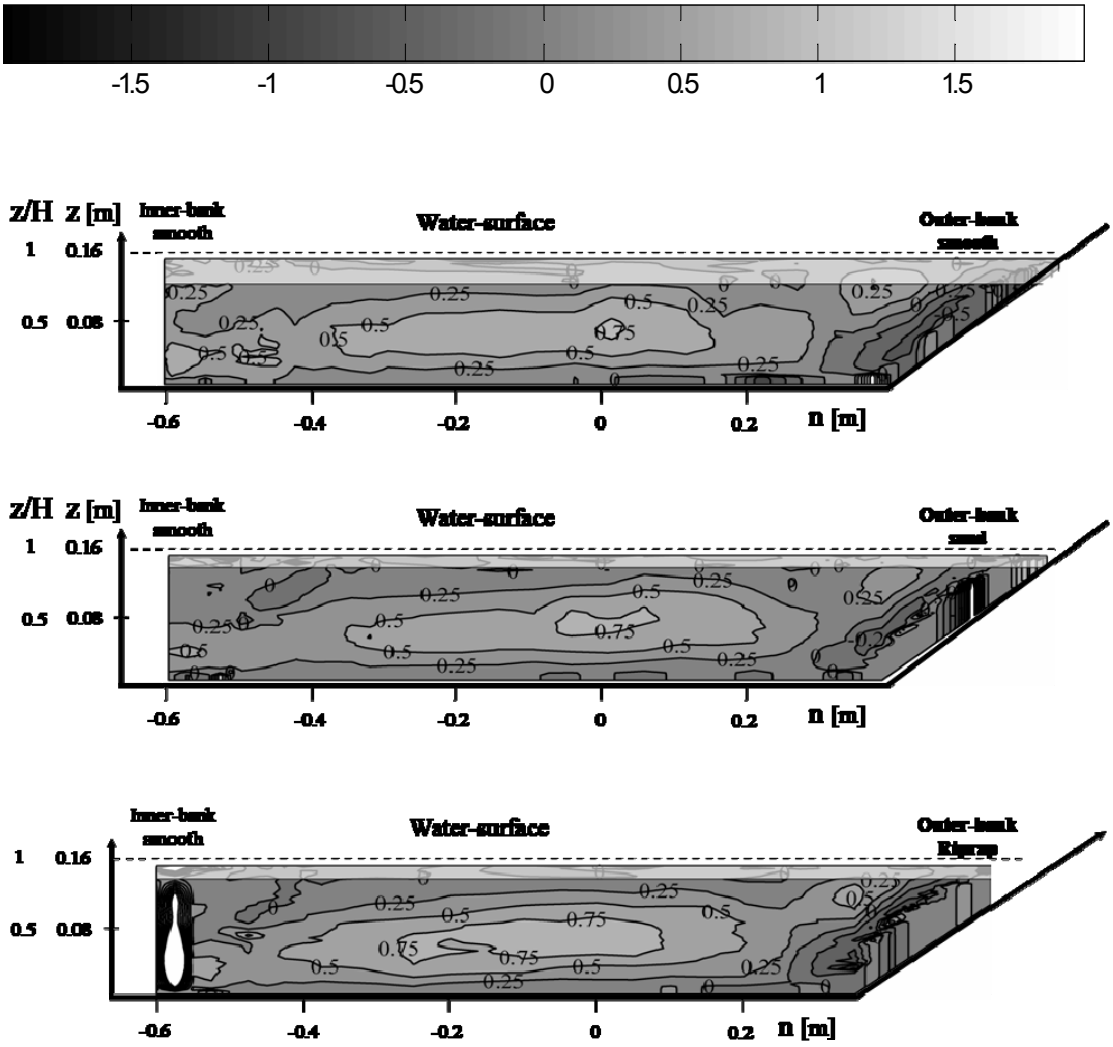

Figure 15

Cross-section at 90°. Isolines of turbulent shear stress $\overline{v_n' v_z'} / u_*^2$
F16_30_00 (Top); F16_30_02 (Middle) and F16_30_30 (Bottom).

4 Mechanisms underlying circulation cells

Blanckaert & de Vriend (2004) methodology, relevant terms of the downstream vorticity equation and the kinetic energy fluxes, is used to study the underlying mechanisms of the circulation cells. The downstream vorticity equation, Equation (7), is obtained by cross-differentiation of the transverse and vertical momentum equations for incompressible flow (Schlichting & Gersten, 2000).

$$\frac{\partial \omega_s}{\partial t} = -\left(\frac{1}{1+n/R} v_s \frac{\partial \omega_s}{\partial s} + v_n \frac{\partial \omega_s}{\partial n} + v_z \frac{\partial \omega_s}{\partial z} \right)$$
$$+ \frac{1}{1+n/R} \omega_s \frac{\partial v_s}{\partial s} + \left[\omega_n \frac{\partial v_s}{\partial n} + \omega_z \frac{\partial v_s}{\partial z} + \frac{1}{1+n/R} \frac{v_n w_s}{R} - \frac{1}{1+n/R} \frac{v_s w_n}{R} \right] - \frac{1}{1+n/R} \frac{\partial}{\partial z} \left(\frac{\overline{v_s'^2}}{R} \right)$$
$$+ \frac{\partial^2}{\partial z \partial n} \left(\overline{v_n'^2} - \overline{v_z'^2} \right) + \frac{1}{1+n/R} \frac{1}{R} \left(\overline{\frac{\partial v_n'^2}{\partial z}} \right) + \left(\frac{1}{1+n/R} \frac{\partial^2}{\partial z^2} - \frac{\partial}{\partial n} \left(\frac{1}{1+n/R} \frac{\partial}{\partial n} \right) \right) \left((1+n/R) \overline{v_n' v_z'} \right)$$
$$+ \upsilon \left(\nabla^2 \omega_s + \frac{2}{(1+n/R)^2} \frac{1}{R} \frac{\partial \omega_n}{\partial s} - \frac{1}{(1+n/R)^2} \frac{1}{R^2} \omega_s \right) \qquad (7)$$

The relevant terms are marked by rectangles. In the second line, the terms within the rectangle represent skewing induced vorticity redistribution by quasi-inviscid deflection of existing mean vorticity. Through several operations (e.g. Blanckaert & de Vriend, 2004) these terms are transformed into:

$$-\frac{1}{1+n/R} \frac{\partial}{\partial z} \left(\frac{v_s^2}{R} \right) + \frac{1}{1+n/R} \frac{v_n \omega_s}{R} + \left[\frac{1}{1+n/R} \frac{\partial v_n}{\partial s} \frac{\partial v_s}{\partial z} - \frac{\partial v_z}{\partial s} \frac{\partial}{\partial n} \left(\frac{1}{1+n/R} v_s \right) \right] \qquad (8)$$

In the red rectangle the term associated with the centrifugal force (CT) is shown. Skewing-induced vorticity is generated by CT.

In the third line, the first term in the left is the cross-stream turbulent anisotropy term (CSTA) and the last term is the cross-stream shear term (CSS), representing the influence of cross-stream turbulent stress components on the vorticity field.

Energy fluxes per unit mass take place through work done by the turbulent stresses as the mean flow deforms (Equation 9). The sum of these energy fluxes is mostly positive i.e.

from mean flow to turbulence. It is called the production or generation of turbulent kinetic energy.

$$P = -\left[\left(\overline{v_s'^2} - \frac{2}{3}k\right)e_{ss} + \left(\overline{v_n'^2} - \frac{2}{3}k\right)e_{nn} + \left(\overline{v_z'^2} - \frac{2}{3}k\right)e_{zz} + 2\overline{v_s'v_n'}e_{sn} + 2\overline{v_s'v_z'}e_{sz} + 2\overline{v_n'v_z'}e_{nz}\right] \quad (9)$$

wherein e_{ij} (i,j = s,n,z) are the strain rates (Batchelor 1970, p.600).

The $2\overline{v_n'v_z'}e_{nz}$ term is shown hereafter (within a rectangle) as it represents the energy flux between mean flow and turbulence and it is correlated with the circulation cells (Figure 15).

4.1 Patterns of normalized centrifugal term in the cross-section at 90°

Figure 16 shows that CT normalized by $\frac{U^2}{H^2}$ is positive in the upper inner part of the channel due to the maximum downstream velocity mid-depth location. The $CT/\left(U^2/H^2\right)$ is negative when integrated over the water depth in the central part of the cross-section and so in agreement with the CRC rotation sense for all experiments as $\omega_s H/U$ values are also negative (Figure 8). In the upper outer part of the cross-section the values are positive and also in compliance with the OBC rotation sense.

With outer-bank roughness increase the OBC and CRC cell corresponding $CT/\left(U^2/H^2\right)$ patterns have small changes being in agreement with previous results that suggest the small effect of bank roughness on the circulation cells for half-trapezoidal channel.

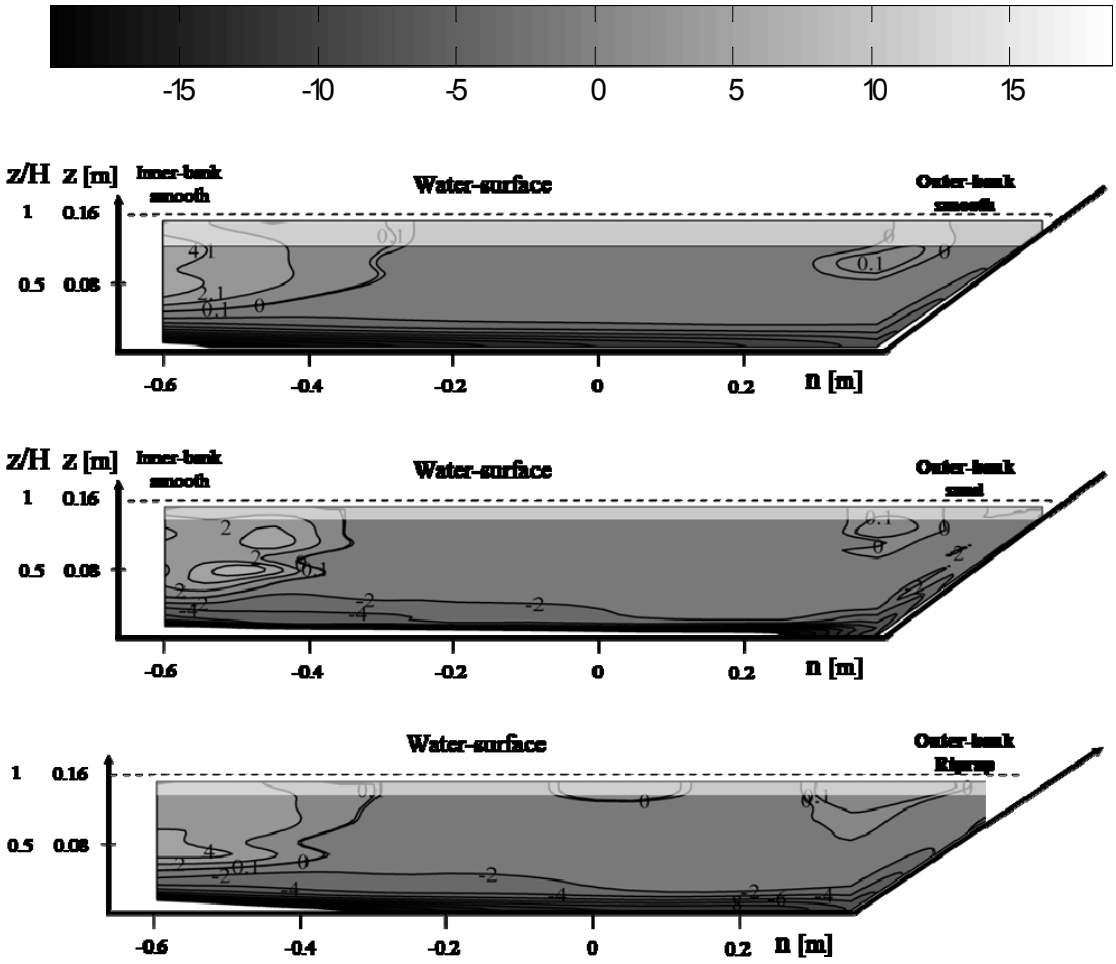

Figure 16
Cross-section at 90°. Isolines of vorticity equation centrifugal term $CT/\left(U^2/H^2\right)$
F16_30_00 (Top); F16_30_02 (Middle) and F16_30_30 (Bottom).

4.2 Patterns of normalized cross-stream anisotropy terms in the cross-section at 90°

Figure 17 shows that normalized CSTA by $\frac{U^2}{H^2}$ is negative in the upper inner part of the cross-section attributed to flow separation. $CSTA/\left(U^2/H^2\right)$ is slightly positive in the central part of the cross-section, and so, not favoring the CRC rotation sense. $CSTA/\left(U^2/H^2\right)$ maximum peak is close to the free-surface in the outer-bank part at about the separation of both cells. $CSTA/\left(U^2/H^2\right)$ is negative in the upper right part of the cross-section and so not favoring OBC rotation sense. These results match well with $CT/\left(U^2/H^2\right)$ patterns and circulation cells patterns. With increasing outer-bank

roughness the $CSTA/\left(U^2/H^2\right)$ patterns do not change significantly, again, agreeing with the circulation cells patterns.

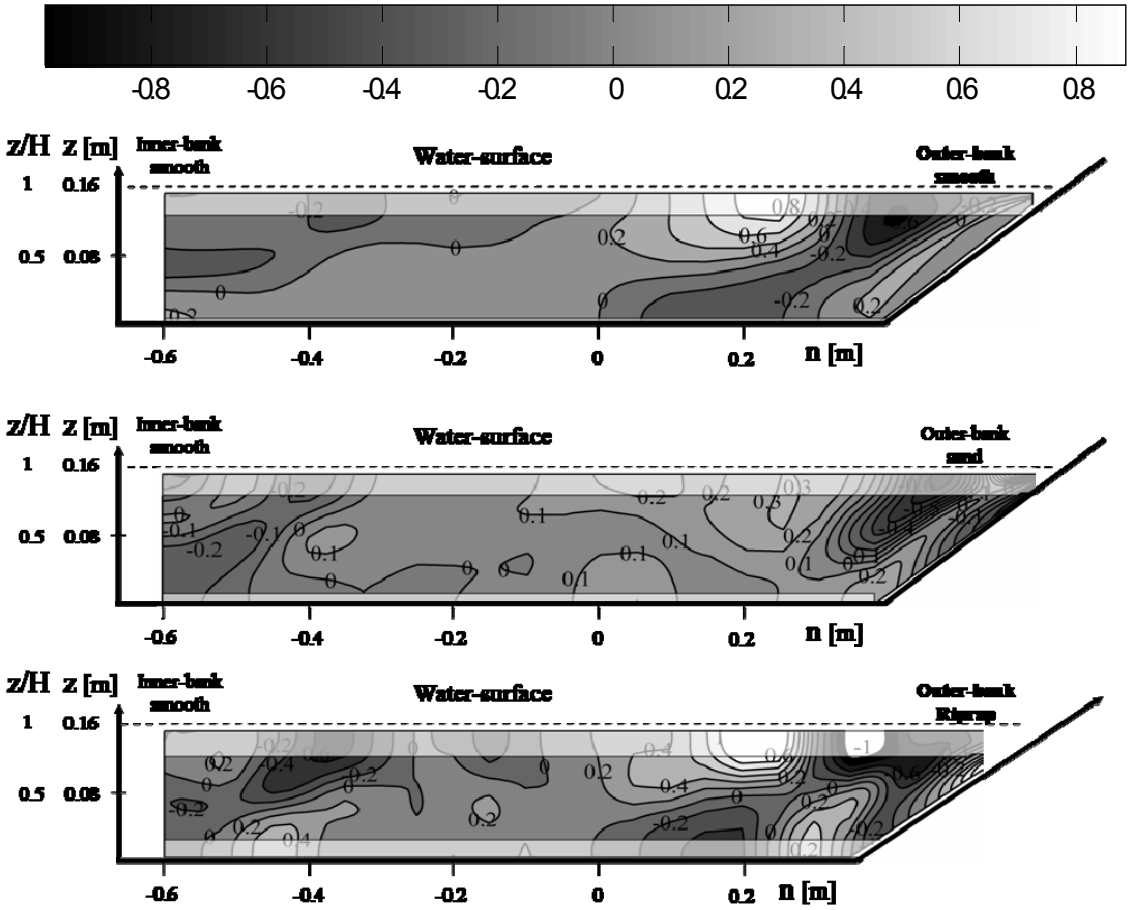

Figure 17

Cross-section at 90°. Isolines of normalized cross-stream turbulence anisotropy term $CSTA/\left(U^2/H^2\right)$ PVC F16_90_00 (Top); F16_90_02 (Middle) and F16_90_30 (Bottom).

4.3 Patterns of normalized cross-stream shear stress terms in the cross-section at 90°

Figure 18 shows isolines of normalized CSS by $\frac{U^2}{H^2}$. The magnitude of this term is higher at channel center. $CSS/\left(U^2/H^2\right)$ positive values at the channel center do not favor the CRC. The outer-bank zone has positive and negative values. The positive values seem to be located over the OBC zone favoring the OBC rotation sense. With increasing outer-bank roughness the $CSS/\left(U^2/H^2\right)$ patterns are also unaffected.

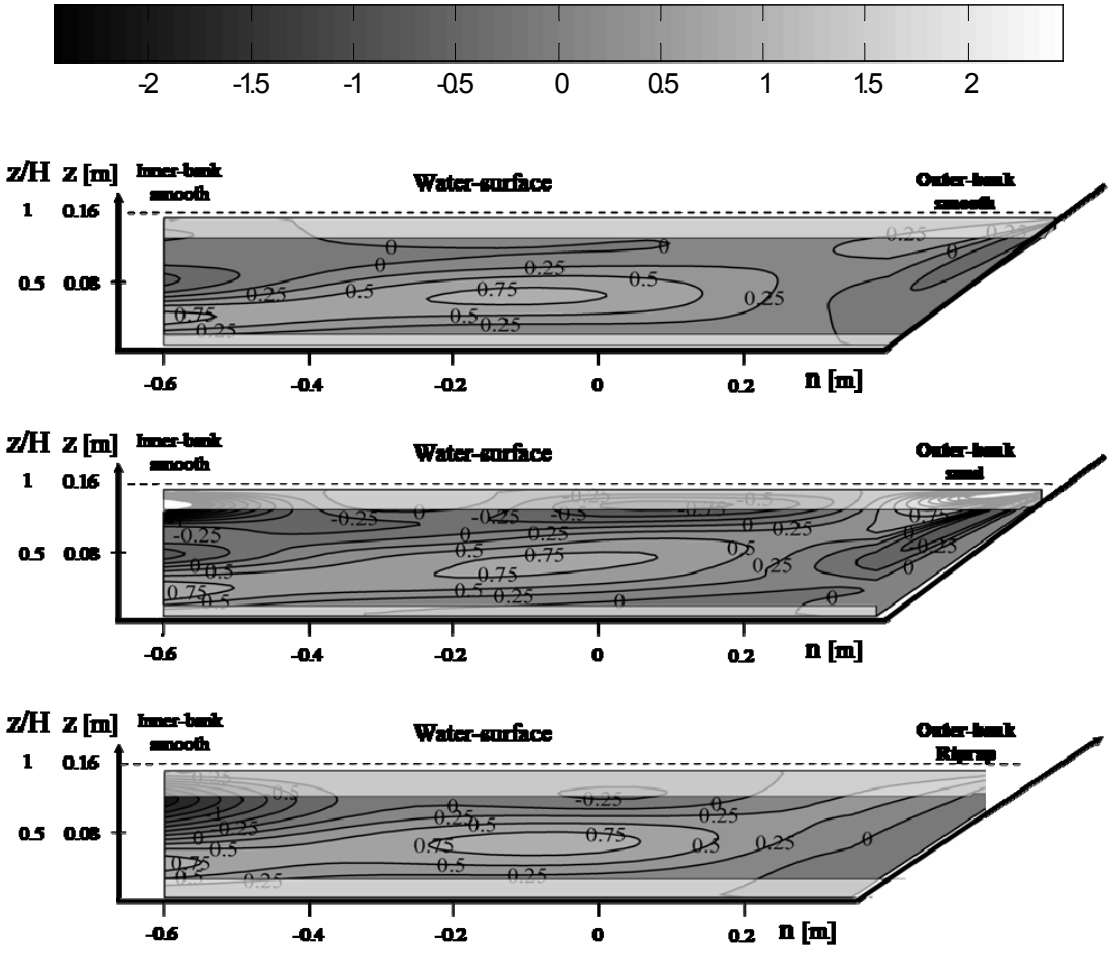

Figure 18

Cross-section at 90°. Isolines of normalized cross-stream turbulence shear stress term $CSS/\left(U^2/H^2\right)$ PVC F16_90_00 (Top); F16_90_02 (Middle) and F16_90_30 (Bottom).

4.4 Patterns of normalized cross-stream kinetic energy fluxes in the cross-section at 90°

Figure 19 shows normalized cross-stream kinetic energy fluxes via $\overline{v_n' v_z'}$ (cf. Equation 9) by $\left(u_*^3 / H\right)$. High kinetic energy fluxes from mean flow to turbulence are observed in the CRC. In the OBC, kinetic energy fluxes are very small, which is in agreement with Blanckaert and de Vriend (2004) even for trapezoidal channels. Negative and positive values in the OBC suggest transfer of kinetic energy from turbulence to mean flow in both senses for trapezoidal channels with varying outer-bank roughness. In order to accurately reproduce the OBC turbulence closures models have to include the possibility of kinetic energy transfer between turbulence and mean flow in either direction.

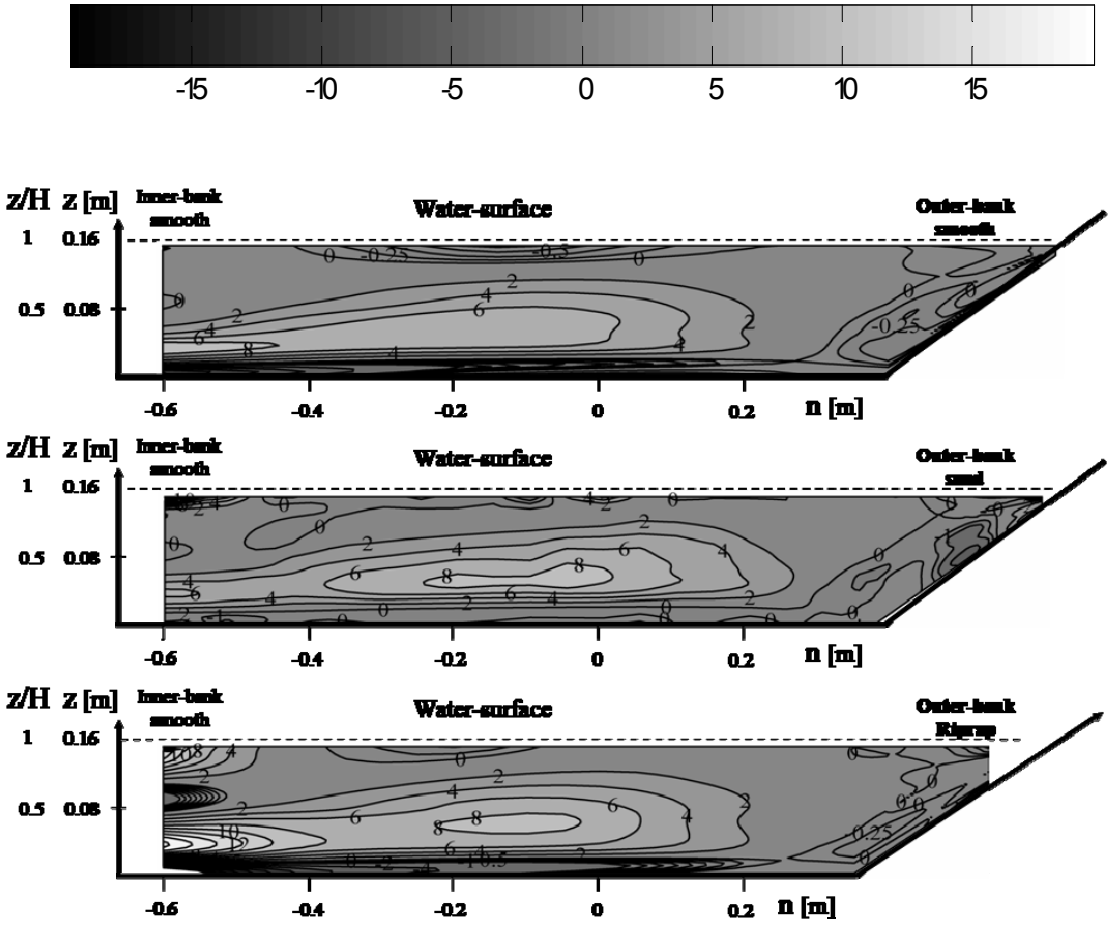

Figure 19
Cross-section at 90°. Isolines of the normalized kinetic energy fluxes between mean flow and the turbulence via cross-stream turbulent stress, $\frac{2\overline{v_n' v_z'} e_{nz}}{\left(u_*^3 / H\right)}$
F16_30_00 (Top); F16_30_02 (Middle) and F16_30_30 (Bottom).

5 Discussion

5.1 Explanation of underlying mechanisms

In order to understand the observations found in this paper Blanckaert & de Vriend (2004) methodology is used. It consists of downstream vorticity equation term-by-term evaluation and also by kinetic energy fluxes analysis.

Tables 3 and 4 show $\omega_s H/U$, area/(BH), $CT/\left(U^2/H^2\right)$, $CSTA/\left(U^2/H^2\right)$, $CSS/\left(U^2/H^2\right)$ and $\frac{2\overline{v_n' v_z'} e_{nz}}{\left(u_*^3/H\right)}$ values from the CRC and OBC centers. Despite the values present in Tables 3 and 4 the evaluation is only qualitative due to the errors associated with derivatives and double derivatives of small quantities.

Table 3
CRC average downstream vorticity equation relevant values and kinetic fluxes

	$\omega_s H/U$ Figure 8	area/(BH)	$CT/\left(U^2/H^2\right)$ Figure 16	$CSTA/\left(U^2/H^2\right)$ Figure 17	$CSS/\left(U^2/H^2\right)$ Figure 18	$\frac{2\overline{v_n' v_z'} e_{nz}}{\left(u_*^3/H\right)}$ Figure 19
F16_30_00	**-0.75**	**0.4**	**-1**	**0.1**	**0.75**	**6**
F16_30_02	**-0.75**	**0.4**	**-1**	**0.1**	**0.75**	**6**
F16_30_30	**-0.75**	**0.4**	**-1**	**0.1**	**0.75**	**8**

Table 4
OBC average downstream vorticity equation relevant values and kinetic fluxes

	$\omega_s H/U$ Figure 8	area/(BH)	$CT/\left(U^2/H^2\right)$ Figure 16	$CSTA/\left(U^2/H^2\right)$ Figure 17	$CSS/\left(U^2/H^2\right)$ Figure 18	$\frac{2\overline{v_n' v_z'} e_{nz}}{\left(u_*^3/H\right)}$ Figure 19
F16_30_00	**0.2**	**0.07**	**0.1**	**-0.7**	**0.25**	**<0**
F16_30_02	**0.2**	**0.07**	**0.1**	**-0.7**	**0.25**	**<0**
F16_30_30	**0.2**	**0.08**	**0.1**	**-0.7**	**0.25**	**<0**

Table 3 shows that CRC is basically favored by centrifugal term, $CT/\left(U^2/H^2\right)$ (as it has the same sign as $\omega_s H/U$ values) and not favored by the cross-stream turbulent shear stress terms ($CSTA/\left(U^2/H^2\right)$ and $CSS/\left(U^2/H^2\right)$). $CT/\left(U^2/H^2\right)$ is the dominant term as it is ten times the cross-stream turbulent shear stress terms. This is in agreement with simplified models for the CRC (e.g. van Bendegom, 1947, Rosovskii, 1957 or Blanckaert and de Vriend, 2004). $\frac{2\overline{v_n' v_z'} e_{nz}}{\left(u_*^3/H\right)}$ positive values indicate a flux of energy from the mean

flow to turbulence. With increasing bank roughness the CRC normalized downstream vorticity value and area are almost constant. The vorticity equation terms are constant which is in agreement with the CRC unchanged status.

Table 4 shows that $CSTA/\left(U^2/H^2\right)$ is the highest term. However, $CT/\left(U^2/H^2\right)$ and $CSS/\left(U^2/H^2\right)$ values have the same order of magnitude. These values suggest that OBC in trapezoidal channels have the characteristics of 1st and 2nd kind of Prandtl's secondary currents. $CSS/\left(U^2/H^2\right)$ and $CT/\left(U^2/H^2\right)$ values are positive in the upper outer-bank zone and so favoring the OBC as they have the same sign of $\omega_s H/U$ whereas $CSTA/\left(U^2/H^2\right)$ does not. A flux of energy from turbulence to mean flow is detected by $\frac{2\overline{v_n' v_z'} e_{nz}}{\left(u_*^3/H\right)}$ negative values for all experiments. So, with increasing outer-bank roughness the vorticity equation terms do not change being in agreement with the OBC $\omega_s H/U$ constant values.

5.2 Comparison with Chapter III and Jin, Y-C et al (1990)

With increasing outer-bank roughness the circulation cells are not affected as well the normalized downstream velocity. This contrast with the curved flows with rectangular channel where the outer-bank roughness increase strongly affects the circulation cells (Chapter III). It seems that low outer-bank inclination hinders the effect of roughness on the OBC. By other hand, the wetted perimeter shear stress distribution is affected, mainly the outer-bank shear stresses, as the mean and maximum values, strongly increase with increasing outer-bank roughness despite the unchanged status of the OBC.

Jin, Y-C et al (1990) results suggest that when a trapezoidal channel has rougher bank than bed a strong peak of shear stress close to the bank toe is generated along the bend. They correlate the shear stress peak with the bank roughness and circulation cells. However, the circulation cells patterns were not measured. In this work, the circulation cells measured did not vary with increasing bank roughness, still a strong peak of shear stress close to the bank toe was observed. Thus it is suggested that only the bank roughness is responsible for surge of bank shear.

6 Conclusions

Experiments were carried out in a sharply 193°-curved laboratory bend with half trapezoidal cross-section, with a 30°-inclined outer-bank, under similar hydraulic conditions for three different roughnesses applied to the outer bank.

The conclusions for the entire bend:

1) The maximum downstream velocity is advected by the center-region cell (CRC) from the inner bank at bed entrance towards the outer-bank at about bend exit.

2) The depth-averaged downstream velocity over the bank toe is similar for all experiments regardless of the outer-bank roughness, except at bend exit where increasing bank roughness decrease depth-averaged downstream velocity.

The conclusions for the cross-section at 90°:

1) In all experiments, the pattern of cross-stream circulation is characterized by the CRC and outer bank cell (OBC).

2) With increasing outer bank roughness, the OBC extension is not significantly affected.

3) 2D-depth averaged simulations assume that Chezy factor is constant over the bottom. For trapezoidal channel with 30°-inclined outer-bank it is found to be a good approximation regardless the outer-bank roughness. However, in the inner-bank region the Chezy factor oscillates strongly due to flow separation caused by the strong bend curvature.

4) Turbulence values close to the outer-bank are unchanged with increasing outer-bank roughness.

5) Bank shear stress maximum is located close to the bank toe. The outer-bank mean and maximum shear stress values increase with increasing bank roughness.

6) CRC is favored by centrifugal term (CT) and opposed by cross-stream shear term (CSS) and cross-stream turbulent anisotropy (CSTA).

7) OBC is favored by CT and CSS and opposed by CSTA.

8) Kinetic energy fluxes have a key role on the OBC generation for trapezoidal curved flows regardless outer-bank roughness as positive and negative values are found in the outer zone of the channel. So, linear numerical models are not able to simulate correctly the OBC as they consider the flux to be always positive from mean flow to turbulence.

REFERENCES

Batcheleor, G.K. (1970). "An introduction to fluid dynamics." Cambridge Univ. press, Cambridge, U.K.

Bathurst, J.C., Throne, C.R. & Hey, R.D. (1979). "Secondary flow and shear stress at river bends." J. Hydr. Div., ASCE, 105 (10), 1277-1295.

Blanckaert, K., & Graf, W.H. (2001). "Mean flow and turbulence in open-channel bend." J. Hydr. Engng. 127(10):835-847.

Blanckaert, K. (2002). "Flow and turbulence in sharp open-channel bends." Ph.D dissertation N°. 2545, Swiss Federal Institute of Technology, Lausanne.

Blanckaert, K., & de Vriend, H.J. (2003). "Non-linear modeling of mean flow redistribution in curved open channels." Water Resources Research, AGU, 39 (12):1375.

Blanckaert, K. & de Vriend, H.J. (2004). "Secondary flow in sharp open-channel bends." J. Fluid Mech., Cambridge Univ. Press, 498: 353-380.

Blanckaert, K. & Graf, WH (2004). "Momentum transport in sharp open-channel bends." J. Fluid Mech., Cambridge Univ. Press, Volume 130, Issue 3, pp. 186-198.

Blanckaert, K. & de Vriend, H.J. (2005). "Turbulence characteristics in sharp open-channel bends." J. Fluid Mech., Cambridge Univ. Press.

Blanckaert, K. & Lemmin, U. (2006). "Means of noise reduction in acoustic turbulence measurements." J.Hydr. Res., 44(1), 3-17.

Blanckaert, K. (2009). "Laboratory experiments on straight and sharply curved open-channel flows. Experimental techniques, data treatment and selected results." In preparation.

Booij, R. (2003). "Measurements and large eddy simulations of the flows in some curved flows." J. Turbulence 4 1-17.

de Vriend, H.J. (1981). "Velocity redistribution in curved rectangle channels". J. Fluid Mech., Cambridge Univ. Press, Vol. 107(6), 429-439.

Einstein, H. A., & Li, H. (1958). "Secondary currents in straight channels." Trans. Am. Geophys. Union, 39 (6) , 1085-1088.

Gosh, S.N. & Roy, N. (1970). "Boundary shear stress distribution in open-channel flow." J. Hydr. Div., ASCE, 96(4), 967-994.

Hersberger, D. (2002). “Measurement of 3D flow field in a 90° bend with ultrasonic Doppler velocity.” Proc.3th Int. Symp. ultrasonic Doppler Meth. for fluid Mech. and Fluid Eng., Lausanne, Switzerland, 59-66.

Hurther, D., & Lemmin, U. (2001). “A correction method for turbulence measurements with a 3-D acoustic Doppler velocity profiler.” J. Atm. Oc. Techn, Vol.18, 446-458.

Ippen, A.T. & Drinker, P.A. (1962). “Boundary shear stress in curved trapezoidal channels.” J.Hydr. Div., ASCE, 88(5), 143-179.

Jin,Y.C., Peter, Steffler, M. & Hicks, F.E. (1990). “Roughness effects on flow and shear stress near outside bank of curved channel.” J.Hydr. Div., ASCE, 88(5), 143-179.

Mockmore, C.A. (1943). “Flow around bends in stable channels.” Transactions, ASCE, Vol.109, 593-628.

Naot, D. (1983). “Response of channel flow to roughness heterogeneity.” J. Hydr. Eng., ASCE, 110(11), 1568-1587.

Nezu, I., Nakagawa, H. & Tominaga, A. (1985). “Secondary currents in a straight channel flow and the relation to its aspect ratio.” Turbulent shear flows 4, Springer-Verlag.,246-290.

Nezu, I. & Nakagawa, H. (1993). “Turbulence in open-channel flows.” Balkema, Rotterdam, The Netherlands.

Perkins, H.J. (1970). “The formation of streamwise vorticity in turbulent flow.” J. Fluid Mech., 44(4), 721-740.

Prandtl, L. (1942) “Füher durch die Strömungslehre”. Vieweg, Braunschweig.

Rolland, T. (1994). “Dévelopment d’une instrumentation Doppler ultrasone adaptée à l’étude hydraulique de la turbulence dans les cannaux.” PhD dissertation N°. 1281, Swiss Federal Institute of Technology, Lausanne.

Rozowskii, I.L. (1957). “Flow of Water in Bends of Open-Channels.” Ac. Sc. Ukr.SSR, Isr. Progr. Sc.Transl., Jerusalem.

Shen, C. (1997). “An acoustic instantaneous particle flux profiler for turbulent flow.” PhD dissertation N°. 1630, Swiss Federal Institute of Technology, Lausanne.

Schlichting, H. & Gersten, K. (2000). Boundary-Layer Theory, 8th edt, Springer, Berlin.

Thorne, C. R. (1982). ‘‘Processes and mechanisms of river bank erosion.’’Gravel-bed rivers, R. D. Hey, J. C. Bathurst, et al., eds., Wiley, NewYork, 227–259.

Tominaga, A., Nezu, I., Ezaki, K. & Nakagawa, H. (1989). "Three-dimensional turbulent structure in straight open-channel flows." J.Hydr. Res. 27,149-173.

Tominaga, A. & Nagao, M. (2002). "Secondary flow structures in bends of narrow open channels with various cross-sections." Proc. Of 4th Intenational conference on hydroscience and Engineering, in CD-ROM.

van Bendegom, L. (1947). "Eenige beschouwingen over riviermorphologie en rivierverbetering." De Ingenieur, 59(4), 1-11 (in Dutch).

Yen, B.C. (1965) "Characteristics of subcritical flow in a meandering channel." Inst. for Hydr. Res., Univ. of Iowa, Iowa City, Iowa.

Chapter VI

CONCLUSIONS

1 Introduction and objectives

Bank erosion is a crucial problem in fluvial hydraulics and it is far from being fully understood and therefore modeled. Despite that, experimental investigation is scarce. Without experimental research the understanding of complex three-dimensional flow and therefore the development of numerical tools is compromised.

This work investigates systematically the influence of the outer bank inclination and roughness on the patterns of main flow, secondary flow, turbulence and outer-bank shear stress in a straight channel and in a sharply curved open-channel laboratory bend.

Experiments were carried out in a laboratory open-channel. It consists of a 9 m long straight entry reach, followed by a 193° bend with constant centerline radius of curvature of R=1.7 m and a 5 m long straight exit reach. The flume width is B = 1.3 m. The bed of the flume has glued quasi-uniform sediments of d = 0.002 m. The inner bank is made of smooth PVC. The outer-bank inclination and roughness elements were varied throughout the work (Table 1). Table 1 also shows the organization of this report.

Table 1
Experiments per chapter

Inclination of outer bank ⇒ / ***Roughness of outer bank*** ⇓	30°	45°	90°
Smooth PVC	Chapter 4/Chapter 5	Chapter 4	Chapter 2/Chapter4
k_s = 0.002 m (sand)	Chapter 5	Appendix	Chapter 2
k_s = 0.03 m (riprap)	Chapter 5	Appendix	Chapter 2

Hence, this work's goals are:

i) To measure in a systematic way straight and curved open-channel flows with varying bank inclination and roughness, including all three mean velocity components and all six Reynolds stresses on a fine grid.

ii) To gain insight in the relevant physical mechanisms responsible for the patterns observed.

iii) To provide an extensive data set and guide lines for numerical modeling.

2 Conclusions

Two main topics were investigated: i) The influence of bank inclination and roughness on straight-channel flow patterns; ii) The influence of outer-bank inclination and roughness on curved flow patterns.

2.1 Straight-channel flow

Tables 1 and 2 show bank and bed maximum values from experiments, Chow (1959) and *Knight's method*. Chow (1959) wetted perimeter shear stress distribution is in agreement with the measurements for channel with quasi-homogeneous roughness distribution. Chow (1959) method is not longer suitable for channels with difference between bank and bed roughnesses. *Knigth's method* estimations are in full agreement with the experiments. The small differences observed are attributed to the fact that the channel is half-trapezoidal and not trapezoidal (as supposed by the *Knigth's method*).

Table 1
Maximum bank shear stress values for trapezoidal channels obtained in this work, Chow (1959) [ ] and Knight's equations ( )

Inclination of outer bank ⇒ / ***Roughness of outer bank*** ⇓	30°	45°
Smooth PVC	0.52[1] (0.57)	0.5 [1] (0.49)
k_s = 0.002 m (sand)	0.9 [1] (1.28)	0.89 [1] (1.18)
k_s = 0.03 m (riprap)	1.8[1] (2.1)	1.8[1] (2)

Table 2
Maximum bed shear stress values for trapezoidal channels obtained in this work, Chow (1959) [ ] and Knight's equations ()

Inclination of outer bank ⇒ / ***Roughness of outer bank*** ⇓	30°	45°
Smooth PVC	1.44 [1.3] (1.33)	1.33 [1.3] (1.29)
k_s = 0.002 m (sand)	1.3 [1.3] (1.17)	1.3 [1.3] (1.19)
k_s = 0.03 m (riprap)	1.16[1.3] (0.98)	1.15 [1.3] (1)

The downstream velocity patterns and circulation cells analyses are useful for the comprehension of the wetted perimeter shear stress values obtained. It was measured that with increasing outer-bank roughness the number of circulation cells increase mainly at channel center. The maximum downstream velocity increases and decreases at about channel center and over the inclined bank, respectively, with increasing outer-bank roughness. These results are in agreement with the high shear stress values at

channel center. The downstream velocity patterns and circulation cells agree with the wetted perimeter shear stress distribution which reinforces the values presented in Tables 1 and 2.

2.2 Curved flow

Curved flows results confirm circulation cells paramount importance on downstream velocity and thereby on wetted perimeter shear stress distribution. In rectangular curved channel three cells were observed regardless outer-bank roughness. The center-region cell (CRC), the outer-bank cell (OBC) and the lower outer-bank cell (LOBC). For trapezoidal channels only CRC and OBC were observed regardless bank roughness and inclination combination.

Regarding the interaction between the cells, it was concluded that OBC has a vital role on the circulation cells patterns, as the OBC widening or shift inwards affects the others circulation cells, CRC and LOBC.

2.2.1 OBC

For rectangular channel, the OBC amplifies and widens considerably with increasing outer bank roughness. Hence the near-bank cells protective effect on the outer bank and adjacent bed is amplified. The OBC widening increases the LOBC size.

For trapezoidal channel, the OBC looses strength and size with decreasing outer-bank angle. The OBC is located over the bank toe for trapezoidal channel along most of the bend. Despite OBC smaller and weaker situation it manages to halt the CRC. Hence, OBC location is very important in protecting the outer-bank regardless its strength or size.

For 30°-inclined outer-bank channels, the OBC does not shift or widen with increasing outer bank roughness. This is an interesting result as it contrasts with rectangular channels (where increasing outer-bank roughness produces a wider OBC).

The mechanisms underlying the OBC are disclosed by analyzing the downstream vorticity equation main terms. All terms follow the variation of the OBC size and strength with outer-bank geometry. The centrifugal term (CT) favors always the OBC whereas the cross-stream turbulent anisotropy term (CSTA) does not. The cross-stream shear term (CSS) is more complex as it favors the outer-bank cell rotation for all experiments except for one, the rectangular channel with riprap outer-bank test. In OBC zone, the kinetic energy transfer between turbulence and mean flow is in both senses for all experiments, confirming and extending Blanckaert (2002) findings.

2.2.2 CRC

The CRC causes a gradual outward shift of the core of maximum downstream velocity along the bend from the inner bank towards the outer bank. The CRC also varies with the cross-section shape and bank roughness. The CRC variation is due to OBC. For rectangular channels, with increasing outer-bank roughness the CRC diminishes. For trapezoidal channels, with decreasing outer-bank angle the CRC diminishes. However, with increasing outer-bank roughness for channels with 30°-inclined bank the CRC size

rests constant. CRC known mechanisms are confirmed for all experiments, hence, CRC is favored by CT and opposed by CSS and CSTA.

2.2.3 Turbulence

Turbulence close to the outer-bank in curved flows is known to be low from foregoing experiments. Despite its low values, it continues to be affected by the bank roughness and bank inclination. For rectangular channels, low-turbulence zone spans inwards with increasing outer-bank roughness. For trapezoidal channels, low-turbulence zone spans inwards with decreasing bank slope. For 30°-inclined bank channels, the turbulence close to the bank does not vary with increasing outer-bank roughness. Turbulence maximums are located at about channel center mid-depth and at about CRC and OBC separation close to the water surface for all experiments. Turbulence maximum at channel center is unchanged with varying outer-bank roughness and inclination angle however the maximum located in the outer-bank follows the trend describe above for the low-value close to the outer-bank.

2.2.4 Bank shear stress

For rectangular curved flows the bank shear stress increases with increasing outer-bank roughness and the maximum is located at about mid-depth where OBC and LOBC converge. For trapezoidal curved flows, with increasing outer-bank roughness the bank shear stress increases, the bank shear stress distribution amplitude range widens and its maximum comes closer to the bank toe. For the trapezoidal curved flow, the outer-bank angle has small impact.

2.2.5 Trapezoidal curved flow with 45°-inclined bank and varying bank roughness

Appendix shows the experiments made on curved flows with 45°-inclined outer-banks with sand and riprap roughnesses. The size of the OBC, OBC strength, the downstream vorticity equation terms and bank shear stresses values are in full agreement with Chapters III to V, so reinforcing all conclusions made on this work.

3 Future work

The paramount role of OBC in curved flows as function of the outer-bank inclination or roughness is shown in this report. However more experiments are needed to confirm in a broader spectrum the trend suggested by the 9 experiments performed. Figures 1 and 2 results are shown as suggestion of future work.

Figure 1 shows the CRC and OBC separation location from the outer-bank (n = 0.65 m) whereas Figure 2 shows the OBC strength. Figures 1 and 2 were made by nine points from the nine experiments and interpolation between points. Interpolation is a weak point which imposes confirmation from future works.

3.1 CRC OBC separation locus

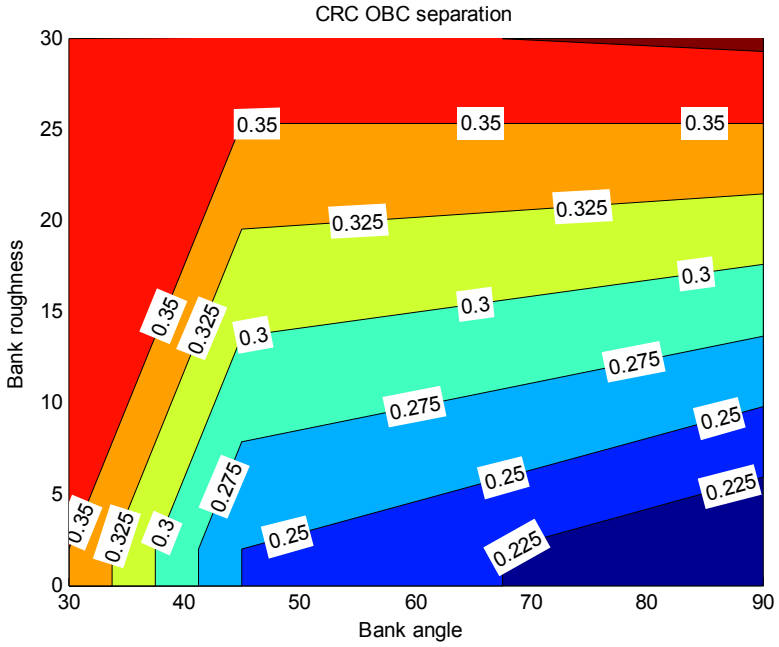

ω_s *H/U-0 isoline*	30°	45°	90°
k_s = 0.03 m (riprap)	0.35	0.37	0.38
k_s = 0.002 m (sand)	0.35	0.25	0.2
Smooth PVC	0.35	0.25	0.2

Figure 1 Distance of the CRC OBC separation line to the outer-bank

Figure 1 shows the distance from normalized downstream vorticity ω_s *H/U-0* isoline to the outer-bank (outer-bank and water surface spanswise location, n = 0.65 m) representing the distance from the CRC and OBC separation to the outer-bank. Figure 1

shows that 30°-bank inclination channels regardless the bank roughness and outer-bank with riprap channels produce smaller CRC as the separation of CRC and OBC is further away from the bank.

3.2 OBC strength

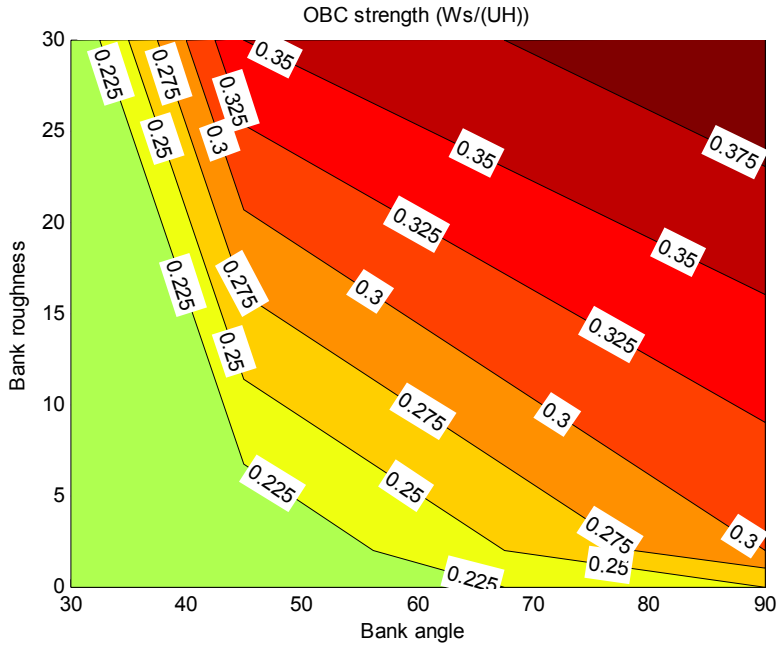

$\omega_s H/U$	30°	45°	90°
k_s = 0.03 m (riprap)	0.2	0.35	0.4
k_s = 0.002 m (sand)	0.2	0.2	0.3
Smooth PVC	0.2	0.2	0.25

Figure 2 OBC strength

Figure 2 shows that OBC from rectangular channel with riprap is the strongest whereas from 30°-inclined bank is the weakest. With decreasing bank angle the OBC strength decreases mainly if the outer-bank is rough.

APPENDIX

F16_45_02 AND F16_45_30 RELEVANT RESULTS

F16_45_02

Patterns of normalized downstream velocity, boundary shear stress, depth-averaged downstream velocity and Chezy factor in the cross-section at 90°

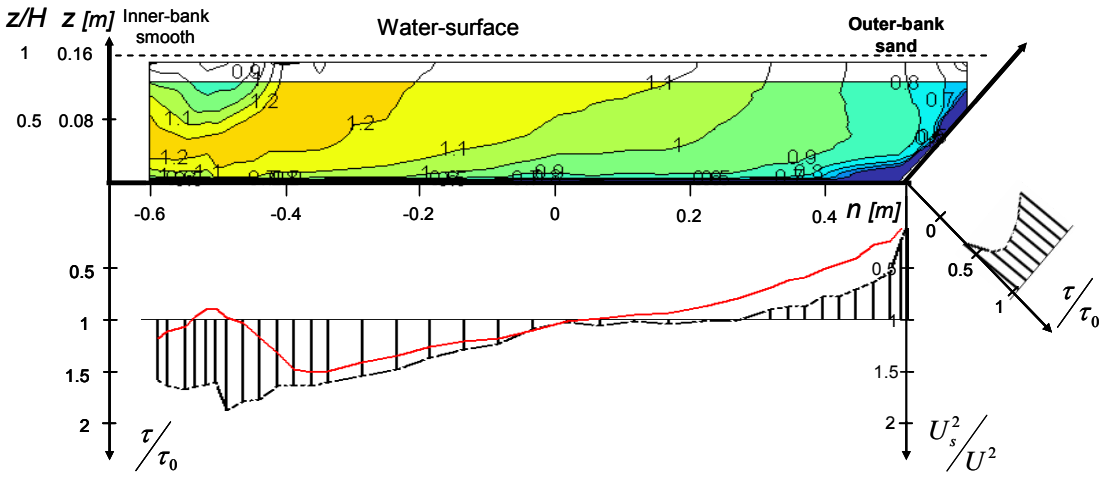

Patterns of normalized cross-stream velocities in the cross-section at 90°

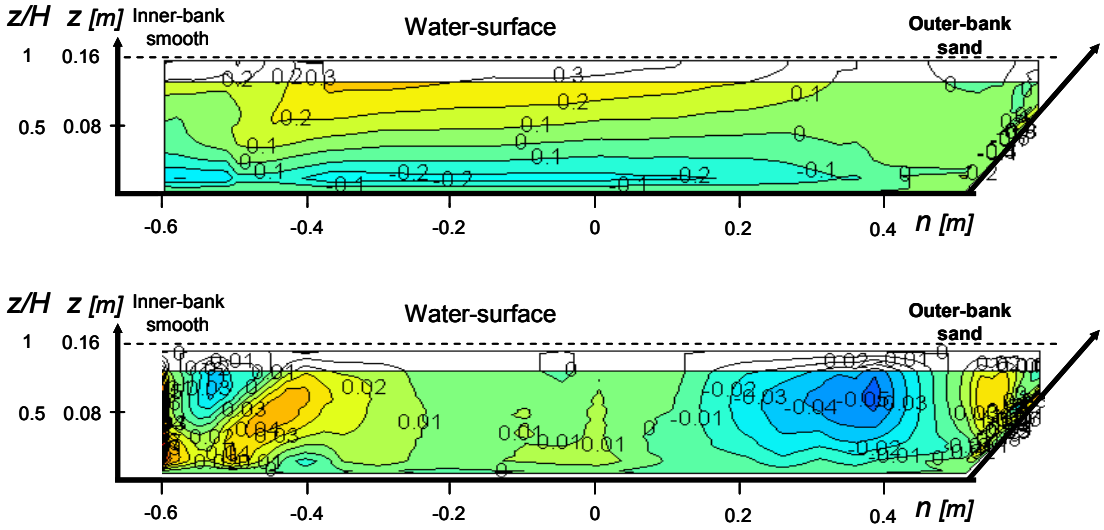

Patterns of normalized downstream vorticity in the cross-section at 90°

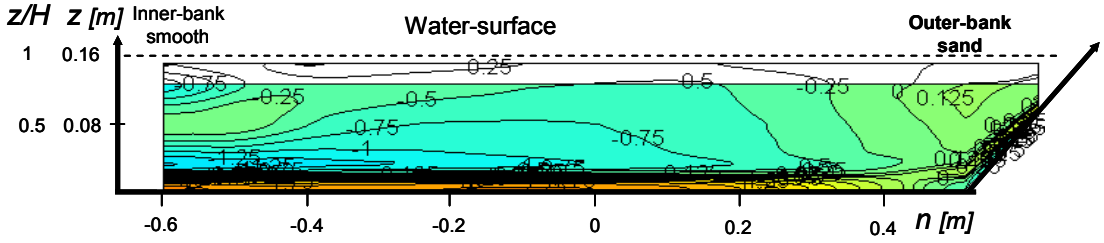

Patterns of normalized turbulent kinetic energy in the cross-section at 90°

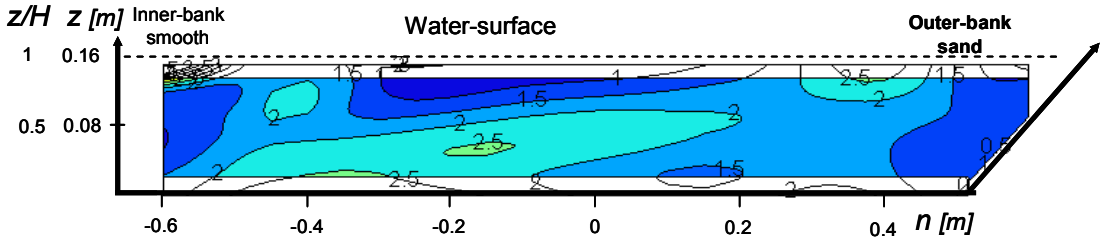

Patterns of normalized normal stress difference in the cross-section at 90°

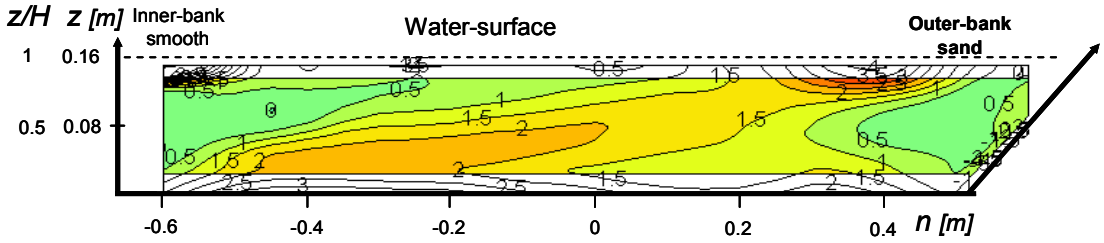

Patterns of normalized cross-stream $\overline{v_n' v_z'} / u_*^2$ in the cross-section at 90°

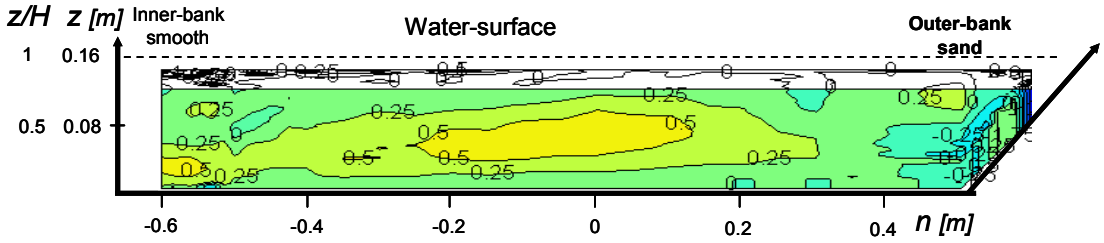

Patterns of normalized centrifugal term in the cross-section at 90°

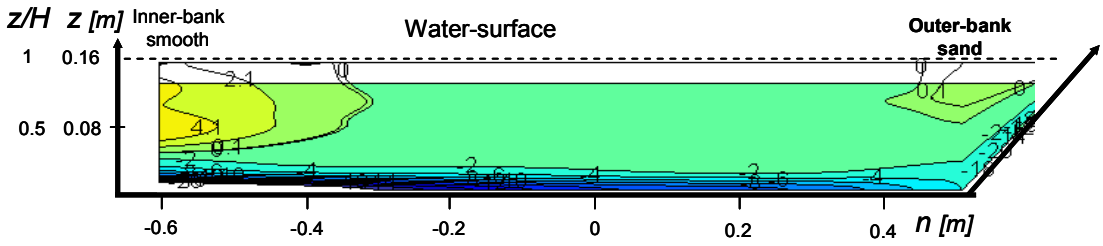

Patterns of normalized cross-stream anisotropy terms in the cross-section at 90°

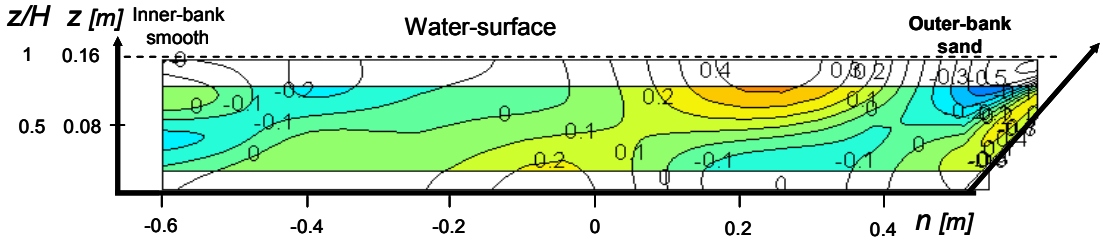

Patterns of normalized cross-stream shear stress terms in the cross-section at 90°

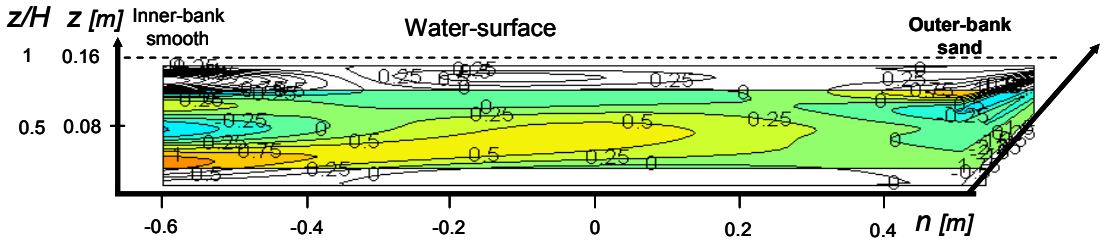

Patterns of normalized cross-stream kinetic energy fluxes in the cross-section at 90°

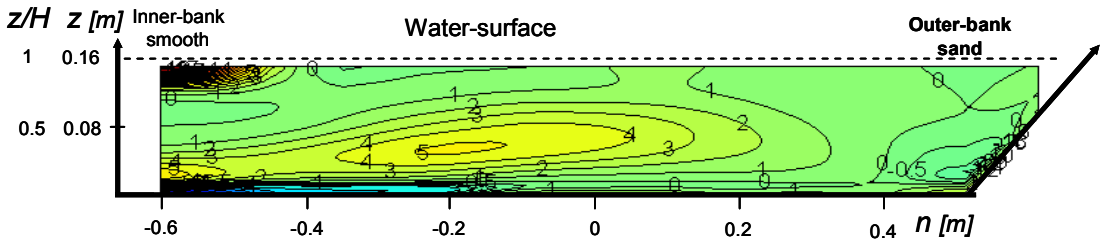

F16_45_30

Patterns of normalized downstream velocity, boundary shear stress, depth-averaged downstream velocity and Chezy factor in the cross-section at 90°

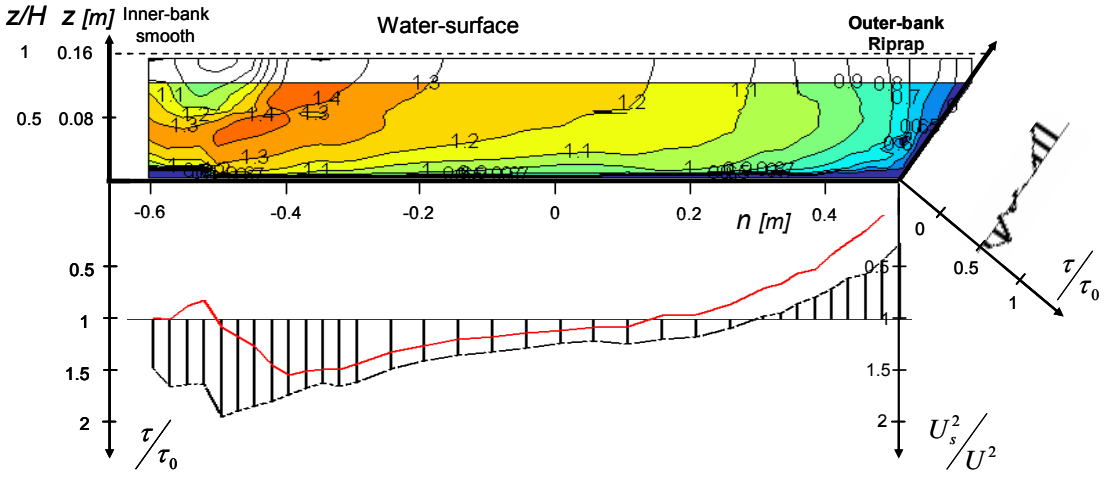

Patterns of normalized cross-stream velocities in the cross-section at 90°

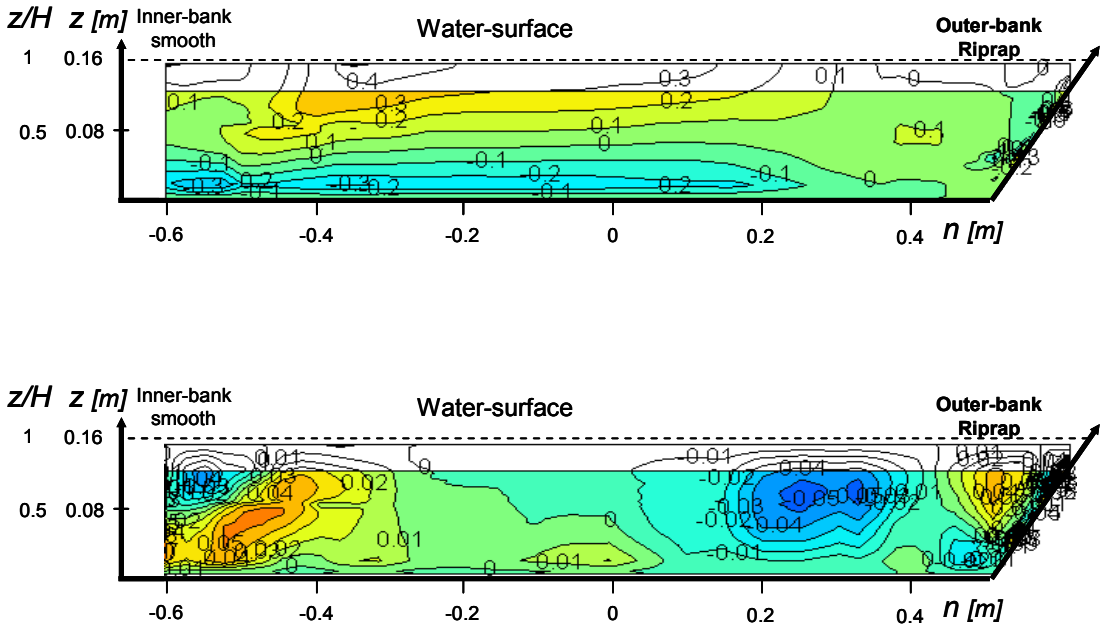

Patterns of normalized downstream vorticity in the cross-section at 90°

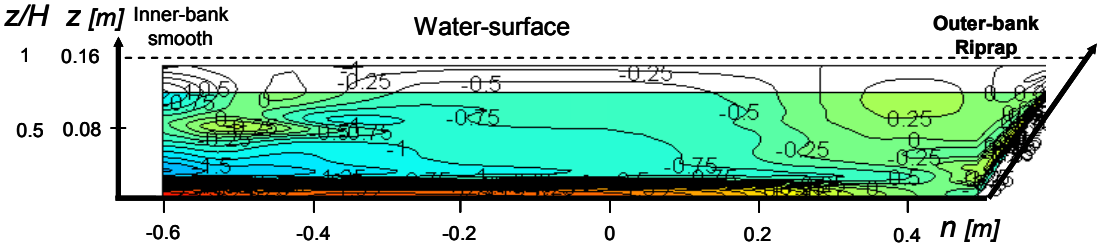

Patterns of normalized turbulent kinetic energy in the cross-section at 90°

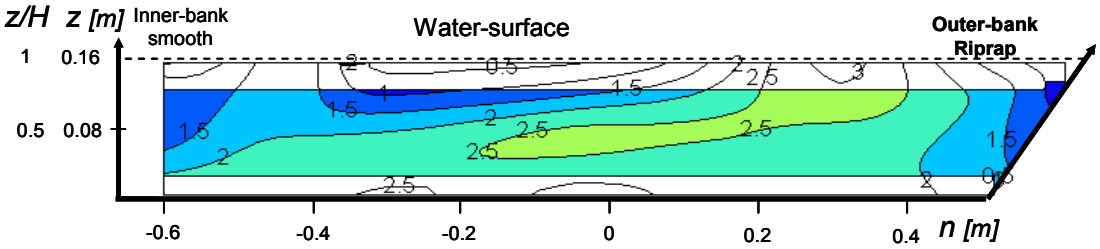

Patterns of normalized normal stress difference in the cross-section at 90°

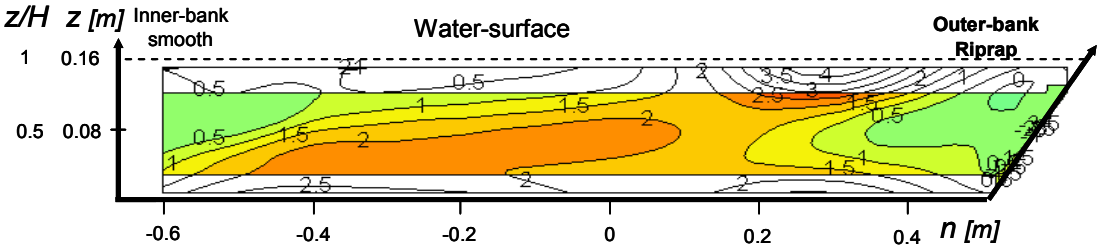

Patterns of normalized cross-stream $\overline{v_n' v_z'} / u_*^2$ in the cross-section at 90°

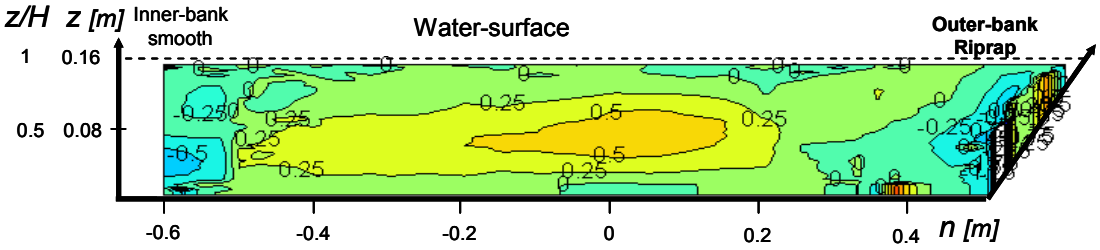

Patterns of normalized centrifugal term in the cross-section at 90°

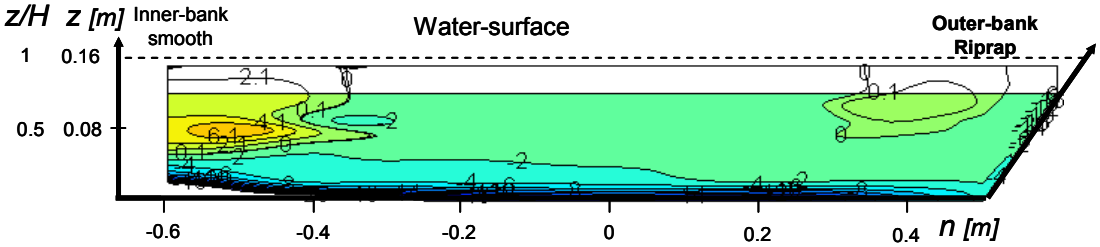

Patterns of normalized cross-stream anisotropy terms in the cross-section at 90°

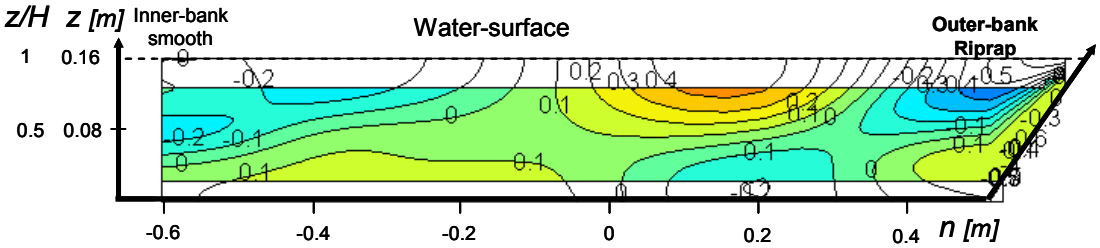

Patterns of normalized cross-stream shear stress terms in the cross-section at 90°

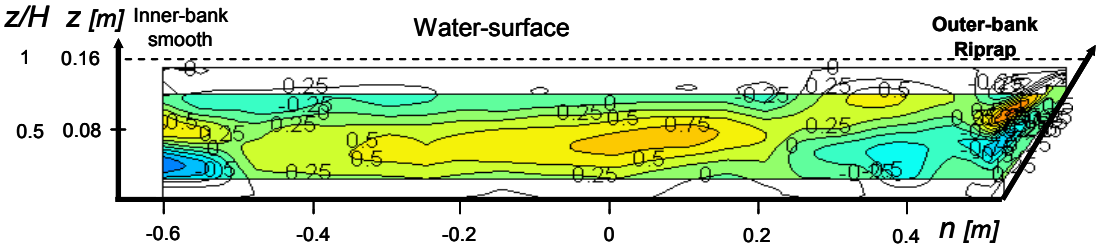

Patterns of normalized cross-stream kinetic energy fluxes in the cross-section at 90°

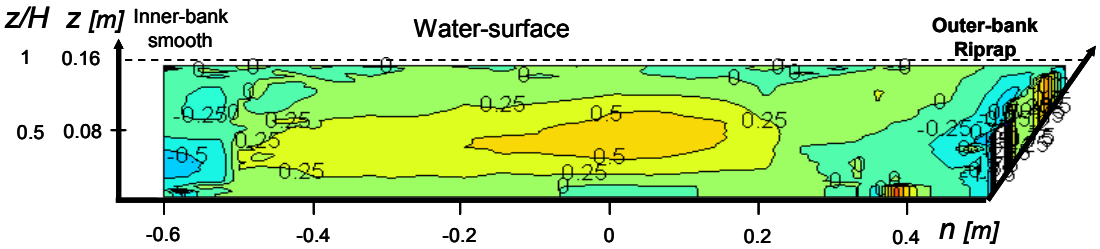

Communications du Laboratoire de Constructions Hydrauliques ISSN 1661-1179
Ecole Polytechnique Fédérale de Lausanne
Editeur: Prof. Dr A. Schleiss

N° 28 2007 A. Vela Giró
Bank protection at the outer side of curved channels by an undulated concrete wall

N° 29 2007 F. Jordan
Modèle de prévision et de gestion des crues - Optimisation des opérations des aménagements hydroélectriques à accumulation pour la réduction des débits de crue

N° 30 2007 P. Heller
Méthodologie pour la conception et la gestion des aménagements hydrauliques à buts multiples

N° 31 2007 P. Heller
Analyse qualitative des systèmes complexes à l'aide de la méthode de Gomez & Probst

N° 32 2007 J. García Hernández, F. Jordan, J. Dubois, J.-L. Boillat
Routing System II - Modélisation d'écoulements dans des systèmes hydrauliques

N° 33 2007 Symposium - Flussbauliche Massnahmen im Dienste des Hochwasserschutzes, der Umwelt, Gesellschaft und Wirtschaft / Mesures d'aménagement des cours d'eau pour la protection contre les crues, l'environnement, la société et l'économie

N° 34 2007 B. Rosier
Interaction of side weir overflow with bed-load transport and bed morphology in a channel

N° 35 2007 A. Amini
Contractile floating barriers for confinement and recuperation of oil slicks

N° 36 2008 T. Meile
Influence of macro-roughness of walls on steady and unsteady flow in a channel

N° 37 2008 S. A. Kantoush
Experimental study on the influence of the geometry of shallow reservoirs on flow patterns and sedimentation by suspended sediments

N° 38 2008 F. Jordan, J. García Hernández, J. Dubois, J.-L. Boillat
Minerve - Modélisation des intempéries de nature extrême du Rhône valaisan et de leurs effets

N° 39 2009 A. Duarte
An experimental study on main flow, secondary flow and turbulence in open-channel bends with emphasis on their interaction with the outer-bank geometry

ISSN 1661-1179

Prof. Dr A. Schleiss
Laboratoire de constructions hydrauliques - LCH
EPFL, Bât. GC, Station 18, CH-1015 Lausanne
http://lchwww.epfl.ch
e-mail: secretariat.lch@epfl.ch